

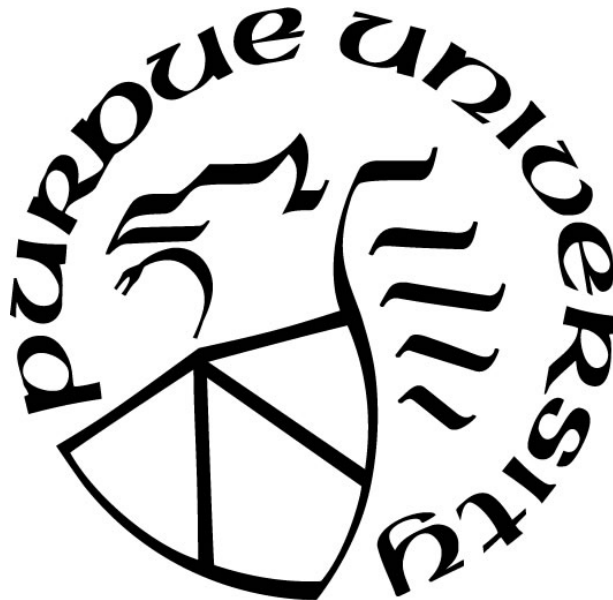
**EFFICIENT UNCERTAINTY CHARACTERIZATION FRAMEWORK IN  
NEUTRONICS CORE SIMULATION WITH APPLICATION TO  
THERMAL-SPECTRUM REACTOR SYSTEMS**

by  
**Dongli Huang**

**A Dissertation**

*Submitted to the Faculty of Purdue University  
In Partial Fulfillment of the Requirements for the degree of*

**Doctor of Philosophy**



School of Nuclear Engineering  
West Lafayette, Indiana  
May 2020

**THE PURDUE UNIVERSITY GRADUATE SCHOOL  
STATEMENT OF COMMITTEE APPROVAL**

**Dr. Hany S. Abdel-Khalik, Chair**

School of Nuclear Engineering

**Dr. Lefteri H. Tsoukalas**

School of Nuclear Engineering

**Dr. Yunlin Xu**

School of Nuclear Engineering

**Dr. Alberto Talamo**

Argonne National Laboratory

**Approved by:**

Dr. Seungjin Kim

*To Mom, Dad, and Liren*

## ACKNOWLEDGMENTS

First and foremost, I would like to express my sincere gratitude and appreciation to my advisor, Dr. Hany S. Abdel-Khalik, who has guided me, supported me, and provided me abundant opportunities throughout my graduate studies and professional development. It is a great honor and pleasure for me to spend my Ph.D. life under your advisory. I appreciate your invaluable ideas and intelligence, heuristic and patient education, and scientific insights and perspectives throughout my doctoral program. You have always encouraged me and offered me opportunities to participate in conferences, workshops, summer schools, and internships, supporting me from every aspect of educational and professional development. Without your guidance and help, I would never be able to make current progress and accomplishment.

My appreciation also goes to my advisory committee: Dr. Linyun Xu, Dr. Lefteri H. Tsoukalas, and Dr. Alberto Talamo for their insightful and critical comments and discussions.

Besides, I am grateful to Dr. Congjian Wang, who has been my mentor at the beginning of my graduate school at Purdue and great mentor at Idaho National Laboratory for my first internship. Your genuine suggestions and precious guidance have helped me go through the difficulties in my educational and professional development. Special thanks goes to Dr. Ugur Mertuyurek for being my mentor during my internship at Oak Ridge National laboratory. I have learnt a lot from the enlightening and delightful discussion with you.

I would also like to thank my fellows and friends at Purdue, Yeni Li, Jia Zhou, Gang Yang, Zhuoran Dang, Guanyi Wang, Arvind Sundaram, Jeongwon Seo, Haoxuan Wang and many other people who have created a wonderful graduate life and research environment and provided me company and encouragement during my journey towards a doctorate. I would give my special thanks to Dr. Mengnan Li, who has been a great friend and companion since my undergraduate and pursued a doctoral degree with me in US.

Last but not least, I have dedicated this dissertation to my beloved mother Qinghe Yu and father Hui Huang, who have always been unconditionally supporting me, believing in me, and encouraging me with love throughout my journey.

# TABLE OF CONTENTS

LIST OF TABLES .....	9
LIST OF FIGURES .....	10
NOMENCLATURE .....	13
ABSTRACT.....	16
1. INTRODUCTION .....	18
1.1 Overview and Motivation .....	18
1.2 Challenges and Objectives.....	20
1.3 Scope and Layout of Dissertation .....	25
1.3.1 Scope of dissertation work.....	25
1.3.2 Organization of dissertation.....	28
1.4 References.....	30
2. UNCERTAINTY SOURCES IN NEUTRONICS CALCULATIONS.....	33
2.1 Uncertainty Classification.....	34
2.2 Uncertainty Representation.....	35
2.3 Uncertainty Sources in Computational Modeling and Simulation .....	37
2.3.1 Parameter uncertainties.....	37
2.3.2 Modeling uncertainties .....	38
2.3.3 Numerical uncertainties .....	39
2.4 Propagation of Uncertainty Sources in Neutronic Simulation Stages .....	39
2.4.1 Uncertainties in pointwise cross-section generation.....	40
2.4.2 Uncertainties in multi-group cross-section generation .....	41
2.4.3 Uncertainties in lattice calculations .....	42
2.4.4 Uncertainties in core calculations .....	44
2.5 References.....	45
3. LITERATURE REVIEW OF UNCERTAINTY ANALYSIS METHODS IN NEUTRONICS CALCULATIONS.....	46
3.1 Uncertainty Quantification Approaches .....	48
3.1.1 Stochastic methods .....	48

3.1.2	Deterministic methods .....	50
3.2	Efficiency-based Uncertainty Propagation Methods .....	51
3.2.1	Surrogate model.....	52
3.2.2	Dimensionality reduction.....	52
3.2.3	Fitting approximation .....	53
3.3	Sensitivity Analysis Approaches .....	53
3.4	Background and Status in Modeling Uncertainty Propagation.....	54
3.5	References.....	55
4.	METHODOLOGIES IN PROPOSED UCF.....	58
4.1	PCM Methodology.....	58
4.1.1	PCM problem setup .....	61
4.1.2	PCM Implementation Algorithm: .....	61
4.1.3	PCM results interpretation.....	63
4.2	Dimensionality Reduction in ROM .....	65
4.2.1	ROM background .....	65
4.2.2	DR problem setup and error bounding .....	67
4.2.3	RFA algorithm for active subspace construction.....	70
4.2.4	DR results interpretation.....	73
4.3	References.....	74
5.	PROPOSED UNCERTAINTY CHARACTERIZATION APPROACHES .....	76
5.1	Proposed Uncertainty Propagation Approaches .....	76
5.2	Propagation of Parameter Uncertainties .....	81
5.2.1	Uncertainty propagation algorithms .....	81
5.2.2	Branch uncertainty representation and reduction .....	84
5.2.3	ROM-based implementation.....	89
5.3	Propagation of Modeling Uncertainties .....	92
5.3.1	Linearity verification exercises.....	93
5.3.2	Evaluation of modeling uncertainty impact.....	95
Modeling assumptions in few-group parameter uncertainty propagation.....		96
5.4	Sensitivity Analysis and Priority Ranking .....	98
5.5	References.....	99

6. APPLICATION TO BWR CORE UNCERTAINTY PROPAGATION AND SENSITIVITY ANALYSIS.....	100
6.1 Dimensionality Reduction of Few-Group Cross-Section Uncertainties.....	100
6.1.1 BWR lattice model setup.....	101
6.1.2 Branch models impact on few-group uncertainty space.....	104
6.1.3 Burnup impact on few-group uncertainty space.....	108
6.1.4 Dimensionality reduction on few-group cross-section uncertainty space.....	110
6.1.5 Multiple lattices impact on few-group uncertainty compression.....	113
6.2 Uncertainty Quantification and Sensitivity Analysis on Core Simulation.....	115
6.2.1 BWR core model setup.....	115
6.2.2 UQ and SA results on BWR core simulation.....	115
6.2.3 Priority ranking on major few-group uncertainty sources.....	120
6.3 Conclusions.....	123
6.4 References.....	123
7. APPLICATION TO CANDU CORE UNCERTAINTY PROPAGATION.....	125
7.1 Dimensionality Reduction of Few-Group Parameter Uncertainties.....	126
7.1.1 CANDU-6 lattice model setup.....	126
7.1.2 CANDU few-group parameter uncertainties.....	129
7.1.3 Correlation among few-group parameters along burnup.....	132
7.1.4 Compressed CANDU few-group uncertainty space.....	133
7.1.5 CANDU branch and device uncertainties.....	137
7.2 ROM-based Uncertainty Propagation Results on CANDU Core Simulation.....	140
7.2.1 CANDU-6 core model setup.....	140
7.2.2 ROM-based few-group uncertainty propagation results on CANDU core responses	148
7.2.3 sUncertainties propagation results in Core CVR.....	152
7.2.4 Uncertainty Propagation Results in LOCA Core Model.....	153
7.3 Conclusions.....	157
7.4 References.....	157
8. MODELING ERROR IN CANDU CORE UNCERTAINTY PROPAGATION.....	158
8.1 Modeling Assumptions Setup.....	159

8.2	Modeling Uncertainties in CANDU Lattice Modeling.....	160
8.3	Modeling Assumptions Impact during Parameter Uncertainty Propagation .....	165
8.3.1	Assessing impact of uncertainty propagation method .....	167
8.3.2	Assessing impact of modeling approximations .....	171
8.4	Modeling Uncertainties Interaction with Parameter Uncertainties.....	174
8.5	Conclusion .....	182
8.6	References.....	182
9.	CONCLUSION AND FUTURE WORK .....	183

## LIST OF TABLES

Table 6-1 List of branch cases at 34.5 GWD/MTU.....	105
Table 6-2 Mean values for samples in branch and base calculations. ....	106
Table 6-3 Correlation coefficients of branch vs. base cases. ....	106
Table 6-4 Correlation coefficients of high vs. low burnup cases. ....	108
Table 6-5 Priority ranking for individual $u_i$ vector to k-eff or axial power shape uncertainties. .....	121
Table 7-1 Energy boundaries in few-group structure. ....	129
Table 7-2 List of all types of few-group parameters required in NESTLE-C. ....	141
Table 7-3 Parameters of core configurations. ....	142
Table 7-4 Reference k-eff and comparison in various core models. ....	145
Table 7-5 Deterministic- vs. stochastic-based uncertainty. ....	152
Table 7-6 Core CVR uncertainties via deterministic vs. via stochastic approaches.....	153
Table 8-1 Core models and reference cross-section libraries with abbreviations in the thesis context. .....	160
Table 8-2 Few-group uncertainties generation in group structure and number of samples through NEWT calculation. ....	165
Table 8-3 Core k-eff uncertainty quantification through deterministic vs. stochastic approach. ....	169

## LIST OF FIGURES

Figure 1-1 Concept of safety margins defined in [10] and its comparison to acceptance criterion defined in terms of conservative bounds or BEPU.....	19
Figure 2-1 Schematic of neutronics simulation and major uncertainty sources at each stage.....	40
Figure 4-1 Layout of model validation problem setup. ....	59
Figure 4-2 Layout of PCM methodology for uncertainty mapping.....	60
Figure 4-3 Example of joint PDF by mapping uncertainties from the experimental domain to the application domain.....	64
Figure 4-4 Example of maximum error resulting from dimensionality recution vs active rank. .	74
Figure 5-1 Layout of proposed uncertainty propagation process with compressed sources of uncertainties starting from multi-group uncertainty to responses of core simulation. ....	80
Figure 6-1 BWR lattice model layout by NEWT. ....	102
Figure 6-2 Layout of Peach Bottom Type 3c lattice model by NEWT. ....	103
Figure 6-3 Layout of Peach Bottom Type 1 lattice model by NEWT.....	104
Figure 6-4 Joint PDFs of fission cross-section - branch vs. base. ....	107
Figure 6-5 Joint PDFs of cross-sections of high burnup vs. low burnup.....	109
Figure 6-6 Joint PDFs of cross-sections of high burnup vs. low burnup – with isotopics uncertainties. ....	109
Figure 6-7 Error reduction vs. active rank throughout depletion - fixed reaction type and energy group. ....	111
Figure 6-8 Error reduction vs. active rank throughout depletion - fixed energy group.....	112
Figure 6-9 Error Reduction vs. Active Rank throughout Depletion – All Reaction Types and Energy Groups Included .....	113
Figure 6-10 Plot of error reduction vs. rank across depletions – all reaction types and energy groups included.....	114
Figure 6-11 Partial uncertainty of k-eff along burnup.....	117
Figure 6-12 Integral uncertainty of k-eff along burnup.....	117
Figure 6-13 Partial uncertainty of axial power shape along burnup.....	118
Figure 6-14 Integral uncertainty of axial power shape along burnup.....	119
Figure 7-1 Lattice layout by SERPENT geometry engine.....	127
Figure 7-2 Lattice layout by NEWT geometry engine. ....	128

Figure 7-3 Burnup-dependent few-group parameter – parameter values of reference and random samples from SAMPLER. ....	131
Figure 7-4 Correlation coefficients among lattice parameters across burnup. ....	133
Figure 7-5 ROM-based maximum reconstruction errors of few-group parameter uncertainties. ....	136
Figure 7-6 Normalized singular values of few-group parameter uncertainties. ....	137
Figure 7-7 Correlations between few-group parameters of base and branch cases. ....	138
Figure 7-8 Correlations between base and device cross-sections. ....	139
Figure 7-9 Radial core channel burnup distribution. ....	143
Figure 7-10 Radial core channel power distribution. ....	144
Figure 7-11 Channel power distributions in three steady-state core models w/ HELIOS-based cross-section library. ....	146
Figure 7-12 Reference channel power distribution w/ SERPENT- or NEWT-based cross-section library in four-group energy structure. ....	147
Figure 7-13 Reference channel power uncertainty distribution w/ HELIOS-based or SERPENT-based cross-section library in two-group energy structure. ....	147
Figure 7-14 ROM-based core k-eff uncertainty. ....	148
Figure 7-15 ROM-based core channel power uncertainty at certain channel. ....	149
Figure 7-16 Histograms of core attributes via stochastic approach. ....	151
Figure 7-17 ROM-based core CVR uncertainty. ....	153
Figure 7-18 Reference core attributes in LOCA core model. ....	154
Figure 7-19 Uncertainty of transient core power. ....	155
Figure 7-20 Uncertainties of core power at selected time steps. ....	156
Figure 8-1 Discrepancies in CANDU bundle k-eff generated by different lattice calculation codes. ....	161
Figure 8-2 SERPENT vs. NEWT few-group cross-section modeling discrepancies. ....	162
Figure 8-3 Burnup-dependent modeling and cross-Section uncertainties. ....	164
Figure 8-4 Percentage discrepancy of channel power between different reference cross-section libraries. ....	166
Figure 8-5 Scatter plot of channel power uncertainty quantified via deterministic vs. stochastic approach. ....	170

Figure 8-6 Comparison of core k-eff uncertainty under different modeling assumptions and approximations, including impact of few-group structures, number of basis from ROM-based compression, core models, and reference cross-section libraries. .... 172

Figure 8-7 Scatter plot of channel power uncertainty based on two-group vs. four-group few-group energy structures. .... 173

Figure 8-8 Scatter plot of channel power uncertainty based on LATTICECELL vs. MULTIREGION resonance treatment..... 173

Figure 8-9 Scatter plot of channel power uncertainty based 300 vs. 50 few-group uncertainty source basis. .... 174

Figure 8-10 ROM-based core k-eff uncertainty with selected reference cross-section libraries.176

Figure 8-11 Relationship between modeling and parameter uncertainties. .... 178

Figure 8-12 Decomposition of modeling errors along parameter uncertainties. .... 179

Figure 8-13 Decomposition of modeling errors based on reaction type of few-group parameters. .... 180

Figure 8-14 Scatter plot of percentage power distribution uncertainties between selected (indicated in the axis label) reference cross-section libraries, implying the impact of modeling uncertainties by switching the reference values. .... 181

## NOMENCLATURE

<i>a</i>	coefficients
<i>f</i>	function
<i>m</i>	number of responses
<i>M</i>	number of experiments
<i>n</i>	number of parameters
<i>N</i>	number of random samples
<i>p</i>	probability density function
<i>r</i>	rank, active degrees of freedom
<i>T</i>	temperature, K
<i>u</i>	control parameters of experiment
<i>v</i>	control parameters of application
<i>x</i>	input, basic physics parameters (cross-section)
<i>y</i>	output, response of interest
<i>z</i>	random variable

### Greek Letters

$\Delta$	difference
$\varepsilon$	error tolerance
$\mu$	mean value
$\Omega$	function of buffer code
$\Pi$	function in terms of cross-section
$\sigma$	cross-section
$\hat{\Sigma}$	few-group parameter represented by polynomials

### Matrices and Operators

<b>A</b>	triangular matrix by Cholesky decomposition
<b>C</b>	covariance matrix
<b>H</b>	matrix operator to convert raw data
<b>I</b>	identity matrix
<b>⊖</b>	zero matrix
$\mathbb{R}$	domain
<i>s</i>	singular value
<b>S</b>	sensitivity profile
$\Sigma$	diagonal matrix from SVD, containing singular values as diagonal elements
<i>u</i>	singular vector
<b>U</b>	orthonormal matrix from SVD, containing singular vectors as columns
<b>V</b>	orthonormal matrix from SVD, containing weighting vectors as columns
<b>X, Y</b>	standardized parameter matrix

## Subscripts and Superscripts

app	application domain
Base	variable of base case
Branch	variable of branch case
cal	computational calculated results
CS	Core Simulation
eff	effective
exp	experiment domain
f	fuel
fast	fast group (neutron energy group)
FG	Few-Group
g	group index
i	experiment index
j	coefficient index
map	mapping response
MG	Multi-Group
msr	experimental measured results
raw	unprocessed raw few-group cross-section data
rel	relative
ROM	ROM-based
T	Transpose
x	reaction type index

## Acronyms and Abbreviations

ADF(s)	Assembly Discontinuity Factor(s)
BE	Best-Estimate
BEUP	Best-Estimate-Plus-Uncertainty
BWR	Boiling Water Reactor
CANDU	CANada Deuterium Uranium (nuclear reactor)
CVR	Coolant Void Reactivity
DR	Dimensionality Reduction
DOF	Degree of Freedom
DR	
ENDF	Evaluated Nuclear Data File
FORM	First-Order Reliability Method
GRS	Gesellschaft für Anlagen- und Reaktorsicherheit (in German)
HELIOS	a generalized-geometry lattice physics code
HO	High Order
KDE	Kernel Density Estimation
KENO	a three-dimensional Monte Carlo criticality transport program
KENO-CE	KENO with Continuous Energy cross-section library
LHS	Latin Hypercube Sampling
LWR	Light Water Reactor
LOCA	Loss-Of-Coolant Accident
NRC	Nuclear Regulatory Commission

NEM	Nodal Expansion Method
NESTLE	Few-Group Neutron Diffusion for Steady-State and Transient Problems by Nodal Expansion Method (computer program)
NESTLE-C	NESTLE CANDU version
NEWT	New ESC-based Weighting Transport code, deterministic transport solver
OAT	One-at-A-Time
OECD	Organization for Economic Cooperation and Development
ORNL	Oak Ridge National Laboratory
PCM	Physics-guided Coverage Mapping
PDF	Probability Density Function
PWR	Pressurized Water Reactor
RFA	Range Finding Algorithm
RoIs	Responses of Interest
ROM	Reduced Order Modeling
SA	Sensitivity Analysis
SAMPLER	a module statistically samples the input data and analyzes the output distribution for SCALE sequences
SERPENT	a Monte Carlo reactor physics burnup calculation code
STD	STandard Deviation
SCALE	Standardized Computer Analyses for Licensing Evaluation (computer software system)
SORM	Second-Order Reliability Method
SVD	Singular Value Decomposition
T2N	Triton-to-NESTLE
TMC	Total Monte Carlo method
TRITON	control module for transport, depletion, sensitivity and uncertainty analysis in SCALE
wt	weight
UAM	Uncertainty Analysis in Modeling
UC	Uncertainty Characterization
UCF	Uncertainty Characterization Framework
UM	Uncertainty Mapping
UQ	Uncertainty Quantification
ZO	Zero Order
<b>Unit</b>	
GWd/MTU	common unit for burnup, gigawatt days per metric ton of uranium
MWD/kgHM	unit for burnup, MegaWatt Days per kilogram Heavy Metal
mk	unit for reactivity, milli-k
pcm	unit for reactivity, per cent mille

## ABSTRACT

This dissertation is devoted to developing a first-of-a-kind uncertainty characterization framework (UCF) providing comprehensive, efficient and scientifically defensible methodologies for uncertainty characterization (UC) in best-estimate (BE) reactor physics simulations. The UCF is designed with primary application to CANDU neutronics calculations, but could also be applied to other thermal-spectrum reactor systems. The overarching goal of the UCF is to propagate and prioritize all sources of uncertainties, including those originating from nuclear data uncertainties, modeling assumptions, and other approximations, in order to reliably use the results of BE simulations in the various aspects of reactor design, operation, and safety. The scope of this UCF is to propagate nuclear data uncertainties from the multi-group format, representing the input to lattice physics calculations, to the few-group format, representing the input to nodal diffusion-based core simulators and quantify the uncertainties in reactor core attributes.

The main contribution of this dissertation addresses two major challenges in current uncertainty analysis approaches. The first is the feasibility of the UCF due to the complex nature of nuclear reactor simulation and computational burden of conventional uncertainty quantification (UQ) methods. The second goal is to assess the impact of other sources of uncertainties that are typically ignored in the course of propagating nuclear data uncertainties, such as various modeling assumptions and approximations.

To deal with the first challenge, this thesis work proposes an integrated UC process employing a number of approaches and algorithms, including the physics-guided coverage mapping (PCM) method in support of model validation, and the reduced order modeling (ROM) techniques as well as the sensitivity analysis (SA) on uncertainty sources, to reduce the dimensionality of uncertainty space at each interface of neutronics calculations. In addition to the efficient techniques to reduce the computational cost, the UCF aims to accomplish four primary functions in uncertainty analysis of neutronics simulations. The first function is to identify all sources of uncertainties, including nuclear data uncertainties, modeling assumptions, numerical approximations and technological parameter uncertainties. Second, the proposed UC process will be able to propagate the identified uncertainties to the responses of interest in core simulation and provide uncertainty quantifications (UQ) analysis for these core attributes. Third, the propagated uncertainties will be mapped to a wide range of reactor core operation conditions. Finally, the

fourth function is to prioritize the identified uncertainty sources, i.e., to generate a priority identification and ranking table (PIRT) which sorts the major sources of uncertainties according to the impact on the core attributes' uncertainties. In the proposed implementation, the nuclear data uncertainties are first propagated from multi-group level through lattice physics calculation to generate few-group parameters uncertainties, described using a vector of mean values and a covariance matrix. Employing an ROM-based compression of the covariance matrix, the few-group uncertainties are then propagated through downstream core simulation in a computationally efficient manner.

To explore on the impact of uncertainty sources except for nuclear data uncertainties on the UC process, a number of approximations and assumptions are investigated in this thesis, e.g., modeling assumptions such as resonance treatment, energy group structure, etc., and assumptions associated with the uncertainty analysis itself, e.g., linearity assumption, level of ROM reduction and associated number of degrees of freedom employed. These approximations and assumptions have been employed in the literature of neutronic uncertainty analysis yet without formal verifications. The major argument here is that these assumptions may introduce another source of uncertainty whose magnitude needs to be quantified in tandem with nuclear data uncertainties. In order to assess whether modeling uncertainties have an impact on parameter uncertainties, this dissertation proposes a process to evaluate the influence of various modeling assumptions and approximations and to investigate the interactions between the two major uncertainty sources. To explore this endeavor, the impact of a number of modeling assumptions on core attributes uncertainties is quantified.

The proposed UC process has first applied to a BWR application, in order to test the uncertainty propagation and prioritization process with the ROM implementation in a wide range of core conditions. Finally, a comprehensive uncertainty library for CANDU uncertainty analysis with NESTLE-C as core simulator is generated compressed uncertainty sources from the proposed UCF. The modeling uncertainties as well as their impact on the parameter uncertainty propagation process are investigated on the CANDU application with the uncertainty library.

# 1. INTRODUCTION

## 1.1 Overview and Motivation

A nuclear reactor is a device to initiate and control a sustained nuclear chain reaction aiming at energy produce. The main purpose of reactor simulation is to predict the behaviors of nuclear chain reaction systems. A computational model/simulation sequence of a nuclear reactor is a set of mathematical representations to describe the theoretical physics of the reactor system, whose solutions/responses of interest are used to analyze the performance of the system. With the increasing power of scientific computing, the accuracy of reactor calculations has been continuously improved by increasing the fidelity of the model and the complexity of the model descriptions, which in turn improves the understanding of the physics in nuclear reactor benefiting the design, operation and safety assessment. Despite the improvement of prediction accuracy, uncertainties are unavoidable in nuclear reactor simulation due to the discrepancies between the reality and the models that the simulations are based on. Since the nuclear reactor is a high consequence system, uncertainty quantification and understanding of the uncertainty sources is indispensable in reactor calculations to ensure the safety and reliability of the reactor designs under normal operation and transient scenarios.

Many nuclear engineering studies and applications have benefited from the noticeable growth in the development of uncertainty analysis techniques. For example, spent fuel analysis employs uncertainty analysis to estimate uncertainties of the heat load and radiotoxicity resulting from the burnt fuel isotopics whose uncertainties are dominated by cross section uncertainties and irradiation history. Burnup credit calculations employ uncertainty analysis to assess the degree of spent fuel subcriticality. Fuel cycle studies focus on estimating uncertainties in burnup, cycle length, concentration of recycled fuel isotopes, etc. Core load follow calculations are concerned with the estimation of uncertainties of key core attributes such as the critical eigenvalue, power distribution, discharge burnup, etc. For criticality safety studies, measurements of flux, eigenvalue, critical size are typically made, and are compared against their predicted values and their propagated uncertainties. In similarity studies, employing similarity indices [1] or representativity factors [2], one judges the relevance of experiments to given applications based solely on the cross sections sensitivities (first order derivatives of key attributes such as the eigenvalue with respect

to cross sections) and their prior uncertainties. In Bayesian inference, also referred to as Bayesian calibration or cross section adjustment techniques [3-5], the main premise is that cross sections may be adjusted within their prior uncertainties to explain the discrepancies between measurements and predictions. The implication is that the adjusted cross sections may be used in lieu of the original cross sections to improve predictions for a wider range of applications.

Uncertainty analysis is an essential component of best-estimate (BE) reactor analysis calculations as it provides reliable metrics by which the quality of the predictions can be assessed. The original nuclear reactor designs for safety analysis require very conservative assumptions to meet the design margins [6]. With the U.S. Nuclear Regulatory Commission (NRC)'s shift [7] from overly conservative bounding-type analyses to best-estimate plus uncertainty (BEPU) [8, 9], the requirements for rigorous, comprehensive and efficient methodologies for uncertainty quantification have greatly increased. The concept of safety margins and its relationship with the acceptance criterion accepted by the regulatory body are illustrated in Figure 1-1. The safety margin can either be measured by the discrepancy between the safety limit and the real value or the acceptance criterion. Figure 1-1 also presents the comparison between the two ways to define the acceptance criterion, which are the conservative analysis and the BEPU analysis.

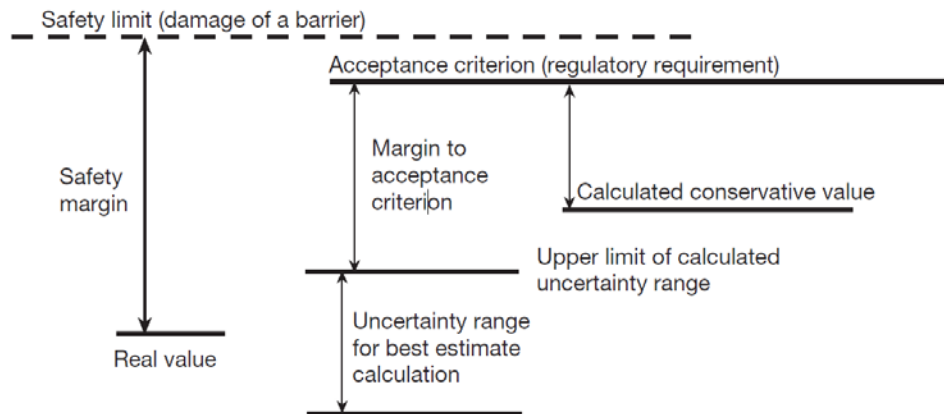


Figure 1-1 Concept of safety margins defined in [10] and its comparison to acceptance criterion defined in terms of conservative bounds or BEPU.

Although direct comparison against measurements provides the ultimate evidence that simulation predictions are reliable, the true value of any best-estimate simulation lies in its ability to analyze reactor conditions for which measurements are not available. Therefore, there is a clear need to characterize, i.e., propagate and prioritize, all sources of uncertainties in order to reliably

use the results of BE calculations in the various aspects of reactor design, operation, and safety. Characterization of uncertainties refers to all engineering analyses conducted to provide scientifically-defendable quantities that measure the reliability of the reactor simulation predictions. This characterization of uncertainties involves three primary processes. The first process, referred to as uncertainty quantification (UQ), propagates all known sources of simulation uncertainties in order to understand their impact on the reactor behavior. The second process, referred to as sensitivity analysis (SA), acts in conjunction with UQ to help identify the key sources of uncertainties. The third process, referred to as uncertainty mapping (UM), represents the ultimate value of any uncertainty analysis, that's to predict the real behavior for a system based on the combined use of UQ, SA, and experimental results.

This thesis work has been focusing on developing an uncertainty characterization framework (UCF) to accomplish the three primary processes above as well as a prior process to identify all sources of uncertainties including not only nuclear data uncertainties, but also modeling assumptions and numerical approximations throughout reactor physics simulations.

## **1.2 Challenges and Objectives**

The last two decades have witnessed a huge growth in the number of publications [10-16] in the area of uncertainty analysis for reactor physics calculations focusing on neutronic sources of uncertainties. The common objective to these developments has been focused on the propagation of nuclear data uncertainties starting with the ENDF (Evaluated Nuclear Data Files) level and heading downstream to the quantities of interest for the various applications, e.g. core simulation [16], criticality safety [17, 18], spent fuel characterization [19], etc. Although methods have been developed to propagate other sources of uncertainties, such as those originating from boundary/initial conditions, geometry, composition, other non-neutronic physics, the discussion in this paper will be limited to what is referred to as “standalone neutronic uncertainty analysis” [10]. Most of the literature on standalone neutronic uncertainty quantification has focused on nuclear data uncertainties [20], which are classified as parameter uncertainties since nuclear data are the input parameters to reactor simulations in this dissertation. The classifications and sources of uncertainties are presented in detail in Chapter 2.

The common assumption in current standalone neutronic uncertainty analyses is that modeling uncertainties have minimal impact on the propagated cross section uncertainties and the

cross-section adjustments, and if present, they may be treated as independent sources of uncertainty. Modeling uncertainties, sometimes referred to as errors or biases are introduced from the numerous simplifying assumptions and approximations made throughout the calculations. For example, in lattice cell calculations, the assumption of reflective boundary conditions represents a source of modeling uncertainties because it ignores the neutron leakage between the assembly and its neighbors. The use of flux weighting to collapse cross sections and the various associated resonance treatment models are other sources of modeling uncertainties. Each type of deterministic solver for radiation transport introduces different type of modeling uncertainties. For example, the discrete ordinary method, the method of characteristics, or collision probability method [21], each introduces its own assumptions and thus will produce different modeling uncertainties. Use of a deterministic solver as compared to a probabilistic particle-tracking solver, e.g., Monte Carlo radiation transport, represents another fundamental source of modeling uncertainties.

The order of magnitude of contributions to the multiplication factor uncertainty from nuclear data and other uncertainty sources in a standalone steady-state assembly calculation is discussed in table of Ref [22]. The nuclear data uncertainty is the dominant uncertainty source contributing to the assembly  $k_{inf}$  uncertainty in an order of 500 [pcm] while other uncertainty sources such as methods and models are less than 100 [pcm]. Thus, most of the literature has focused on the propagation of parameter uncertainties only. However, at the core simulations level, the neutronic calculations are performed in a wide burnup range and various local conditions or even transient scenarios, giving rise to the significance of impact from other sources of uncertainty, such as modeling uncertainties [23]. Despite the unneglectable effect of modeling uncertainties on core responses of interest uncertainties, few literatures has included uncertainty sources other than nuclear data uncertainties in core-wise uncertainty quantification. Ref. [24, 25] are examples evaluating the impact of modeling uncertainties in the boundary conditions and fuel geometries, etc., but the uncertainty analysis is still applied at lattice calculation level.

Therefore, analysis in this thesis work aims at the propagation of all sources related to the neutronic modeling to preserve the accuracy and confidence of the uncertainty characterization exercise. If comprehensively done, this would include the propagation of the basic ENDF data uncertainties, referred to as parameter uncertainties as well as the modeling uncertainties resulting from downstream modeling or data processing, including simplifying assumptions/approximations associated with radiation transport models, e.g., Monte Carlo continuous cross-section models vs.

multi-group deterministic methods, homogenization and/or collapsing procedures employed to reduce dimensionality of the cross-sections, resonance self-shielding calculations, etc. Challenges here are how to define the modeling uncertainties in neutronic calculations, how to propagate modeling uncertainties and evaluate the impact of them on the core responses of interest, and how to develop systematic approach for the propagation of modeling uncertainties incorporation with parameter uncertainties in the uncertainty analysis.

Another challenge results from the feasibility and efficiency of propagation of all sources of uncertainties. Despite the importance of uncertainties, the existing nuclear simulation codes have always lacked an integrated framework for their characterization. This is primarily due to:

- 1) The complex nature of nuclear models, i.e., based on a multi-level homogenization strategy where a number of models are linked together to account for the wide range of physical phenomena involved, the large variations in energy and length scales, and the various forms of feedback mechanisms;
- 2) The individual simulations codes requiring long execution times and being associated with voluminous size of input and output data streams;
- 3) The recent advances in uncertainty algorithms have been primarily demonstrated for modern software platforms, i.e., new codes; it is however difficult to incorporate these advances in some of the legacy codes used extensively in the design and regulatory spaces.

Focusing on neutronics calculations, a nuclear reactor calculations start with basic nuclear data which describe cross-sections variations as a function of the incident neutron energy, referred to as pointwise continuous cross-sections. Considering the level of heterogeneity of a nuclear core, modeling the core using the pointwise nuclear data is a herculean task that is not suitable for day-to-day engineering analysis. Hence, the primary job of a reactor physicist is to devise recipes by which cross-sections can be condensed into small number of groups to render core simulation computationally feasible. This is done using customized recipes, referred to as collapsing and homogenization techniques, where collapsing refers to reducing the number of energy groups require to represent nuclear data, and homogenization refers to reducing the spatial heterogeneity that is characteristic of any commercial-size nuclear reactor. For example, in typical core simulation, each assembly is replaced by 10-20 axial nodes, where each node represents a homogeneous mixture of fuel, coolant, and cladding material that preserves the reaction rates in

order to accurately calculate the core eigenvalue as well as the local pin powers. Collapsing relies on the use of representative energy-dependent weighting flux to reduce the initial energy dependence from the pointwise format down to the multi-group format. This is typically done at the pin cell level, which preserves the relative amounts of fuel-to-coolant, representing a key quantity in determining the flux spectrum. Homogenization relies on detailed modeling of all fuel lattices present in the core (a lattice is a 2D slice of a fuel assembly) to smear away the heterogeneous details of a fuel lattice into the so-called few-group parameters. In doing so, the few-group parameters develop new dependencies to ensure reactions rates are preserved locally, i.e., at the lattice level. Some of these dependencies include fuel composition, fuel temperature, coolant temperature or voiding, boron dilution, control rod insertion, reactivity devices, etc. To obtain these dependences, lattice physics calculations must be repeated many times to generate the few-group parameters at many conditions, which are fitted using polynomial regression, and are later interpolated at the local conditions for core-wide simulation. The number of lattice physics calculations is typically measured by the number of different fuel lattices times the number of burnup steps times the number of branch cases per burnup step, resulting in a high dimensional table containing  $10^4$ - $10^6$  parameters. All these parameters are input to downstream core-wide simulation either in their raw format or after some preprocessing to facilitate their interpolation for core simulation.

A buffer code is typically used to read all the few-group parameters generated by lattice physics and convert them into polynomial coefficients as input parameters to the core simulator, such that every few-group parameter, e.g., fast absorption, thermal fission, etc., is written as a polynomial in terms of local conditions, such as burnup, fuel temperature, etc. The number of polynomial coefficients is approximately the same as the number of raw data. This follows because for example to generate a 2<sup>nd</sup> order polynomial to functionalize a few-group parameter in terms of say moderator density, one needs two additional branch cases in addition to the base case to estimate three polynomial terms, a constant term representing the value of the cross-section at the base case, and a linear and 2<sup>nd</sup> order terms that are functions of the deviations of the few-group parameter from the base case. A base case refer to a depletion of the lattice at multiple time steps from zero up to a representative end of life discharge burnup. Branch cases refer to additional flux evaluations off of each base case, where only a single condition is changed to estimate the impact on the few-group parameters, e.g., an increase or decrease in fuel temperature, coolant density, etc.

A core simulator reads the polynomial coefficients directly instead of the raw few-group parameters. The implication of this is that an uncertainty analysis procedure must first propagate the multi-group cross-section uncertainties to all few-group parameters generated by the lattice physics calculations, and then through the buffer code used to generate their equivalent polynomial representation, ending with uncertainties for the polynomial coefficients input to the core simulator. The uncertainty analysis must be able to propagate the uncertainties in the core simulator's few-group parameters to the core attributes of interest. Finally, the core simulator is executed in either quasi steady-state mode where one is interested in doing load-follow calculations over a representative cycle of depletion, or in transient mode, where one is interested in the solution over multiple time steps to trace a certain transient, e.g., rod ejection accident, power manoeuvre transient, etc. In both cases, the core responses of interest, sometimes referred to as attributes, could include the spatially and temporally distributed responses in either transient or steady state calculations, e.g., power distribution, and the eigenvalue for steady state calculations. If one is interested in distribution-type responses, the number of responses could be in the order of  $10^4$ - $10^6$  or more, depending on the level of mesh refinement used by the numerical solver.

Given these challenges, any successful propagation of uncertainties must employ efficient techniques to reduce the computational cost required to propagate and prioritize uncertainties, which is otherwise intractable with conventional uncertainty analysis techniques.

Based on the motivations and challenges discussed above, the overarching goal of this UCF is to provide a comprehensive and scientifically defensible methodology for characterizing uncertainties in all BE reactor analysis calculations including both steady state and transient simulations, while balance the accuracy, confidence and efficiency during this process. To achieve the ultimate goal, the dissertation will make effort on the following three objectives:

1. Develop a framework to accomplish four tasks in uncertainty characterization:
  - a. Identify all sources of uncertainty in neutronic simulation process;
  - b. Propagate all major sources of uncertainty;
  - c. Mapping of uncertainties between different operational conditions;
  - d. Prioritize the propagated uncertainty sources.

The first three tasks may be referred to as part of an UQ analysis, while the last one is commonly known as sensitivity analysis. These tasks will be discussed in detail in Chapter 3.

2. Develop a reduced order modeling (ROM)-based uncertainty propagation method to ensure computational feasibility of this framework. The employed ROM technique should be able to provide a metric to measure/bound the errors introduced by the dimensionality reduction of the space of uncertainty sources. The ROM-based uncertainty propagation can be implemented to automate the generation of uncertainty libraries for existing core simulation code.
3. Develop a method to evaluate the interaction between the two major uncertainty sources, the modeling uncertainty and the parameter uncertainty, in order to develop insight for follow-up analysis to reduce cross-section uncertainties using calibration techniques. An important objective of the proposed framework is to study the correlations between modeling and parameter uncertainties. This is important to support many of the studies that focus on improving the quality of reactor physics calculations, focused on the removal or reduction of cross-section uncertainties. The idea is that if the modeling errors are heavily correlated with cross-section uncertainties, any change to the cross-sections using conventional calibration techniques, e.g., Bayesian analysis, could impact the quality of the models when extrapolated to other operating conditions. To limit the scope for this exploratory study, we will focus on how the discrepancies in the multi-group cross-sections, as calculated by different lattice physics codes and/or assumptions, correlate with the variations in the multi-group cross-sections due to propagated cross-section uncertainties.

### **1.3 Scope and Layout of Dissertation**

#### **1.3.1 Scope of dissertation work**

The uncertainty characterization exercises can be experimentally-based or code-based [26], which is necessary to distinguish between in this context, with the latter being the focus of this thesis work.

An *experimentally-based* UC exercise involves a direct comparison between simulation predictions and real experimental measurements, which typically is referred to as *bias*. The advantage of the experimentally-based UC exercise is that it provides a clear-cut quantification of the bias between simulation and the reality. Its disadvantage is that it does not explain how the

bias magnitude relates to the various sources of uncertainties inherent in the simulation. This is the reason that it is difficult to map this bias to other conditions not covered by the available experiments.

A *code-based* UC exercise, however, implies a self-assessment of the uncertainty sources, i.e., the code propagates its own known uncertainties, and provides them as part of the standard output along with best-estimate results. With the code-based uncertainty analysis, one can apportion the propagated uncertainties to the various sources of uncertainties, and can devise methods for their mapping to other operating conditions. The primary disadvantage of code-based UC techniques is that it propagates the “known” sources of uncertainties only, implying that all modeling inadequacies that are unknown to the modeler cannot be properly quantified. Ideally, one should employ a combination of the two exercises to fully characterize uncertainties and devise methods for uncertainty mapping to all operational conditions of interest.

This thesis work employs a code-based UC and its scope is limited to the propagation of nuclear data uncertainties from the multi-group energy structure to the core-wide simulation in standalone neutronics calculations. The dissertation represents effort towards the development of an integrated framework for UC with primary application to thermal reactor, including both light and heavy water reactors, taking both steady-state and transient scenarios in to consideration.

The envisioned UCF will take into account for a wide range of uncertainty sources in uncertainty propagation. The first phase of the UCF focuses on the propagation of parameter uncertainties, including all uncertain parameters from lattice physics calculations, such as assembly discontinuity factor and delay neutron fraction as well as cross-section uncertainties, to responses of interests in core simulation. The uncertainty correlations between different simultaneous core conditions and different lattice types are explored. Given the voluminous size of few-group parameter uncertainty space and the large number of lattice physics model executions required to prepare the few-group parameters, ROM techniques are employed to compress the uncertainty space of the few-group parameters. The modeling uncertainties are minimized by employing a continuous cross-section Monte Carlo transport model to generate the reference cross-sections for core-wide calculations in different group formats. In the second phase, the sensitivity of the propagated uncertainties are measured by repeating the UQ analysis with different modeling assumptions to generate the reference cross-sections. The approach is justified to provide an estimate of the impact of modeling uncertainties on the propagated parameter uncertainties.

Product of this work is to develop and implement the ROM-based UQ for applications to existing computational sequences for nuclear reactor calculations. Specifically, NESTLE [27] and NESTLE-C [28] are employed as core simulator for a light water system, the BWR Peach Bottom reactor, and a heavy water system, CANDU reactor, respectively. NESTLE is a core simulator employing a few-group neutron diffusion representation which is approximated using the Nodal Expansion Method (NEM), whose CANDU version is NESTLE-C. It allows both steady state and transient calculations. The focus is to estimate both the effective critical eigenvalue and the power distribution uncertainties in both scenarios. The few-group parameters are calculated through the SCALE's NEWT [29] code and the SERPENT [30] code as input to NESTLE/NESTLE-C for core-wide calculations.

As the work starts from the multi-group uncertainties, the SCALE's SAMPLER [31] is employed for the propagation of multi-group cross-section uncertainties to few-group parameters through NEWT. The SERPENT code is used to generate the reference two-, four-, and eight-group libraries, and to verify the reference NEWT models. This is because the NEWT is a deterministic neutron transport model which employs a number of standard modeling assumptions, e.g., group structure, resonance treatment, etc., while SERPENT is based on a continuous cross-section Monte Carlo transport model which is considered a gold standard for neutron transport calculations. By employing both models, the impact of modeling uncertainties can be initially assessed on the propagated parameter uncertainties.

The rendering algorithms for ROM as well as uncertainty propagation have been encoded in a python script to allow for seamless re-generation of the NESTLE-C cross-section uncertainty library. The script is designed for a variable number of few-groups as input to NESTLE, including two, four and eight groups. The generated library is tested using a number of representative CANDU-6 core models including a reference model at full power, a voided core model to estimate the voiding coefficient of reactivity, a toy model excluding thermal-hydraulics feedback, and a LOCA transient model. The python script is designed to automate multiple functionalities including

- (a) reading the sampled few-group parameters as calculated by NEWT
- (b) processing of the results in a compressed format using ROM techniques

- (c) generation of a set of NESTLE-C libraries that span the uncertainty space using both stochastic and deterministic uncertainty propagations (different uncertainty analysis methods will be discussed in Chapter 3).

### **1.3.2 Organization of dissertation**

The organization of this dissertation is presented as follows.

Chapter 2 discusses the uncertainty sources in the processes of neutronics core simulations as to identify all sources uncertainties is one of the bases to develop a comprehensive UCF. It first provides a review on uncertainty classification and representation in general modeling and simulation process. Further, uncertainty sources including parameter uncertainties, modeling uncertainties and numerical uncertainties and their contributions in the UQ process are discussed. Additionally, the propagation of major uncertainty sources in each stage of neutronics simulation is presented from pointwise level, to multi-group level, through few-group level and down to the core simulation level.

Chapter 3 provides a literature review of the related uncertainty quantification methods in two aspects, considering in both theoretical uncertainty propagation procedures and efficiency improvement made with the methods. Specifically, the stochastic UQ and deterministic (including forward and adjoint) UQ method are discussed in detail. The efforts made by practitioners to reduce the computational expense of the UQ exercises as well as their advantages and limitations are described. Finally, a literature review on background of modeling uncertainty and the status of its impact evaluation is provided.

Chapter 4 describes the methodologies employed and developed in this UCF, including the physics-guided coverage mapping (PCM) methodology and the ROM methodology, as well as their implementation algorithms. The PCM method is originally designed in support of model validation, but is treated as the mapping strategy in this dissertation to accomplish the uncertainty mapping task and to perform an initial reduction in the few-group parameters uncertainty space by evaluate the correlation between a wide range of core conditions. The ROM approaches and the range finding algorithm (RFA) are presented to reduce the parameter space into a manageable number of active degrees of freedoms (DOFs). Interpretation of results generated by each methodology is described at the end of each subsection.

Chapter 5 states the proposed approaches to accomplish the framework. It starts with a mathematical description of the uncertainty propagation problem in this framework and the process of proposed approaches. The approaches to measure the impact of parameter uncertainties and modeling uncertainties are presented respectively in the following two sections. In parameter uncertainty propagation, both stochastic and deterministic UQ methods implementation, reduction on space of few-group parameter uncertainties under various core conditions and the ROM-based UQ process are described in detail. The modeling uncertainty propagation are presented with respect to the discussions of modeling assumptions and the proposed approach to evaluate the impact of modeling uncertainty propagation on core responses. Furthermore, the sensitivity analysis method and the algorithm to prioritize the uncertainty sources from reduced parameter uncertainty space are expressed.

Chapter 6-8 demonstrate the applications of the developed UCF on reactor simulations, propagating parameter uncertainties from multi-group cross-sections to core simulation and analyzing the modeling uncertainties impact and the interactions with parameter uncertainties on core response uncertainties.

Specifically, Chapter 6 describes the application on a BWR system with implementation process and results of the dimensionality reduction on few-group cross-sections in aspects of branch conditions, burnup and multiple lattice types, as well as the ROM-based UQ/SA on core responses of interest. A priority-ranking table on major few-group uncertainties is provided at the end. Numerical results in Chapter 6 imply the nearly perfect correlations between simultaneous core conditions indicating that few-group uncertainty space could be reduced by getting rid of the branch uncertainties.

Chapter 7 illustrates the application of ROM-based UQ of parameter uncertainty propagation results on a CANDU reactor system. The first section explores the few-group parameter uncertainty space by looking into the uncertainty propagated from multi-group cross-section uncertainties along burnup, the correlation among burnup-dependent few-group parameters and the reducibility of few-group parameter uncertainties of CANDU bundle model. The second section presents results of ROM-based uncertainty propagation applied on CANDU core models including the steady-state reference core model, coolant-voided core model and a transient LOCA core model.

Chapter 8 evaluates the impact of modeling uncertainty in the nuclear data uncertainty propagation process on the CANDU application. Various modeling assumptions and approximations are investigated include those related with the uncertainty propagation method employed, e.g., deterministic vs. stochastic, the few-group energy structure employed to represent the cross-sections, the resonance treatment in lattice physics calculation, the reference values for the cross-section, and the number of samples employed to render ROM compression. Results indicate that some of the modeling assumptions could have a non-negligible impact on the core responses propagated uncertainties, highlighting the need for a more comprehensive approach to combine parameter and modeling uncertainties.

Finally, Chapter 9 summarizes the dissertation work and provides recommendations for future work.

## 1.4 References

1. Broadhead, B.L., et al., *Sensitivity-and uncertainty-based criticality safety validation techniques*. Nuclear science and engineering, 2004. **146**(3): p. 340-366.
2. Palmiotti, G. and M. Salvatores, *Developments in sensitivity methodologies and the validation of reactor physics calculations*. Science and Technology of Nuclear Installations, 2012. **2012**.
3. Broadhead, B., *Nuclear data adjustment methodology utilizing resonance parameter sensitivities and uncertainties*. 1984, Oak Ridge National Lab., TN (USA).
4. Jessee, M., H. Abdel-Khalik, and P. Turinsky, *Evaluation of BWR core attributes uncertainties due to multi-group cross-section uncertainties*. Proc. of M&C, 2007.
5. Sobes, V., et al., *Resonance parameter adjustment based on integral experiments*. Nuclear Science and Engineering, 2016. **183**(3): p. 347-355.
6. Commission, U.N.R., *Best-Estimate Calculations of Emergency Core Cooling System Performance, Regulatory Guide 1.157*. Washington, DC, May, 1989.
7. NRC, U., *NRC Regulations Title 10, Code of Federal Regulations*. 2009.
8. D'Auria, F., C. Camargo, and O. Mazzantini, *The Best Estimate Plus Uncertainty (BEPU) approach in licensing of current nuclear reactors*. Nuclear Engineering and Design, 2012. **248**: p. 317-328.
9. Sollima, C., G. Petrangeli, and F. D'Auria. *Framework and strategies for the introduction of best estimate models into the licensing process*. in *17th International Conference on Nuclear Engineering*. 2009. American Society of Mechanical Engineers Digital Collection.
10. Ivanov, K., et al., *Benchmarks for Uncertainty Analysis in Modelling (UAM) for the Design, Operation and Safety Analysis of LWRs-Volume I: Specification and Support Data for Neutronics Cases (Phase I)*. 2013, Organisation for Economic Co-Operation and Development.
11. Williams, M.L., et al., *Applications of nuclear data covariances to criticality safety and spent fuel characterization*. Nuclear Data Sheets, 2014. **118**: p. 341-345.

12. Zwermann, W., et al., *Nuclear data uncertainty and sensitivity analysis with XSUSA for fuel assembly depletion calculations*. Nuclear Engineering and Technology, 2014. **46**(3): p. 343-352.
13. Abdel-Khalik, H.S., P.J. Turinsky, and M.A. Jessee, *Efficient subspace methods-based algorithms for performing sensitivity, uncertainty, and adaptive simulation of large-scale computational models*. Nuclear science and engineering, 2008. **159**(3): p. 256-272.
14. Rochman, D., et al., *Nuclear data uncertainty propagation: perturbation vs. Monte Carlo*. Annals of Nuclear Energy, 2011. **38**(5): p. 942-952.
15. Rearden, B.T. and D.E. Mueller, *Recent use of covariance data for criticality safety assessment*. Nuclear Data Sheets, 2008. **109**(12): p. 2739-2744.
16. Yankov, A., et al., *A two-step approach to uncertainty quantification of core simulators*. Science and Technology of Nuclear Installations, 2012. **2012**.
17. Roberts, J.A., B.T. Rearden, and P.P. Wilson, *Determination and Application of Partial Biases in Criticality Safety Validation*. Nuclear Science and Engineering, 2013. **173**(1): p. 43-57.
18. Kiedrowski, B.C., et al., *Whisper: Sensitivity/uncertainty-based computational methods and software for determining baseline upper subcritical limits*. Nuclear Science and Engineering, 2015. **181**(1): p. 17-47.
19. Leray, O., et al., *Nuclear data uncertainty propagation on spent fuel nuclide compositions*. Annals of Nuclear Energy, 2016. **94**: p. 603-611.
20. Smith, D., *Nuclear data uncertainty quantification: past, present and future*. Nuclear Data Sheets, 2015. **123**: p. 1-7.
21. Stamm'ler, R.J. and M.J. Abbate, *Methods of steady-state reactor physics in nuclear design*. Vol. 111. 1983: Academic Press London.
22. Castro González, E., *Methodologies for sensitivity/uncertainty analysis using reactor core simulators with application to Pressurized Water Reactors*. 2018, Industriales.
23. Huang, D. and H.S. Abdel-Khalik, *INVESTIGATIVE STUDY ON IMPACT OF MODELING UNCERTAINTIES IN UNCERTAINTY QUANTIFICATION OF NEUTRONICS CORE SIMULATION*. 2019, Proceedings of M&C: Portland, ON (United States).
24. Zeng, K., et al., *Uncertainty Quantification and Propagation of Multiphysics Simulation of the Pressurized Water Reactor Core*. Nuclear Technology, 2019: p. 1-20.
25. Macian, R., M.A. Zimmermann, and R. Chawla, *Statistical uncertainty analysis applied to fuel depletion calculations*. Journal of nuclear science and technology, 2007. **44**(6): p. 875-885.
26. Abdel-Khalik, H.S., *Feasibility Study of An Integrated Framework for Characterization of Uncertainties with Application to CANDU Steady State and Transient Reactor Physics Simulation*. 2015.
27. Turinsky, P.J., et al., *NESTLE: Few-group neutron diffusion equation solver utilizing the nodal expansion method for eigenvalue, adjoint, fixed-source steady-state and transient problems*. 1994, EG and G Idaho, Inc., Idaho Falls, ID (United States); Los Alamos National ....
28. Turinsky, P. and H. Sarsour, *NESTLE-C: Few-group neutron diffusion equation solver utilizing the nodal expansion method for eigenvalue, adjoint, fixed-source steady-state and transient problems: CANDU version*. 2003, North Carolina State University: Raleigh, NC (United States).

29. DeHart, M. and M. Jessee, *NEWT: a new transport algorithm for two-dimensional discrete ordinates analysis in non-orthogonal geometries*. ORNL/TM-2005/39, Oak Ridge National Laboratory, 2005.
30. Leppänen, J., et al. *The Serpent Monte Carlo code: Status, development and applications in 2013*. in *SNA+ MC 2013-Joint International Conference on Supercomputing in Nuclear Applications+ Monte Carlo*. 2014. EDP Sciences.
31. Williams, M.L., et al., *A statistical sampling method for uncertainty analysis with SCALE and XSUSA*. Nuclear technology, 2013. **183**(3): p. 515-526.
32. Bang, Y., H.S. Abdel-Khalik, and J.M. Hite, *Hybrid reduced order modeling applied to nonlinear models*. International Journal for Numerical Methods in Engineering, 2012. **91**(9): p. 929-949.
33. Huang, D., et al., *Dimensionality reducibility for multi-physics reduced order modeling*. Annals of Nuclear Energy, 2017. **110**: p. 526-540.

## 2. UNCERTAINTY SOURCES IN NEUTRONICS CALCULATIONS

A theoretical model of an engineering system is a set of mathematical equations and conditions to describe the physical phenomena governing the behavior of the engineering system, whose solution can be used as a representative of the real performance of the system. It reflects the physicists or theoreticians' knowledge based on the observations and analysis to the reality. Uncertainties and errors are introduced in this stage because of lack of knowledge. Furthermore, in most of the circumstances it is infeasible to obtain an analytical solution for a complicated system. With the power of computational science, the equations of the theoretical model are manipulated into best-estimate (BE) simulation code to make the model depend on input parameters and be able to generate output responses, which can be considered as a measurement of the performance of the engineering system. The manipulating process, including assumptions, simplifications, discretization, etc., will further introduce uncertainties to the BE prediction. Obviously, uncertainties and errors introduced in each modeling and simulation stage will lead to discrepancies between the prediction from execution of the BE simulation and the real performance of the reality from the measurement, resulting in the definition of uncertainty in responses of interest. More discussions on the modeling and simulation phases and the uncertainties and errors can be referred to Ref. [1].

The most direct way to evaluate the propagated uncertainties is to quantify the discrepancies between the BE prediction and reality of the responses of interest which can be measured through experiment. Nevertheless, the true value of the response of interest is not always available because of insufficient knowledge or limited precision of the measuring experiment. The indirect evaluations of the responses of interest uncertainty require more information about the uncertainty sources and the proper method to propagate each source of uncertainty. A precise quantification of uncertainties provides a reliable metric for the best-estimate reactor analysis simulation by evaluating the quality of the predictions. Therefore, this chapter focuses on identifying all major sources of uncertainties and propagate these uncertainties properly throughout the reactor simulation process. This chapter first discussed the origins of the uncertainties during the modeling and simulation sequences and the classifications of the uncertainties. The following subsection deals with the identification of uncertainty sources in computational calculations, especially in reactor physics calculations. The third subsection will provide a mathematical representation of

uncertainties that will be propagated during the calculations and be quantified on the responses of interest. Finally, the last subsection will present an overview of the nuclear reactor calculation process and deal with the propagation of major uncertainty sources in each step of neutronics calculation throughout the core simulations. Contents in this chapter are inspired by insight of Dr. Abdel-Khalik [2].

## 2.1 Uncertainty Classification

Uncertainties are fundamentally classified into two categories, the aleatory and the epistemic uncertainty [3, 4]. Aleatory uncertainty, which is also called irreducible uncertainty or stochastic uncertainty in the literature, originates from inherent randomness in the physical model, which is a property of the system. The aleatory uncertainty is usually described by probability distribution as the true value varies from measurement to measurement in a certain range and cannot be minimized or reduced with additional measurements. An example of the aleatory uncertainty is the number of counts registered in a detector. The number of counts is inherently random - the associated standard deviation of the counts will depend on the nature the radiation interactions inside the detector volume and therefore cannot be reduced even if the counting experiment is repeated an infinite number of times.

Epistemic uncertainty, which is also referred to as reducible uncertainty or systematic uncertainty, is uncertainty raised from lack of knowledge to the system model [5]. The epistemic uncertainties are usually considered as biases in the calculations resulting from approximations, assumptions, or lack of knowledge about the true value of model input data. For example, if the nominal value of  $\nu$ , the neutron fission yield, used in BE calculations is lower than its true value, the associated reactor analysis model will consistently under-predict the core's critical eigenvalue. Epistemic uncertainties are reducible in principle with additional measurements. For example, by repeating the experiments used to measure  $\nu$ , better estimates of its true value can be evaluated.

The distinction between the two types is important and must be done carefully. By way of an example, in the above detector example, the number of counts measured is subject to an aleatory uncertainty; however the mean value of the counts measured over a given time interval suffers from an epistemic uncertainty, implying that a better estimate of the mean can be obtained with additional measurements.

Both aleatory and epistemic uncertainties exist in reactor physics analysis and should be quantified carefully. Examples of aleatory uncertainties include the dimensions and compositions of the various materials comprising the reactor core, all subject to manufacturing tolerances. This follows because any manufacturing process cannot render the exact engineering specifications, and hence a level of uncertainty is to be expected. Epistemic uncertainties include nuclear data, e.g., microscopic cross-sections, thermal-hydraulics data, e.g., heat transfer coefficients, and systematic errors resulting from numerical, e.g., discretization and iterative techniques, and modeling approximations, e.g., use of homogenization theory.

There have been discussion on necessity of distinguishing between uncertainty and error [1], as the error is defined as recognizable inaccuracy, either acknowledged or unacknowledged by the analyst, which is not caused by lack of knowledge. This distinction is not needed in our context, and hence the two terms will be used interchangeably.

## **2.2 Uncertainty Representation**

Probabilistic analysis is the most widely used method for representing and describing uncertainty in physics systems and models. The uncertainty is usually represented as intervals or probability distributions [5-7]. The uncertainty quantification (UQ) process devises a metric that is used to measure uncertainties. The measurement process may be thought of as a hypothetical, i.e., virtual, experiment that determines all possible outcomes/states/results/values of the phenomenon under consideration [8]. An important part of this process is to assign probabilities to the various possibilities.

As described in the uncertainty classification, the aleatory uncertainties are usually described by well-defined probability distributions for the physical quantities because of the randomness in nature; while the epistemic uncertainties are usually represented by sparse point value or interval data, since the true value of quantity is based on the experiments, expert judgment, etc. Despite the distinction between the two types of uncertainty, both of them can be represented using the likelihood-based probabilistic expression [9]. The combined possibilities and their associated probabilities are often described by a probability density function (PDF) or a histogram which may be viewed as the metric by which uncertainty are measured, i.e., quantified. The expression for

likelihood/probability (  $P(a \leq x \leq b)$  ) of the uncertain quantity  $x$  with condition  $K$  can be described in terms of the conditional PDF  $f_x(x|K)$  [10]:

$$P(a \leq x \leq b) = \int_a^b f_x(x|K)dx$$

where  $x$  is in a general interval  $[a,b]$ , and samples of  $K$  can be drawn from the corresponding PDF,  $f_K(K)$ , to construct conditional PDF for  $X$ ,  $f_x(x|K)$ .

The most common PDF is the normal Gaussian distribution, which is described by a mean value representing the nominal value for input parameters used in BE calculations, and a standard deviation describing either the modeler's confidence in the mean value for epistemic uncertainties, or the inherent randomness of aleatory uncertainties. With multiple input data, the uncertainty can be described in matrix form. The mean values of input parameters can be described by a vector  $x_\mu$  such that the  $i^{\text{th}}$  component  $[x_\mu]_i$  is the mean value of the  $i^{\text{th}}$  input data  $[x]_i$ , and the multivariate uncertainty are described by a covariance matrix  $\mathbf{C}_x$  to characterize the uncertainties and correlations between input parameters. For Gaussian parameters, a covariance matrix is sufficient to describe all correlations. Its diagonal elements represent the variance (square of standard deviation) of the individual input data, and the off-diagonal elements are measures of the correlations between two input components. A diagonal matrix with zero off-diagonal elements implies a set of input data that are uncorrelated. The covariance matrix is symmetric and of the form:

$$[\mathbf{C}]_{ij} = \rho_{ij}\sigma_i\sigma_j$$

where  $[\mathbf{C}]_{ij}$  denotes the element at the intersection of the  $i^{\text{th}}$  row and  $j^{\text{th}}$  column. The  $\rho_{ij}$  is the standard correlation coefficients between the  $i^{\text{th}}$  and  $j^{\text{th}}$  input data, whose value ranges from -1.0 (perfect negative linear correlation) to 1.0 (perfect positive linear correlation); while  $\sigma_i$  is the standard deviation of the  $i^{\text{th}}$  parameter.

Based on matrix notations discussed above, the PDF representation of the uncertain parameters  $x$  is proportional to:

$$\exp\left[-\frac{1}{2}(x-x_\mu)^T \mathbf{C}_x^{-1}(x-x_\mu)\right]$$

Other metrics that are functions of the resulting PDF or histogram could also be employed to measure uncertainties, such as kurtosis of the PDF or the histogram; and tail probability that is the probability to exceed a certain value, commonly referred to as failure probability.

The covariance matrix may also be decomposed using rank revealing decompositions [11] to reduce the effective number of input data, which will be discussed in Chapter 4 as reduced order modeling (ROM) techniques to achieve significant dimensionality reduction by identifying all the correlations between multiple input parameters.

## **2.3 Uncertainty Sources in Computational Modeling and Simulation**

This section presents the uncertainty sources in the UC process and discusses how each uncertainty source will be dealt with in this thesis. Three major uncertainty sources are generally considered in computational nuclear reactor simulation, parameter uncertainties, modeling uncertainties and numerical uncertainties.

### **2.3.1 Parameter uncertainties**

The parameter uncertainties originate from uncertainties of input data. All input data to a computational model, typically referred to as parameters, could contain uncertainties which propagate throughout the model and give rise to response uncertainties. Input data uncertainties are unavoidable because input data are either experimentally evaluated or generated using pre-processor codes. The objective of UQ is to determine all possible variations for the responses of interest, often described in the form of a PDF, due to all possible input data variations within their known ranges of uncertainties.

In uncertainty propagation through neutronics calculations, parameter uncertainties emanate from the differential cross-section measurements and the subsequent data assimilation against the integral experiment measurements, and propagate to each level of simulations. Thermal-hydraulics parameters also contain uncertainty information at the core simulator level, but will be excluded from discussion since this Ph.D. work focuses on uncertainty propagation in neutronics

calculations. The uncertainties of responses due to all possible input data uncertainties can be evaluated via either deterministic and stochastic methods and efficiency can be controlled with recent advances in ROM techniques, which will be discussed in detail in Chapter 4.

The parameter uncertainties are the simplest source of uncertainties to quantify via standard sampling-based UQ approach, which will be presented in Chapter 3. However, to propagate all parameter uncertainties through a sampling-based UQ approach or to prioritize the dominant sources of uncertainties through a conventional sensitivity analysis (SA) approach is computationally infeasible as the number of input parameters for a reactor model is enormous. Fortunately, with the recent advance of ROM algorithms, the dimensionality of input parameter uncertainties can be reduced to a manageable size to enable uncertainty propagation and prioritization in a computational efficient manner.

### **2.3.2 Modeling uncertainties**

The modeling uncertainties, sometimes referred to as modeling errors in this context, originate from either the theoretical model deviation from the reality, or the modeling simplifications and approximations introduced to achieve computational efficiency.

The discrepancies between the reality and the physics model rises from incomplete knowledge about the physics governing the system. This type of modeling uncertainty is most difficult to quantify since it requires one to make quantitative statements about one's lack of knowledge. The resulting uncertainty can only be reduced with improvement of knowledge for the system and can only be quantified with access to the experimental data. Since this work focus on neutronics phase only, and the physics of neutron behavior in nuclear reactor is well understood and described, the uncertainties due to imperfect knowledge will be considered negligible.

The modeling uncertainties due to the numerous simplifying assumptions and approximations made throughout the calculations, such as using diffusion theory instead of transport theory, using energy group instead of continuous energy, etc., can be quantified in principle. This requires the development of algorithms to capture the effect of the modeling simplifications and approximations, as well as how they propagate and interact with other sources of uncertainties.

One of the tasks of this Ph.D. work is to investigate the effects of modeling uncertainties and their interaction with parameter uncertainties in the uncertainty propagation process. The common

uncertainty analyses assume that modeling uncertainties have minimal impact on the propagated cross section uncertainties and the cross-section adjustments, and if present, they may be treated as independent sources of uncertainty. For example, in lattice cell calculations, the assumption of reflective boundary conditions represents a source of modeling uncertainties because it ignores the neutron leakage between the assembly and its neighbors. The use of flux weighting to collapse cross sections and the various associated resonance treatment models are other sources of modeling uncertainties. Each type of deterministic solver for radiation transport introduces different type of modeling uncertainties.

The focus will be on the modeling uncertainties originating from modeling simplifications and approximations only, such as the multi-group approximations, numerical transport solver assumptions, etc. The proposed approach to propagate discussed in detail in Chapter 5.

### **2.3.3 Numerical uncertainties**

The numerical uncertainties arise from numerical discretization for implementation of computational codes to describe the physics models, such as introducing integral and/or differential operators, or generating a set of algebraic equations that can be manipulated further by computers. In our context of deterministic radiation transport, both the modeling errors and numerical uncertainties are considered in modeling uncertainties. There have been great amount of research characterizing uncertainties from numerical errors [12]. Furthermore, the numerical uncertainties can always get reduced by increasing the computational power. Applications in this Ph.D. work are thermal reactors, in which the numerical uncertainties are considered to be negligibly small given the short mean free path of the neutrons.

## **2.4 Propagation of Uncertainty Sources in Neutronic Simulation Stages**

In reactor physics calculations, uncertainties arise from many sources, including uncertainties from basic nuclear parameters, i.e., point-wise cross-sections, manufacturing tolerances on geometry, burnt fuel isotopics, etc. Uncertainties also originate from modeling approximations and assumptions often introduced to render practical execution, e.g., multi-group approximation, reflective boundary conditions assumption in cell lattice calculations, etc. Finally,

numerical approximations, resulting from discretizing the continuous equations into algebraic forms amenable for computer manipulation, also introduce uncertainties in the simulation results.

The neutronic computational sequence can be divided into four stages as shown in Figure 2-1. In this section, a description of each stage and how uncertainties are introduced into each stage of the neutronic simulation is provided in each of the following subsection.

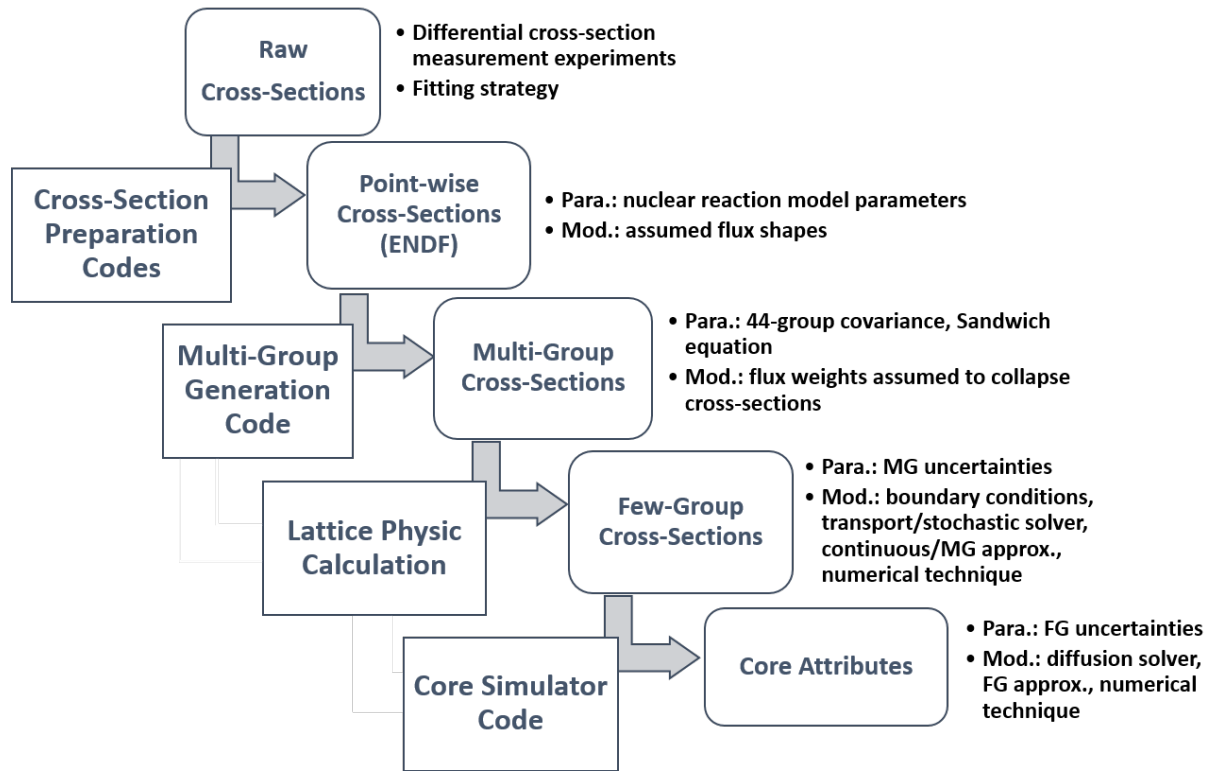


Figure 2-1 Schematic of neutronics simulation and major uncertainty sources at each stage.

### 2.4.1 Uncertainties in pointwise cross-section generation

The first stage of neutronics simulation is common to calculations of all different types of reactors. It is done once by differential cross-section measurement experiments, and is typically repeated only when new cross-section measurements become available. The product is an Evaluated Nuclear Data Files (ENDF) library that can be used by reactor analysts for all reactor types. The raw cross-section measurements are referred to as differential measurements. These measurements are fitted to analytical models, which contain a number of undetermined coefficients, referred to as nuclear reaction model parameters. An example of nuclear reaction model parameter is the resonance width and center when the fitting is done under a resonance. These analytical

models are based on nuclear theories such as the R-matrix theory. An example of a code that performs these calculations is the SAMMY [13]. The fitting procedure is based on a generalized least-squares procedure, also known as Bayesian Estimation, which requires some initial guesses for the nuclear reaction model parameters. The measurements are fed in a sequential manner to the algorithm, wherein the model parameters determined from a previous iteration (i.e., with a given set of measurements) are used as the initial guess for the next iteration (i.e., the next batch of measurements). The process is repeated a number of times until all available measurements are employed. In doing so, the measurements containing outliers, i.e., measurements with high uncertainties that are not consistent with the rest of measurements, will be discarded. An important result of the least-squares fitting procedure is the uncertainties (in the form of covariance matrices) of the reaction model parameters.

The uncertainties in this stage originate from two sources, the differential cross-section measurements uncertainties, and the nuclear reactor model forms used to describe the continuous cross-sections. Given the maturity of nuclear models and the evaluation procedure, the cross-section fitting results are considered by most practitioners to be satisfactory for all reactor analysis calculations. Accordingly, the basic assumption in most neutronic UQ studies is that nuclear reaction model parameters represent the main source of uncertainty for all downstream calculations.

#### **2.4.2 Uncertainties in multi-group cross-section generation**

The second stage collapses the pointwise cross-sections into a multi-group format using assumed flux shapes. The number of groups are typically selected based on a combination of expert judgment and a trial-and-error approach that attempts to resolve all aspects of the flux spectrum, expected to affect the integral quantities of interest such as eigenvalue, reaction rates, etc. This stage is specific to the flux spectrum expected in the reactor, and hence must be repeated for different reactor types. Regarding the uncertainties of the multi-group cross-sections, they can be estimated by propagating the uncertainties of the nuclear reaction model parameters using the standard sandwich relationship, which will be described in Chapter 5. A typical computer code that performs this stage is the PUFF code of the SCALE's code package, developed by ORNL [14].

The multi-group cross-sections contain essentially two different sources of uncertainties, one originating from the nuclear reaction parameters used to construct the continuous cross-sections, and the other from the assumed flux shape. Most of the current multi-group generation codes account only for the first source of uncertainty (under the constraints of linearity assumption), implying that the flux shape is assumed to have no uncertainty. This latter source of uncertainty is difficult to estimate because the real flux shape is unknown a priori. Therefore, assumed flux shape uncertainty must be treated as a source of modeling uncertainty using a decision variable. To estimate this source, one must be able to compare the predictions against a high fidelity model that directly uses the continuous cross-sections, i.e., without any collapsing. The discrepancies between the predictions of the low and high fidelity models can be used estimate the modeling bias, which has to be repeated to take into account its dependence on other modeling conditions, such as composition, temperature, etc., i.e., control parameters.

### **2.4.3 Uncertainties in lattice calculations**

In the third stage, the few-group cross-sections are calculated for the cell lattices expected to be loaded in the core simulation. These calculations must be repeated every time a new cell lattice design is introduced. Cell lattice calculations start with the multi-group cross sections, and calculate the few-group cross-sections for a wide range of core conditions. The product of this stage is a very large matrix of few-group cross-sections, which are fitted to polynomial expressions to facilitate their interpolation in downstream core-wide calculations. The brute force application of the forward-based (sampling-based) UQ approach would prove to be computationally expensive, even if one is not interested in capturing sensitivity information. This is because the UQ computational cost will be few to several hundred times higher than the cost required to generate the reference few-group cross-sections (discussed in Section 3.1.1), which is large considering the wide range of conditions that must be captured to properly functionalize cross-sections.

Since this stage is within the scope of this thesis, an idea about the size of the data streams flowing through cell lattice calculations is provided here, considering a typical transport code that is used to calculate the few-group cross-sections. The number of few-group parameters functionalized in terms of core conditions is roughly the product of (1) the number of burnup steps, (2) the number of branch cases required to functionalize cross-section dependence on core conditions such as fuel and coolant temperature, coolant voiding, boron content, etc., and (3) the

number of cell lattice types in the core. This product can easily reach the order of  $10^3$  for typical reactor cores. To propagate uncertainties, the number of model executions is expected to be few to several hundred greater than the number of uncertain parameters. This results in the order of  $10^5$  model executions which is infeasible in practical applications. If Monte Carlo model is employed to propagate the uncertainties, e.g., using a Total Monte Carlo approach [15], the cost gets multiplied by another factor representing the ratio of the computational cost of executing Monte Carlo to that of an equivalent deterministic code. This factor is typically in the order of 100, and could be more if responses include space and energy-resolved data.

Further, an integrated UC process should not only quantify the propagated uncertainties, but also identify the dominant contributors to the propagated uncertainties. This is usually done via an SA, where the number of model executions is proportional to the number of multi-group parameters. For typical multi-group libraries, this number is in the order of  $10^5$  for typical lattice calculations to account for tracking about 70 isotopes using few hundred energy groups, and two to four reactions per nuclide, e.g., fission, absorption, scattering, capture, etc. This increases the number of required code runs to be in the order of  $10^6$  to  $10^9$  executions, which is infeasible despite the expected increase in computer power.

In this stage, two sources of uncertainties are introduced, one from the multi-group cross-sections propagated from the previous stage, and the other resulting from the modeling assumptions, such as the use of reflective boundary conditions, the use of a deterministic transport solver, and the use of multi-group instead of continuous cross-sections. The first source is straightforward to account for. The computational cost becomes impractical when sensitivity information is required, i.e., to understand the contribution of the individual multi-group cross-sections on the propagated few-group uncertainties. The second source depends on the modeling decisions taken and therefore must be treated as a source of modeling errors. First, regarding the use of deterministic transport solver and multi-group cross-sections, this source could be identified by comparing model predictions against a high fidelity continuous cross-section Monte Carlo model. The second source is more difficult to account for because it depends on the type of neighboring bundles in the reactor core. To account for that source, one must emulate the impact of the neighbors via a super cell lattice calculations.

Therefore, similar to the previous stage, the correlations between the multi-group uncertainties and the modeling uncertainties from modeling assumptions and approximations are to be investigated by the proposed research.

#### **2.4.4 Uncertainties in core calculations**

The last stage involves the calculation of core-wide power distribution during steady state and transient conditions starting with the few-group parameters (cross-section data) as input. For typical thermal reactor models, the number of few-group parameters is equal to the number of cell lattice executions times the number of few-group parameters generated by a single lattice model execution, which is in the order of 10, representing the thermal and fast absorption cross-sections as well as the reaction types, such as transport, fission, absorption, prompt neutron yield, and Xe and Sm fast and thermal absorption cross-sections, etc. The resulted number is roughly in the order of  $10^4$ .

The sources of uncertainties in core-wide calculations include:

- (1) Uncertainties from the few-group parameters;
- (2) Uncertainties from the radiation transport model employed (e.g., nodal diffusion theory assumptions, and two energy-group cross-section representation);
- (3) Uncertainties from non-neutronic models, e.g., thermal-hydraulics models, and their associated correlations used to describe the transfer of the heat from the fuel to the coolant, and the corresponding feedback into neutronics calculations, e.g., fuel temperature feedback, coolant and moderator temperature and density feedbacks;
- (4) Uncertainties from the control parameters such as the lattice dimensions, fuel composition, flowrates, inlet coolant temperatures, etc.

The first source, i.e., few-group parameter uncertainties, can be treated using a standard sampling-based UQ approach as described in Section 5.2.1. The second source, i.e., the radiation transport model, can be estimated using the core-wide Monte Carlo models. This will also require the mapping algorithm to allow the efficient mapping of uncertainties to the wide range of core configurations due to the infeasibility to execute core-wide Monte Carlo simulations for all conditions of interest.

## 2.5 References

1. Oberkampf, W.L., et al., *Error and uncertainty in modeling and simulation*. Reliability Engineering & System Safety, 2002. **75**(3): p. 333-357.
2. Abdel-Khalik, H.S., *Feasibility Study of An Integrated Framework for Characterization of Uncertainties with Application to CANDU Steady State and Transient Reactor Physics Simulation*. 2015.
3. Der Kiureghian, A. and O. Ditlevsen, *Aleatory or epistemic? Does it matter?* Structural Safety, 2009. **31**(2): p. 105-112.
4. Oberkampf, W.L. and C.J. Roy, *Verification and validation in scientific computing*. 2010: Cambridge University Press.
5. Helton, J.C., J.D. Johnson, and W.L. Oberkampf, *An exploration of alternative approaches to the representation of uncertainty in model predictions*. Reliability Engineering & System Safety, 2004. **85**(1-3): p. 39-71.
6. Zio, E. and N. Pedroni, *Literature review of methods for representing uncertainty*. 2013: FonCSI.
7. Helton, J.C., et al., *Representation of analysis results involving aleatory and epistemic uncertainty*. International Journal of General Systems, 2010. **39**(6): p. 605-646.
8. Hubbard, D.W., *How to Measure Anything: Finding the Value of Intangibles in Business*. 2010: Wiley.
9. Sankararaman, S. and S. Mahadevan, *Likelihood-based representation of epistemic uncertainty due to sparse point data and/or interval data*. Reliability Engineering & System Safety, 2011. **96**(7): p. 814-824.
10. Jaynes, E.T., *Probability theory: The logic of science*. 2003: Cambridge university press.
11. Meyer, C.D., *Matrix analysis and applied linear algebra*. Vol. 71. 2000: Siam.
12. Roy, C. *Review of discretization error estimators in scientific computing*. in *48th AIAA Aerospace Sciences Meeting Including the New Horizons Forum and Aerospace Exposition*. 2010.
13. Larson, N.M., *Updated Users' Guide for SAMMY Multilevel R-matrix Fits to Neutron Data Using Bayes' Equation*. 1998, Oak Ridge National Lab., TN (US).
14. Wiarda, D. and M. Dunn, *PUFF-IV: A Code for Processing ENDF Uncertainty Data into Multigroup Covariance Matrices*. ORNL/TM-2006/147, Oak Ridge National Laboratory (October 2006), 2006.
15. Rochman, D., et al., *Efficient use of Monte Carlo: uncertainty propagation*. Nuclear Science and Engineering, 2014. **177**(3): p. 337-349.

### **3. LITERATURE REVIEW OF UNCERTAINTY ANALYSIS METHODS IN NEUTRONICS CALCULATIONS**

This chapter presents literature review on the uncertainty analysis methods applied in neutronics calculations including subjects of uncertainty quantification (UQ) and sensitivity analysis (SA). Although there are many different classifications for UQ methods, we select two selection criteria for our discussion, each discussed in a following section. The first criterion differentiates methods based on the calculation procedure into probabilistic/stochastic or deterministic as discussed in the first section. The second section presents development in UQ methods classified by the second criterion, comparing methods based on the efficiency achieved either via automation or algorithmic improvements. Sensitivity analysis approaches are introduced in the following third section to prioritize the uncertainty sources. The presented UQ/SA methods in the first three sections focus on propagation and quantification of the parameter uncertainty. The final section provides a review on the status of modeling uncertainty impact evaluation.

The body of uncertainty analysis literature accumulated over the past two decades may be categorized into two fundamental groups, one focusing on the development of enabling computational tools to automate the propagation of uncertainties, and the other on the development of mathematical algorithms to cut down the cost in terms of computer power and storage requirements. In the first group, researchers have focused on building automated sequences for uncertainty propagation, such as the GRS method developed in Germany [1], the Sampler super-sequence developed by ORNL [2], the RAVEN environment developed by INL [3], the Total Monte Carlo (TMC) methodology developed by the NRG group in the Netherlands [4, 5], and the benchmark for uncertainty analysis in modeling (UAM) [6], etc. The other group of researchers has focused on improving the performance of existing algorithms by replacing the original models with inexpensive surrogate amenable for fast execution [7-9], reducing the dimensionality of the uncertainty space [10-12], or by using intelligent sampling strategies [13, 14].

To set the stage for the discussion, a high level description of the general procedure to propagate uncertainties is first introduced. Any method begins with a best estimate model and a set of input parameters along with their prior uncertainties. The model represents the best available approximation of reality short of knowledge of the exact values of the parameters, which are treated as epistemic sources of uncertainties. The "epistemic" is a Greek-origin adjective denoting

lack of knowledge, which is mathematically described using a probability density function (PDF). A uniform PDF implies complete lack of knowledge, whereas a PDF peaking around a given value indicates a high degree of belief exists that the true value lies at or around the peak location. Complete knowledge would be described by a Dirac delta function centered around the true value of the parameter.

The goal of the uncertainty analysis is to estimate the PDFs of the output quantities of interest, typically referred to as attributes or responses. A PDF may be used to draw samples or calculate moments, and conversely, samples or moments may be used to reconstruct and/or approximate a PDF. A moment is a function of a PDF such as the mean and standard deviation. Analogous to a Taylor series expansion of a function, any PDF may be described using an infinite series expansion, using the so-called moment generating function [15]. Different PDFs require different number of moments for their expansion. For example, the exponential PDF, commonly used to describe radioactive decay, is expanded using a single moment, the mean value; a Gaussian PDF needs two moments, the mean and standard deviation. A PDF may be reconstructed exactly if all its moments are known, or approximated using available moments according to E. T. Jaynes [16] to find the PDF with maximum entropy whose moments match the available moments. Samples could also be used to reconstruct and/or approximate a PDF. Different from using moments, the approximation accuracy using samples is inversely proportional to the square of the number of samples, with the approximation error going to zero as the number of samples goes to infinity. Mathematically, this is described as follows:

$$\sigma_R = \frac{C}{\sqrt{N}}$$

where the subscript  $R$  is a feature derived from the response PDF,  $N$  is the number of samples, and  $C$  is the proportionality constant, and  $\sigma_R$  is the standard deviation of the response  $R$ , typically used as a measure of confidence one has in the value of  $R$ . The first implication is that an order of magnitude improvement in  $\sigma_R$  requires two orders of magnitude increase in the number of samples,  $N$ . Second, the constant  $C$  is dependent on the topology of the probability space in terms of the model form, i.e., linear vs nonlinear as well as the degree of nonlinearity, and the shapes of the prior parameters PDF. If one is interested in rare events, also known as extreme quantile estimation, that is the probability of the response exceeding a threshold value, the constant  $C$  becomes very small, forcing one to use many samples to reach the sought level of confidence

in  $R$ . Further, if one is interested in apportioning the variance in  $R$  to each of the  $n$  input parameters, the number of samples required becomes dependent on  $n$ , which could be computationally infeasible to achieve given the high dimensionality of the input parameters for most realistic neutronic problems (as discussed in Section 2.4.3 and 2.4.4).

### 3.1 Uncertainty Quantification Approaches

As described in Chapter 2, the uncertainty propagation for standalone core simulation is divided in three processes, from pointwise to multi-group level through cell physics, from multi-group to few-group level through lattice physics, and from few-group to full core level through core simulation. The UQ approaches employed in core simulation can be either stochastic or deterministic. There are also hybrid methods that combine the advance of the two methods, as two-step method [17] for example.

#### 3.1.1 Stochastic methods

The stochastic methods try to determine the probability distribution of responses by executing the model many times with different samples for the uncertain input parameters. In the core simulation UQ process, the stochastic approach generates a set of  $N$  random few-group libraries as input to the core simulator. The statistical quantities, such as mean value, standard deviations and higher order moments, of the core responses can be obtained by executing the  $N$  random samples and collecting the results as PDF or histogram.

Different stochastic methods can be discussed in five aspects [18].

1. Determine the probability distribution to characterize the uncertainty of each input parameter. The best way to determine the PDF of the uncertainty parameter is to use measurement data, which, in reality, not available. Thus, the determination on the input uncertainty distribution is usually based on expert judgement. In reactor core simulations, the input parameter uncertainties are commonly assigned uniform or normal distribution [19]. On the other hand, the dependencies between different uncertain input parameters need to be taken into consideration when applicable. However, the dependencies information is not always available, so that input parameters are sometimes assumed to be independent in the sampling methods.

2. Select the sampling techniques employed to generate random samples of uncertain input parameters. Several techniques have been proposed to sample the input parameters from their prior uncertainty such as Simple Random Sampling and the Latin Hypercube Sampling (LHS) [13]. The resulting difference among different sampling techniques are not significant, while the LHS technique shows better performance considering the required number of samples and region coverage in some literature [19, 20].
3. Determine the required number of samples or number of model executions. The determination method could be parametric or nonparametric. With parametric sampling, the number of samples depends on the number of uncertain input parameters, resulting in computational infeasibility with large number of input parameters, which applied in reactor core simulation. The required number of samples could be greatly reduced with nonparametric sampling [21] with a statistical confidence. Many researches in UQ of neutronics calculation employed this nonparametric sampling [1, 22, 23]. However, with number of samples determined by the nonparametric sampling, the PDF of responses could not be constructed based on this reduced number of model executions.
4. Determine the representation for the uncertainty analysis results of the responses. Mean values and standard deviations are common presentation of the response uncertainties. In spite of reduced information comparing to the PDF and histograms, mean values and standard deviations do not require large number of random samples.
5. Perform sensitivity analysis to determine how the uncertainty of input parameters affect the uncertainty of responses. The sampling-based methods enable the global sensitivity analysis by randomly sampling all the input parameters simultaneously and generating responses uncertainties according to different sources of uncertainties in the model parameters [24].

Stochastic methods have found a lot of popularity in engineering applications due to their non-intrusive nature, which translates to ease of implementation, and their ability to propagate uncertainties without making any assumptions about the shapes of the probability distributions of the input parameters, the output response, and the degree of nonlinearity of the model. In fact, one can show that the only factor that influences the accuracy of the propagated uncertainties is the number of model executions that can be afforded. In addition, if one is interested only in confidence intervals for the quantities of interest rather than the full probability distribution, the

cost of the simulation could be reduced significantly using order statistics, e.g., Wilks formula [21] which requires 59 samples to obtain 95/95 confidence interval for the upper limit of the quantities of interest, under some minimal assumptions. If one requires the estimation of the sensitivities of the various parameters, that's the contribution of each parameter to the propagated uncertainties, the cost of the analysis is no longer dependent on the number of samples only but also on the number of input parameters. Typically, one requires an additional factor of 10 times the number of parameters to obtain reliable estimates of the various parameters contributions to the propagated uncertainties. The sensitivities evaluated are referred to as global sensitivities, because they average the model behavior over the range of random samples, hence local sensitivity information cannot be identified. In fact, two models with significantly different local behavior but similar global behavior will be indistinguishable using stochastic methods.

### **3.1.2 Deterministic methods**

Deterministic methods are generally more effective in estimating local sensitivities and less effective in estimating the general shape of the responses PDF. This follows because they employ local sensitivity information, e.g., first and/or higher order variations, to propagate only select moments of the PDFs, e.g., mean and standard deviation. According to Jaynes, the number of moments propagated defines the shape of the PDF that can be used to describe the responses uncertainties, which may not be an accurate representation of the true PDF. If the true PDFs are well-approximated by Gaussian PDFs [16], deterministic adjoint-based methods tend to be more effective than stochastic methods when the number of model parameters is large. Prioritization of the key contributors to the propagated uncertainties is possible using deterministic methods, when the Gaussian assumption is invoked. When general PDFs are involved, stochastic methods are more effective in prioritizing key contributors to the propagated uncertainties.

In the context of reactor physics uncertainty literature, both stochastic and deterministic methods, including both forward and adjoint methods, have been developed with hybrid recipes thereof representing the most effective approach nowadays. In typical reactor physics problems, one has covariance information about the multi-group cross-sections, and wishes to calculate the uncertainties in the core responses, e.g., eigenvalue and power distribution. To achieve that, one has to calculate the few-group cross-sections uncertainties, which are typically very large in dimensionality because they have to be functionalized in terms of a wide range of local conditions,

e.g., burnup, fuel and coolant temperature, boron dilution, etc. Many approaches have been proposed to achieve this. In one approach, the multi-group cross-sections are propagated through lattice physics calculations using a stochastic approach to determine the few-group cross-sections uncertainties [23]. To ensure computational efficiency, all major few-group cross-section dependencies are dropped to render a small number of lattice physics calculations, i.e., no dependence on burnup, fuel temperature, coolant voiding, etc. This results in about 10 few-group cross-sections as the whole input parameter space. In another approach, adjoint methods could be used to estimate the few-group cross-sections, again by dropping dependencies to ensure only a few number of adjoint evaluations [17], since each response requires a single adjoint evaluation. The next step is to propagate uncertainties through core calculations which is straightforward using either stochastic or deterministic methods since the number of few-group cross-sections is small.

In another approach, the few-group cross-sections are calculated as a function of burnup only, and their effective number is reduced using reduced order modeling (ROM) techniques [12]. Although the number of time steps is typically in the order of 30-50 steps, the effective number of degrees of freedom (DOFs) across burnup is only in the order of 5, implying an increase in the total number of DOFs from ten (without any dependencies as mentioned before) to about 35-50 (with burnup dependence only). Earlier work has shown that one can extend this idea to account for all other cross-section dependencies [25]. In fact, research has shown that there exists high degree of correlation between the branch cases, reaching a value of near perfect correlations for all major branch cases, such as increase or decrease of fuel temperature, coolant temperature, and void fraction. This idea is employed in existing work to render a reduction in the size of the uncertainty space before executing core calculations. This approach represents the most effective approach that currently exists for propagating cross-sections uncertainties through lattice physics and core calculations.

### **3.2 Efficiency-based Uncertainty Propagation Methods**

As noted earlier, the uncertainty quantification literature may be classified into two groups, a group focusing on rendering efficiency via building automated procedures for uncertainty analysis and another via design of new algorithms. With regard to the second group, new algorithmic developments are deemed necessary when the cost of the uncertainty analysis becomes

prohibitively expensive due to the associated cost of repeated model execution. Three prominent algorithmic strategies for rendering efficiency are highlighted here.

### **3.2.1 Surrogate model**

The first strategy focuses on replacing the forward model with a surrogate model, that is an approximate model, whose predictions are close enough to the original model, but can be executed as many times as required to reach the desired level of confidence in the quantities of interest. There exists a plethora of surrogate construction techniques, wherein the associated cost is dependent on the number of input parameters and the degree of model nonlinearity. Adjoint methods have also been used to construct surrogate models, based on the estimation of first and/or higher order variations. The difference between adjoint and forward models is that one can show that the first order variations for a given response can be evaluated using a single adjoint calculation, which makes adjoint methods superior when one is interested in few responses only. However, when higher order variations are required, the cost of the analysis becomes dependent on the number of parameters as well as the number of responses, which renders forward methods more effective for general nonlinear models with large number of responses. With first order variations estimated either using adjoint or forward methods, one can estimate the standard deviation of the responses in terms of the standard deviations of the parameters. This is a popular approach in the neutronic community and is typically referred to as the Sandwich equation, expressed mathematically later in the discussion. Other surrogate methods could also be employed such as the use of lower-fidelity models to serve as surrogates, the use of Gaussian process models [26, 27], neural networks [28, 29], and polynomial chaos expansions [8]. The primary challenge of surrogate models is that it is difficult to assess the errors resulting from the use of the surrogate model over the entire range of parameters variations.

### **3.2.2 Dimensionality reduction**

The second strategy employed to reduce the cost of uncertainty analysis beings with an initial reduction of the size of the uncertainty space for both the input parameters and output responses. The idea here is that most complex models have responses that are highly correlated, implying the true number of independent degrees of freedom is much less than the nominal number of responses.

Similarly, one can show that the null space of the operator is effectively large, indicating that there exists many combination of input parameter variations that produce negligible variations in the responses, and hence propagating uncertainties along these directions is of minimal value. Dimensionality reduction techniques for both the input parameter and output response spaces have been developed in earlier work [12, 30, 31]. Unlike surrogate model construction, the errors resulting from discarding the null space components could be accurately estimated using randomized range finding algorithms [32].

### **3.2.3 Fitting approximation**

The final strategy focuses on the use of intelligent sampling techniques to provide a more efficient coverage of the parameter space. Examples include hypercube sampling which attempts to spread the samples evenly over the space, proving to be an effective strategy in extreme quantile estimation. Adaptive sparse-grid methods [33] cut down the number of samples in areas of the parameter space with weak impact on the responses of interest, and trades that for more samples in the areas showing higher variations. Quasi Monte Carlo methods [34] employ fixed sequences to cover the space which can be shown to result in lower variances for the response of interest. Each method comes with its own advantage/disadvantages, but one can show that for models with sufficiently high number of parameters, pure Monte Carlo sampling remains the most efficient and reliable methodology to cover the uncertainty space. The literature is replete with methods attempting to hybridize the above methods.

## **3.3 Sensitivity Analysis Approaches**

Sensitivity analysis determines the importance of different uncertainty sources in input data contributing to the system response uncertainties. The results of sensitivity analysis are useful in providing information of most influential contributors to responses of interest uncertainties . This could be used to prioritize the key uncertainty sources contributing to responses uncertainties and to render reduction in the parameter uncertainty space with ROM-based UQ in this work. Additionally, SA may be used to perform model calibration and model validation [35]. SA methods can be classified into local and global methods.

Local SA employs one-at-a-time (OAT) methods, which execute the model sample by varying the inputs one-at-a time while holding the other inputs fixed. Simplicity of this method makes it the most utilized method in practical applications. However, local SA is computationally inefficient when the number of input parameters is very large. Moreover, local SA cannot identify the correlation between input parameters, as the inputs are never perturbed simultaneously. Besides, most of the implementations of this method require linear model assumption and only first order derivatives of responses with respect to input parameters are determined.

Global SA considers the entire range of variation of input parameters with the aim of accounting for the entire output uncertainty according to the different sources of uncertainties in the model inputs [36]. This method is advantageous because of its ability to obtain detailed (i.e., all moments) PDFs for all responses and deal with nonlinear models. The limitation is that sensitivity information is more difficult to infer and the number of model executions can be too large to render the approach practical for high dimensional models.

Sensitivity analysis in this work combines the benefits of both local and global SA methods while circumventing some of their deficiencies. In principle, the ROM techniques provide the means to render simultaneous reduction for both the input parameters space and responses space. This is achieved over two steps. In the first step, local methods are employed to identify a subspace that captures the dominant parameters and their cross-interactions in order to account for all high orders effects inherent in the original nonlinear model. In the second step, global methods are used to build a surrogate which restricts the samples to the active subspace only, thereby reducing the effective dimensionality of the input parameters space, and rendering the construction of the surrogate model computationally feasible.

### **3.4 Background and Status in Modeling Uncertainty Propagation**

Despite the notable success in improving the efficiency of propagating uncertainties, most of the previous work has focused on propagation of parameter uncertainties only, and very few have considered the effects of modeling uncertainties [37].

The quantification of modeling uncertainties is conceptually more difficult than the quantification of parameter uncertainties. This follows because the quantification of parameter uncertainties is concerned with characterizing the variations in the responses of interest due to variations in the model parameters. This is a straightforward task if one has good estimate of the

model parameters prior uncertainties, and can be accomplished via a brute force approach in which the model is executed numerous times with different parameter samples. The challenge is typically computational in nature, that's how to reduce the cost of the required model runs to obtain full PDFs for the responses of interest. Modeling uncertainties however are concerned with characterizing the differences between model predictions and real behavior which is unknown, and can only be estimated using experimentally-based UQ. Evidently, it is not practical to run experiments for all conditions expected during operation, which renders the quantification of modeling uncertainties a conceptually difficult endeavor.

To our knowledge, no work has been reported on the impact of the modeling uncertainties on the propagated parameter uncertainties. This work may thus be considered as a first-of-a-kind exploration into the impact of modeling uncertainties and their interaction with cross-section uncertainties. Alarming, results indicate that there exists non-negligible [38], and sometimes significant, interaction between the two sources of uncertainties, which calls into question the value of uncertainty analysis if this interaction is not properly understood.

### 3.5 References

1. Glaeser, H., *GRS method for uncertainty and sensitivity evaluation of code results and applications*. Science and Technology of Nuclear Installations, 2008. **2008**.
2. Williams, M.L., et al., *A statistical sampling method for uncertainty analysis with SCALE and XSUSA*. Nuclear technology, 2013. **183**(3): p. 515-526.
3. Alfonsi, A., et al. *Raven as a tool for dynamic probabilistic risk assessment: Software overview*. in *Proceeding of M&C2013 International Topical Meeting on Mathematics and Computation*. 2013.
4. Rochman, D., et al., *Efficient use of Monte Carlo: uncertainty propagation*. Nuclear Science and Engineering, 2014. **177**(3): p. 337-349.
5. Pecchia, M., et al., *Advanced calculation methodology for manufacturing and technological parameters' uncertainties propagation at arbitrary level of lattice elements grouping: Physor2014*. Journal of Nuclear Science and Technology, 2015. **52**(7-8): p. 1084-1092.
6. Ivanov, K., et al., *Benchmark for uncertainty analysis in modeling (UAM) for design, operation and safety analysis of LWRs*. 2007: Citeseer.
7. Jessee, M.A., M.L. Williams, and M.D. Dehart. *Development of generalized perturbation theory capability within the SCALE code package*. in *Proc. International Conference on Mathematics, Computational Methods & Reactor Physics (M&C 2009)*. 2009.
8. Ayres, D. and M. Eaton, *Uncertainty quantification in nuclear criticality modelling using a high dimensional model representation*. Annals of Nuclear Energy, 2015. **80**: p. 379-402.
9. Roderick, O., et al., *Stochastic finite-element approach in nuclear reactor uncertainty quantification*. Transactions of American Nuclear Society, 2009. **100**: p. 317-318.

10. Abdel-Khalik, H.S., P.J. Turinsky, and M.A. Jessee, *Efficient subspace methods-based algorithms for performing sensitivity, uncertainty, and adaptive simulation of large-scale computational models*. Nuclear science and engineering, 2008. **159**(3): p. 256-272.
11. Wang, C., J. Hite, and H.S. Abdel-Khalik, *Intersection subspace method for uncertainty quantification*. Transactions of the American Nuclear Society, 2014. **111**: p. 1384-1387.
12. Bang, Y., H.S. Abdel-Khalik, and J.M. Hite, *Hybrid reduced order modeling applied to nonlinear models*. International Journal for Numerical Methods in Engineering, 2012. **91**(9): p. 929-949.
13. Helton, J.C. and F.J. Davis, *Latin hypercube sampling and the propagation of uncertainty in analyses of complex systems*. Reliability Engineering & System Safety, 2003. **81**(1): p. 23-69.
14. Talbot, P.a.P.A., *Sparse-grid stochastic collocation uncertainty quantification convergence for multigroup diffusion*. Transactions of the American Nuclear Society, 2014. **111**: p. 747-750.
15. Sahoo, P., *Probability and mathematical statistics*. University of Louisville, USA, 2013.
16. Jaynes, E.T., *Information theory and statistical mechanics*. Physical review, 1957. **106**(4): p. 620.
17. Yankov, A., et al., *A two-step approach to uncertainty quantification of core simulators*. Science and Technology of Nuclear Installations, 2012. **2012**.
18. Helton, J.C., et al., *Survey of sampling-based methods for uncertainty and sensitivity analysis*. Reliability Engineering & System Safety, 2006. **91**(10-11): p. 1175-1209.
19. Mesado, C., et al., *Uncertainty and Sensitivity of Neutron Kinetic Parameters in the Dynamic Response of a PWR Rod Ejection Accident Coupled Simulation*. Science and Technology of Nuclear Installations, 2012. **2012**.
20. Hernández-Solís, A., *Uncertainty and sensitivity analysis applied to LWR neutronic and thermal-hydraulic calculations*. 2012: Chalmers University of Technology.
21. Wilks, S.S., *Determination of sample sizes for setting tolerance limits*. The Annals of Mathematical Statistics, 1941. **12**(1): p. 91-96.
22. Wieselquist, W., et al., *PSI methodologies for nuclear data uncertainty propagation with CASMO-5M and MCNPX: Results for OECD/NEA UAM benchmark Phase I*. Science and Technology of Nuclear Installations, 2013. **2013**.
23. Zeng, K., et al., *Uncertainty Analysis of Light Water Reactor Core Simulations Using Statistic Sampling Method*. M&C 2017, 2017.
24. Saltelli, A., K. Chan, and M. Scott, *Sensitivity analysis. Probability and statistics series*. John and Wiley & Sons, New York, 2000.
25. Huang, D., et al. *Efficient Evaluation of Core Simulator Few-Group Cross-Section Uncertainties via PCM*. in *Proceedings of the 2017 ANS Winter Meeting*. 2017.
26. Helgesson, P. and H. Sjöstrand, *Treating model defects by fitting smoothly varying model parameters: Energy dependence in nuclear data evaluation*. Annals of Nuclear Energy, 2018. **120**: p. 35-47.
27. Higdon, D., et al., *Calibration of tuning parameters in the FRAPCON model*. Annals of Nuclear Energy, 2013. **52**: p. 95-102.
28. Phung, V.-A., et al., *Prediction of in-vessel debris bed properties in BWR severe accident scenarios using MELCOR and neural networks*. Annals of Nuclear Energy, 2018. **120**: p. 461-476.

29. Back, J.H., et al., *Prediction and uncertainty analysis of power peaking factor by cascaded fuzzy neural networks*. *Annals of Nuclear Energy*, 2017. **110**: p. 989-994.
30. Huang, D. and H.S. Abdel-Khalik. *Development of Uncertainty Quantification Capability for NESTLE*. in *2017 25th International Conference on Nuclear Engineering*. 2017. American Society of Mechanical Engineers Digital Collection.
31. Huang, D., et al., *Dimensionality reducibility for multi-physics reduced order modeling*. *Annals of Nuclear Energy*, 2017. **110**: p. 526-540.
32. Abdo, M.G., H.S. Abdel-Khalik, and C. Wang. *Further investigation of error bounds for reduced order modeling*. in *Proceedings of Int. Conf. Math and Comp., Nashville, TN 2015*. 2015.
33. Constantine, P.G., M.S. Eldred, and E.T. Phipps, *Sparse pseudospectral approximation method*. *Computer Methods in Applied Mechanics and Engineering*, 2012. **229**: p. 1-12.
34. Owen, A.B., *Monte Carlo, quasi-Monte carlo, and randomized quasi-Monte Carlo*, in *Monte-Carlo and Quasi-Monte Carlo Methods 1998*. 2000, Springer. p. 86-97.
35. Wu, X., *Metamodel-based inverse uncertainty quantification of nuclear reactor simulators under the Bayesian framework*. 2017, University of Illinois at Urbana-Champaign.
36. Saltelli, A., et al., *Global sensitivity analysis: the primer*. 2008: John Wiley & Sons.
37. Todorova, N., et al., *Sensitivity Studies on Cross-section Generation and Modeling for BWR Core Simulation Using SAPHYR Code System*. 2004.
38. Huang, D. and H.S. Abdel-Khalik, *INVESTIGATIVE STUDY ON IMPACT OF MODELING UNCERTAINTIES IN UNCERTAINTY QUANTIFICATION OF NEUTRONICS CORE SIMULATION*. 2019, Proceedings of M&C: Portland, ON (United States).

## 4. METHODOLOGIES IN PROPOSED UCF

This chapter introduces two methodologies employed in the uncertainty characterization framework (UCF), the Physics-guided Coverage Mapping (PCM) method and the reduced order modeling (ROM) techniques. The first section illustrates the PCM methodology, serving as the method for similarity studies and mapping of uncertainties in this UCF. The PCM methodology description as well as the implementation algorithms are presented, followed by the interpretation of generated joint probability density function (PDF) via PCM. The second section discusses dimensionality reduction (DR) via ROM techniques, serving as the compression strategy to reduce the dimensionality of few-group parameter uncertainties to make the UCF feasible and efficient. The ROM section first provides background of ROM techniques and DR applications. The implementation of ROM technique in this UCF relies on the range-finding algorithm (RFA) to identify the active subspace, denoted as active degrees of freedoms (DOFs), with a preset error bound/tolerance. An interpretation of the DR results following the RFA algorithm is provided at the end of this section.

Part of the PCM descriptions is presented in previous publications [1, 2], as PCM methodology has been developed by the research group in support of model validation [3]. A full description of PCM is reproduced here for the sake of comprehensive discussion. The ROM techniques applied in this UCF have also been published in previous work [4-6].

### 4.1 PCM Methodology

The PCM methodology is designed to preclude the need for model calibration in support of model validation. Nuclear model validation provides a metric to measure the degree to which a given model prediction is a true representation of the real reactor behavior in conditions of interest. The model validation practice contains two subjects, the experiment and application. The “experiment” or “experimental domain” refers to small-scale or separate effects experiments, which are employed to calibrate the physics models in order to minimize the discrepancies between model predictions and measurements over the range of experimental conditions in model calibration. The “application” or “application domain” is the full-scale system such as a reactor under operation conditions during normal operation and accident scenarios. The layout of model

validation problem setup is depicted in Figure 4-1, where the experiment and application share the same prior parameter uncertainties. Both the experiment and application have calculation/simulation models providing predictions, while measurements are only available in experimental domain. Model validation is concerned with the following question: how can one assess the adequacy of a model for a given domain of application when the experimental data are only available at a range of conditions that is much smaller than the application domain.

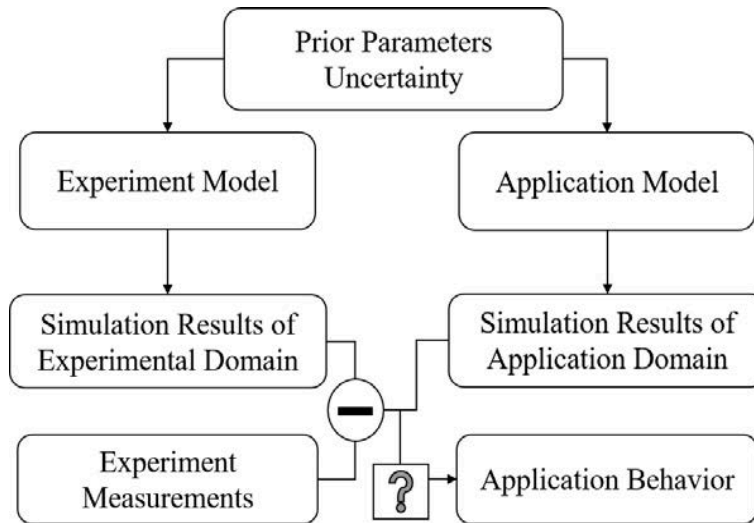


Figure 4-1 Layout of model validation problem setup.

Model calibration is one approach that is heavily employed in engineering wherein available experimental data are employed to adjust uncertain model parameters in order to reduce the discrepancies between the measured and model predictions for the experimental conditions. The adjusted parameters are then used to estimate model behavior over the wider domain of application. The calibration-based approach has many challenges such as relying on adjustment on basic physics parameters, the definition of discrepancy and the criteria used to minimize the discrepancies between measurement and predictions of experiment, etc. [1, 3].

Instead, PCM avoids any calibration of model parameters and directly calculates the biases for the responses of interest in the application domain using all available experimental data, and physics models for both the experimental and application domains. In doing so, the uncertainty of the bias may be evaluated based on an information-theoretic approach [7, 8] that takes into account all sources of uncertainties in both the application and experimental domains. The process of PCM methodology for uncertainty mapping on reactor application behavior is illustrated in Figure 4-2.

The central idea of PCM is to find a pattern or relationship, usually in the form of a PDF, between the experimental and application responses, shown as uncertainty mapping in the PCM layout. A pseudo response in terms of all available experimental responses which has the highest mutual information with the application response of interest will be built [1]. Mutual information is an information-theoretic measure that quantifies the degree of correlation between two random variables [8]. High mutual information implies that the two variables are highly correlated. To provide the best mapping of biases and uncertainties between the experimental and application domain, a joint PDF between responses of application and the experiment pseudo response is constructed indicating the coverage of uncertainties from experimental domain to application domain. The application behavior will be predicted with the measurements of experiment and the mutual information, represented as joint PDF, between the experiment and application.

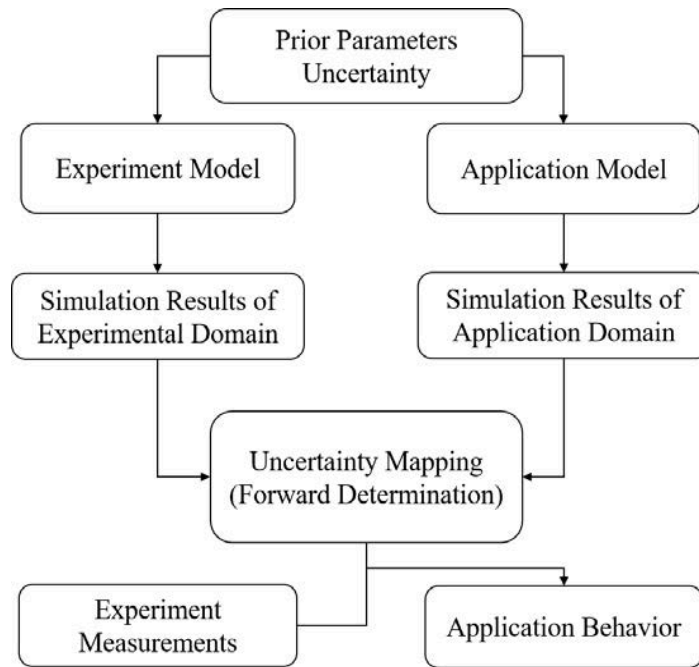


Figure 4-2 Layout of PCM methodology for uncertainty mapping.

This idea is employed in this thesis work by assuming that the experimental domain represents the uncertainties one can afford to calculate, while the application domain refers to the spectrum of conditions which should be evaluated for a comprehensive propagation of uncertainties. For example, if one could afford to calculate uncertainties using a single train of historical base conditions with no branching. The few-group parameters from this train would represent the experimental domain data as defined by PCM. The application domain would

represent the cross-sections that should be evaluated at all the other base and branch cases. The goal is to use PCM to assess the correlations between the application and experimental conditions, and provide means by which the uncertainties and their correlations can be mapped between the two sets of conditions.

#### 4.1.1 PCM problem setup

Mathematically, the physics models describing the experiment and application are given by:

$$y_{exp} = f_{exp}(x, u), \text{ and} \quad (4-1)$$

$$y_{app} = f_{app}(x, v) \quad (4-2)$$

where  $y_{exp}$  and  $y_{app}$  refer to the responses, as modeled by in the experiment and application domain, respectively;  $x$  are basic physics parameters (such as cross-sections) that are common to both the experiment and application domains, while  $u$  and  $v$  are control parameters (such as the geometry, and composition specifications, etc.) that are not common to both domains. In our context,  $u$  and  $v$  would be used to specify the branch cases differences.

In the experimental domain, one has access to both measurement, denoting as  $y_{exp}^{msr}$ , and analysis results, denoting as  $y_{exp}^{cal}$ , whereas in the application domain one has analysis results  $y_{app}^{cal}$  only, and one is interested in predicting the expected bias between model predictions and the true system behavior for the application. The central idea of PCM is to find a relationship in the form of a PDF  $p(y_{exp}, y_{app})$  between the experimental and application responses. This PDF is subsequently used to map the biases from the experimental to application conditions using any number of nonparametric techniques, such as the Kernel Density Estimation (KDE) [9] to be used in this work.

#### 4.1.2 PCM Implementation Algorithm:

A mathematical description of the steps required to implement PCM is given as follows. Assume that one is starting with M different experiments and a single application. Assume each experiment comes with a measured value for the response of interest, denoted as  $y_{exp}^{msr,(i)}$ ,

$i = 1, \dots, M$ . Next, execute the forward models for the application and the  $M$  experiments and obtain the reference values for the application response  $y_{app}$ , and that of the experiments  $y_{exp}^{(i)}$ ,  $i = 1, \dots, M$ . The goal is to employ the biases  $y_{exp}^{(i)} - y_{exp}^{msr.(i)}$ ,  $i = 1, \dots, M$  to determine a bias for the application response.

- 1) Identify all sources of uncertainties in the experiments and the application. Let  $x$  denote the common sources of uncertainties, while  $u_i$  refers to the sources unique to experiment  $\#i$ , and  $v$  the application's unique sources of uncertainties. For example,  $x$  denotes cross-sections;  $u_i$  denotes the fuel to moderator ratio, the geometry of the unit cell, etc., in the experiment  $\#i$ , and  $v$  denotes uncertainties in one of the core control parameters in the reactor application, e.g., the flow rate. Note that  $u_i$  and  $v$  are independent of one another.
- 2) Generate  $N$  random samples of  $x$ ,  $u_i$ , and  $v$  according to their prior distributions. Note that, if  $v$  and  $u_i$  do not have any uncertainties, their samples are to be fixed at their reference values.
- 3) Execute the application and  $M$  experiment computational models  $N$  times using the generated random samples. This step is essentially an uncertainty analysis done for each of the experiments and the application.
- 4) Let the  $N$  responses from the application and experiment  $\#i$  be denoted by vectors  $y_{app}$  and  $y_{exp}^{(i)}$  both of length  $N$ , respectively, where  $i = 1, \dots, M$ .
- 5) Assimilate all  $M$  experimental responses into a new response, referred to as mapping response,  $y_{app}^{map.(i)}$  selected to maximize its mutual information with the application response. This can be done using nonparametric estimation techniques, such as alternating conditional estimation. The use of nonparametric estimation allows the algorithm to pick the best relationship for the mapping response, as compared to parametric methods which constrain the relationship to some pre-determined surface, such as linear regression techniques.
- 6) Using the  $N$  samples for both application response and mapping response, generate a joint PDF,  $p(y_{app}^{map}, y_{app})$ . If the experiments are indeed perfectly representative of the application, one would get a contour that relates the two quantities, i.e., a function, or a PDF with zero spread. In reality, the scattered points will define a trend which describes the dependence of the application on the experiments, and the degree of the scatter will determine the uncertainty of this dependence.

- 7) Determine the PDF of  $y_{app}^{map}$ , denoted by  $p(y_{app}^{map,msr})$ , using the measured experimental responses PDFs,  $p(y_{exp}^{(i)})$ . Note that in Step 5  $y_{app}^{map}$  is determined as a function of the experimental responses. This function is derived solely from the  $N$  samples generated by the physics models. However, its PDF is calculated based on the PDFs of the experimental response. This step emulates a basic uncertainty propagation exercise, in which input variables PDF are propagated through a black-box or a function to get the output PDF. In many situations, only the means and standard deviations of the responses are measured/evaluated. In this case, one can assume the PDFs for all responses to be Gaussian. Note also that, since the relationship between the mapping response and the experimental response will not be generally a linear function, the PDF for the mapping response may not be Gaussian, even if all measured responses are Gaussian.
- 8) Using the joint PDF constructed in step 6, and the PDF determined for the mapping response, evaluate the PDF for the application response.

### 4.1.3 PCM results interpretation

As stated above, a joint PDF will be generated between the pseudo/mapping response and the calculation values of application as the result of applied PCM method. Note that the calculation values in experimental domain can be responses from either a single experiment or a representative of several ( $M$ ) experiments available. An example of the joint PDF built in PCM is given in Figure 4-3.

The result can be interpreted as follows:

- (1) Each data point on the scatter plot (on XY-plane) represents a pair of experiment response and the corresponding application response sharing the same prior parameter uncertainty. Number of model executions is independent on the number of parameters or responses, as PCM requires two uncertainty analyses for experiment model and application model each, which are forward non-intrusive uncertainty analyses.
- (2) The spread of the scatter plot indicates the presence and impact of additional sources of uncertainties that are not common to the experiment and application

models. The predicted application uncertainty comes from two uncertainty sources, the experiment uncertainty and the spread of the scatter plot.

- (3) The correlation between experiment and application responses is implied by the spread of the scatter plot. If there is zero or little spread, the correlation between the experiment and application will be high, which means the experiment is a perfect representative of the application. Conversely, large spread of the scattered points indicates loose correlation between experiment and application, response can be mapped to predict application with high uncertainty. The scattered points define a trend which describes the dependence of the application on the experiments, and the degree of spread will determine the uncertainty of this dependence.
- (4) Z-axis represents the probability density value of the PDF whose integral over the X-Y range is 1.0. The absolute value in Z-axis will not provide additional information.

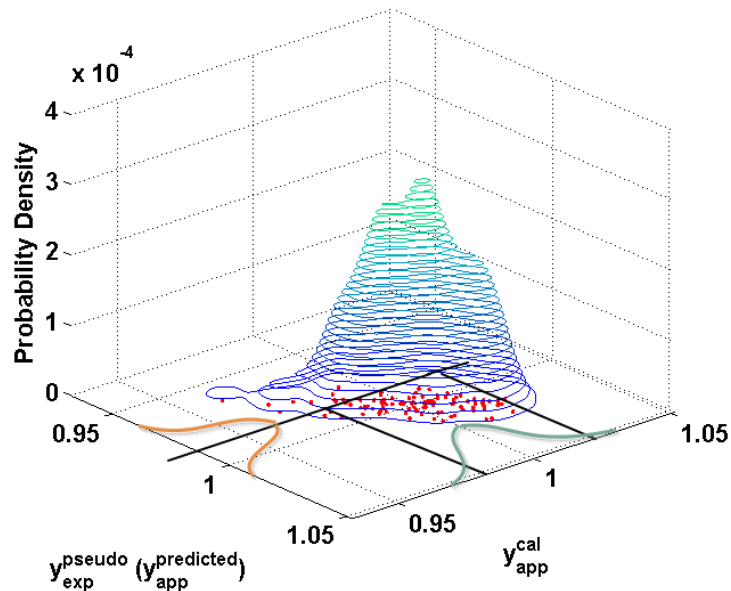


Figure 4-3 Example of joint PDF by mapping uncertainties from the experimental domain to the application domain.

## 4.2 Dimensionality Reduction in ROM

### 4.2.1 ROM background

ROM includes any process that reduces the complexity of the analysis models in one or more aspects. Uncertainty characterization (UC) exercise usually requires the ROM techniques as it requires amount of repeated model executions helping quantify and prioritized various sources of uncertainties. In UC of reactor core simulations, the analysis model contains more than ten thousand input parameters and detailed equation sets describing behavior of reactor in terms of various scales and physics feedback, which requires millions of model executions of complex system. The high computational expense makes the UC analysis practically infeasible, which is a major challenge in any UCF.

ROM-based methods achieve computational efficiency in one of two approaches, either by reducing the dimensionality of the uncertainty space, or by building a surrogate model that can be used in lieu of the original model. On one hand, the computational burden can be reduced by reducing the number of uncertainty sources in input parameters, which will reduce the number of required model runs. This type of reduction is referred to as dimensionality reduction. On the other hand, reducing the complexity helps reduce the cost of the calculations which renders number of repeated model executions to be affordable. This type of reduction constructs a model of reduced complexity that can be used in lieu of the original model, hence the common terminology of surrogate model, which can be used to replace/represent the original model for the sake of completing UC analysis.

The surrogate model construction relies on function approximation techniques, which replace the original model in terms of input parameters and responses, with an approximate function with lower complexity. Function approximation techniques can be classified into mathematical-based and physics-based categories. The mathematical-based function approximation attempted to find a relationship between the input parameters and responses in the form of a parametric analytic expression with a number of undetermined coefficients. The form of the approximate function is determined based on the expert judgement or modeler's experience. And the unknown coefficients are determined by executing the model a number of times. Example of the applications are response surface methodologies [10], polynomial chaos expansion [11], stochastic collocation techniques [12], etc. The advantage of this ROM approach is that it does not require knowledge of the model equations, i.e. the model can be treated as a black-box. However,

it introduces two challenges in reactor physics applications. First, the number of model executions required to determine the coefficients ensuring the surrogate as a representative of the real model, would be unrealistically high. This follows because the number of model executions is a function of the number of parameters, which is in the order of  $10^4$ - $10^6$  in reactor core simulations, as well as the order of nonlinearity of the model. Second, it is very difficult to assess the quality of the surrogate model and quantify the errors resulting from the approximation, as the form of the approximate function is based on modeler's decisions. The physics-based function approximation is constructed based solely on the physics of the model. An example of this ROM techniques applied to the reactor physics simulations is the exact-to-precision generalized perturbation theory (EpGPT) [13] with implementation [14], replacing the transport solver by an analytical expression with much lower computational time consuming. The advantage of the physics-based function approximation is that the error of the surrogate model can be bounded, which makes quantification of modeling discrepancies possible. However, this approach requires intimate knowledge of and complete access to the original model, as sometimes the adjoint-solver is required. Therefore, the surrogate model techniques are not practically feasible to make this UCF computationally affordable.

Instead of function approximations, the DR approach reduces the effective number of degrees of freedom used to describe the input data, so that the original model remains unchanged. The advantage of DR techniques is that one can upper-bound with high confidence the errors resulting from the reduction, which allows one establish a scientific approach that ensures the reliability of the reduced models. DR operates on the assumption that a large part of the uncertainty space is discarded completely from the analysis, as it is deemed to be non-influential with respect to the quantities of interest. The DR approaches are based on either gradient-based or gradient-free reduction algorithms, both of which employ a Range Finding Algorithm (RFA) [15] with randomized model executions as snapshots and rank revealing decompositions [16] to identify the active DOFs. The DR approach can sometimes combine both gradient-based and gradient-free algorithms [17]. The gradient-free reduction is employed in this UCF as the gradient-based reductions requires adjoint capability of the neutronics solver to calculate the derivatives of responses with respect to nuclear data.

## 4.2.2 DR problem setup and error bounding

ROM-based DR techniques is employed in this work to provide a rigorous mathematical approach by which the uncertainty space can be effectively shrunk into a manageable size to enable the practical application of UC techniques. The idea is to identify the active DOFs, which is a small subset of effective parameter uncertainty space that can be used to describe the majority of the response variations. Inactive DOFs denote directions in the parameter space that have negligible impact on the responses of interest. The number of active DOFs in reactor physics calculations is in the order of a few tens to hundreds, which is considerably smaller than the nominal size of the uncertainty space in the order of millions to billions in various reactor types [18-20]. The implication is that one can recast all UC algorithms in terms of the active DOFs which renders the process computationally manageable. The construction of ROM-based DR employed in this work can be described as follows.

Consider a model described by a general function (linear or nonlinear)  $f$  with  $n_x$  input model parameters  $x \in \mathbb{R}^{n_x}$  generating  $n_y$  output responses  $y \in \mathbb{R}^{n_y}$  as:

$$y = f(x) \quad (4-3)$$

Description here limits the reduction to the model parameters only to minimize the notational cluttering. In principle, the reduction can be applied to all input parameters including both model and control parameters in the UCF application when the function is expressed as  $f(x, \alpha, \eta)$  where  $\alpha$  and  $\eta$  are control parameters and modeling decisions respectively.

The objective of DR is to identify the active subspace for the input parameter space and the response space, denoting by  $\mathbf{K}_x \in \mathbb{R}^{n_x \times n_x}$  and  $\mathbf{K}_y \in \mathbb{R}^{n_y \times n_y}$  respectively. The model can be rewritten in the following expression:

$$\mathbf{K}_y y = f(\mathbf{K}_x x) \quad (4-4)$$

The objective of the RFA is to identify two subspaces, one for the input and another for the output spaces, denoted respectively by two matrix operators  $\mathbf{K}_x$  and  $\mathbf{K}_y$ . The matrix  $\mathbf{K}_z$  (where  $z$  denotes respectively  $x$  and  $y$ ) is extremely rank-deficient, i.e., its rank is much smaller than its dimensions:

$$\mathbf{K}_z \in \mathbb{R}^{n_z \times n_z} \quad \text{and} \quad \text{rank}(\mathbf{K}_z) = r_z \ll n_z \quad (4-5)$$

These matrices are used to restrict the variations of the respective model interface variables, i.e., the input parameters and output responses, on hyperplanes, i.e., mathematical subspaces. This restriction may be described by a projection operation as follows:

$$x^{(r)} = \mathbf{K}_x x \quad \text{and} \quad y^{(r)} = \mathbf{K}_y y \quad (4-6)$$

where the (r) superscripts denotes that the respective variables are constrained to a subspace. A rank-deficient matrix may be written using an orthogonal decomposition as follows:

$$\mathbf{K}_z = \mathbf{Q}_z \mathbf{Q}_z^T, \quad (4-7)$$

where  $\mathbf{Q}_z \in \mathbb{R}^{n_z \times r_z}$  is a skinny orthonormal matrix (i.e., the number of its columns is much smaller than the rows, with the columns being orthogonal and of unit Euclidean length) with  $r_z$  columns representing a basis for a subspace, denoted hereinafter by the active subspace,

$$\mathbf{Q}_z = \left[ [\mathbf{Q}_z]_{*1} \quad [\mathbf{Q}_z]_{*2} \quad \cdots \quad [\mathbf{Q}_z]_{*r_z} \right] \quad (4-8)$$

where  $[\mathbf{Q}_z]_{*i} \in \mathbb{R}^{n_z \times 1}$  is the  $i^{th}$  column of the matrix  $\mathbf{Q}_z$ . An active subspace for the input parameter space, by definition, spans all input parameters variations that have dominant impact on the output responses. Said differently, the output responses are insensitive to parameter variations that are orthogonal to the active parameters subspace.

The proposed surrogate model takes advantage of this behavior by limiting parameter variations to the active parameters subspace. Similarly, an active subspace in the output space implies that the majority of the output variations are contained in the active response subspace, with the variations in the orthogonal complement of that subspace being very small and can therefore be discarded in the construction of the surrogate model.

Next, we would like to distinguish here between the pre- and post-reduction variables for the various models interfaces. Consider for example a generic  $z$  interface where the original space has dimension  $n_z$ , implying that  $z$  has  $n_z$  degrees of freedom. The reduced variable  $z^{(r)}$  also lives in the original space and has  $n_z$  components, however its variation is constrained to a subspace of dimension  $r_z$ , implying that there are  $(n_z - r_z)$  perfect correlations inside its  $n_z$  components. The  $r_z$  components of  $z$  along the active subspace are described by another vector that lives in an  $r_z$  dimensional space, referred to as the active DOFs of the variable  $z$ . This smaller vector is important

as it will be used to construct the surrogate model. The relationships between these variables are described by the following equations:

$$z^{(r)} = \mathbf{K}_z z, \quad z_{DOF}^{(r)} = \mathbf{Q}_z^T z, \quad \text{and} \quad z^{(r)} = \mathbf{Q}_z z_{DOF}^{(r)} \quad (4-9)$$

The first equation on the LHS implies  $z^{(r)}$  is the projection (i.e. the orthogonal shadow) of  $z$  along the active subspace, that is spanned by the columns of the matrix  $\mathbf{Q}_z$ . The second equation calculates the  $r_z$  components of  $z^{(r)}$  along the active subspace and aggregates them in a vector  $z_{DOF}^{(r)}$ . The last equation describes how one may reconstruct the reduced variables from the active DOFs. Note that in this reconstruction  $z_{DOF}^{(r)}$  has  $r_z$  components, while  $z^{(r)}$  has  $n_z$  components, which follows from the fact that  $\mathbf{Q}_z$  has  $n_z$  rows and  $r_z$  columns.

A general matrix  $\mathbf{X} \in \mathbb{R}^{m \times N}$  can be written in the form of summation of mutually orthogonal outer products via a Singular Value Decomposition (SVD) with  $r$  singular vectors as:

$$\mathbf{X} = \mathbf{U} \mathbf{\Sigma} \mathbf{V}^T \quad (4-10)$$

where both  $\mathbf{U} \in \mathbb{R}^{m \times r}$  and  $\mathbf{V} \in \mathbb{R}^{r \times N}$  are orthonormal matrices, and  $\mathbf{\Sigma} \in \mathbb{R}^{r \times r}$  is a diagonal matrix. This expression can also be written as summation format:

$$\mathbf{X} = \sum_{i=1}^r s_i u_i v_i^T \quad (4-11)$$

where  $u_i$  and  $v_i$  refer to the columns of  $\mathbf{U}$  and  $\mathbf{V}$  respectively and  $s_i$  are scalars. This expression involves a summation of  $r$  outer products, implying that when the matrix  $\mathbf{X}$  multiplies a vector  $x$ , only  $r$  degrees of freedom of the vector  $x$  will be projected and rotated by the operator  $\mathbf{X}$ . Since  $x$  lives in an  $n$  dimensional space, the implication is that  $n - r$  degrees of freedom will be lost upon multiplying  $x$  by  $\mathbf{X}$ . This represents the basic idea of DR.

Quantification of reduction errors is an essential requirement of the DR approach employed here. As described by Eq. (4-4), the original function remains unchanged, and the reduction errors are resulting solely from constraining input parameter variations to the active parameter subspace, and the output variations to the active response subspace. Quantification of errors resulting from reduction in the input space [21], for reduction errors in the output space [22], and for the simultaneous reduction in both input and output space [23] are presented here. It is important to mention here that for a given selection of the active subspaces, one can create upper-bounds on the errors resulting from the reduction [22, 23]. And for a given upper-bound on the error, one

could find an infinite number of active subspaces that satisfy this upper-bound. First, consider the errors resulting from the input parameter space reduction,

$$e_x = \|f(x) - f(\mathbf{K}_x x)\| \leq \varepsilon_x \quad \text{over all } x \in S_x \quad (4-12)$$

where  $e_x$  describes the errors in the output responses due to a reduction in the input parameter space, with  $\varepsilon_x$  representing an upper-bound for all possible  $x$  values. The second source of errors is due to reduction in the response space:

$$e_y = \|f(x) - \mathbf{K}_y f(x)\| \leq \varepsilon_y \quad \text{over all } x \in S_x \quad (4-13)$$

This reduction implies that the responses are constrained to an active subspace assumed to contain the majority of response variations. Finally, the combined error for two simultaneous reductions in both the input parameter and output response spaces is given by:

$$e_{xy} = \|f(x) - \mathbf{K}_y f(\mathbf{K}_x x)\| \leq \varepsilon_{xy} \quad \text{over all } x \in S_x \quad (4-14)$$

where  $S_x$  specifies the range of allowable  $x$ .

### 4.2.3 RFA algorithm for active subspace construction

To determine the effective rank  $r$ , a RFA [15, 18] developed in earlier work, is used to identify the best linear transformation with smallest number of active DOFs that can approximate the few-group covariance matrix to a preset tolerance. The RFA algorithm is described below for generic model receiving  $n_x$  input parameters aggregated in a vector  $x$  and produces  $n_y$  outputs in a vector  $y$ . The goal is to find active DOFs for the output response.

- 1) Specify the range of allowable  $x$  variations, contained in the volume  $S_x \in \mathbb{R}_x$ . In the current context,  $S_x$  represents the range of parameters variations as defined by the prior uncertainties.
- 2) Specify preset tolerance  $\varepsilon_y$ , i.e., upper-bound, on the reduction errors for the responses.
- 3) Generate  $l + l_s$  random samples for  $x$ , i.e.,  $\{x_i\}_{i=1}^{l+l_s} \in S_x$ .
- 4) Generate  $l + l_s$  realizations of  $y$ , i.e.,  $\{y_i\}_{i=1}^{l+l_s}$  and form two matrices  $\mathbf{Y} = [y_1 \ y_2 \ \dots \ y_l] \in \mathbb{R}^{n_y \times l}$  and  $\mathbf{Y}_s = [y_{l+1} \ y_{l+2} \ \dots \ y_{l+l_s}] \in \mathbb{R}^{n_y \times l_s}$ .

- 5) Update  $\mathbf{Y}$  and  $\mathbf{Y}_s$  by standardizing the matrices. Standardization implies subtraction and division by some reference value, selected in the current context as the mean value over  $N$  samples.
- 6) Use  $\mathbf{Y}$  to compute orthonormal basis  $\mathbf{U}_y$  with rank  $r_y$ .
- 7) Use  $\mathbf{Y}_s$  to assess whether  $\mathbf{U}_y$  satisfies the tolerance  $\varepsilon_y$ .
- 8) If the desired tolerance is not met, increase  $l$ .

The volume  $S_x$  in step 1, defined by the user, identifies the allowable ranges for the parameters. This volume can be defined in a number of ways depending on the modeling conditions. For example, the simplest approach is to define an interval range for each of the parameters. If a parameter represents the concentration of a given material, then the interval can be selected to span the expected range of that concentration variation over the envisaged horizon of operation. If the parameter represents a technological quantity, i.e., a dimension subject to manufacturing uncertainty, then the range may be selected to cover the range of uncertainty expected, i.e., two or three standard deviations around its mean value. If the parameter represents a physical quantity, e.g., thermal conductivity, subject to a general aleatory or epistemic uncertainty, then the associated parameter PDF is to be specified to sample the random parameter values in step 3. If the parameters are measured experimentally in a manner that introduces correlations between their uncertainties, e.g., nuclear cross-sections, then the covariance matrix describing their uncertainties must be used to constraint their sampled values. Similarly, if the parameters are calculated from an upstream physics model, correlations between their variations are expected, and must be specified to ensure that the samples generated in step 3 are consistent with the upstream physics model.

The  $y$  realizations in step 4 may be generated directly using the model function, i.e.,  $y_i = f(x_i)$ . If the function  $f$  is too expensive to evaluate, other approximate approaches may be used. For example, a lower fidelity model may be used, e.g., a diffusion model in lieu of a transport model, a deterministic in lieu of a probabilistic model. While all these approaches introduce additional errors resulting in an increase in the size of the active subspace, it can be shown that the associated reduction errors can still be upper-bounded [24].

Note that in step 3 two sets of random samples are generated. The first set contains  $l$  samples which are used for the construction of the active subspace, referred to as the snapshots set.

The second set contains  $l_s$  samples which are used solely for calculating an upper-bound on the active subspace in step 7. This set is referred to as the oversamples set. It is important to distinguish between these two sets, because as mentioned earlier, the realizations used for the construction of the active subspace, i.e., the snapshots set, could be generated using an approximate model for the function  $f$ . However, the oversamples set must be calculated using the original function  $f$  to ensure reliable determination of the upper-bound. Secondly, the size of the snapshots set needs to be at least as big as the size of the sought active subspace; however the oversamples set may be set to a fixed value (typically less than 10), which are used to specify a probabilistic confidence in the estimation of the error upper-bound. Also note that if the snapshots set is too small to meet the user-defined tolerance on the reduction errors (step 8), additional snapshots must be added, however the oversamples set need not be reevaluated or expanded, as it can be used to test multiple active subspaces.

Step 5 is particularly required when the components of the response  $y$  are of different units and/or scales. For example if  $y$  contains outputs from a typical core simulator such as the critical eigenvalue, pin powers, and the fuel isotopic composition, it is important to standardize  $y$  by centering it around and/or dividing it by the mean values of the samples. This is also important because the user-defined tolerance for the different components of the response vectors are expected to be different.

In step 6, an orthonormal basis for the active subspace is calculated. This may be done using any rank-revealing decomposition such as the SVD or the Gram-Schmidt QR factorization, or any of their numerous variations. This process generates a matrix  $\mathbf{Q}_y$  with  $r_y$  columns. The premise is that this matrix can be used to reconstruct the model response realizations for any input parameter  $x \in S_x$  such that the discrepancies between the original model responses and the reconstructed responses are upper-bounded by the user-defined bound  $\varepsilon_y$ . This may be written as follows:

$$\|(\mathbf{I} - \mathbf{Q}\mathbf{Q}^T)f(x)\| \leq \varepsilon_y \quad (4-15)$$

where  $\mathbf{Q}_y^T f(x) \in \mathbb{R}^{r_y}$  represents the  $r_y$  components of the response along the active subspace (referred to as the responses active DOFs), and  $\mathbf{Q}_y \mathbf{Q}_y^T f(x) \in \mathbb{R}^{n_y}$  is the reconstructed response vector in the response space. Note that the vector  $\mathbf{Q}_y \mathbf{Q}_y^T f(x)$  has  $n_y$  components just like the

original response vector  $f(x)$ . However, the variations of these  $n_y$  components is restricted to an  $r_y$  active subspace.

The error upper-bound  $\varepsilon_y$  is calculated in step 8 as follows:

$$\varepsilon_y = 10\sqrt{\frac{2}{\pi}} \max_{i=1,\dots,s} \left\| (\mathbf{I} - \mathbf{Q}_y \mathbf{Q}_y^T) [\mathbf{Y}_s]_{*i} \right\|, \text{ such that } p(e_y(x) \geq \varepsilon_y) = 10^{-s} \quad (4-16)$$

where  $[\mathbf{Y}_s]_{*i}$  is the  $i^{\text{th}}$  column of the matrix  $\mathbf{Y}_s$  and  $e_y(x)$  is the error for any given  $x$  as defined in Eq. (4-12). This upper-bound is met in a probabilistic fashion, implying that there is a probability of  $10^{-s}$  ( $s$  the size of the oversamples set) that the actual error  $e_y(x)$  will exceed the bound  $\varepsilon_y$  for some parameter value  $x$  that belongs to the allowable range of parameter variations  $S_x$ . This probability is denoted as the failure probability, i.e., denoting the failure of the active subspace to upper-bound the errors resulting from the reduction.

#### 4.2.4 DR results interpretation

Applying the RFA algorithm on the randomized parameter space generates an error vs active rank plot as illustrated in Figure 4-4. The maximum error declines with more DOFs involved in the reconstruction of the original matrix, i.e. with  $r$  increasing. The active rank can be determined with a user-defined preset tolerance.

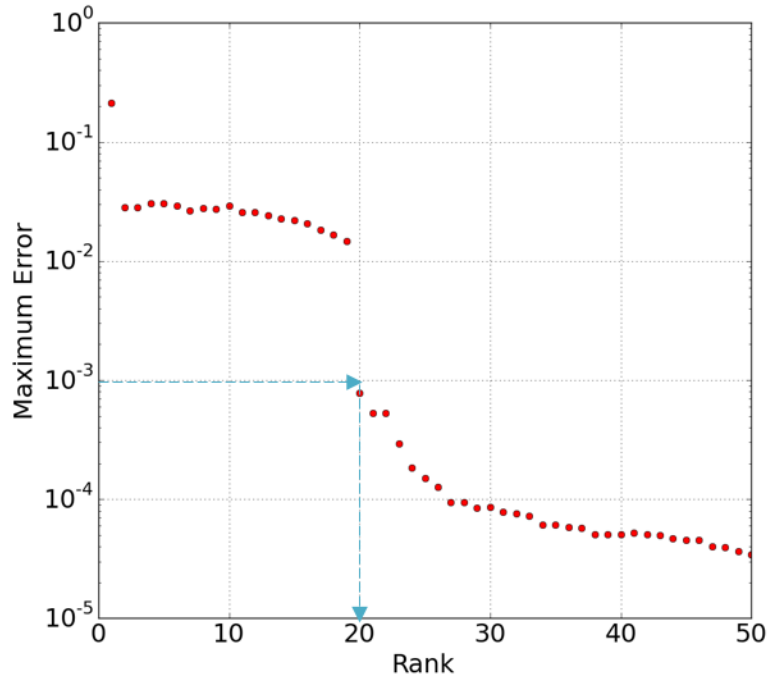


Figure 4-4 Example of maximum error resulting from dimensionality reduction vs active rank.

### 4.3 References

1. Huang, D. and H. Abdel-Khalik. *Construction of optimized experimental responses in support of model validation via physics coverage mapping methodology*. in *Proceedings of PHYSOR*. 2016.
2. Huang, D., et al. *Efficient Evaluation of Core Simulator Few-Group Cross-Section Uncertainties via PCM*. in *Proceedings of the 2017 ANS Winter Meeting*. 2017.
3. Abdel-Khalik, H.S., A. Hawari, and C. Wang, *Physics-guided Coverage Mapping (PCM): a new methodology for model validation*. 2015.
4. Huang, D., et al., *Dimensionality reducibility for multi-physics reduced order modeling*. *Annals of Nuclear Energy*, 2017. **110**: p. 526-540.
5. Huang, D. and H.S. Abdel-Khalik. *Development of Uncertainty Quantification Capability for NESTLE*. in *2017 25th International Conference on Nuclear Engineering*. 2017. American Society of Mechanical Engineers Digital Collection.
6. Huang, D., et al., *Further development of few-group cross-section uncertainty quantification techniques for core simulation*. 2018.
7. Athe, P. and H. ABDEL-KHALIK, *Mutual Information: A Generalization of Similarity Indices*. *Trans. Am. Nucl. Soc*, 2014. **111**: p. 751.
8. Cover, T.M. and J.A. Thomas, *Elements of information theory*. 2012: John Wiley & Sons.
9. Trumpler, R.J. and H.F. Weaver, *Statistical astronomy*. 1953: Univ of California Press.
10. Box, G.E. and N.R. Draper, *Empirical model-building and response surfaces*. 1987: John Wiley & Sons.
11. Choi, S.-K., et al., *Polynomial chaos expansion with latin hypercube sampling for estimating response variability*. *AIAA journal*, 2004. **42**(6): p. 1191-1198.

12. Eldred, M. *Recent advances in non-intrusive polynomial chaos and stochastic collocation methods for uncertainty analysis and design.* in *50th AIAA/ASME/ASCE/AHS/ASC Structures, Structural Dynamics, and Materials Conference 17th AIAA/ASME/AHS Adaptive Structures Conference 11th AIAA No.* 2009.
13. Wang, C. and H.S. Abdel-Khalik, *Exact-to-precision generalized perturbation theory for eigenvalue problems.* Nuclear Engineering and Design, 2013. **256**: p. 130-140.
14. Mertyurek, U., et al., *CRANE: A Prototypic SCALE Module for Reduced Order Modeling.* Transactions of the American Nuclear Society, Reno NV, 2014.
15. Halko, N., P.-G. Martinsson, and J.A. Tropp, *Finding structure with randomness: Probabilistic algorithms for constructing approximate matrix decompositions.* SIAM review, 2011. **53**(2): p. 217-288.
16. Meyer, C.D., *Matrix analysis and applied linear algebra.* Vol. 71. 2000: Siam.
17. Wang, C., J. Hite, and H.S. Abdel-Khalik, *Intersection subspace method for uncertainty quantification.* Transactions of the American Nuclear Society, 2014. **111**: p. 1384-1387.
18. Bang, Y., H.S. Abdel-Khalik, and J.M. Hite, *Hybrid reduced order modeling applied to nonlinear models.* International Journal for Numerical Methods in Engineering, 2012. **91**(9): p. 929-949.
19. Abdel-Khalik, H.S., P.J. Turinsky, and M.A. Jessee, *Efficient subspace methods-based algorithms for performing sensitivity, uncertainty, and adaptive simulation of large-scale computational models.* Nuclear science and engineering, 2008. **159**(3): p. 256-272.
20. Jessee, M.A., *Cross-section adjustment techniques for BWR adaptive simulation.* 2008.
21. Abdo, M.G. and H.S. Abdel-Khalik, *Propagation of error bounds due to active subspace reduction.* Transactions of American Nuclear Society, Summer, 2014.
22. Abdo, M.G. and H.S. Abdel-Khalik. *Probabilistic error bounds for reduced order modeling.* in *Proceedings of International Conference on Mathematics and Computations in Nuclear Science and Engineering, Nashville, TN.* 2015.
23. Abdo, M.G. and H.S. Abdel-Khalik. *Development of multi-level reduced order modeling methodology.* in *ANS Annual Meeting.* 2015.
24. Abdo, M.G.M.M., *Multi-level reduced order modeling equipped with probabilistic error bounds.* 2016: North Carolina State University.

## **5. PROPOSED UNCERTAINTY CHARACTERIZATION APPROACHES**

This chapter discusses a number of algorithms to propagate uncertainties in an efficient manner, as well as algorithms to verify the validity of the linearity assumption, and assess the impact of modeling uncertainties. The first section describes the approach employed in the proposed uncertainty quantification (UQ) process, providing an integral picture. The section discusses the algorithms employed to propagate parameter uncertainties using both deterministic, e.g., sandwich equation, and stochastic approaches as well as how reduced order modeling (ROM) techniques and Physics-guided Coverage Mapping (PCM) methodology can be used to cut down the cost of uncertainty propagation. The next section discusses assumptions in modeling uncertainty propagation and exercises to check the validity of the linearity assumption, followed by how to quantify the impact of modeling errors. The final section presents the sensitivity analysis (SA) approach and the prioritization of the uncertainty sources.

The PCM methodology and the ROM-based dimensionality reduction (DR) approaches are presented in Chapter 4 of this dissertation. Part of the uncertainty propagation algorithms has been published in [1].

### **5.1 Proposed Uncertainty Propagation Approaches**

The proposed approaches rely on two basic strategies to evaluate the assumptions of uncertainty propagation and the active degrees of freedom (DOFs) of uncertainty space in core simulation process. The first is the PCM methodology [2], recently introduced to support model validation, to identify the similarities between two courses of domains, which reduces the computational cost required for the preparation of the few-group cross-sections, while maintaining all the dependency details of the few-group cross-sections. The overarching goal is to render computational efficiency while maximizing the insight that can be obtained from the uncertainty characterization exercise. The second is the range finding algorithm (RFA) developed in reduced order modeling (ROM) techniques, employed as compression approach to identify the best linear transformation with smallest number of active DOFs that can approximate the covariance matrix for core simulation to a preset tolerance [3]. Details of the PCM methodology and the ROM

techniques can refer to Chapter 4. The sensitivity analysis will be done based on the active DOFs identified by RFA. Besides, the impact of multiple lattice models on uncertainty space will also be based on the PCM strategy.

Earlier research has employed ROM techniques [3] to demonstrate how efficiency can be attained in uncertainty propagation exercises by exploiting correlations between variables at each model-to-model interface. In the current context, the few-group parameters represent the interface between lattice physics and core-wide calculations. ROM is manifested by finding another set of variables, referred to the active DOFs, which can be used to calculate to near-exact (within a preset tolerance) estimates of the few-group parameter variations resulting from the multi-group uncertainties. The implication is that instead of propagating the uncertainties of the few-group parameters, one only needs to propagate the uncertainties of the active DOFs, thereby significantly reducing the cost of the uncertainty propagation exercise. Research has shown that the active DOFs are related to the original variables, e.g., few-group parameters, by simple linear transformations which can be obtained using matrix decomposition techniques. Further, past research has developed numerous methods for the identification of the DOFs under different scenarios. For example, adjoint methods can be used to identify the active DOFs at the input model parameters levels, forward methods can be used to identify the active DOFs at the output response level, and hybrid adjoint-forward methods can be used to determine the minimum number of active DOFs for general nonlinear models. Intersection methods have also been developed to calculate the intersection of the active DOFs at the interface between two different codes in a multi-physics code sequence. In our work, we focus on the use of forward methods only due to the lack of the adjoint capability for the majority of reactor physics tools currently being used for production calculations. In this approach, one can perform ROM at the intersection between two codes, where the reduction is first determined by the upstream code. The identified active DOFs can be further reduced using a sensitivity analysis through the downstream code. This sensitivity analysis is typically affordable because the number of active DOFs determining by the upstream code is small.

Except from ROM-based dimensionality reduction, we show PCM methodology can be used to perform an initial reduction of the number of responses, representing the few-group parameters at a wide range of conditions required for few-group parameter functionalization for downstream core-wide calculations. This method is superior to ROM in our context, because ROM expects one to generate all responses from a single code execution, and then performs multiple

randomized executions to find the active DOFs. In our context, the responses from lattice physics calculations include all raw few-group parameters at a large number of conditions, which requires many executions of the lattice physics calculations for a single randomized realization by the ROM approach, which makes the computations unreasonably taxing. Hence, PCM is used instead because it allows one to perform initial correlation analysis between the different conditions used for the generation of the cross-sections. Results indicate the raw few-group parameters exhibit near-perfect correlations between the different conditions used for few-group parameters functionalization, which significantly reduces the computational overhead of executing lattice physics calculations as shown in the applications in Chapter 6.

Figure 5-1 shows the layout of the proposed uncertainty propagation process, including the variables associated therewith, and the methods (PCM, ROM, SA) employed for UQ and DR.

The starting point for the proposed uncertainty analysis will be the multi-group cross-section. It will be assumed that cross-section uncertainties are available at the multi-group level, implying that they have already been propagated from ENDF level through the given collapsing procedure. This work has already been demonstrated by others, see Oak Ridge National Laboratories' (ORNL) work on estimating the covariance matrix of the multi-group cross-sections, available in generic group structure that is suitable for a wide range of reactor types [4]. As pointed out earlier, the collapsing procedures introduces its own assumptions and associated errors which are expected to impact the quality of the multi-group cross-sections, however this is considered outside the scope of this manuscript. Thus, our focus will be on propagating the multi-group cross-sections to the few-group parameter and ultimately to core responses of interest. The multi-group cross-section uncertainties are propagated to the lattice physics solver through stochastic UQ process, generating a set of  $N$  few-group parameter samples. The  $\sigma_{MG}$  denotes the multi-group cross-sections input to lattice physics calculations.

The few-group uncertainties are propagated to core simulator after compression to obtain the uncertainties of core responses of interest. The first reduction step employs PCM to assess the degree of correlations between the various conditions used for few-group parameters functionalization to perform an initial reduction in the number of few-group parameters, whose uncertainties is to be propagated through downstream core-wide calculations. The ROM technique is then employed to compress the few-group parameter uncertainties into a compressed few-group covariance matrix as well as the few-group mean values. A set of samples for few-group parameter

library are generated based on the compressed covariance and the reference values of few-group parameters and then propagated to core simulator to obtain the core response uncertainties through either a stochastic or deterministic UQ process. When the stochastic method is employed to propagate the compressed few-group uncertainties, the samples refer to randomly perturbed samples following Eq. (5-30) and Eq. (5-31) while the deterministic UQ is used, the samples refer to the reference values perturbed by the active DOFs of the few-group uncertainties, following the expression of Eq. (5-28).

The resulting few-group parameters are denoted as  $\sigma_{FG}^{raw}$ , which are processed into a format suitable for core simulation, denoted by  $\sigma_{FG}^{CS}$ . Sensitivity information will be generated through UQ process to further reduced using the results of a sensitivity analysis. Finally, a priority ranking is performed to determine the important sources of uncertainties. The end result is to calculate the uncertainties for  $y$ , the core responses of interest. The uncertainties are described using standard deviations  $\sigma_y$  for the responses  $y$ .

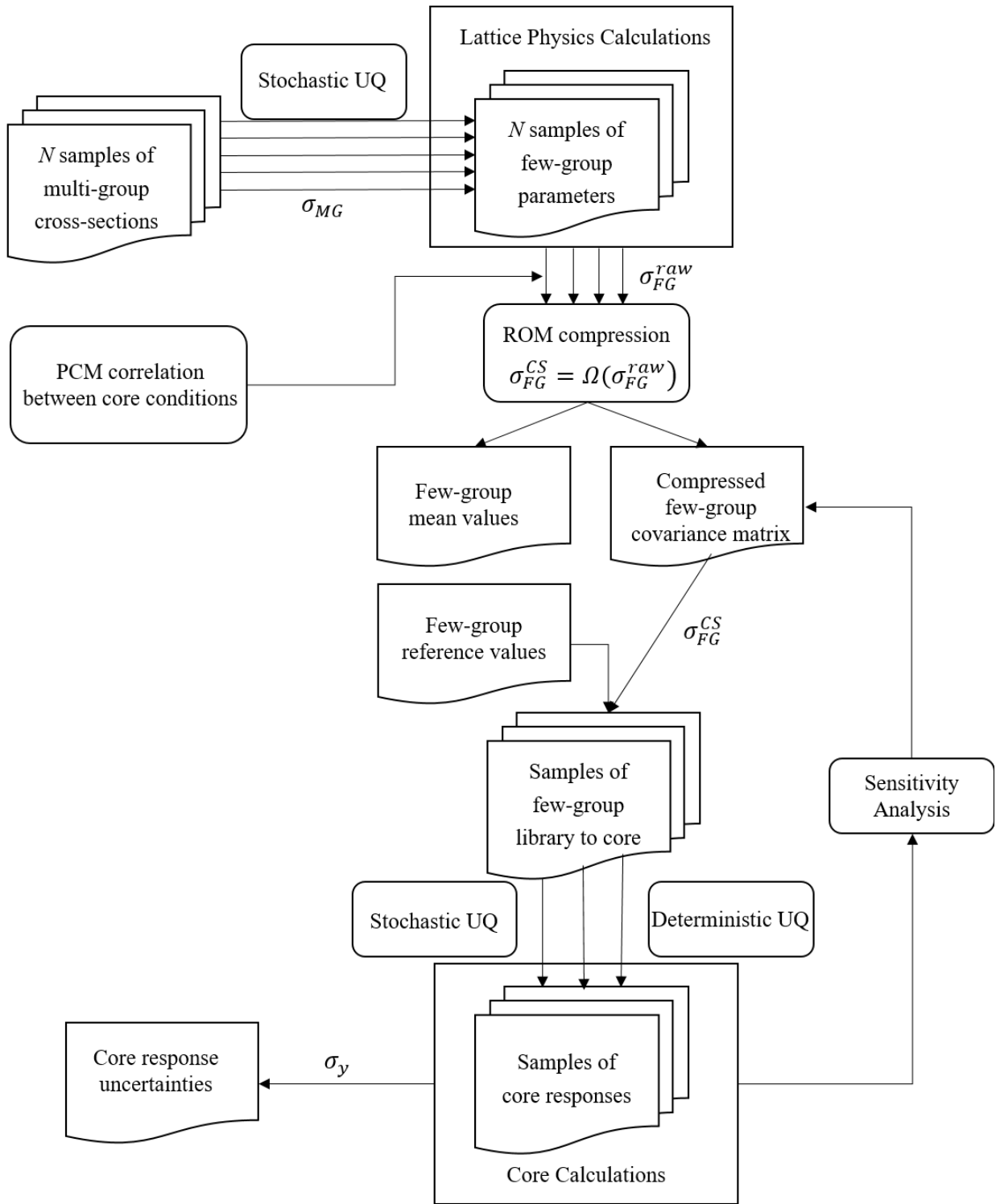


Figure 5-1 Layout of proposed uncertainty propagation process with compressed sources of uncertainties starting from multi-group uncertainty to responses of core simulation.

## 5.2 Propagation of Parameter Uncertainties

This section provides a generic discussion of stochastic and deterministic UQ, applied to a generic model with  $m$  input parameters and  $n$  output responses. This generic representation can be used to describe the propagation of uncertainties through lattice physics and core-wide calculations. In our implementation, stochastic UQ is used for the lattice physics calculations, and both the deterministic and stochastic approaches are allowed for core-wide calculations.

### 5.2.1 Uncertainty propagation algorithms

Consider the model's input parameters uncertainties to be defined using normal distribution which is fully determined by  $(\sigma_0, \mathbf{C}_\sigma)$ , where  $\sigma_0 \in \mathbb{R}^m$  represents the best estimate values for the model parameters, i.e., cross-sections, and  $\mathbf{C}_\sigma \in \mathbb{R}^{m \times m}$  the covariance matrix, and  $m$  denotes the number of input parameters. This representation is used for both the multi-group and few-group parameters.

Let the forward model relating responses and parameters for a given model, i.e., lattice physics or core-wide calculations, be given by:

$$y = f(\sigma) \quad (5-1)$$

where  $y$  is a vector representing the model's responses, i.e., few-group cross-sections in lattice calculations, and core responses in core-wide calculations. The  $\sigma$  is a vector representing the model's input parameters, i.e., multi-group cross-sections for lattice physics calculations, and the few-group parameters for core-wide calculations.

The core attributes uncertainties are expressed with mean values and corresponding covariance matrices for both approaches, denoted by  $(y_\mu, \mathbf{C}_y)$ , although the stochastic approach is able to provide the probability density distribution of the responses. Uncertainties can be propagated stochastically by drawing  $N$  samples of the parameters from their prior distributions, calculating the corresponding responses by executing the forward model, and condensing the results in the form of mean and covariance matrix for the responses as follows:

$$y_\mu = \frac{1}{N} \sum_{i=1}^N y_i, \quad \mathbf{C}_y = \frac{1}{N-1} \sum_{i=1}^N (y_i - y_\mu)(y_i - y_\mu)^T \quad (5-2)$$

Since one has  $N$  recorded samples for each response, one can histogram the samples to approximate the true PDF of the response. This can be done using both parametric and nonparametric techniques. A common approach employed is the kernel density estimation [5], which approximates the responses PDF as the sum of kernel functions, each centered around the sampled values. The width of each kernel function is a user-selected parameter to control the smoothness of the resulting PDF - recipes exist for its optimum selection [6].

$$p(y) = \sum_{i=1}^N h_i \left( \frac{y - y_i}{\delta_i} \right) \quad (5-3)$$

In our implementation, although the few-group parameters uncertainties will be propagated through lattice physics using stochastic approach, a simple normal distribution representation will be used, as measured by a vector of means and a covariance matrix. The adequacy of this representation will not be questioned in the current work. Future work could investigate the value for propagating other higher order moments of the distribution, e.g., skewness and kurtosis.

In a deterministic treatment, only few moments of the model parameters uncertainty distributions are propagated. With normal distribution, one propagates only the vector of mean values and covariance matrix. Under the assumption of model linearity within the range of parameter variations, the resulting responses mean values and covariance matrix can be calculated as follows:

$$y_\mu = f(\sigma_0), \mathbf{C}_y = \mathbf{S} \mathbf{C}_\sigma \mathbf{S}^T \quad (5-4)$$

where  $\mathbf{S} \in \mathbb{R}^{n \times m}$  is the sensitivity matrix of the model, representing the first order derivatives of the  $n$  responses with respect to the  $m$  model parameters. The  $\mathbf{S}$  matrix can be evaluated using either adjoint or forward methods. If adjoint methods are employed, one requires  $n$  adjoint executions of the adjoint code, wherein each execution, the right hand side of the equations is updated using the respective response definition. This approach is considered ineffective when one is interested in propagating uncertainties for models with many responses, e.g., estimating uncertainties of nodal power distribution, estimating uncertainties of the few-group parameters with all their dependencies taken into account. If forward approach is employed, one needs to execute the forward model  $m$  times, wherein each time one parameter is perturbed to calculate via finite differencing one column of the  $\mathbf{S}$  matrix. In many engineering applications, one expects  $n \ll m$  as there are usually a significant number of input parameters, and relatively few responses of interest. However,

this may not be the case when distribution-type data are treated as responses, e.g. power distribution.

Note that the first equation of Eq. (5-2) implies that the mean value is obtained by simply executing the forward model using the reference (also assumed to be the mean) value for the input parameters. If the linearity assumption is not adequate, one would expect discrepancies in the mean values and the covariance matrices as calculated by the stochastic and deterministic approaches.

Applying the process above to the different layers of the calculational sequence shown in Figure 5-1. The first layer is described as follows:

$$\sigma_{FG}^{raw} = \Pi(\sigma_{MG}) \quad (5-5)$$

The second layer, representing the buffer code to the core simulator is described by:

$$\sigma_{FG}^{CS} = \Omega(\sigma_{FG}^{raw}) \quad (5-6)$$

The third layer, representing the core simulator is described by:

$$y = \Pi(\sigma_{FG}^{CS}) \quad (5-7)$$

The uncertainties are initially available at the multi-group cross-section level in the form of mean values and covariance matrix denoted by:  $(\sigma_{MG,\mu}, \mathbf{C}_{MG})$ . The goal is to quantify the core responses uncertainties in terms of their mean and covariance matrix, denoted by:  $(y, \mathbf{C}_y)$ . In doing so, one must go through the few-group parameters, hence one must be able to approximate:  $(\sigma_{FG,\mu}^{raw}, \mathbf{C}_{FG}^{raw})$  and  $(\sigma_{FG,\mu}^{CS}, \mathbf{C}_{FG}^{CS})$ . To render computational efficiency, our goal is to represent the few-group parameters uncertainties in a suitable compressed format, denoted by:

$$\sqrt{\|\mathbf{C}_{FG}^{raw} - \mathbf{C}_{FG,ROM}^{raw}\|} \leq \varepsilon \quad \text{and} \quad \sqrt{\|\mathbf{C}_{FG}^{CS} - \mathbf{C}_{FG,ROM}^{CS}\|} \leq \varepsilon \quad (5-8)$$

where  $\varepsilon$  is a very small tolerance, e.g.,  $\varepsilon = 10^{-4}$  or smaller if one wishes.

In standard deterministic approach, the uncertainties in the core responses can be related to the multi-group cross-sections as follows:

$$\mathbf{C}_y = \mathbf{S}\mathbf{C}_{MG}\mathbf{S}^T \quad (5-9)$$

where  $\mathbf{S}$  is the so-called sensitivity matrix, containing the first order derivatives of the responses with respect to the multi-group cross-section. One can easily show that this matrix may be rewritten using the chain rule of differentiation as follows:

$$\mathbf{S}^T = \mathbf{S}_{MG-FG^{raw}}^T \mathbf{S}_{FG^{raw}-FG^{CS}}^T \mathbf{S}_{FG^{CS}-y}^T \quad (5-10)$$

where each of these matrices is associated with one of the three layers denoted above, i.e., one evaluates the derivatives of the raw few-group parameters with respect to the multi-group cross-sections, another evaluates the sensitivities resulting from the polynomial fitting buffering for the core simulation, and the last contains the derivatives of the core responses with respect to the polynomial coefficients that are input to the core simulator.

Regarding the first term,  $\mathbf{S}_{MG-FG^{raw}}$ , it can be evaluated either using finite differencing techniques or adjoint techniques. In the former, one will have to execute the lattice physics code a number of times equal to the number of multi-group cross-sections, typically in the order of  $10^4$  times, representing about 100-300 energy groups times 5-10 reactions per group times at least ten isotopes times the number of times required to fully functionalize the few-group parameters in terms of local conditions as discussed earlier. This is clearly computationally intractable. In adjoint setting, the number of code runs would be proportional to the number of responses, representing the few-group parameters which are also too many to render the process feasible. Earlier work has shown that a combined use of forward and adjoint methods could be used to reduce the cost required to approximate this matrix. This work has shown that one needs an order of  $r$  forward and  $r$  adjoint model runs, with  $r$  being in the order of 100, which renders the process computationally feasible [7]. Regarding the third derivative term,  $\mathbf{S}_{FG^{CS}-y}$ , this matrix is also very big in size, rendering both forward and adjoint methods computationally infeasible for its full evaluation.

### 5.2.2 Branch uncertainty representation and reduction

The correlations between the few-group cross-sections as evaluated over the range of conditions typically used for their functionalization.

A buffer code is typically used to read all the few-group parameters generated by lattice physics and convert them into polynomial coefficients, such that every few-group parameter, e.g., fast absorption, thermal fission, etc., is written as a polynomial in terms of local conditions, such as burnup, fuel temperature, etc. The number of polynomial coefficients is approximately the same as the number of raw data. This follows because for example to generate a 2<sup>nd</sup> order polynomial to functionalize a few-group parameter in terms of say moderator density, one needs two additional branch cases in addition to the base case to estimate three polynomial terms, a constant term

representing the value of the cross-section at the base case, and a linear and 2<sup>nd</sup> order terms that are functions of the deviations of the few-group parameter from the base case.

A base case refer to a depletion of the lattice at multiple time steps from zero up to a representative end of life discharge burnup. Branch cases refer to additional flux evaluations off of each base case, where only a single condition is changed to estimate the impact on the few-group parameters, e.g., an increase or decrease in fuel temperature, coolant density, etc. A core simulator reads the polynomial coefficients directly instead of the raw few-group parameters.

Both the historical and instantaneous effects of these conditions must be investigated. This follows because, for example, the thermal fission cross-section evaluated at a given burnup would depend on both the instantaneous fuel temperature as well as the average fuel temperature that was used to deplete the fuel. Thus our goal is to investigate the correlations between the different instantaneous conditions and the historical conditions. A typical example of the conditions used to functionalize cross-sections are as follows:

- 1) Generate multiple depletion trains, each from zero burnup, until end of life, as measured in burnup units, e.g., 70 GWD/MTU. Each train is defined by historical parameters, including fixed fuel temperature, coolant voiding, and boron concentration. These parameters are kept constant during depletion. These cases are referred to as historical base cases. There are typically three base cases to cover the historical fuel temperature variations, three voiding base cases, to simulate low, intermediate, and high historical voiding, controlled depletion, that's a depletion with control rod inserted throughout depletion. In this study, we will investigate the impact of burnup on the few-group cross-sections, that's the correlations between the cross-section uncertainties at different burnup values.
- 2) Branching off of each burnup step, instantaneous branch cases are developed, where in each case one parameter is changed at a time, e.g., increase or decrease in fuel temperature, change voiding from the historical value, insertion of control rod in a non-controlled historical case, etc. This is done while keeping the isotopic concentrations fixed, i.e., no depletion. In this study, we will illustrate the impact of fuel temperature, control rod insertion, and voiding branches on the correlations between the few-group parameters.

At each burnup step from the previous trains, change one parameter at a time and re-evaluate the flux, and all associated few-group cross-sections. For example, increase or decrease the fuel temperature, and re-evaluate the cross-sections. This is done while keeping all isotopic

concentrations constant. These evaluations are referred to as branch cases. For example, for non-controlled depletion base cases, the control rod is inserted as an instantaneous effect. Another example is the change in voiding. If the base voiding is at low, two instantaneous changes towards intermediate and high voiding will be made. In this study, we will illustrate the impact of fuel temperature, control rod insertion, and voiding branches on the correlations between the few-group cross-sections.

Regarding the second term of Eq.(5-10),  $\mathbf{S}_{FG^{CS}-y}$ , it is expected to be a square matrix, where the number of polynomial coefficients is often selected to be the same as the number of raw data employed to generate the fits, e.g., a 2<sup>nd</sup> order polynomial is described by three coefficients which requires three raw points for their evaluation. As currently implemented in NESTLE, all polynomials contain a constant term plus higher order terms, thus one can write:

$$\begin{bmatrix} \sigma_{FG,ZO}^{CS} \\ \sigma_{FG,HO}^{CS} \end{bmatrix} = \sigma_{FG}^{CS} = \mathbf{S}_{FG^{raw}-FG^{CS}} \sigma_{FG}^{raw} = \mathbf{S}_{FG^{raw}-FG^{CS}} \begin{bmatrix} \sigma_{FG,Base}^{raw} \\ \sigma_{FG,Branch}^{raw} \end{bmatrix} \quad (5-11)$$

This representation implies that the raw few-group parameters can be split into two blocks of data, one representing the base cross-sections at different depletion steps, and branch cross-sections calculated as multiple perturbations off of the base cross-sections. On the left hand side, the polynomial coefficients can be split into two blocks, one representing the Zero Order (ZO) terms, representing the constant terms for the polynomials and the Higher Order (HO) terms representing the 1<sup>st</sup>, 2<sup>nd</sup>, 3<sup>rd</sup>, etc. order terms. This representation proves useful when leveraging the correlation between the base and branch cases as shown next.

PCM can expose the perfect correlations between the branch and base case cross-sections. For example, consider the thermal fission cross-section evaluated at two different fuel temperatures to be represented by two random variables, one representing a base and the other a branch cross-section, and both are expected to be impacted by the uncertainties of the multi-group cross-sections. If these two variables are perfectly correlated, the implication is that the uncertainty for one variable can be used to infer the other. This observation may be leveraged to significantly reduce the cost of uncertainty propagation by redefining the raw few-group parameters as follows:

$$\sigma_{FG}^{raw} = \begin{bmatrix} \sigma_{FG,Base}^{raw} \\ \Delta\sigma_{FG,Branch}^{raw} \end{bmatrix} = \mathbf{H} \begin{bmatrix} \sigma_{FG,Base}^{raw} \\ \sigma_{FG,Branch}^{raw} \end{bmatrix} \quad (5-12)$$

where the second block contains cross-section differences due to the different changes introduced for the branch cases, e.g., fuel temperature increase or decrease, coolant temperature increase or decrease, etc. The  $\mathbf{H}$  operator is a simple matrix operator to convert the raw cross-sections into two sets, one representing the base cross-sections, and the other the branch cases' differences. One can easily show that:  $\mathbf{H}^2 = \mathbf{I}$ , the identity matrix, which renders the conversion between the two formats seamless via a multiplication by the  $\mathbf{H}$  matrix, demonstrated below for a pair of cross-sections, say the fast fission at one reference fuel temperature and a branch case thereof, denoted respectively by:  $\sigma_f^{fast}(T_{f,Base})$  and  $\sigma_f^{fast}(T_{f,Branch})$ . A simplified version of Eq. (5-12) for this pair of cross-sections reduces to:

$$\begin{aligned} \begin{bmatrix} \sigma_f^{fast}(T_{f,Base}) \\ \Delta\sigma_f^{fast}(T_{f,Branch}) \end{bmatrix} &= \begin{bmatrix} 1 & 0 \\ 1 & -1 \end{bmatrix} \begin{bmatrix} \sigma_f^{fast}(T_{f,Base}) \\ \sigma_f^{fast}(T_{f,Branch}) \end{bmatrix} \\ \begin{bmatrix} \sigma_f^{fast}(T_{f,Base}) \\ \sigma_f^{fast}(T_{f,Branch}) \end{bmatrix} &= \begin{bmatrix} 1 & 0 \\ 1 & -1 \end{bmatrix} \begin{bmatrix} \sigma_f^{fast}(T_{f,Base}) \\ \Delta\sigma_f^{fast}(T_{f,Branch}) \end{bmatrix} \end{aligned} \quad (5-13)$$

$$\mathbf{H} = \mathbf{H}^{-1} = \begin{bmatrix} 1 & 0 \\ 1 & -1 \end{bmatrix}$$

With the assumption of perfect correlation between base and branch case uncertainties, the uncertainties in the differences can be set to zero, resulting in a covariance matrix of the form:

$$\mathbf{C}_{FG}^{raw} = \begin{bmatrix} \mathbf{C}_{FG,Base}^{raw} & 0 \\ 0 & 0 \end{bmatrix} \quad (5-14)$$

According to the definition of covariance matrix, the few-group covariance matrix can be generated with the following expression:

$$\mathbf{C}_{FG} = \frac{1}{N-1} \mathbf{X}\mathbf{X}^T, \quad \mathbf{X} \in \mathbb{R}^{m \times N} \quad (5-15)$$

where  $\mathbf{C}_{FG}$  denotes for the general expression of few-group covariance matrix, either for raw few-group parameters generated by lattice physics calculation or after being processed by a buffer code for core simulation;  $\mathbf{X}$  contains the relative difference of all few-group parameters, i.e. after subtracting and dividing by the mean value for each respective parameter. Via a Singular Value Decomposition (SVD) of  $\mathbf{X}$  shown in equation below, the few-group uncertainty space can be represented with  $r$  singular vectors:

$$\mathbf{X} = \left[ \Delta\sigma_{FG,1}^{rel} \quad \Delta\sigma_{FG,2}^{rel} \quad \dots \quad \Delta\sigma_{FG,N}^{rel} \right] = \mathbf{U}\mathbf{\Sigma}\mathbf{V}^T, \quad \mathbf{U} \in \mathbb{R}^{m \times r}, \mathbf{\Sigma} \in \mathbb{R}^{r \times r} \quad (5-16)$$

The corresponding decomposition for the covariance matrix is given by:

$$\mathbf{U}\mathbf{\Sigma}^2\mathbf{U}^T = \sum_{i=1}^r s_i^2 \mathbf{u}_i \mathbf{u}_i^T \doteq \mathbf{C}_{FG}^{raw} = \begin{bmatrix} \mathbf{C}_{FG,Base}^{raw} & 0 \\ 0 & 0 \end{bmatrix} = \begin{bmatrix} \mathbf{U}_{FG}^{Base} \mathbf{\Sigma}_{FG}^{Base} \\ 0 \end{bmatrix} \begin{bmatrix} \mathbf{U}_{FG}^{Base} \mathbf{\Sigma}_{FG}^{Base} \\ 0 \end{bmatrix}^T \quad (5-17)$$

where  $\mathbf{u}_i$  and  $s_i$  refer to the singular vector and singular value of the covariance matrix from the SVD respectively. The ROM-based approximation covariance matrix is defined by retaining only the first  $r$  singular vectors to meet a user-preset tolerance as implied by Eq. (5-8), where

$$\mathbf{C}_{FG,ROM} = \sum_{i=1}^r s_i^2 \mathbf{u}_i \mathbf{u}_i^T.$$

Next, these few-group parameters are processed through the buffer code to generate the cross-section library in the format required by the core simulator. As stated in the scope of this work (Section 1.3.1), NESTLE and its CANDU version, NESTLE-C, are employed in this framework as the core simulator. NESTLE/NESTLE-C employs polynomial fitting and stores the coefficients of the polynomials as input to the core simulator. The expression of macroscopic cross-section of reaction type  $x$  and energy group  $g$  in the core simulator format is shown in the following equation [8]:

$$\begin{aligned} \hat{\Sigma}_{xg} = & a_{1_{xg}} + \sum_{n=1}^2 a_{(n+1)_{xg}} (\Delta\rho_c)^n + \sum_{n=1}^2 a_{(n+3)_{xg}} (\Delta T_c)^n + \sum_{n=1}^2 a_{(n+5)_{xg}} (\Delta\sqrt{T_{F_{eff}}})^n \\ & + \sum_{n=1}^2 a_{(n+7)_{xg}} (\Delta P_c)^n + \sum_{n=1}^2 a_{(n+9)_{xg}} (\Delta P_m)^n + \sum_{n=1}^2 a_{(n+11)_{xg}} (\Delta N_{sp})^n \end{aligned} \quad (5-18)$$

where  $a_{j_{xg}}$  are the polynomial coefficients apply to a specific core condition defined by coolant density ( $\rho_c$ ), coolant temperature ( $T_c$ ), fuel temperature ( $T_{F_{eff}}$ ), coolant purity ( $P_c$ ), moderator purity ( $P_m$ ), and soluble poison number density ( $N_{sp}$ ). The macroscopic cross-section with notation  $\hat{\Sigma}_{xg}$  could be part of the few-group lattice parameters for core simulation, denoted as  $\sigma_{FG}^{CS}$ . In this circumstance,  $a_{1_{xg}}$  coefficients are the zero order terms while  $a_{j_{xg}}$ ,  $j \geq 2$  coefficients are the higher order terms.

One can re-write Eq. (5-11) in terms of the differences between the branch and base cases as follows:

$$\sigma_{FG}^{CS} = \begin{bmatrix} \sigma_{FG,ZO}^{raw} \\ \sigma_{FG,HO}^{raw} \end{bmatrix} = \mathbf{H} \begin{bmatrix} \sigma_{FG,Base}^{raw} \\ \Delta\sigma_{FG,Branch}^{raw} \end{bmatrix} \quad (5-19)$$

This suggests that the few-group parameters for the core simulation can be written in terms of the few-group raw parameter from the base calculation and the difference from the branch calculations:

$$\sigma_{FG}^{CS} = \begin{bmatrix} \sigma_{FG,ZO}^{raw} \\ \sigma_{FG,HO}^{raw} \end{bmatrix} = \begin{bmatrix} \mathbf{I}_{FG,Base-FG_{ZO}^{CS}} \\ \mathbf{\Theta}_{FG,Branch-FG_{HO}^{CS}} \end{bmatrix} \begin{bmatrix} \sigma_{FG,Base}^{raw} \\ \Delta\sigma_{FG,Branch}^{raw} \end{bmatrix} = \mathbf{S}_{\Delta FG^{raw}-FG^{CS}} \sigma_{FG}^{raw} \quad (5-20)$$

where

$$\mathbf{S}_{\Delta FG^{raw}-FG^{CS}} = \begin{bmatrix} \mathbf{I}_{FG,Base-FG_{ZO}^{CS}} \\ \mathbf{\Theta}_{FG,Branch-FG_{HO}^{CS}} \end{bmatrix}$$

represents the transformations through the buffer code.

Since the  $\Delta\sigma_{FG,Branch}^{raw}$  have zero uncertainties, one can easily show that the higher order polynomial terms will also have zero uncertainties, thus confining the uncertainties to the zero-order terms only, which greatly simplifies the analysis.

### 5.2.3 ROM-based implementation

The ROM technique takes advantage of the correlations that may be present in the parameters and/or the responses. The employed ROM-based implementation is demonstrated here for parameter correlations only. For full discussion on taking advantage of all correlations, consult an earlier publication [12, 21]. This can be achieved by first decomposing the covariance matrix as follows:

$$\mathbf{C}_\sigma = \mathbf{U}\mathbf{\Sigma}^2\mathbf{U}^T = \sum_{i=1}^m \xi_i^2 \mathbf{u}_i \mathbf{u}_i^T \quad (5-21)$$

The  $\mathbf{u}_i$  are referred to as the singular vectors of the covariance matrix and they are selected to be orthonormal. The  $\xi_i$  are the singular values ordered from high to low. This decomposition is exact if the summation is extended to  $m$ . One can however show that the matrix can be approximated to a high degree of accuracy with very few components, such that:

$$\sqrt{\left\| \mathbf{C}_\sigma - \sum_{i=1}^r \xi_i^2 \mathbf{u}_i \mathbf{u}_i^T \right\|} = \varepsilon \quad (5-22)$$

where  $\varepsilon$  is a very small preset tolerance. This can be shown to be attributed to the sharp decline in the singular values of the matrix  $\mathbf{C}_\sigma$ . This idea has been explored by many researchers. In the context of ROM, earlier work has shown that it can be generalized for both linear and nonlinear models [3], single and multi-physics models [9]. One can trace its roots to the Karhunen Loeve expansion or the principal component analysis approaches [10, 11], both typically involving the use of singular value decomposition approach. The distinct differences between these different approaches is considered outside the scope of this article. Reader is recommended to consult the noted references for more details.

The implication of this decomposition is that the true number of DOFs in the uncertainty space, can be reduced from  $m$  down to  $r$ , and  $\xi_i$  represents the standard deviation of the  $i^{\text{th}}$  DOFs. Each DOF is defined by one of the singular vector of the covariance matrix,  $\mathbf{u}_i$ . Another interpretation of this decomposition is that while the original space contains  $m$  uncertain generally correlated parameters, one could find a smaller number  $r$  of uncertain uncorrelated parameters via a linear transformation,  $\mathbf{U}$ , where each of the new parameters is referred to as an active DOF, defined by  $\mathbf{u}_i^T (\sigma - \sigma_0) / \sigma_0$ . The active DOFs covariance matrix is diagonal and equal to  $\mathbf{\Sigma}^2$ .

With the active DOFs determined, one can recast the stochastic and deterministic algorithms in the previous subsections in terms of the active DOFs. These data may be used to update the stochastic and deterministic rendition of the previous uncertainty algorithms in terms of the active DOFs.

With regard to the stochastic approach, the samples are now rendered as follows:

$$\sigma_i = \sigma_0 \left( 1 + \sum_{j=1}^r \alpha_j^i \xi_j \mathbf{u}_j \right), \quad i = 1, \dots, N \quad (5-23)$$

where  $\xi$  is a random variable sampled from a normal distribution  $\mathcal{N}(0,1)$ , i.e., zero mean and unit standard deviation. For the deterministic algorithm rendition, a forward-based sensitivity analysis is employed to perturb the model parameters along each of the singular vectors as follows:

$$\sigma_i = \sigma_0 (1 + \beta \mathbf{u}_i),$$

where  $\beta$  is an arbitrary scalar, to form the  $i^{\text{th}}$  column of the matrix  $\mathbf{S}_U$ :

$$[\mathbf{S}_U]_{*i} = (y(\sigma_i) - y(\sigma_0)) / \beta, \text{ for } i = 1, \dots, r \quad (5-24)$$

The responses samples, obtained after running the code, are combined in the same way for the stochastic approach to calculate the responses PDF or their covariance matrix. For the deterministic approach, the results are combined as follows:

$$\mathbf{C}_y = \mathbf{S}\mathbf{C}_\sigma\mathbf{S}^T = (\mathbf{S}\mathbf{U}\mathbf{\Sigma})(\mathbf{S}\mathbf{U}\mathbf{\Sigma})^T = \mathbf{S}_U\mathbf{S}_U^T = \sum_{i=1}^r [\mathbf{S}_U]_{*i} [\mathbf{S}_U]_{*i}^T \quad (5-25)$$

Eqs.

$$[\mathbf{S}_U]_{*i} = (y(\sigma_i) - y(\sigma_0)) / \beta, \text{ for } i = 1, \dots, r \quad (5-24)$$

and

$$\mathbf{C}_y = \mathbf{S}\mathbf{C}_\sigma\mathbf{S}^T = (\mathbf{S}\mathbf{U}\mathbf{\Sigma})(\mathbf{S}\mathbf{U}\mathbf{\Sigma})^T = \mathbf{S}_U\mathbf{S}_U^T = \sum_{i=1}^r [\mathbf{S}_U]_{*i} [\mathbf{S}_U]_{*i}^T \quad (5-25)$$

imply that for  $r$  active degrees of freedom, the forward model need only be executed  $r+1$  times to evaluate the covariance of the responses, assuming the model behaves linearly in the range of cross-section uncertainties.

With ROM techniques implemented, the covariance matrix of core responses can be described with:

$$\mathbf{C}_y = \mathbf{S}\mathbf{C}_{FG,ROM}^{CS}\mathbf{S}^T = (\mathbf{S}\mathbf{U}\mathbf{\Sigma})(\mathbf{S}\mathbf{U}\mathbf{\Sigma})^T \quad (5-26)$$

where the variance of responses (the diagonal elements of  $\mathbf{C}_y$ ) resulting from uncertainties in the  $r$  active DOFs of the few-group parameters can be calculated as:

$$\sigma_y^2(r) = \frac{1}{N-1} \sum_{i=1}^r [y(\sigma_i) - y(\sigma_0)]^2 s_i^2 \quad (5-27)$$

where each  $i$  refers to a code execution with the few-group parameters perturbed as follows:

$$\sigma_i = \sigma_0(1 + u_i) \quad (5-28)$$

The implication from Eq. (5-27) is that the response uncertainties can be determined with  $r+1$  executions of the core simulation based on the  $r$  active DOFs from lattice parameter uncertainty space, thus emulating a deterministic forward-based approach for uncertainty propagation.

The stochastic approach can also be used to propagate the uncertainties from lattice level by generating  $N$  random samples of the few-group parameters consisting with the few-group

covariance matrix and provides mean and covariance matrix for response by executing the core simulation for  $N$  times. The resulting response uncertainties can be calculated with:

$$y_\mu = \frac{1}{N} \sum_{i=1}^N y_i, \quad \mathbf{C}_y = \frac{1}{N-1} \sum_{i=1}^N (y_i - y_\mu)(y_i - y_\mu)^T \quad (5-29)$$

where  $y_i$  contains responses from the  $i^{\text{th}}$  perturbation. Each random perturbation of the few-group parameters can be designed as follows:

$$\sigma = \sigma_0 + \mathbf{A}^T z \quad (5-30)$$

where  $\mathbf{A}^T$  is the upper triangular matrix by Cholesky decomposition of the few-group parameters covariance matrix, and  $z$  is a random vector drawn from unit normal distribution.

Based on the compressed uncertainty space of lattice parameters described in this context, the  $i^{\text{th}}$  random perturbation can be represented as:

$$\sigma_i = \sigma_0 \left( 1 + \sum_{j=1}^r z_i s_j u_j \right) \quad (5-31)$$

where  $z_i \in \mathbb{R}^{r \times 1}$  is the  $i^{\text{th}}$  random variable.

### 5.3 Propagation of Modeling Uncertainties

In order to elucidate the possible interactions between modeling and parameter uncertainties, the salient features of the general procedure employed to propagate uncertainties are first highlighted along with some of the assumptions commonly made in regarding to modeling uncertainties. Recalling the second classification of uncertainty methods, one can propagate uncertainties either in terms of the parameter samples used to execute the forward model or by directly propagating certain moments of the parameters PDF. In the first case, a response's PDF is approximated using the available samples with the bottleneck being the number of samples that can be afforded to accurately describe the PDF. If, however, the moments are propagated using deterministic methods, the resulting shape of a response's PDF is fixed per Jaynes maximum entropy principle [12]. For example, if one propagates the first and second moments only, the resulting output PDF can only be described using Gaussian distribution. If the model employed exhibits linear behavior meaning response variations around some reference point in the response

space are linear with respect to parameter variations, then input parameters with Gaussian PDF will transform into Gaussian PDF for the output responses.

In the ENDF library, only mean values and covariance information are available for the cross sections. The implication is that one can only describe their PDFs using Gaussian distribution to satisfy Jaynes' maximum entropy principle. Coupling that with the fact that the standard deviations for most important cross sections are within fraction to few percent of their nominal values, most researchers have justified the use of Gaussian distributions for output responses. This is based on the belief that neutronic quantities of interest are expected to behave linearly over the relatively small range of cross section variations due to prior uncertainties. For example, the  $\nu$ , thermal absorption and fast transport cross sections have standard deviations in the order of 0.05%, 0.5%, and 5%, respectively, of their nominal values. This belief to our knowledge has never been assessed rigorously but is entirely based on observation/experience with one-at-a-time parametric studies in which one parameter is adjusted by small amounts to test linearity assumption. We believe this approach is not rigorous enough and can be misleading when there are high order interaction terms between the parameters that cannot be captured using one-at-a-time approaches. For example, a model of the form appears passes the one-at-a-time linearity check:

$$\mathbf{z} = a\mathbf{x} + b\mathbf{y} + c\mathbf{xy}$$

where  $\mathbf{x}$ , and  $\mathbf{y}$  represent uncertain model parameters, and  $\mathbf{z}$  is the response. A direct consequence of the linearity assumption is that if one propagates cross section moments around two different reference points that are close to each other in the parameter space, the output PDFs are expected to be very similar. The differences in the reference values could be due to the use of different cross section libraries or different energy/spatial homogenization strategies. The implication is that modeling assumptions, which introduce some variations in the reference cross sections, are not expected to impact the propagated cross section uncertainties. This assumption is tested in this study using a number of verification exercises described in the next section.

### 5.3.1 Linearity verification exercises

A function is considered linear if its first order derivatives with respect to its parameters do not change if evaluated at multiple points in the parameter space, e.g., a quadratic function changes its slope at different points hence is not linear. Thus, a simple check for linearity is to re-evaluate the local derivatives at different reference points. Further, since the deterministic and

stochastic approaches for propagating uncertainties both rely on the evaluation of the function at multiple points around a reference point, one should expect the results of these analyses to be the same if the reference point changes, assuming the function is indeed linear. Let the reference point be changed as follows  $\sigma_1 = \sigma_0 + d\sigma$ . If the model is linear then:

$$\begin{aligned} y(\sigma_1 + d\sigma_i) - y(\sigma_1) &= \mathbf{S}d\sigma_i \\ &= y(\sigma_0 + d\sigma + d\sigma_i) - y(\sigma_0 + d\sigma) \\ &= y(\sigma_0 + d\sigma_i) - y(\sigma_0) \end{aligned}$$

If this condition is not satisfied, the implication is that the higher order derivatives are not negligible. Therefore, it is the goal of this study to employ rigorous tests for linearity to assess whether modeling assumptions introduce negligible variations on the propagated cross section uncertainties.

Typical linearity tests employ the one-at-a-time approach. This approach could be misleading, depending on the type of nonlinear terms available. For illustration, consider the following simple parametric models

$$y = ax_1^2 + bx_2^2 + cx_1 + dx_2 + e \quad \text{and} \quad y = ax_1 + bx_1x_2 + cx_2 + e$$

The first model will show nonlinear behavior if one variable is kept constant and the other is changed, however the second model will always display linear behavior. To avoid this, we propose another approach in which a random direction in the parameter space is selected and the model response variation along this direction is analyzed. The process is repeated multiple times. If the model has any nonlinearity, it will be discovered by analyzing the model behavior along one or more of these random directions. To explore the effect of the reference point, another random vector is selected to randomize the selection of the reference point around which linearity is tested.

Mathematically, this is described as follows:

```

For  $i = 1, \dots, N_i$ ,
    Select  $d\sigma_i$ ,
    For  $j = 1, \dots, N_j$ ,
        Select  $dz_j$ ,
        For  $k = 1, \dots, N_k$ ,
            Select  $\alpha_k$ ,
             $y(\sigma_0 + d\sigma_i + \alpha_k dz_j) - y(\sigma_0 + d\sigma_i)$ ;
        End;
    End;
End.

```

The outermost loop selects  $N_i$  random reference point. The second loop selected  $N_j$  random directions along which the model behavior is to be analyzed. The innermost loop, for a given reference point, performs  $N_k$  point evaluation of the function along the selected direction, with each point determined using a different scalar  $\alpha_k$ . This produces a total of  $N_i \cdot N_j$  scatter plots. If any of them shows appreciable nonlinear behavior based on some preset error tolerance, then the model is judged to be nonlinear. Further analysis of these plots could help identify the source of nonlinearity. However, this will be considered outside scope of this work, as our goal is to establish whether the linearity assumption is valid.

### 5.3.2 Evaluation of modeling uncertainty impact

The quantification of modeling uncertainties is conceptually more difficult than the quantification of parameter uncertainties in general. This follows because the quantification of parameter uncertainties is concerned with characterizing the variations in the responses of interest due to variations in the model parameters. This is a straightforward task if one has good estimate of the model parameters prior uncertainties, and can be accomplished via a brute force approach in which the model is executed numerous times with different parameter samples. The challenge is typically computational in nature, that's how to reduce the cost of the required model runs to

obtain full PDFs for the responses of interest. Modeling uncertainties however are concerned with characterizing the differences between model predictions and real behavior which is unknown, and can only be estimated using experimentally-based UQ. Evidently, it is not practical to run experiments for all conditions expected during operation, which renders the quantification of modeling uncertainties a conceptually difficult endeavor.

Fortunately, neutronic modeling is extremely well-understood using both probabilistic and deterministic treatments, i.e., respectively the Monte Carlo particle tracking and the integro-differential Boltzmann equation. For example, the Monte Carlo method employing Continuous Cross-sections (denoted for short by MC) has been well validated against real measurements, and is considered by the neutronic community to be the gold standard for radiation transport for a wide range of applications, e.g., reactor and shielding calculations, criticality safety, etc. The implication is that one can rely on MC to estimate modeling uncertainties for a given radiation transport model, e.g., multi-group SN method, by simply comparing the given model predictions against those estimated by MC. This represents the rationale of our approach. Our focus will be on reactor core-wide simulation, where the input parameters represent the few-group parameters determined via homogenization of the cross-sections at various local core conditions using lattice physics calculations. The idea is to use an MC model to calculate reference values for the few-group parameters.

The impact of modeling uncertainties can then be assessed by propagating parameter uncertainties using different reference values as calculated by deterministic models with various modeling assumptions, e.g., using different group structure, different resonance treatment model, etc. This approach, while rudimentary and straightforward, has not been attempted before in the literature; it will serve to develop the initial insight required to assess the impact of modeling uncertainties on the propagated nuclear data uncertainties, and help develop the best strategy for the simultaneous propagation of both sources of uncertainties.

### ***Modeling assumptions in few-group parameter uncertainty propagation***

The following modeling assumptions will be explored to provide an initial estimate of their impact on the propagated cross-sections uncertainties.

Firstly, the UQ approach itself introduces some assumptions, whose impact on the propagated uncertainties has not been documented in the literature. Just like modeling radiation

transport, uncertainties can also be propagated using either probabilistic (stochastic) or deterministic approach. The stochastic approach relies on a brute force random sampling of the parameter values and repeating code execution to build the PDF of the responses of interest. In the deterministic treatment, the goal is to calculate features of the PDF rather than the entire PDF, with features representing key statistical metrics, such as mean values and standard deviation and covariance information. Each of the two treatments comes with its own assumptions, of which two assumptions are relevant to our context.

The second assumption is related to the choice of the mean values of the few-group parameters. Since we will employ a stochastic approach for the propagation of the multi-group cross-sections to the few-group parameters, one expects to get many samples of the few-group parameters. These samples have to be condensed into a vector of mean values and a covariance matrix, which can later be used to propagate uncertainties through downstream core-wide calculations. The vector of mean values for the few-group parameters will not generally be equal to the reference values generated without perturbations. This implies that even with the same lattice physics code, the use of deterministic vs. stochastic approaches for uncertainty analysis is expected to give rise to variations in the mean values of the few-group parameters. Note that with deterministic techniques, the mean values are taken to be equal to the reference values and one only propagates the second moment of the distribution using the so-called sandwich equation. The sandwich equation employs the derivatives of a model response with respect to the model parameters to estimate the standard deviation of the response as a function of the parameters covariance matrix sandwiched between the so-called sensitivity vector which contains the derivatives of the response.

The third approximation is a result of the uncertainty algorithm employed. This follows because each algorithm has its own assumptions and thus is expected to generate different results. For example, the deterministic uncertainty algorithm, commonly used in the neutronic community, propagates only the second moment, i.e., covariance matrix, of the PDF using first-order approximations. This can be done using either the adjoint or forward differencing to calculate the derivatives of the quantities of interest with respect to sources of uncertainties. If the model exhibits nonlinearities, the propagated uncertainties will be impacted. Stochastic uncertainty algorithms do not enforce the linearity assumption if one can execute the original model for all the random samples. Thus, it is important to compare the propagated uncertainties using both the

deterministic and stochastic algorithms, assuming one uses the same code, the same mean values, and the same covariance matrix to isolate the impact of the uncertainty algorithm.

Further, the reference values are expected to differ based on the lattice physics models employed for their calculation, i.e., MC versus a deterministic model and its inherent assumptions. Another interesting situation is when the computer code used to propagate uncertainties is different from the code used for BE calculations. The implication is that the reference values calculated by the two codes will give rise to a discrepancy term which may have an impact on the propagated uncertainties. This may happen if the discrepancy term is large enough to be outside the linear range of response variations with cross-section, thereby giving rise to nonlinear effects.

The discrepancies in the reference values for the few-group parameters as calculated by two different codes originate from different modeling assumptions and numerical approximations made by the different codes, e.g., one code may use a deterministic multi-group radiation transport solver, while the other relies on continuous cross-section Monte Carlo particle transport methodology. While it is possible to avoid this issue completely by employing the same code, this approach may not always be feasible. This is because the code used to generate the reference cross-sections may be a legacy code or a black-box that is not be amenable for propagation of uncertainties, which requires the introduction of perturbations to a code's inputs. Also the BE code may be too expensive to execute repeatedly for propagating uncertainties, forcing the analyst to use another more efficient fast-executing code. Another reason is that the BE code is validated and qualified in tandem with its own cross-sections, forcing the analyst to set the mean values equal to the best-estimate code cross-sections. Thus, it is important to assess the impact of the choice of the mean values as described by the modeling discrepancy vector on the propagated uncertainties. This is achieved by repeating the propagation of uncertainties using the same computer code, the same uncertainty propagation algorithm, the same covariance matrix, and varying the selection of the mean values based on estimates of the modeling discrepancy vector. Different sources for the modeling discrepancies can be analyzed, e.g., the choice of the energy group structure, the resonance treatment, etc.

#### **5.4 Sensitivity Analysis and Priority Ranking**

A sensitivity study is performed to assess the key contributors to core responses uncertainties and determine the minimum rank  $r$  needed. This sensitivity analysis is useful because it provides

guidance on the key sources of uncertainties. Given the small number of active DOFs at the few-group level, one can employ a one-at-a-time approach to complete the sensitivity analysis, where in each code execution, one increases the number of active DOFs by one to measure their individual impact. This is equivalent to re-evaluating Eq. (5-27) with different  $r$  values to identify the impact of each active DOF.

To characterize the importance of contributions from the uncertainty sources to core responses, the impact of each active DOF is prioritized and ranked to generate a table containing the prioritization of the uncertainty sources.

## 5.5 References

1. Huang, D. and H. Abdel-Khalik, *Theoretical Development of Cross-section Uncertainty Library FOR CORE Simulators*. Journal of Nuclear Engineering and Radiation Science, 2019.
2. Huang, D. and H. Abdel-Khalik. *Construction of optimized experimental responses in support of model validation via physics coverage mapping methodology*. in *Proceedings of PHYSOR*. 2016.
3. Bang, Y., H.S. Abdel-Khalik, and J.M. Hite, *Hybrid reduced order modeling applied to nonlinear models*. International Journal for Numerical Methods in Engineering, 2012. **91**(9): p. 929-949.
4. Wiarda, D. and M. Dunn, *PUFF-IV: A Code for Processing ENDF Uncertainty Data into Multigroup Covariance Matrices*. ORNL/TM-2006/147, Oak Ridge National Laboratory (October 2006), 2006.
5. Parzen, E., *On estimation of a probability density function and mode*. The annals of mathematical statistics, 1962. **33**(3): p. 1065-1076.
6. Park, B.U. and J.S. Marron, *Comparison of data-driven bandwidth selectors*. Journal of the American Statistical Association, 1990. **85**(409): p. 66-72.
7. Wang, C. and H.S. Abdel-Khalik, *Exact-to-precision generalized perturbation theory for eigenvalue problems*. Nuclear Engineering and Design, 2013. **256**: p. 130-140.
8. Turinsky, P.J., et al., *NESTLE: Few-group neutron diffusion equation solver utilizing the nodal expansion method for eigenvalue, adjoint, fixed-source steady-state and transient problems*. 1994, EG and G Idaho, Inc., Idaho Falls, ID (United States); Los Alamos National ....
9. Huang, D., et al., *Dimensionality reducibility for multi-physics reduced order modeling*. Annals of Nuclear Energy, 2017. **110**: p. 526-540.
10. Le Maître, O. and O.M. Knio, *Spectral methods for uncertainty quantification: with applications to computational fluid dynamics*. 2010: Springer Science & Business Media.
11. Jolliffe, I.T., *Principal components in regression analysis*. Principal component analysis, 2002: p. 167-198.
12. Jaynes, E.T., *Information theory and statistical mechanics*. Physical review, 1957. **106**(4): p. 620.

## **6. APPLICATION TO BWR CORE UNCERTAINTY PROPAGATION AND SENSITIVITY ANALYSIS**

This chapter exemplifies the application of the proposed uncertainty characterization framework based on a boiling water reactor (BWR) system. Multi-group cross-section uncertainties are propagated to the few-group cross-sections through lattice calculations and down to core responses, including the multiplication factor and the power distribution in steady state core calculations. In this chapter, the first section propagates cross-section uncertainty at BWR lattice level and discusses the compression strategies applied on the few-group cross-section uncertainties; the second section presents the results of uncertainty quantification and sensitivity analysis on propagating the compressed few-group cross-section uncertainties to BWR core simulation, followed by a priority ranking of the propagated few-group uncertainties.

Part of the numerical results presented in this chapter are also published in [1-5].

### **6.1 Dimensionality Reduction of Few-Group Cross-Section Uncertainties**

The Physics-guided Coverage Mapping (PCM) methodology [6] discussed in Chapter 4 serves as the strategy of similarity study, which investigates the possibility of an initial reduction on the few-group uncertainty at a wide range of core conditions by exploring the uncertainty correlation structure among various branch models and the base model. The impact of uncertainties introduced by isotope number densities during depletion is also evaluated and discussed via PCM method. The Reduced Order Modeling (ROM) techniques [7, 8] discussed in Chapter 4 are employed to determine a reduced set, referred to as active Degrees Of Freedom (DOFs), of the few-group parameter uncertainties resulting from the multi-group covariance with a preset tolerance [9]. Both PCM and ROM techniques are used to condense the generated samples into a few-group covariance matrix which is later propagated through core simulation.

The BWR model contains five different lattices which represent the axial variations of a fuel assembly, the focus will be on demonstrating the strong correlations existing between the base and the branch cases. As discussed in Chapter 5, branch cases are required for the functionalization of the few-group parameters in terms of local core conditions. Using initially a single lattice model, the first subsection will show the near perfect correlations existing between the base and branch

cases, which is leveraged using PCM methodology to perform an initial reduction of the number of few-group parameters whose uncertainties need to be propagated. The implication is that the uncertainties of the branch cases are perfectly correlated with the base cases and hence need not be evaluated separately. Next, the BWR model numerical experiment is used to determine the number of active DOFs of the few-group parameters and the sensitivity of this number to the number of lattices. This is possible using a BWR model since it contains five different lattice types, representing the natural uranium, dominant, and power shaping lattices, used over the length of the assembly.

The lattice solver will provide two-group assembly-wise homogenized macroscopic cross-section, which serve as cross-section library of NESTLE [10] through Triton-to-NESTLE (T2N) utility. Five types of cross-section reactions including absorption, fission, transport, nu-fission and kappa-fission are collected.

### **6.1.1 BWR lattice model setup**

The single lattice study on branch correlations employs a  $10 \times 10$  representative BWR lattice model [3, 11] illustrated in Figure 6-1, starting with fresh fuel, consisting of 92  $\text{UO}_2$  fuel pins with 4.0% initial enrichment, 14 out of which contain 5.0% gadolinium, surrounded by coolant, and all of which are included in a channel box.

The lattice calculations are completed with SCALE 6.2beta2 code package, inside which TRITON [12] is employed to deplete the fuel from 0 to 70.5 GWD/MTU in 33 burnup steps, and NEWT [13] is employed to solve neutron transport calculations. Multi-group cross-section library for this model follows a 238-group energy structure. Three hundred random samples for the base case and each branch case are generated by SAMPLER [14] to propagate cross-section uncertainties from the multi-group level to few-group level based on the 56-group covariance library [15] included in SCALE. The 56-group covariance library contains uncertainty information for 402 nuclides, assumed to represent the best state of knowledge about the cross-sections. These covariance library is propagated from the point-wise continuous cross-sections in the ENDF/B-VII.1 library. This covariance library is considered by current practitioners to be adequate for thermal reactors, and is used as the basis for criticality safety and benchmarking of reactor physics models [15]. It is however important to remark here that the quality of the uncertainties in the 56-group covariance library is expected to impact the reliability of any uncertainties propagated

through downstream calculations, e.g., core-wide calculations. For example, if the uncertainties of the ENDF/B data are only available at few temperatures, the uncertainties of the multi-group data will be impacted by how these measurements are employed to characterize uncertainties at the wide range of temperatures expected in real reactor operation. Our goal in this thesis is to focus on the computational tasks required to propagate uncertainties from the multi-group representation, under the reservation that the multi-group cross-sections represent an acceptable measure of uncertainties. Future work should look into the impact of this assumption of the propagated uncertainties. For example, Section 6.1.2 shows that there exists huge correlation between the base and the fuel temperature branch cases. This could be because the uncertainties in the ENDF library are only available at few temperatures. With new ENDF/B evaluations, further analysis could be used to reveal the impact of new measurements on the reliability of the propagated uncertainties. This is however considered outside the scope of this research.

Five types of reaction, absorption, fission, transport, nu-fission and kappa-fission cross-sections are recorded. To investigate the correlations among burnups, 11.25, 34.5 and 58.5 GWD/MTU are selected as representative of low, medium, and high burnup respectively.

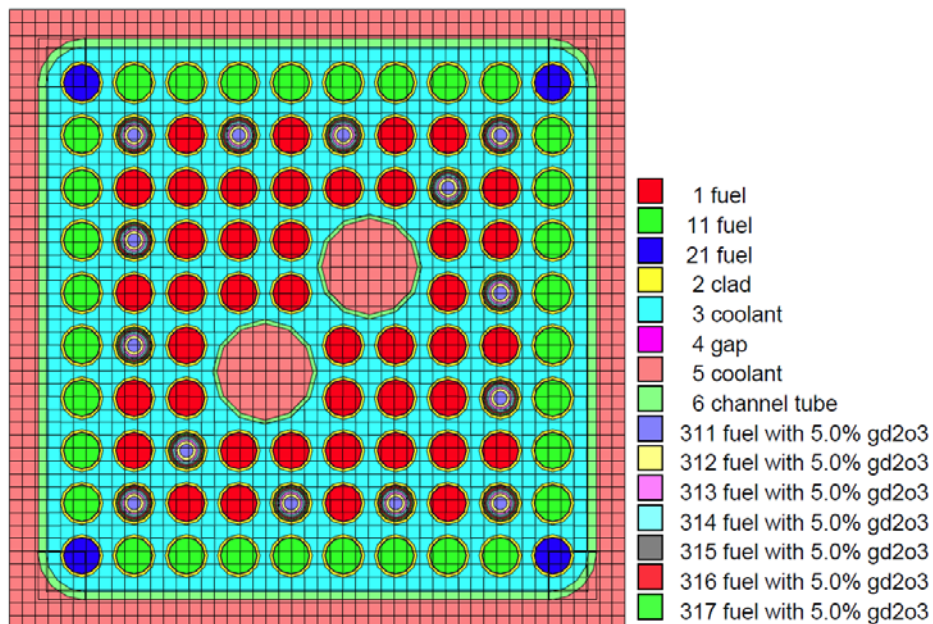


Figure 6-1 BWR lattice model layout by NEWT.

The BWR model contains multiple lattice which provides the means to investigate any possible dependencies. Two BWR lattice models are selected to complete this study. The two

lattices are based on  $7 \times 7$  fuel designs from Peach Bottom Unit 2 cycle 1, 2, 3 [4, 16]. Figure 6-2 and Figure 6-3 depict the layout of Type 3c lattice model and Type 1 lattice model as generated by NEWT. Type 3c lattice consists of 2.50 wt %  $\text{UO}_2$  fuel pins with  $\text{Gd}_2\text{O}_3$  in 5 rods and Type 1 lattice is made up of 1.10 wt %  $\text{UO}_2$  fuel pins without  $\text{Gd}_2\text{O}_3$ .

Both lattices are depleted to 70 GWD/MTU using 32 burnup steps, and the calculations are repeated 96 times using 96 randomized multi-group libraries as generated by SAMPLER. The responses selected for the uncertainty analysis are still the assembly-wise homogenized two-group macroscopic parameters, including the fast and thermal absorption, fission, transport, nu-fission and kappa-fission cross-sections.

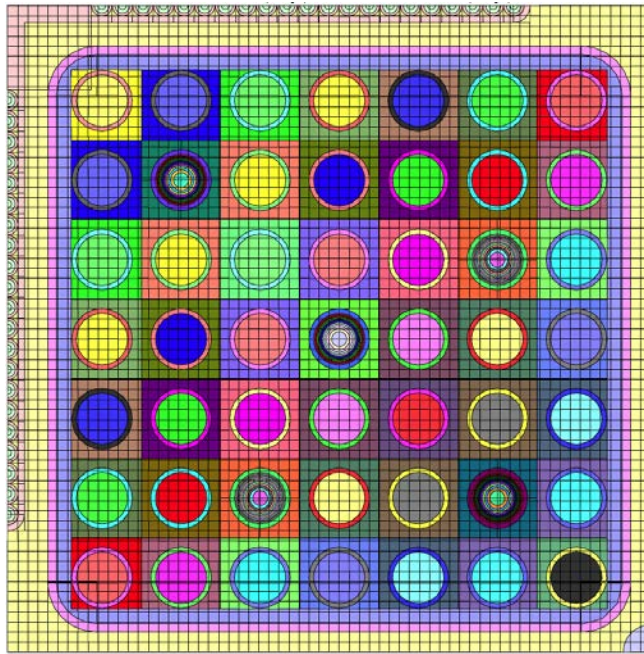


Figure 6-2 Layout of Peach Bottom Type 3c lattice model by NEWT.

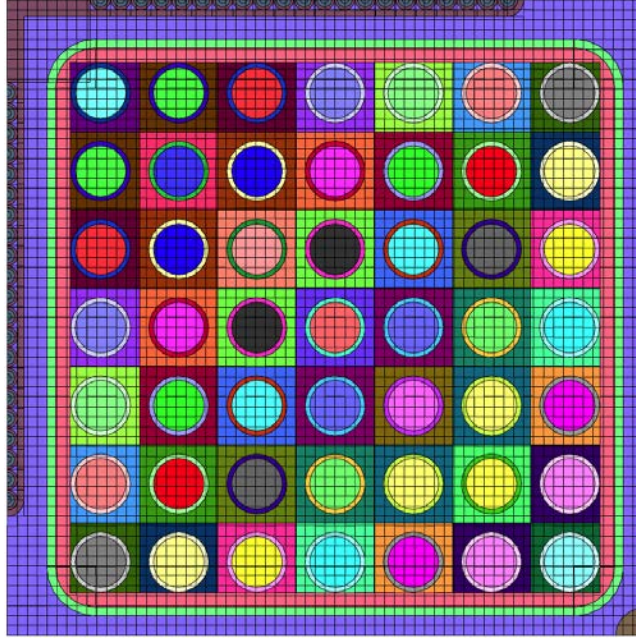


Figure 6-3 Layout of Peach Bottom Type 1 lattice model by NEWT.

### 6.1.2 Branch models impact on few-group uncertainty space

Based on the PCM methodology, the experimental domain will represent the base depletion at a single reference historical condition, and the application domain will represent both the experimental conditions plus branching thereof in terms of moderator voiding, fuel temperature variations and control rod states in this case study. PCM will find a relationship between the experimental (base) and application (one branch condition) responses in the form of Probability Density Function (PDF) for the subsequent mapping of bias.

First, we analyze the correlations between the instantaneous conditions (i.e., branch cases) and the base cases at an intermediate base burnup value with historical 50% voided coolant and 950 K fuel temperature. The responses selected for the uncertainty analysis are the assembly-wise homogenized two-group macroscopic parameters. Although any response can be generated at relatively low cost, only the results of macroscopic fission cross-sections are presented as representative in this manuscript.

Figure 6-4 contains 3D plots of the PCM-determined joint PDFs of the fission cross-sections at the branch cases and those at the base cases. Two representative results of PCM evaluation are shown in Figure 6-4 (a) and (b) at high temperature thermal group branch and high void fast group

branch respectively. All PDFs are centralized around zero by subtracting and dividing by their corresponding mean values, which are listed in Table 6-2. The z-axis represents the value of the PDF whose integral over the uncertainty range is equal to 1.0. Correlations can be visually seen by looking at the scatter plots, which are projections of joint PDF on the x-y plan. Table 6-3 lists the standard linear correlation coefficient between the branch and base cases, whose values vary from 0.89 to 0.99. The linear/Pearson correlation coefficient measures the linear correlation between two variables, ranging from -1 to 1, where 1 indicates perfect positive linearity, 0 presents no linear correlation, and -1 is perfect negative linearity.

Figure 6-4 and Table 6-3 suggest that the branches are perfectly correlated with the base case, implying that the uncertainties for the base cases can be used to predict uncertainties for the branch cases. The indication is that the few-group uncertainties at branch core conditions will not affect the uncertainty propagation in core simulations based on Eq. (5-18), as the branch uncertainties will not increase the uncertainty of the few-group parameter while will only change the reference point. This implication is limited to the tested branch conditions, which applied in the corresponding core simulation, and cannot be extended to prove that all feedbacks have no impact on core simulations. The fuel temperature branch shows fewer variations than coolant void fraction, and cross-sections of a fast group exhibit larger variation than those of thermal group, but the correlation coefficients against base case are all sufficiently close to 1.0.

Table 6-1 List of branch cases at 34.5 GWD/MTU.

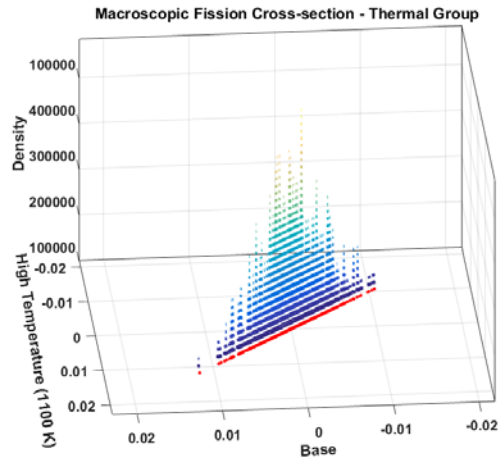
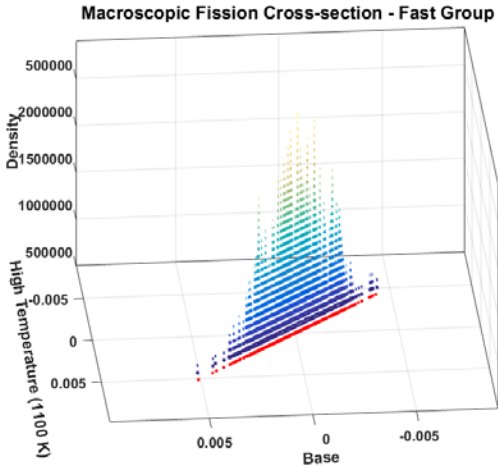
Branch Name	Coolant Void (%)	Fuel Temperature (K)	Control Rod Insertion
Base	50	950	Out
High Void	80	950	Out
Low Void	20	950	Out
High Temperature	50	1100	Out
Low Temperature	50	810	Out
Control Rod Out	50	950	Out
Control Rod In	50	950	In

Table 6-2 Mean values for samples in branch and base calculations.

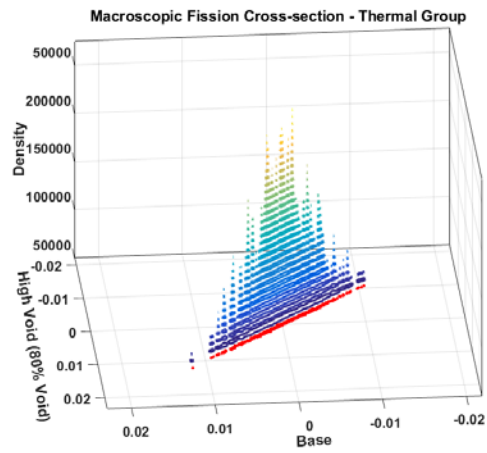
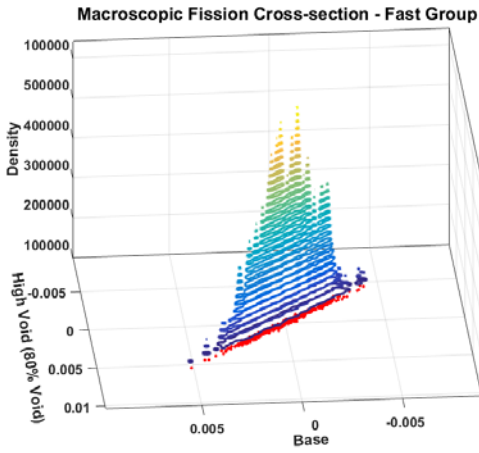
Branch Name	Mean (cm <sup>-1</sup> ) - Group 1	Mean (cm <sup>-1</sup> ) - Group 2
Base – Medium Burnup	0.00157831	0.0351079
High Temperature - Medium Burnup	0.00157656	0.0351144
High Void - Medium Burnup	0.00146860	0.0344346
Control Rod In – Medium Burnup	0.00102106	0.0201783
Base – Low Burnup	0.00229137	0.0427334
Base – High Burnup	0.00122762	0.0271401

Table 6-3 Correlation coefficients of branch vs. base cases.

Correlation Coefficients of Fast Group Fission Cross-Section						
Correlation Coefficient	Base	High Void	Low Void	High Temperature	Low Temperature	Control Rod In
Base	1.0000	0.9952	0.9979	1.0000	1.0000	0.8909
High Void	0.9952	1.0000	0.9868	0.9954	0.9948	0.8669
Low Void	0.9979	0.9868	1.0000	0.9976	0.9981	0.9020
High Temperature	1.0000	0.9954	0.9976	1.0000	0.9999	0.8900
Low Temperature	1.0000	0.9948	0.9981	0.9999	1.0000	0.8917
Control Rod In	0.8909	0.8669	0.9020	0.8900	0.8917	1.0000
Correlation Coefficients of Thermal Group Fission Cross-Section						
Correlation Coefficient	Base	High Void	Low Void	High Temperature	Low Temperature	Control Rod In
Base	1.0000	0.9993	0.9995	1.0000	1.0000	0.9639
High Void	0.9993	1.0000	0.9977	0.9994	0.9992	0.9616
Low Void	0.9995	0.9977	1.0000	0.9994	0.9996	0.9646
High Temperature	1.0000	0.9994	0.9994	1.0000	1.0000	0.9640
Low Temperature	1.0000	0.9992	0.9996	1.0000	1.0000	0.9637
Control Rod In	0.9639	0.9616	0.9646	0.9640	0.9637	1.0000

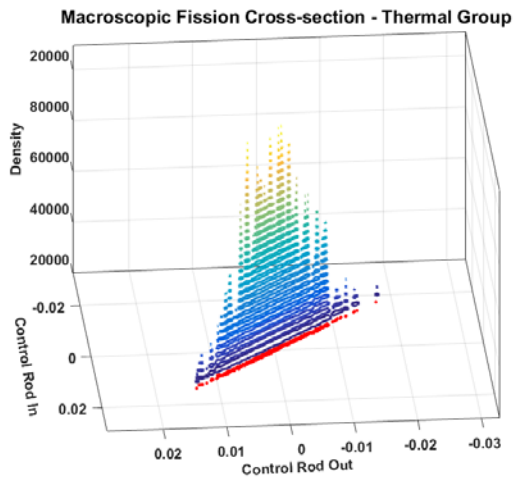
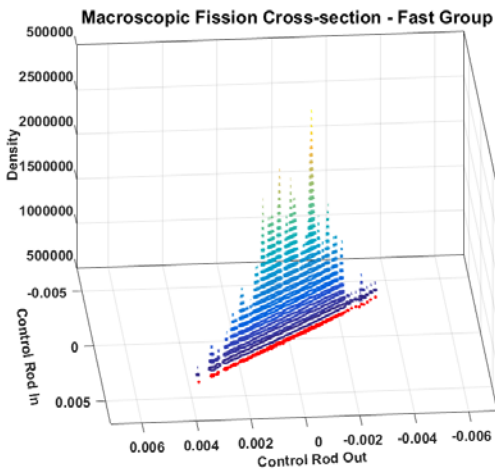


(a) High Temperature Branch vs. Base – Group 1 (b) High Temperature Branch vs. Base – Group 2



(c) High Void Branch vs. Base – Group 1

(d) High Void Branch vs. Base – Group 2



(e) Control Rod In vs. Base – Group 1

(f) Control Rod In vs. Base – Group 2

Figure 6-4 Joint PDFs of fission cross-section - branch vs. base.

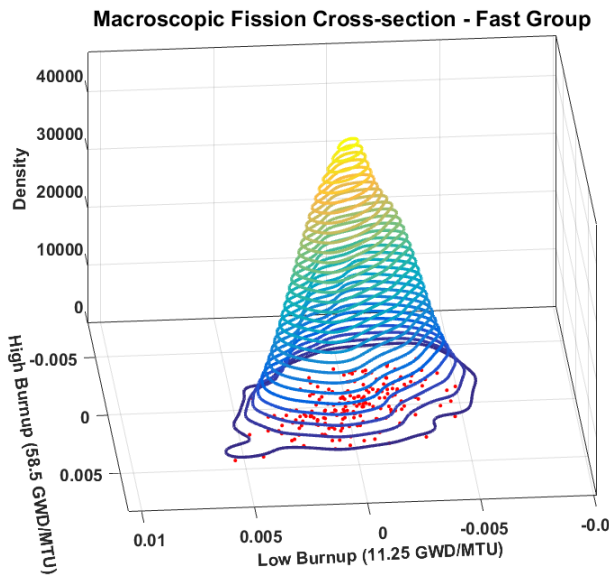
### 6.1.3 Burnup impact on few-group uncertainty space

The correlations between few-group parameters uncertainties evaluated at different burnups are investigated. Here the PCM-designated experimental domain is still the base case at a given burnup, while the application domain is represented by other burnup values. This must be carefully done because the current trend is to perform a single train of depletion and off of that uncertainties in the few-group cross-sections can be evaluated using standard techniques. In doing so, the isotopic concentrations are kept constant as evaluated by the base depletion. In reality, isotopics have their own uncertainties, and they are expected to be correlated across burnup. To illustrate this scenario, we perform two experiments. In the first experiment, the correlations are investigated by assuming the isotopics have no uncertainties, with their values fixed at those predicted by the base depletion. In the second experiment, we include the uncertainties resulting from the isotopics.

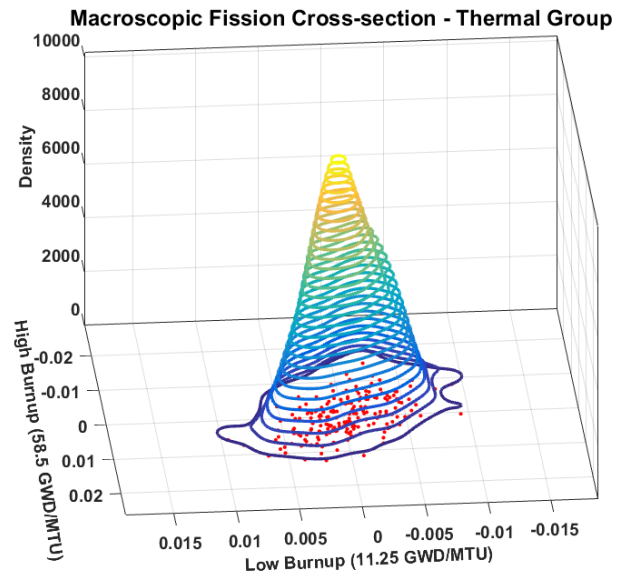
Figure 6-5 and Figure 6-6 present the result of the first experiment in a similar manner to the previous figures/tables. The results suggest the uncertainties are correlated however loosely with correlation coefficients in the order of 0.5. The conclusion from this study is that one must evaluate the uncertainties at all these burnup values since their correlations are not as high as the branch cases. Figure 6-6 shows the results of the second numerical experiment with isotopics uncertainties included. Interestingly, the correlations increase notably by 50%, which highlights a very important remark that is while simplification is typically introduced to reduce the computational cost, they can change the correlation structure, thereby affecting the reliability of uncertainty analysis. Moreover, absent these assumptions, and via a correct implementation of ROM techniques, designed to exploit the high correlations, one can reduce the computational cost without making any assumptions.

Table 6-4 Correlation coefficients of high vs. low burnup cases.

Correlation Coefficient	without Isotopics Uncertainties	with Isotopics Uncertainties
Group 1	0.4793	0.7502
Group 2	0.4832	0.5150

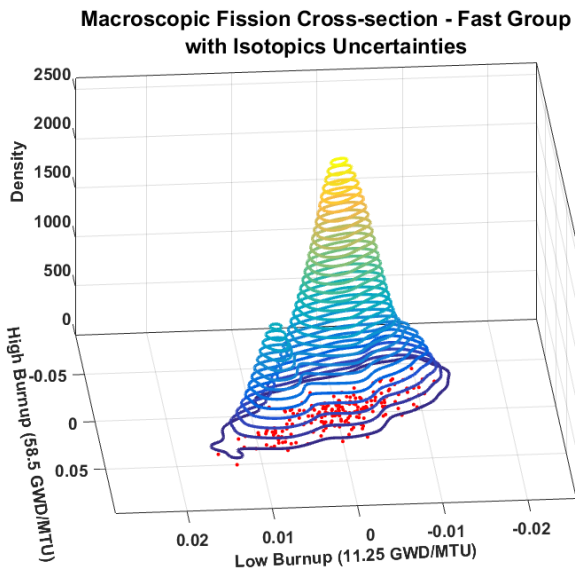


(a) High Burnup vs. Low Burnup - Group 1

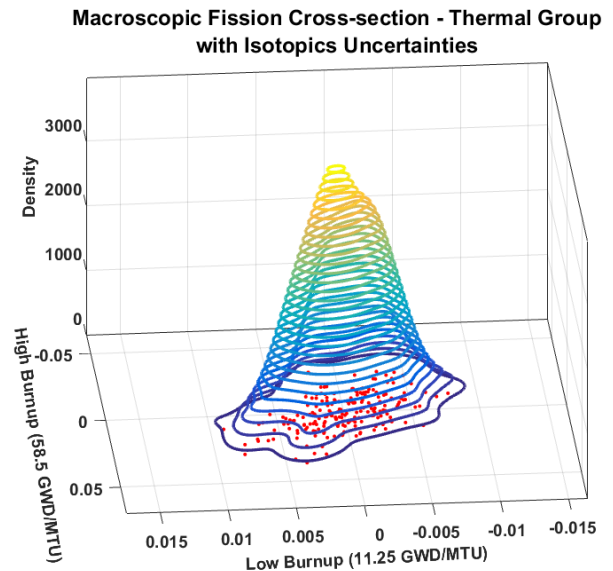


(b) High Burnup vs. Low Burnup - Group 2

Figure 6-5 Joint PDFs of cross-sections of high burnup vs. low burnup.



(a) High Burnup vs. Low Burnup - Group 1



(a) High Burnup vs. Low Burnup - Group 2

Figure 6-6 Joint PDFs of cross-sections of high burnup vs. low burnup – with isotopics uncertainties.

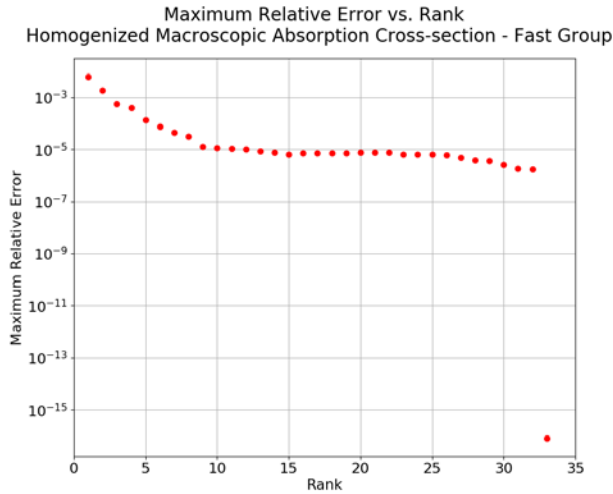
#### 6.1.4 Dimensionality reduction on few-group cross-section uncertainty space

To investigate the reducibility and correlation over burnup steps, ROM techniques are applied to the few-group cross-sections. The  $\mathbf{Y}_{Bu}$  matrix can be constructed as:

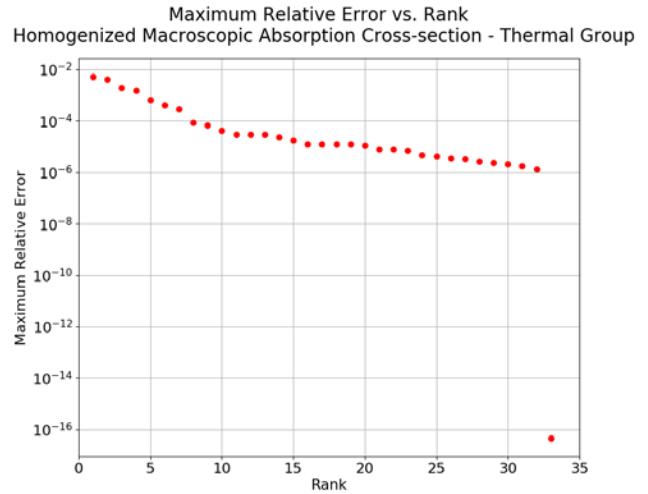
$$\begin{bmatrix} \Sigma_{xg,Bu1,1} & \Sigma_{xg,Bu1,2} & \cdots & \Sigma_{xg,Bu1,200} \\ \Sigma_{xg,Bu2,1} & \Sigma_{xg,Bu2,2} & \cdots & \Sigma_{xg,Bu2,200} \\ \vdots & \ddots & & \vdots \\ \Sigma_{xg,Bu33,1} & \Sigma_{xg,Bu33,2} & \cdots & \Sigma_{xg,Bu33,200} \end{bmatrix} \in \mathbf{R}^{33 \times 200}$$

where subscript  $x$  denotes a certain reaction type,  $g=1,2$  is group number,  $Bui$  represents the burnup step number,  $i=1,2,\dots,33$  since there are 33 depletion steps. Figure 6-7 depicts the results after applying RFA algorithm on the standardized  $\mathbf{Y}_{Bu}$  matrix. We choose homogenized macroscopic absorption and fission cross-section respectively as representatives of certain reaction types and present in the plots. Maximum errors in the figures are calculated by the absolute-value norm of the standardized error matrix ( $\mathbf{Y}_{Bu} - \mathbf{Y}_{Bu,r}$ ). These figures indicate the relationship between errors resulting from the dimensionality reduction and the rank, i.e. reduced dimension, used to reconstruct the model. For a preset user-defined tolerance, the corresponding size of active subspace needed to describe the original space can be obtained from the figure.

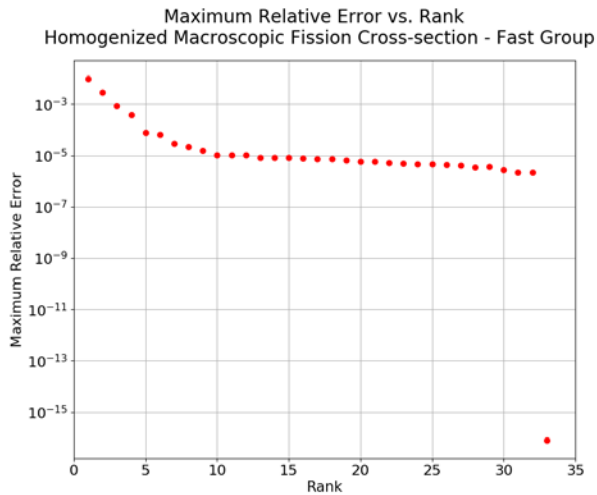
Take the absorption cross-section in thermal group as an example to compare with the original dimension of covariance matrix. Consider burnup dependence only, where reaction type and energy group are fixed, dimension of original covariance matrix for NESTLE cross-section library is  $33 \times 33$ , while the reduced dimension is  $33 \times 5$  for  $\mathbf{U}_r$  and  $5 \times 5$  for  $\mathbf{\Sigma}_r$  with the preset tolerance  $\varepsilon$  is 0.01% as shown in Figure 6-7 (a). Similar behaviors are also indicated from other combination of reaction types and energy groups, suggesting capability of dimensionality reduction in covariance matrix of cross-section library for NESTLE.



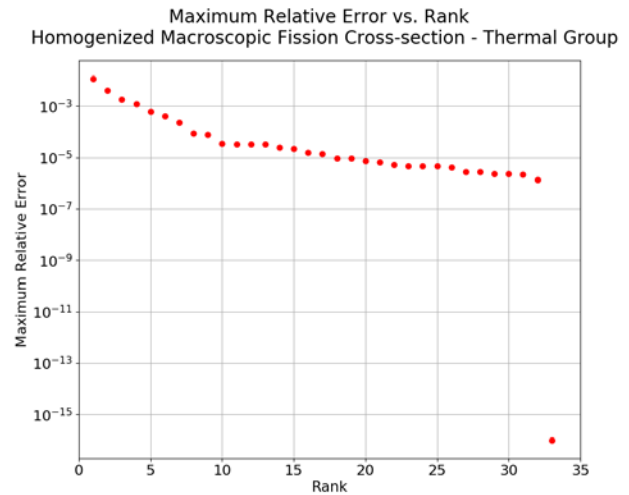
(a) Absorption Cross-Section- Fast Group



(b) Absorption Cross-Section- Thermal Group



(c) Fission Cross-Section- Fast Group



(d) Fission Cross-Section - Thermal Group

Figure 6-7 Error reduction vs. active rank throughout depletion - fixed reaction type and energy group.

The RFA is next applied across burnup steps and all reaction types to investigate the reducibility with fixed energy group. Results of effective rank are shown in Figure 6-8 (a) and (b) for fast group and thermal group cross-sections respectively. The  $Y$  matrix can be presented as:

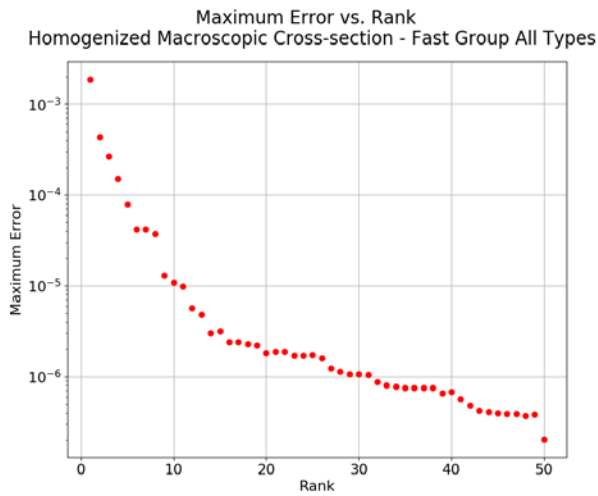
$$\begin{bmatrix}
 \Sigma_{Ab,g,Bu1,1} & \Sigma_{Ab,g,Bu1,2} & \cdots & \Sigma_{Ab,g,Bu1,200} \\
 \Sigma_{Fiss,g,Bu1,1} & \Sigma_{Fiss,g,Bu1,2} & \cdots & \Sigma_{Fiss,g,Bu1,200} \\
 \Sigma_{Tr,g,Bu1,1} & \Sigma_{Tr,g,Bu1,2} & \cdots & \Sigma_{Tr,g,Bu1,200} \\
 \Sigma_{NuFiss,g,Bu1,1} & \Sigma_{NuFiss,g,Bu1,2} & \cdots & \Sigma_{NuFiss,g,Bu1,200} \\
 \Sigma_{\kappa Fiss,g,Bu1,1} & \Sigma_{\kappa Fiss,g,Bu1,2} & \cdots & \Sigma_{\kappa Fiss,g,Bu1,200} \\
 \vdots & & \ddots & \vdots \\
 \Sigma_{Ab,g,Bu33,1} & \Sigma_{Ab,g,Bu33,2} & \cdots & \Sigma_{Ab,g,Bu33,200} \\
 \Sigma_{Fiss,g,Bu33,1} & \Sigma_{Fiss,g,Bu33,2} & \cdots & \Sigma_{Fiss,g,Bu33,200} \\
 \Sigma_{Tr,g,Bu33,1} & \Sigma_{Tr,g,Bu33,2} & \cdots & \Sigma_{Tr,g,Bu33,200} \\
 \Sigma_{NuFiss,g,Bu33,1} & \Sigma_{NuFiss,g,Bu33,2} & \cdots & \Sigma_{NuFiss,g,Bu33,200} \\
 \Sigma_{\kappa Fiss,g,Bu33,1} & \Sigma_{\kappa Fiss,g,Bu33,2} & \cdots & \Sigma_{\kappa Fiss,g,Bu33,200}
 \end{bmatrix} \in \mathbf{R}^{165 \times 200}$$

sweeping with loops for every 200 random samples:

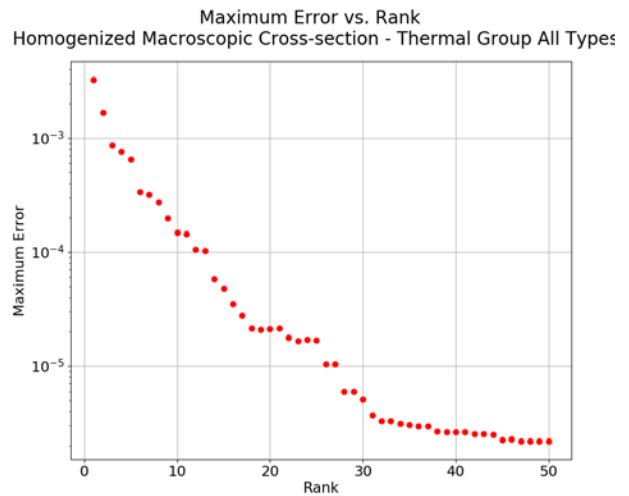
*For each burnup step;*

*For each reaction type.*

For a preset criteria of  $\varepsilon = 0.01\%$ , compared with the original dimension of 33 (burnup steps)  $\times$  5 (reaction types) = 165, active dimension of cross-section for fast group can be reduced to 5, and for thermal group can be reduced to 14.



(a) Fast Group



(b) Thermal Group

Figure 6-8 Error reduction vs. active rank throughout depletion - fixed energy group.

The final investigation on reducibility of cross-section library includes all dependencies on burnup steps, reaction types and energy groups. Results are presented in Figure 6-9. The matrix structure sweeps with loops:

*For each burnup step;*  
*For each reaction type;*  
*For each energy group.*

Figure 6-9 indicates that the effective rank is less than 40 with prior criteria  $\varepsilon = 0.01\%$  considering all dependencies over depletion. Compared to the original parameter dimension of  $33$  (*burnup steps*) $\times 5$  (*reaction types*) $\times 2$  (*groups*) $= 330$ , the record size has been decreased apparently.

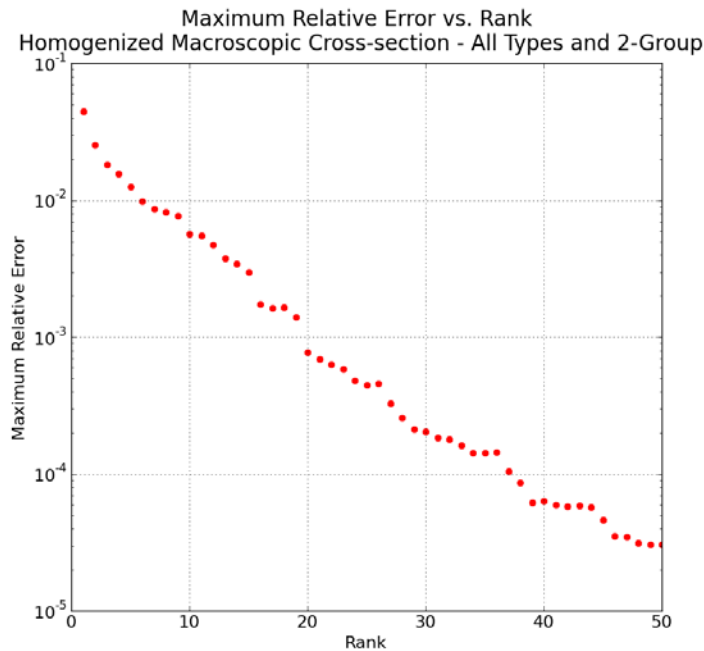


Figure 6-9 Error Reduction vs. Active Rank throughout Depletion – All Reaction Types and Energy Groups Included

### 6.1.5 Multiple lattices impact on few-group uncertainty compression

In order to find the reducibility and correlation across the burnup range, the few-group homogenized macroscopic cross-sections of both Type 3c and Type 1 lattice in all reaction types and energy groups among all burnup steps are collected with the same arrangement, storing in

$\mathbf{Y}_{Type3c}, \mathbf{Y}_{Type1} \in \mathbf{R}^{320 \times 96}$  respectively. The loop sweeps as:

For each burnup step;

For each reaction type;

For each energy group.

The response matrix of multiple lattices  $\mathbf{Y}_{Multiple} \in \mathbf{R}^{640 \times 96}$  is the combination of  $\mathbf{Y}_{Type3c}$  and  $\mathbf{Y}_{Type1}$ . Apply RFA algorithm on uncertainties of both  $\mathbf{Y}_{Type3c}$  and  $\mathbf{Y}_{Multiple} \in \mathbf{R}^{640 \times 96}$ , results of the maximum error resulting from the dimensionality reduction and the rank, i.e. reduced dimension, used to reconstruct the model are depicted in Figure 6-10. With a preset tolerance of relative error 0.1%, the uncertainty space of single lattice is reduced to  $r = 21$ , while of multiple lattices is reduced to  $r = 24$ . This indicates that the size of uncertainty space of few-group cross-sections can be significantly reduced to propagate the uncertainties, and introducing different lattice types will add in only few DOFs to describe the variations of uncertainties. This indicates that the size of uncertainty space of few-group parameters is not significantly impacted due to the introduction of other lattices.

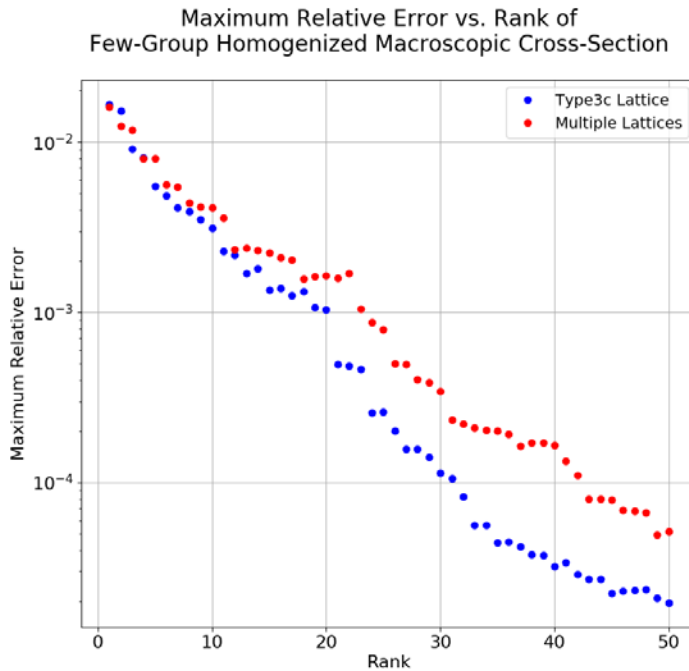


Figure 6-10 Plot of error reduction vs. rank across depletions – all reaction types and energy groups included.

## 6.2 Uncertainty Quantification and Sensitivity Analysis on Core Simulation

Uncertainty quantification (UQ) and sensitivity analysis (SA) results of propagating cross-section uncertainties from the multi-group level to core simulations are presented in this section. The UQ approach employed here is the ROM-based uncertainty propagation implementation.

### 6.2.1 BWR core model setup

The BWR full-core 3D neutronics is modeled by NESTLE, which is a core simulator with few-group neutron diffusion equations spatially discretized utilizing the Nodal Expansion Method (NEM) [10]. Since the full core model is quarter-core symmetry, the model is reduced to quarter its actual size with cyclic inner boundary conditions. 24 axial slices are modeled for the core attributes. There are five BWR assembly layers to model this representative BWR core, Upper Natural, Vanishing, Dominant, Power Shaping and Lower Natural layers from top to bottom. In this preliminary numerical study, we only investigate on the impact of Dominant fuel assembly (Type 3c) layer.

The few-group cross-section library needed for NESTLE core simulation is provided by the TRITON lattice physics calculations. By depleting the lattice model to 70.5 GWD/MTU, all the required cross-sections are available for the quarter-core model. NESTLE reads the 2-group homogenized macroscopic cross-sections output by TRITON in the form of polynomial coefficients as function of each branch cases. The macroscopic cross-section library for NESTLE in a given fuel color, burnup and control rod state can be described in terms of coolant density, coolant temperature, effective fuel temperature and soluble poison number density [10]:

$$\hat{\Sigma}_{xg} = a_{1_{xg}} + \sum_{n=1}^2 a_{(n+1)_{xg}} (\Delta\rho_C)^n + a_{4_{xg}} \Delta T_C + a_{5_{xg}} \Delta\sqrt{T_{F_{eff}}} + \sum_{n=1}^3 a_{(n+5)_{xg}} (\Delta N_{sp})^n$$

where  $x$  and  $g$  represent the reaction type and energy group respectively, and  $a_{j_{xg}}$  are Taylor series expansion coefficients. The definitions of the parameters could be referred to Eq. (5-18).

### 6.2.2 UQ and SA results on BWR core simulation

Analysis in Section 6.1.4 on dimensionality reduction of the few-group cross-section library shows that the active DOFs of uncertainty space is 19 with prior criteria of 0.1% when taking into consideration of all reaction types and energy groups. In the following step, a sensitivity analysis

has been done on the active subspace to determine the importance of each dominant directions on uncertainty analysis. The first 19  $u_i$  vectors are sent through NESTLE respectively and executed by scaling their corresponding singular values by the largest singular value, making the sensitivity analysis on each dominant direction in the same linear range.

Figure 6-11 to Figure 6-14 show the partial or integral uncertainties of representative core attributes, k-effective and axial power shape, versus the burnup. Here “partial” means the contribution to core attributes uncertainty by each individual direction; while “integral” represents the summed contribution to uncertainty by up to the first  $k$   $u_i$  vectors.

Figure 6-11 shows the uncertainty of k-effective that each  $u_i$  vector will add in, from which we can tell that the individual  $u_i$  vector will add in no more than 20 pcm (1/5 of the grid) uncertainty after the first 5 dominant directions. Figure 6-12 indicates that the integral uncertainty of k-effective will change within 10 pcm with more than 10 dominant directions.

In Figure 6-13 and Figure 6-14, sensitivity analysis on axial power shape uncertainties are presented with representatives in bottom, middle and top layer respectively in (a), (b) and (c). Larger power shape uncertainties are detected in top layers. These figures suggest that around 13 dominant directions might be important to uncertainty analysis on axial power shape.

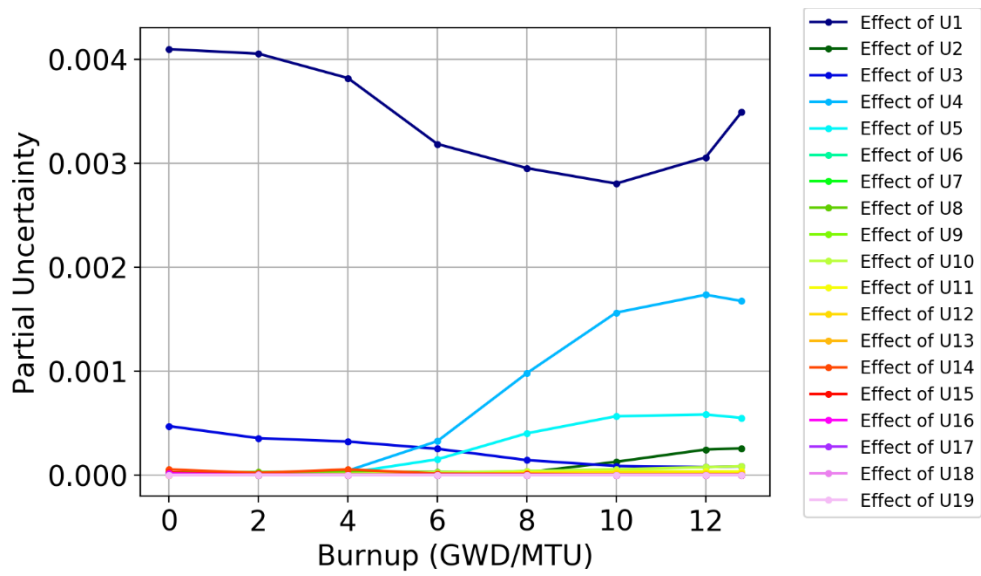


Figure 6-11 Partial uncertainty of k-eff along burnup.

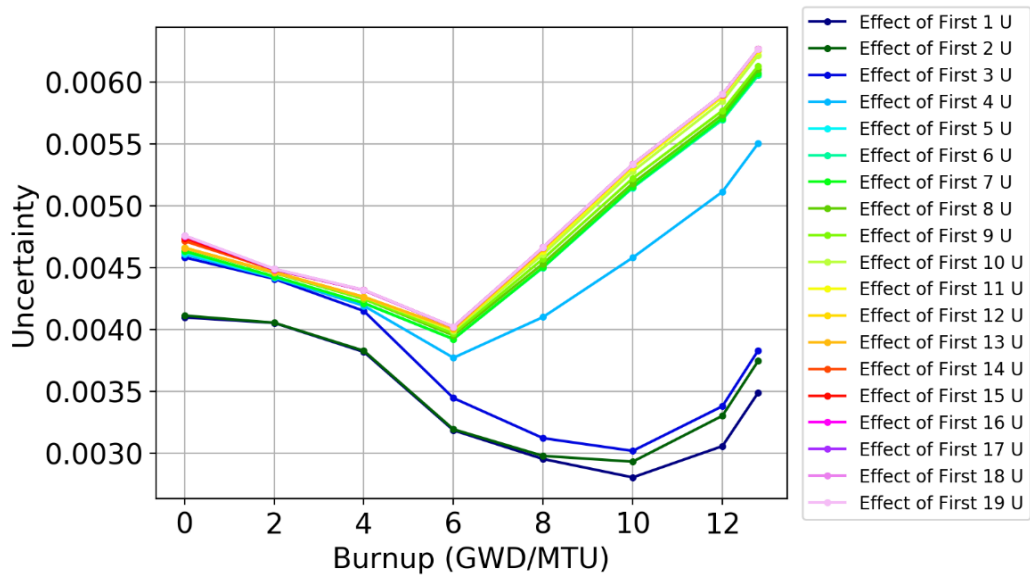
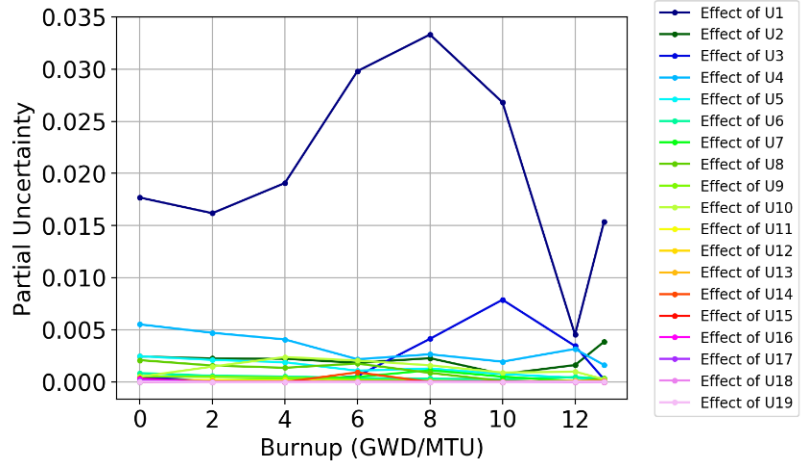
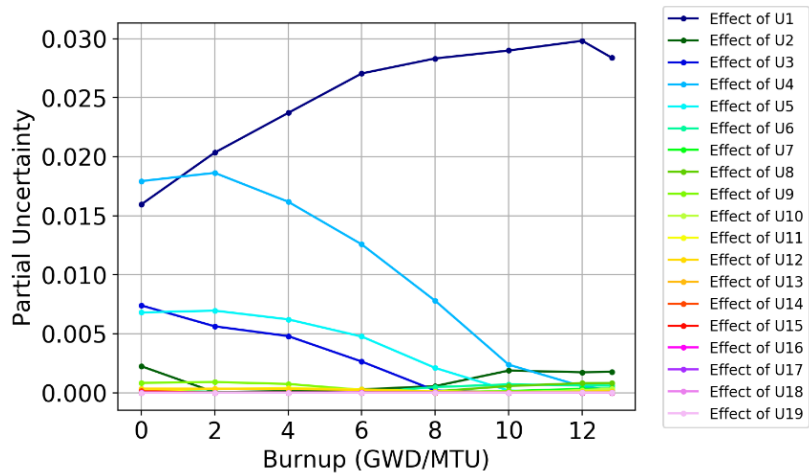


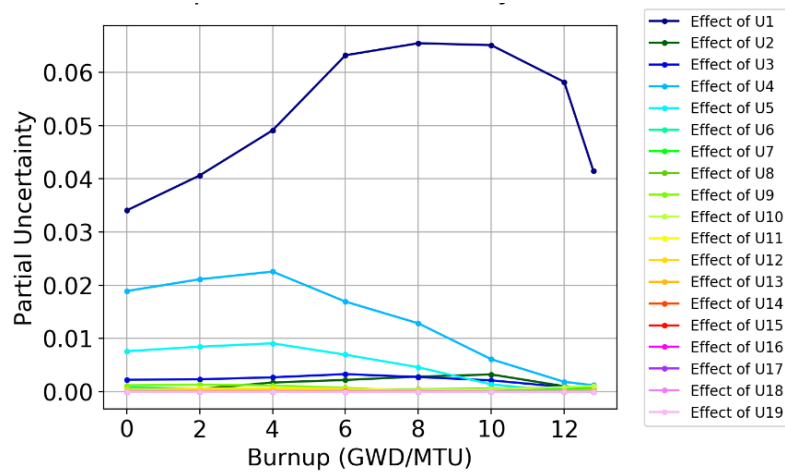
Figure 6-12 Integral uncertainty of k-eff along burnup.



(a) Axial Zone 6 (Bottom Layer)

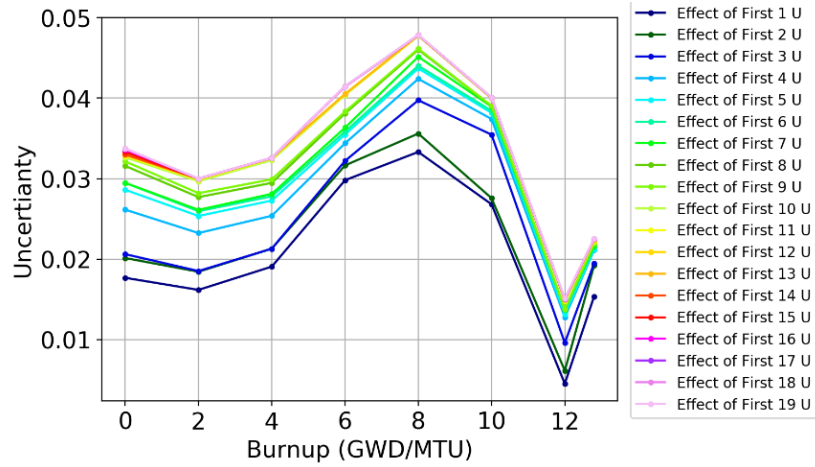


(b) Axial Zone 15 (Middle Layer)

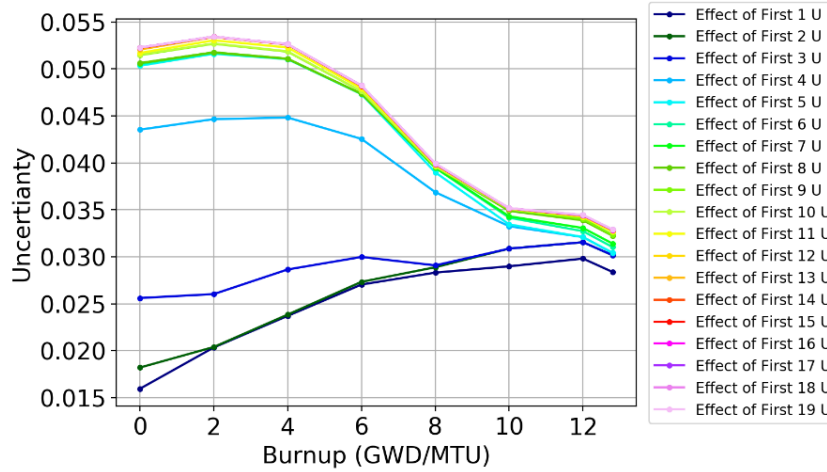


(c) Axial Zone 25 (Top Layer)

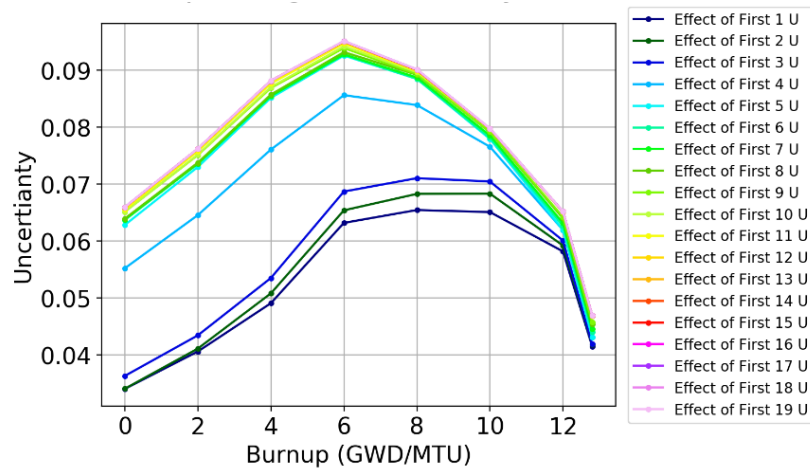
Figure 6-13 Partial uncertainty of axial power shape along burnup.



(a) Axial Zone 6 (Bottom Layer)



(b) Axial Zone 15 (Middle Layer)



(c) Axial Zone 25 (Top Layer)

Figure 6-14 Integral uncertainty of axial power shape along burnup.

### 6.2.3 Priority ranking on major few-group uncertainty sources

To characterize the individual importance of each  $u_i$  vector to different responses, the impact of each direction is prioritized and ranked. There are 24 axial nodes in the NESTLE model, numbered from 4 to 27. Thus, the responses are uncertainties of k-effective as well as these 24 axial powers. Table 6-5 provides a summary of ranked importance of first 19  $u_i$  vectors. Rank “1” represents “the most important”, and rank “19” represents “the least important”. The table indicates that the first 14 directions are important, and we might be able to get rid of the 11<sup>th</sup> to 13<sup>th</sup> U vectors when doing uncertainty analysis on k-effective and axial power shape.

Based on all the results above, we conclude that 14 vectors are important to constrain a 0.1% uncertainty in core simulation.

Table 6-5 Priority ranking for individual  $u_i$  vector to k-eff or axial power shape uncertainties.

	k_eff	Node 4	Node 5	Node 6	Node 7	Node 8	Node 9	Node 10	Node 11	Node 12	Node 13	Node 14	Node 15
<b>Effect of U1</b>	1	1	1	1	1	1	1	1	1	1	1	1	1
<b>Effect of U2</b>	5	2	3	3	3	3	3	4	4	5	5	5	5
<b>Effect of U3</b>	4	4	4	4	4	6	7	8	7	4	4	4	4
<b>Effect of U4</b>	2	3	2	2	2	2	2	2	2	2	2	2	2
<b>Effect of U5</b>	3	5	5	6	5	4	4	3	3	3	3	3	3
<b>Effect of U6</b>	15	8	8	8	8	8	6	5	5	7	7	7	7
<b>Effect of U7</b>	12	9	10	9	9	10	10	11	12	12	12	12	11
<b>Effect of U8</b>	7	6	6	7	7	7	9	9	10	9	9	8	8
<b>Effect of U9</b>	8	10	11	10	10	9	8	6	6	6	6	6	6
<b>Effect of U10</b>	6	7	7	5	6	5	5	7	8	8	8	10	12
<b>Effect of U11</b>	10	12	13	12	11	11	11	10	9	10	10	11	10
<b>Effect of U12</b>	11	13	12	13	12	12	12	12	11	11	11	9	9
<b>Effect of U13</b>	19	16	17	17	18	18	16	14	13	13	13	14	14
<b>Effect of U14</b>	9	11	9	11	13	13	13	13	14	14	14	13	13
<b>Effect of U15</b>	13	14	14	14	15	16	17	17	17	17	18	18	18
<b>Effect of U16</b>	14	15	15	15	14	14	14	15	15	16	17	17	16
<b>Effect of U17</b>	17	17	16	16	16	15	15	16	16	15	15	15	15
<b>Effect of U18</b>	16	19	18	19	19	19	19	19	18	19	19	19	19
<b>Effect of U19</b>	18	18	19	18	17	17	18	18	19	18	16	16	17

Table 6-5 continued

	Node 16	Node 17	Node 18	Node 19	Node 20	Node 21	Node 22	Node 23	Node 24	Node 25	Node 26	Node 27
<b>Effect of U1</b>	1	1	1	1	1	1	1	1	1	1	1	1
<b>Effect of U2</b>	5	5	3	2	5	5	5	5	5	5	5	5
<b>Effect of U3</b>	4	4	4	9	4	4	4	4	4	4	4	4
<b>Effect of U4</b>	2	2	2	4	2	2	2	2	2	2	2	2
<b>Effect of U5</b>	3	3	5	6	3	3	3	3	3	3	3	3
<b>Effect of U6</b>	8	11	12	10	8	8	8	7	7	8	8	8
<b>Effect of U7</b>	11	9	8	7	12	12	12	12	12	12	12	12
<b>Effect of U8</b>	6	6	7	8	9	9	9	9	8	7	7	7
<b>Effect of U9</b>	7	12	13	5	7	6	6	6	6	6	6	6
<b>Effect of U10</b>	12	7	6	3	6	7	7	8	9	9	9	10
<b>Effect of U11</b>	10	10	11	12	11	11	11	10	10	10	10	9
<b>Effect of U12</b>	9	8	10	13	10	10	10	11	11	11	11	11
<b>Effect of U13</b>	15	15	17	18	16	15	14	14	14	14	14	14
<b>Effect of U14</b>	13	13	9	11	13	13	13	13	13	13	13	13
<b>Effect of U15</b>	18	16	15	14	17	17	17	17	17	17	17	17
<b>Effect of U16</b>	14	14	14	15	14	14	15	15	15	15	15	15
<b>Effect of U17</b>	16	18	16	16	15	16	16	16	16	16	16	16
<b>Effect of U18</b>	19	19	19	19	18	18	18	18	18	18	18	18
<b>Effect of U19</b>	17	17	18	17	19	19	19	19	19	19	19	19

### 6.3 Conclusions

To overcome the computational expense of uncertainty propagation due to cross-sections in core simulation, this chapter investigates the correlations among branch and base calculations throughout depletion for lattice physics calculations.

Results show near perfect correlations between the branch cases, and weaker correlation across burnup. Interestingly, the results of uncertainty mapping between different burnup states indicate that ignoring burnup correlations which may be attempted to simply the uncertainty representation (i.e., assuming uncertainties are independent across burnup) over-estimates the true number of degrees of freedom across burnup. In reality, burnup introduces correlations in the cross-sections which should be exploited for further reduction of the computational cost.

ROM techniques are further employed to investigate the true dimension of few-group cross-section library for core simulator. Results indicate that the dimension can be reduced without making adhoc assumptions about cross-sections dependencies.

The sensitivity analysis for core attributes with respect to the few-group cross-sections suggests further reduction for the true dimension of the uncertainty space is possible. For a representative BWR core, these results indicate that only a handful of parameters could be used to describe uncertainties of the dominant lattice.

Furthermore, the case study on impact of multiple lattice models on uncertainty propagation in core simulation imply that introducing more lattice types will not result in significant increase of the few-group cross-section uncertainty space.

### 6.4 References

1. Abdel-Khalik, H.S., et al. *Towards Development of Uncertainty Library for Nuclear Reactor Core Simulation*. in *2018 26th International Conference on Nuclear Engineering*. 2018. American Society of Mechanical Engineers Digital Collection.
2. Huang, D. and H.S. Abdel-Khalik. *Development of Uncertainty Quantification Capability for NESTLE*. in *2017 25th International Conference on Nuclear Engineering*. 2017. American Society of Mechanical Engineers Digital Collection.
3. Huang, D., et al. *Efficient Evaluation of Core Simulator Few-Group Cross-Section Uncertainties via PCM*. in *Proceedings of the 2017 ANS Winter Meeting*. 2017.
4. Huang, D., et al., *Further development of few-group cross-section uncertainty quantification techniques for core simulation*. 2018.

5. Huang, D. and H. Abdel-Khalik, *Application of Cross Sections Uncertainty Propagation Framework to Light and Heavy Water Reactor Systems*. Journal of Nuclear Engineering and Radiation Science, 2019.
6. Huang, D. and H. Abdel-Khalik. *Construction of optimized experimental responses in support of model validation via physics coverage mapping methodology*. in *Proceedings of PHYSOR*. 2016.
7. Huang, D., et al., *Dimensionality reducibility for multi-physics reduced order modeling*. Annals of Nuclear Energy, 2017. **110**: p. 526-540.
8. Bang, Y., H.S. Abdel-Khalik, and J.M. Hite, *Hybrid reduced order modeling applied to nonlinear models*. International Journal for Numerical Methods in Engineering, 2012. **91**(9): p. 929-949.
9. Huang, D. and H. Abdel-Khalik, *Theoretical Development of Cross-section Uncertainty Library FOR CORE Simulators*. Journal of Nuclear Engineering and Radiation Science, 2019.
10. Turinsky, P.J., et al., *NESTLE: Few-group neutron diffusion equation solver utilizing the nodal expansion method for eigenvalue, adjoint, fixed-source steady-state and transient problems*. 1994, EG and G Idaho, Inc., Idaho Falls, ID (United States); Los Alamos National Laboratory.
11. George, N.M., *Assessment of Reactivity Equivalence for Enhanced Accident Tolerant Fuels in Light Water Reactors*. 2015.
12. Jessee, M.A. and M.D. DeHart, *Triton: a multipurpose transport, depletion, and sensitivity and uncertainty analysis module*. Oak Ridge National Laboratory, ORNL/TM-2005/39 Version, 2011. **6**.
13. DeHart, M. and M. Jessee, *NEWT: a new transport algorithm for two-dimensional discrete ordinates analysis in non-orthogonal geometries*. ORNL/TM-2005/39, Oak Ridge National Laboratory, 2005.
14. Williams, M.L., et al., *A statistical sampling method for uncertainty analysis with SCALE and XSUSA*. Nuclear technology, 2013. **183**(3): p. 515-526.
15. Marshall, W.B., Williams, M.L., Wiarda, D., Rearden, B.T., Dunn, M.E., Mueller, D., Clarity, J.B. and Jones, E.L., 2015. *Development and Testing of Neutron Cross Section Covariance Data for SCALE 6.2*. Oak Ridge National Lab.(ORNL), Oak Ridge, TN (United States).
16. Larsen, N., *Core Design and Operating Data for Cycles 1 and 2 of Peach Bottom 2*. 1978, General Electric Co., San Jose, CA (USA). Nuclear Energy Engineering Div.

## 7. APPLICATION TO CANDU CORE UNCERTAINTY PROPAGATION

This chapter exemplifies the application of the proposed uncertainty characterization framework based on a CANDU heavy water reactor system. The scope is limited to the propagation of the nuclear data uncertainty starting with the multi-group cross-section covariance matrix and down to core responses, including the eigenvalue and power distribution in both steady state and transient core wide calculations. The focus of this chapter is to demonstrate how to employ the reduction technique to compress the few-group uncertainty space of CANDU reactor into a very small number of active Degrees Of Freedoms (DOFs) which renders the overall process computationally feasible.

A CANDU-6 model containing single type of lattice is employed as case study. Different from the BWR application with only the few-group cross-section uncertainties propagated, the CANDU application propagates all few-group parameter uncertainties, including the cross-sections, Assembly Discontinuity Factors (ADFs), neutron velocities, and transient parameters. Based on the results from the BWR study, the branch cases are taken to be perfectly correlated with the base depletion case, which allows one to considerably reduce the size of the few-group parameters uncertainty space. Over burnup, the correlations are strong, however not high enough to allow one assume perfect correlation. Thus, ROM techniques are employed to condense the uncertainty space as described in Section 5.2.3. The compressed few-group parameters covariance matrix is propagated to the steady state CANDU-6 core simulation in both deterministic and stochastic manners to compare both approaches.

The first section explores the dimensionality reduction of few-group parameters uncertainty space in terms of the correlations in a wide range of core conditions and across burnup, as well as the ROM-based compression results on the few-group parameter uncertainty space. The second section reports the uncertainty quantification results on core responses of interest, i.e. core multiplication factor, core coolant void reactivity (CVR) and core power distribution, with uncertainty propagation from the compressed few-group parameter uncertainties in both steady-state and transient scenarios.

Part of the numerical results presented in this chapter are also published in [1].

## **7.1 Dimensionality Reduction of Few-Group Parameter Uncertainties**

CANDU-6 has a single lattice type which considerably simplifies the analysis as compared to a Light Water Reactor (LWR) core model which could contain up to a few dozen lattice types. For this phase-one project, the focus will be on estimating the k-eff and the channel power distribution as calculated by the NESTLE-C core simulator [2]. The UQ exercise begins with the uncertainties at the multi-group level, specifically a 56-group format as processed by a previous study conducted by ORNL [3], wherein a 56-group covariance library is generated based on a representative thermal reactor spectrum. One could question the validity of this covariance matrix for CANDU analysis since its production involves a number of modeling assumption and approximation as well, e.g., the choice of the flux weighting used to condense the cross-sections from continuous to multi-group format. This however will be considered outside the scope of this phase-one project.

Lattice physics calculations are employed to propagate the multi-group uncertainties to the few-group uncertainties using the SCALE NEWT and SAMPLER codes. The SERPENT [4] code is also used to model the CANDU-6 lattice to satisfy two objectives. First, it will serve to verify the accuracy of the NEWT reference cross-sections, since it is based on a probabilistic solution methodology utilizing Monte Carlo radiation transport with continuous cross-sections which represents the gold standard for neutronic calculations. Second, it will provide the means to assess the impact of modeling assumptions on the propagated cross-sections uncertainties, serving to provide initial guidance for the following phases of the project, expected to expand the UCF framework to account for other sources of uncertainties. Also, the few-group cross-sections calculated by earlier studies, using HELIOS [5], will be used as a basis for assessing the impact of modeling errors for the two-group case only.

Finally, the covariance of the few-group cross-sections will be calculated in a condensed format to facilitate its propagation through core simulation using the NESTLE-C code. The reference cross-sections for

### **7.1.1 CANDU-6 lattice model setup**

CANDU-6 lattice contains 37 fuel elements containing natural uranium [5] with heavy water serving as both coolant and moderator, albeit at different temperatures. The heavy water inside the

pressure tubes serves as the coolant at a temperature of 563 K, and the heavy waters outside the pressure tubes acts as moderator at a temperature of 341 K. The CANDU-6 lattice is modeled using SERPENT, KENO-CE [6], and NEWT codes to provide initial estimates of the modeling errors, representing the discrepancies in the estimated few-group cross-sections resulting from different modeling assumptions/approximations.

SERPENT is a Monte Carlo Radiation Transport code with depletion capabilities; it uses the ENDF cross-sections in ACE format, and has a capability to collapse the cross-sections into user-specified energy-group format. For this study, we employ a representative two-group energy boundaries, with the thermal boundary extending to 0.625 eV, and the fast group to 20 MeV. Layout of the lattice is shown in Figure 7-1 as generated by the SERPENT geometry engine. Figure 7-2 shows a similar layout as produced by NEWT.

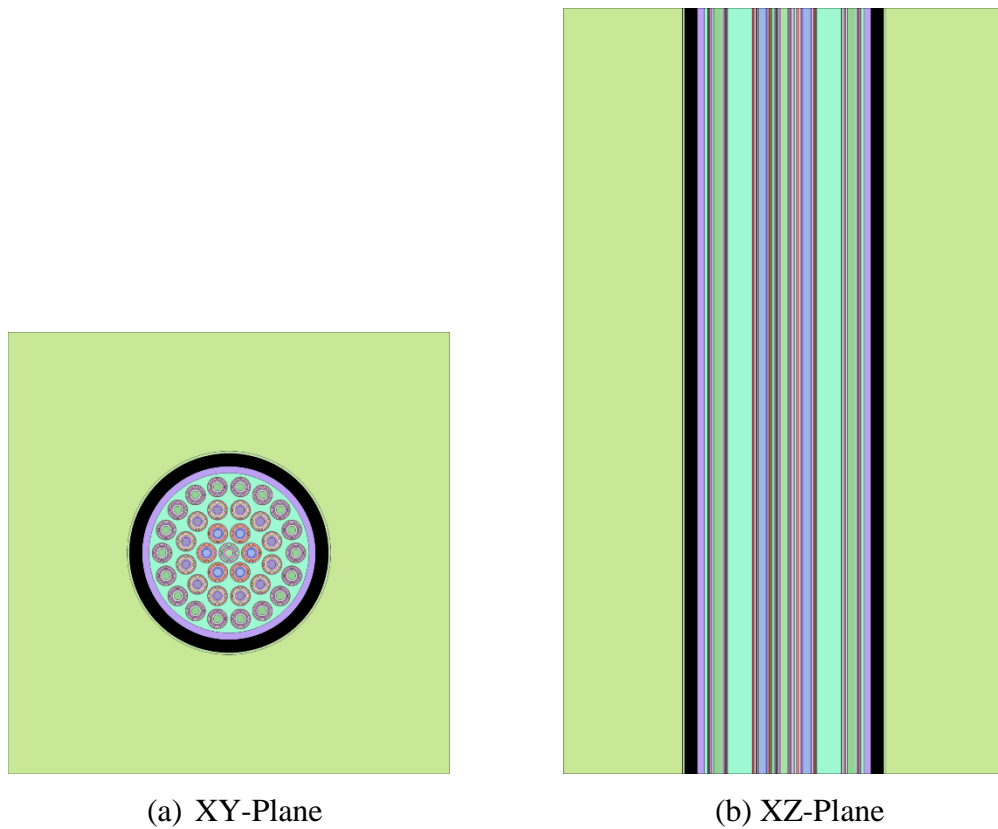


Figure 7-1 Lattice layout by SERPENT geometry engine.

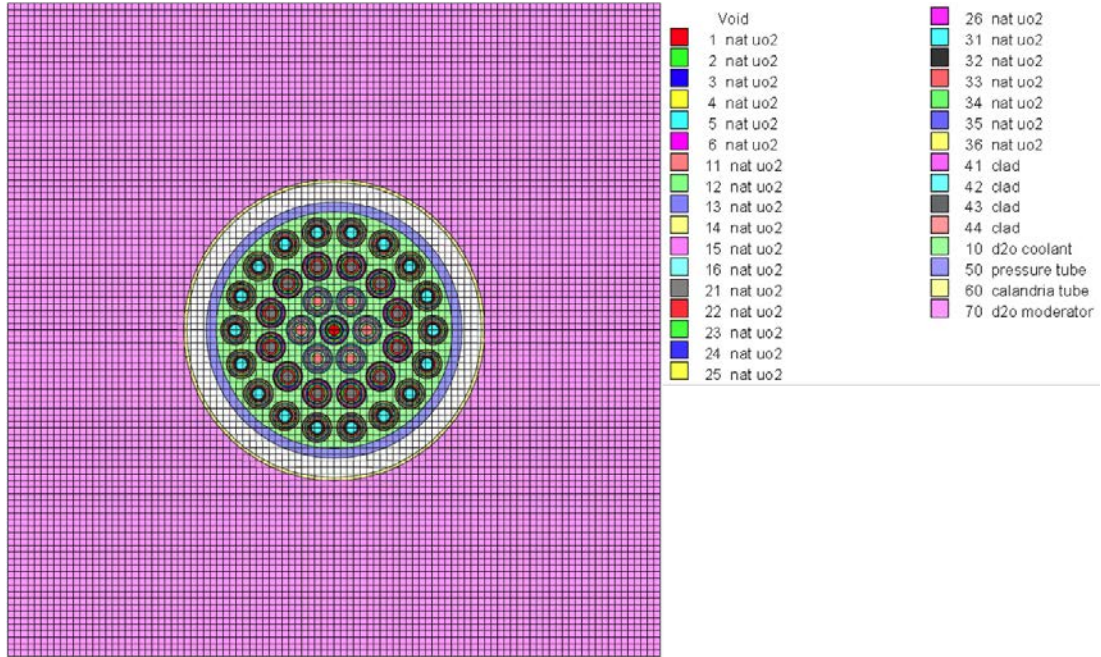


Figure 7-2 Lattice layout by NEWT geometry engine.

To study the impact of the number of few-groups on the propagated core uncertainties, three representative few-group structures, two-, four- and eight-groups are employed, collapsed from 238-group structure in NEWT, and from continuous energy format in SERPENT. The choice of the group boundaries in NEWT suffers from one limitation -- shown in Table 7-1 and compared to SERPENT boundaries -- that the few-group boundaries must be a subset from the multi-group boundaries. SERPENT does not suffer from this limitation since the collapse is done from continuous energy structure. All energy group structures have a lower limit of 0.1 eV and an upper limit of 20 MeV.

Table 7-1 Energy boundaries in few-group structure.

Few-Group Structure	Boundaries [MeV] in SERPENT	Boundaries [MeV] in NEWT
Two-group (2G)	6.25E-7	6.25E-7
Four-group (4G)	6.25E-7	6.25E-7
	1.3007E-4	1.22E-4
	1.8316E-1	2.00E-1
Eight-group (8G)	1.1157E-7	1.00E-7
	6.2506E-7	6.26E-7
	1.3007E-4	1.22E-4
	9.1188E-3	9.50E-3
	1.8316E-1	2.00E-1
	8.2085E-1	9.50E-1
	2.2313	2.3540

### 7.1.2 CANDU few-group parameter uncertainties

The SAMPLER routine is executed to propagate the multi-group uncertainties using the NEWT lattice model. SAMPLER is distributed with 1000 randomly-generated multi-group libraries that are consistent with the multi-group covariance library. The few-group cross-sections covariance matrix may be generated in a brute force manner from these runs using the following expression:

$$\mathbf{C}_{FG} = \frac{1}{N-1} \sum_{i=1}^N \left( \frac{\sigma_i}{\sigma_\mu} - 1 \right) \left( \frac{\sigma_i}{\sigma_\mu} - 1 \right)^T \quad (7-1)$$

$$\text{and } \sigma_\mu = \frac{1}{N} \sum_{i=1}^N \sigma_i$$

where  $\sigma_i$  is a vector of all few-group cross-sections generated using the  $i^{\text{th}}$  randomly-generated multi-group cross-section library, and  $N$  is the number of samples, which is 300 in this case study. In matrix algebra, one cannot divide two vectors, but this abusive notation is used to simplify notation denoting that the covariance is produced in relative units by simply dividing by the mean values of the few-group cross-sections.

Figure 7-3 shows representative set of few-group parameters and their uncertainties as directly calculated by SAMPLER in two-group format. The lines in gold color represent the burnup dependent few-group parameter of the individual samples from NEWT execution, while the red curve is the standard deviation of the corresponding parameter as calculated over all the samples.

Note that in general there are three types of matrices that are typically used to describe the second moments of the responses PDF, referred to as covariance matrices. The first matrix, denoted Type-I, has the square of the units of the response, as it describes the absolute values for the response variances (i.e., square of standard deviations) and covariances thereof. The  $i$ th and  $j$ th element of this matrix can be written in the form:

$$[\mathbf{C}]_{ij}^{Type-I} = \rho_{ij} std_i std_j ,$$

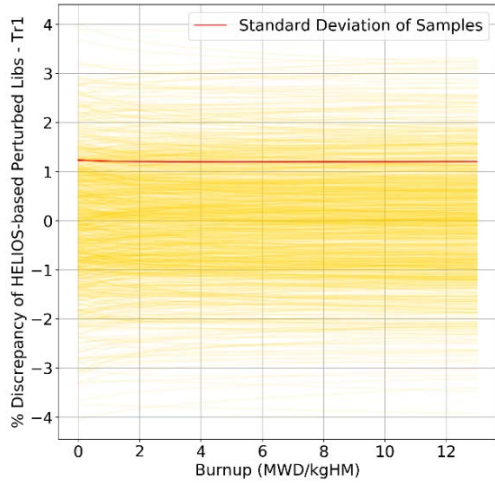
where  $std_i$  is the standard deviation of the  $i^{\text{th}}$  response (this non-conventional notation is used to avoid confusion with the cross-section), and  $\rho_{ij}$  is the standard correlation coefficient between the  $i^{\text{th}}$  and  $j^{\text{th}}$  responses, with values between -1 and 1. The second matrix, denoted Type-II, is unitless, typically referred to as correlation matrix, and is defined by:

$$[\mathbf{C}]_{ij}^{Type-II} = \frac{[\mathbf{C}]_{ij}^{Type-I}}{std_i std_j} = \rho_{ij} ,$$

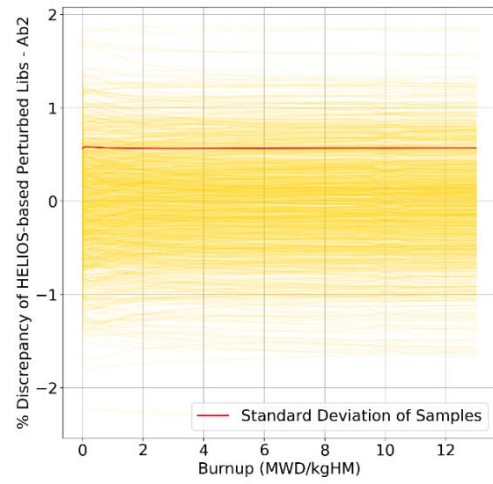
such that all its diagonal elements are equal to 1.0, and the off-diagonal elements are between -1 and 1. This matrix represents a normalized version of the Type-I matrix. Normalization could also be rendered by dividing by the mean values of the responses, resulting in a Type-III matrix, which is the choice selected for our analysis as in Eq. (7-1):

$$[\mathbf{C}]_{ij}^{Type-III} = \frac{[\mathbf{C}]_{ij}^{Type-I}}{mean_i mean_j}$$

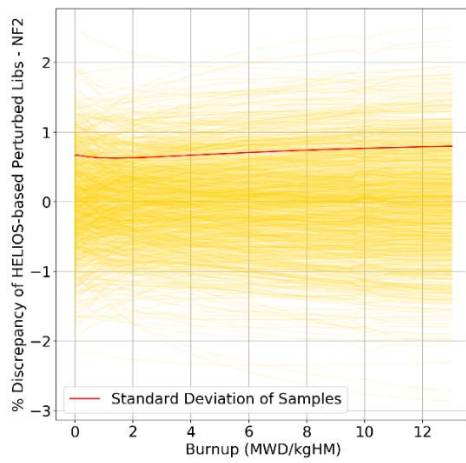
where  $mean_i$  and  $mean_j$  are the mean values for the  $i^{\text{th}}$  and  $j^{\text{th}}$  responses, respectively. This representation is very convenient when working with responses of different units and different ranges. It allows one to design the random samples and/or perturbations as multipliers to the quantities of interest, and provides a meaningful way to compare uncertainties for different responses resulting from different error sources as will be shown later in the discussion.



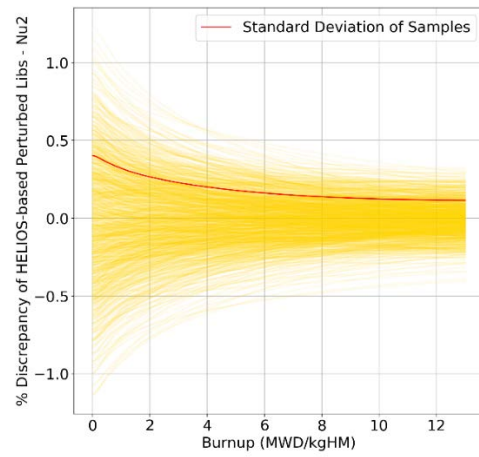
(a) Transport – Group 1



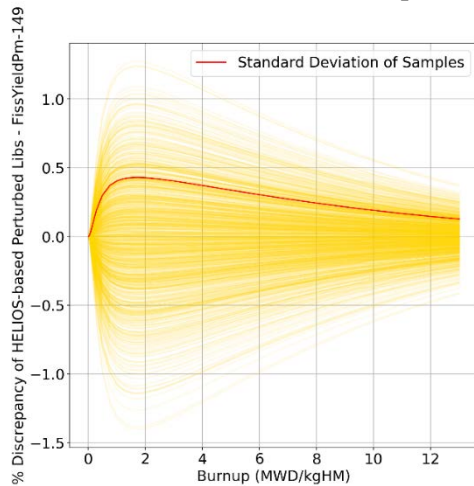
(b) Absorption – Group 2



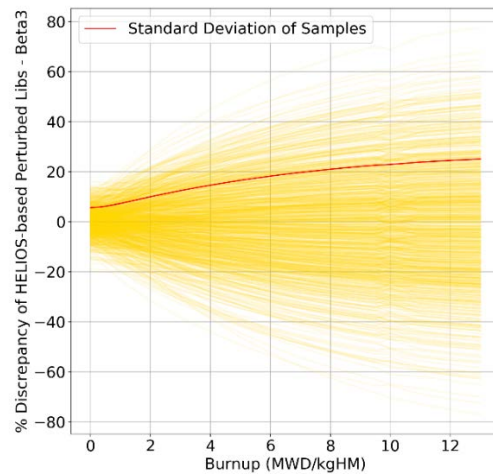
(c) Nu-Fission – Group 2



(d) Nu – Group 2



(e) Fission Yield of Pm-149

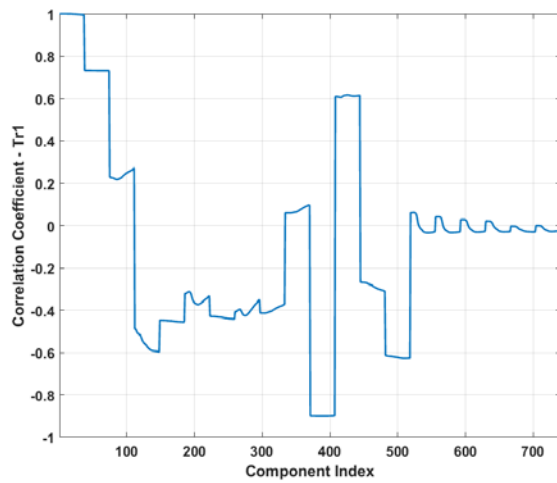


(f) Beta – Group 3

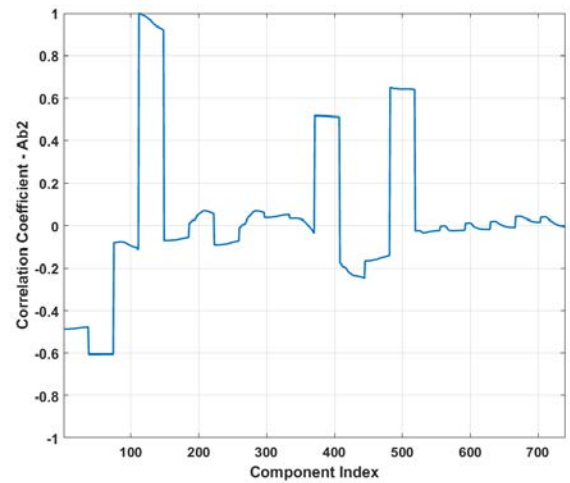
Figure 7-3 Burnup-dependent few-group parameter – parameter values of reference and random samples from SAMPLER.

### 7.1.3 Correlation among few-group parameters along burnup

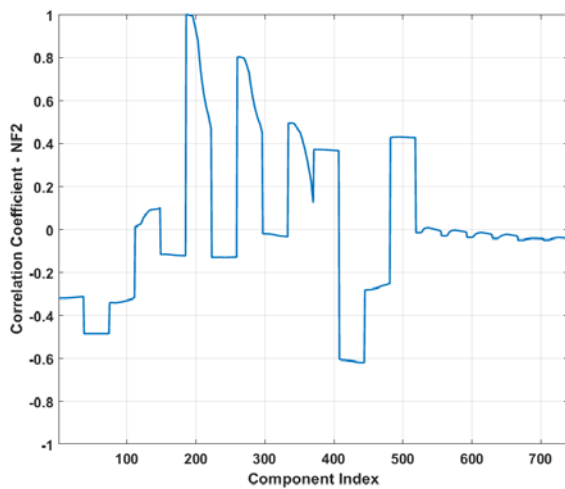
The next set of results investigate the correlations between different few-group burnup-dependent parameters. The correlation coefficients between each few group parameter at a given burnup and all other burnup-dependent parameters are calculated. Representative results are shown in Figure 7-4 for the correlation between the zero burnup value for the parameter with all other parameters. The total number of parameters is equal to 37 (the number of burnup steps) times the number of individual parameters types. The few-group parameters are organized in blocks of 37, where each block represents the correlations of the zero-burnup value of the parameter with its values across burnup. The parameters types are ordered as follows: Tr1, Tr2, Ab1, Ab2, NF1, NF2, KF1, KF2, Nu1, Nu2, ADF1, ADF2,  $\frac{1}{v_1}, \frac{1}{v_2}, \beta_1, \beta_2, \beta_3, \beta_4, \beta_5, \beta_6$  respectively. For example, Figure 7-4 (a) shows the correlation between the zero burnup values of the fast transport cross-section with all few-group parameters. The first 37 elements along the x-axis show the correlations with the burnup dependent values for the fast transport cross-sections. These results indicate that the zero-burnup fast transport cross-section is perfectly correlated with all its values across burnup, and approximately 0.73 correlation with the thermal transport cross-section, and near zero correlation with the thermal prompt neutron fraction and all six delayed neutron fractions. Figure 7-4 (d) shows that the delayed neutron fractions are near independent of all the other cross-section types, and their individual correlations across burnup are strongly varying. The implication is that one can treat the delayed neutron fractions are independent, but must account for their burnup dependence when doing transient analyses. These results provide great level of insight to the analyst to make additional simplifying assumptions for their particular application.



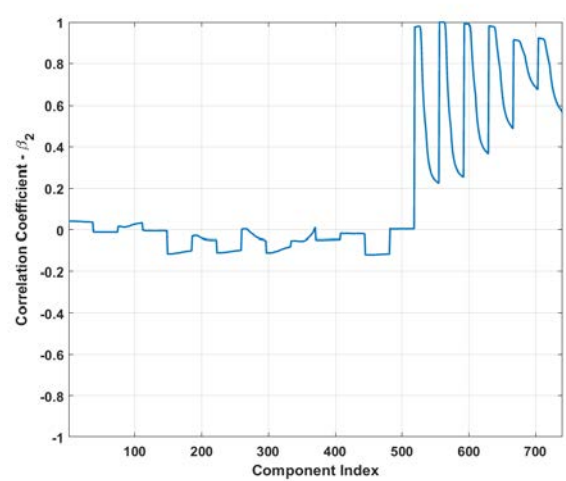
(a) Transport Cross-Section – Group 1



(b) Absorption Cross-Section – Group 2



(c) Nu-Fission – Group 1



(d) Delayed Neutron Fraction – Group 2

Figure 7-4 Correlation coefficients among lattice parameters across burnup.

### 7.1.4 Compressed CANDU few-group uncertainty space

In practice, the size of the vector  $\sigma_i$ , denote it by  $m$ , is very large because as it contains cross-sections at all conditions required for proper cross-section functionalization. This includes all burnup steps (in the order of several tens) to get the cross-section dependence on burnup, and all branch cases, evaluated at each burnup step (in the order of few tens per burnup step) to calculate cross-section corrections due to changing local conditions such as fuel temperature, and coolant temperature, and device cross-sections to calculate corrections resulting from insertion of

reactivity devices. The matrix  $\mathbf{C}_{FG}$  will thus be extremely large if calculated directly using the expression in Eq. (7-1). Instead, we rely on an ROM approach, which constructs a compressed representation for the  $\mathbf{C}_{FG}$  as follows:

$$\begin{aligned} \mathbb{R}^{m \times N} \ni \mathbf{X}_\sigma &= [\sigma_1 \quad \sigma_2 \quad \dots \quad \sigma_N] = \mathbf{U}\mathbf{S}\mathbf{V}^T, \mathbf{U} \in \mathbb{R}^{m \times r}, \mathbf{S} \in \mathbb{R}^{r \times r} \\ \mathbf{C}_{FG} &= (\mathbf{U}\mathbf{\Sigma})(\mathbf{U}\mathbf{\Sigma})^T, \text{diag}(\mathbf{\Sigma}) = \frac{1}{\sqrt{N-1}} \text{diag}(\mathbf{S}) \end{aligned} \quad (7-2)$$

This approach implies an initial SVD decomposition of the matrix containing the  $N$  realizations of the few-group cross-sections, denoted by  $\mathbf{X}_\sigma$ , which determines the effective rank of the  $\mathbf{C}_{FG}$  matrix. One can easily show that the  $\mathbf{U}$  matrix calculated from the decomposition of  $\mathbf{X}_\sigma$  is the same as that obtained from the decomposition of  $\mathbf{C}_{FG}$  matrix, and the singular values are related by simple scalar relationship as shown in Eq. (7-2). Thus, the  $\mathbf{C}_{FG}$  matrix is never constructed, but represented in a compressed form with a compression factor of  $(m+1)r/m^2$ . Typical values for  $m$  and  $r$  for CANDU reactor core models employing macroscopic depletion are in the order of  $10^4$ , and 10, respectively, implying a compression factor of approximately 0.001. If microscopic depletion models are employed,  $m$  is expected to increase by a factor equal to the number of tracked isotopes. Earlier LWR-based work has however shown that  $r$  only slightly increases due to the significant inherent correlations between the tracked isotopes.

The results of this ROM-based compression on the two- (2G), four- (4G) and eight-group (8G) lattice parameters uncertainties are shown in Figure 7-5, which shows the decline of the maximum errors resulting from the compression as a function of the first  $r$  singular vectors in the sense of equation below:

$$\sqrt{\left\| \mathbf{C}_\sigma - \sum_{i=1}^r \xi_i^2 \mathbf{u}_i \mathbf{u}_i^T \right\|} = \varepsilon$$

where  $\varepsilon$  is a very small preset tolerance. This can be shown to be attributed to the sharp decline in the singular values of the matrix  $\mathbf{C}_\sigma$ .

The sharp decline of the errors indicate that one can significantly compress the uncertainty space, as described by the covariance matrix, while keeping a reasonable reconstruction accuracy. The implication is that the number of active DOFs required to propagate uncertainties downstream through core calculations is significantly reduced. In our context, an active DOF refers to one

column of the  $\mathbf{U}$  matrix, which determines how the few-group parameters are perturbed in a manner that respects their correlations. If  $r$  is sufficiently small, the implication is that there exist many directions in the few-group parameters uncertainty space which have very small uncertainty, and hence need not be sampled for downstream core-wide calculations.

One can also plot the singular values of the covariance matrix, which show the same type of decline with the rank. Different from the maximum error plot in Figure 7-5, the singular values have a physical meaning: the standard deviation associated with each of the active DOFs. Figure 7-6 shows a representative set of singular values graphs, plotted for different cross-section types. As noted, each cross-section type shows a different rate of decline, which can be used to provide insight into the relative sources of uncertainties for the various cross-sections. The covariance matrix for each parameter is generated based on all the samples of the corresponding parameter across burnup. Singular values in Figure 7-6 are normalized with the maximum singular value among all parameters, which is 7.0648 in this case belonging to the delayed neutron fraction covariance.

Comparison of singular values among all parameters indicates that the delayed neutron fractions (Betas) have relatively large uncertainty comparing to other parameters, up-scattering to the fast group (MacroScatt1) and product of fission cross-section and number of neutrons per fission in thermal group also have larger uncertainties. The uncertainties in fission product yields are two to four orders of magnitude less than the Beta uncertainties, while other parameter uncertainties are one to two orders of magnitude lower than Beta uncertainties.

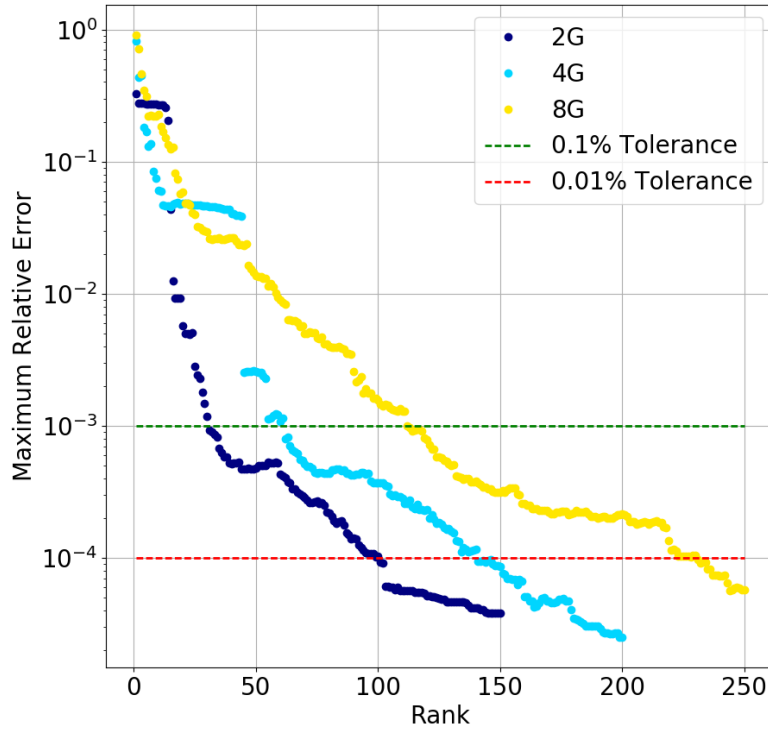


Figure 7-5 ROM-based maximum reconstruction errors of few-group parameter uncertainties.

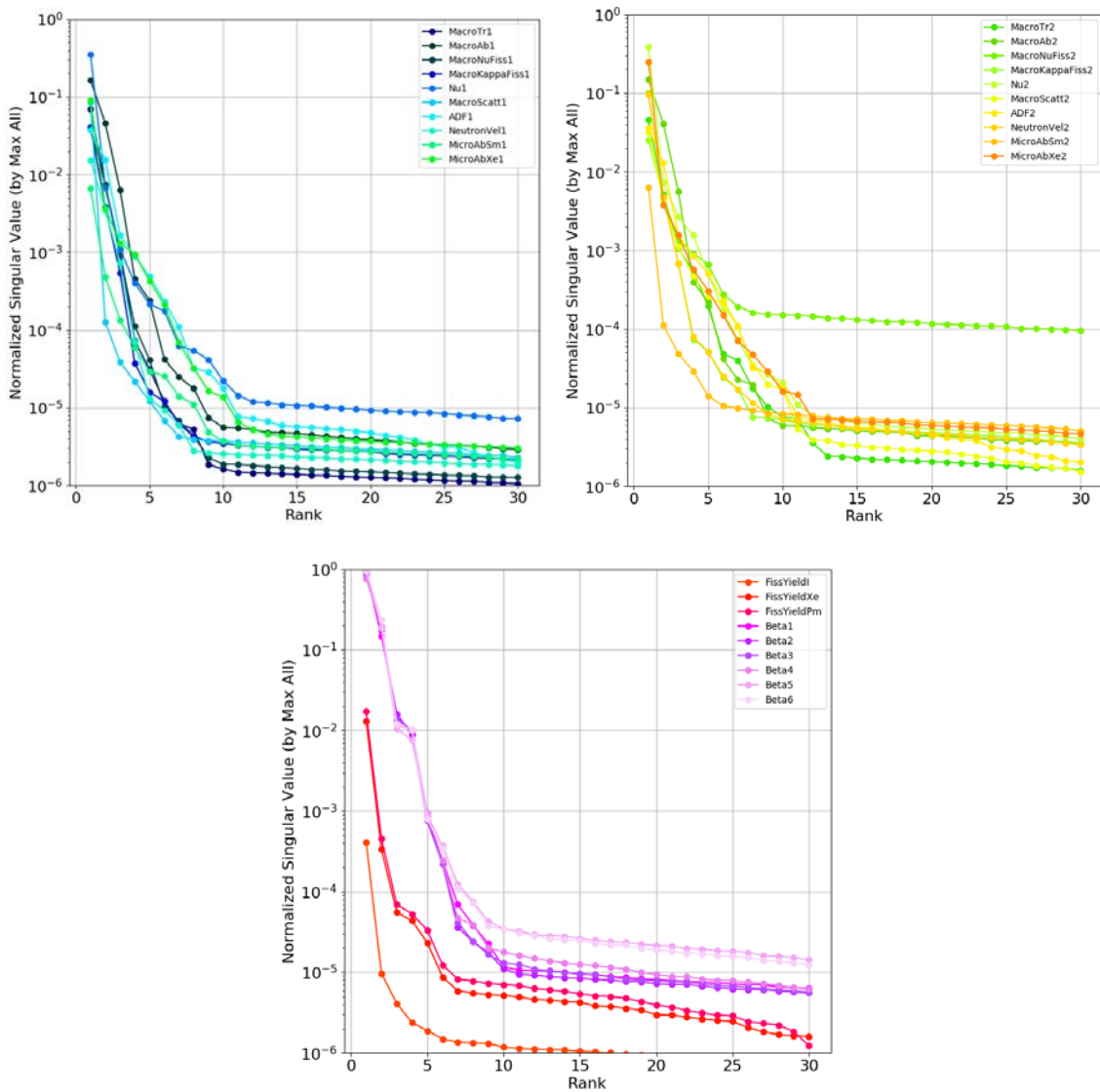


Figure 7-6 Normalized singular values of few-group parameter uncertainties.

### 7.1.5 CANDU branch and device uncertainties

In regard to the branch and device calculations, the figures below show representative sampled lattice parameters' values depicting the strong correlations with the base values. For example, the first subplot in Figure 7-7 shows the lattice k-eff values (measured as deviation from the reference unperturbed value) at a representative base case versus the k-eff value at the fuel temperature increase branch case (also measured as deviation from the reference branch case value). The base fuel temperature is 950 K, whereas the branch value is 1673 K. Results indicate

near correlation between these two conditions. Similar results are shown for representative lattice parameters in the other two subplots.

For the device calculations, deviation of the lattice parameters from their reference values are scatter-plotted in Figure 7-8. The x-axis represents the variations in the lattice parameters at the base case at an intermediate burnup value without the inclusion of the device, whereas the y-axis shows the variations at the same burnup when the device is inserted. Data points shown in both Figure 7-7 and Figure 7-8 are percentage discrepancies from the unperturbed calculation values. With NESTLE-C reading the incremental change in the parameters due to device insertion at a single intermediate burnup value, these results indicate that the device incremental values will have very small uncertainties due to the observed near perfect correlation of the lattice parameters at the two conditions, i.e., the base case and the case with device insertion.

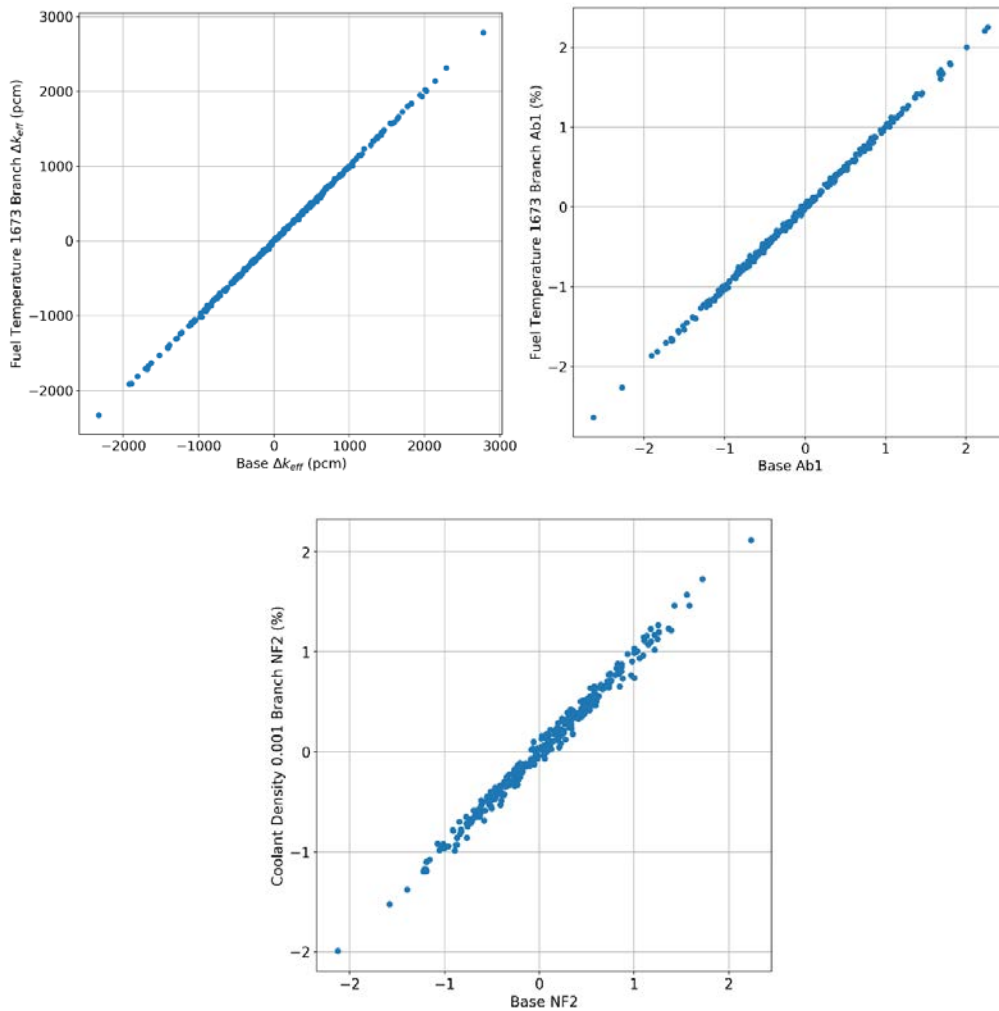


Figure 7-7 Correlations between few-group parameters of base and branch cases.

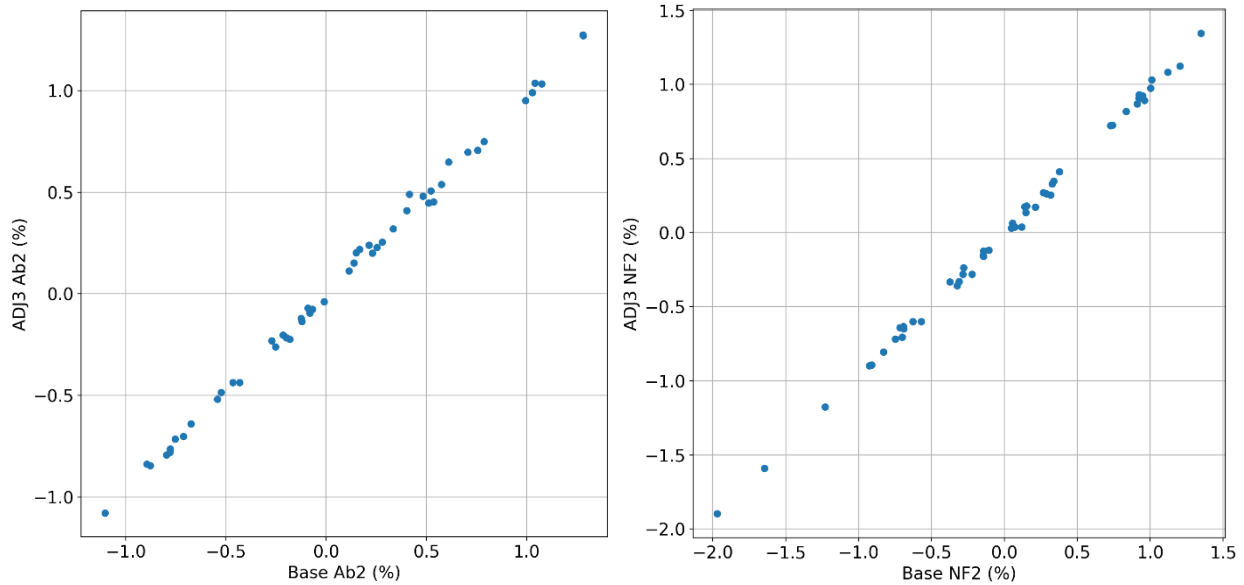


Figure 7-8 Correlations between base and device cross-sections.

These results are employed to justify the use of a single active DOF to describe the correlations between the branch, devices, and base cross-sections. The implication of this assumption for the NESTLE-C library is as follows. First with regard to the branch cross-sections, NESTLE-C does not employ the raw branch cross-sections directly. Instead it relies on preprocessing in which the cross-sections (base and branch) are fitted to polynomials, and the resulting polynomial coefficients are stored in NESTLE-C input cross-section library. One can then calculate the uncertainties in the polynomial coefficients based on the uncertainties in the raw cross-sections. Simple algebra shows that if the raw cross-sections for the branch cases are perfectly correlated with the base cross-sections, then the uncertainty in all higher order polynomial coefficients (except the constant term) will be zero. With regard to the device cross-sections, a similar situation is encountered, where NESTLE-C reads the differences between the device cross-sections and the base cross-sections (without the devices inserted). Again, if the two are perfectly correlated, the difference will have zero uncertainty. The implication is that for NESTLE-C one needs to perturb only the zero-order (constant) term in the polynomial fit and leave the higher order coefficients as well as the device incremental cross-sections unperturbed. This was considered an appropriate approximation during phase-one of this project, given that other terms are found to have more pronounced impact on the propagated uncertainties such as group structure, and resonance treatment, etc.

## 7.2 ROM-based Uncertainty Propagation Results on CANDU Core Simulation

### 7.2.1 CANDU-6 core model setup

The NESTLE-C core model requires a standard set of few-group parameters filed in a cross-section data input script (referred to as cross-section library in this context), as listed in Table 7-2, to calculate core-wide behavior.

The few-group parameter names and their aliases in the context are provided in first and second columns of Table 7-2 respectively. Parameters in fuel region are burnup dependent, while in reflector region they are assumed burnup-independent.

The third column (number of parameters per burnup step) indicates whether the few-group parameter is energy-dependent, where ‘NumFG’ represents number of energy groups in the few-group structure. The fission yield data and delayed neutron fractions are not energy-dependent.

Most of the few-group parameters are functionalized in terms of a wide range of core conditions, e.g., fuel burnup, fuel temperature, coolant and moderator density, etc., in order to capture impact of local neutronic/thermal-hydraulic feedback. This dependence is indicated in the fourth column (core conditions).

Moreover, to capture the impact of reactivity device insertions, some of the cross-sections are modified by incremental amounts, which are denoted in the fifth column (device increments).

The last column indicates whether the respective parameter is included in this framework. The buckling uncertainty is supposed to be zero in the uncertainty study, and the prompt fission spectrum shows no uncertainty in two-group structure from the lattice calculation, and trivial uncertainty in four- and eight-group structure. Thus, they are not included in this uncertainty study.

Table 7-2 List of all types of few-group parameters required in NESTLE-C.

Parameter Type	Alias	#/ Burnup Step	Core Conditions	Device Increments	Included in UQ Study
Transport Cross-Section	Tr	NumFG	Yes	Yes	Yes
Absorption	Ab	NumFG	Yes	Yes	Yes
Nu*Fission	NF or NuFiss	NumFG	Yes	Yes	Yes
Kappa*Fission	KF or KappaFiss	NumFG	Yes	No	Yes
Nu	Nu	NumFG	Yes	No	Yes
Scattering	Scatt	NumFG* (NumFG-1)	Yes	Yes	Yes
Buckling	N/A	NumFG	No	No	No
Prompt Fission Spectrum	N/A	NumFG	No	No	No
Discontinuity Factors	ADF	NumFG	No	Yes	Yes
Neutron Velocity	nVel	NumFG	No	No	Yes
Sm-149 Absorption	MicroAbSm	NumFG	Yes	No	Yes
Xe-135 Absorption	MicroAbXe	NumFG	Yes	No	Yes
I-135 Fission Yield	FissYieldI	1	No	No	Yes
Xe-135 Fission Yield	FissYieldXe	1	No	No	Yes
Pm-149 Fission Yield	FissYieldPm	1	No	No	Yes
Delayed Fractions (beta)	Beta	6	No	No	Yes

The CANDU core contains 380 horizontal channels, each loaded with 12 fuel bundles. The CANDU core model is analyzed using the NESTLE-C core simulator. The core specifications are given in Table 7-3. For reference, the channel burnup and power distribution calculated by NESTLE-C are shown in Figure 7-9 and Figure 7-10 respectively.

Table 7-3 Parameters of core configurations.

<b>Parameter</b>	<b>Dimension</b>
Lattice pitch (square)	28.575 cm
Length of bundle	49.53 cm
Core length	594.36 cm
Core radius	379.7 cm
Channel count	380
Fuel bundles per channel	12
Fuel type	Natural Uranium
Fuel bundle type	37-element
Heavy Water Moderator Purity	99.97 wt% D <sub>2</sub> O
Heavy Water Coolant Purity	99.20 wt% D <sub>2</sub> O
# LZCs	14
# SORs	28
# ARs	21
# MCA	0

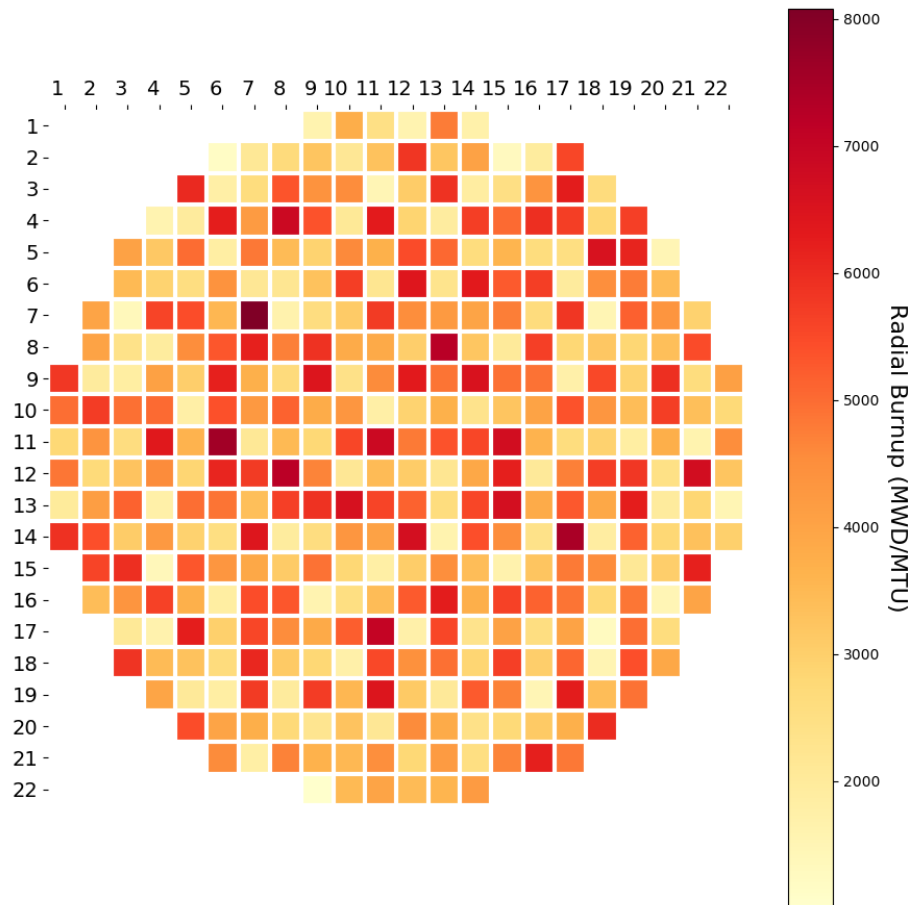


Figure 7-9 Radial core channel burnup distribution.

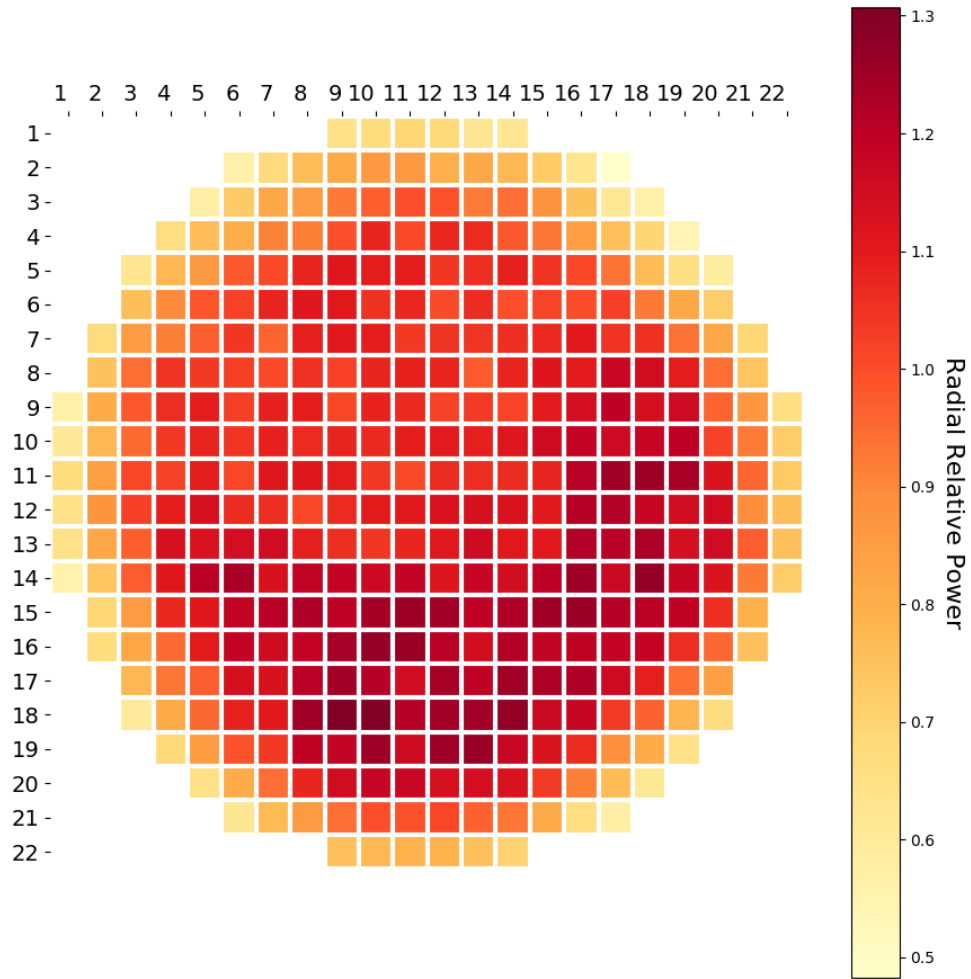


Figure 7-10 Radial core channel power distribution.

The analyzed NESTLE-C core models include three steady-state CANDU-6 models and one LOCA (loss-of-coolant accident) transient model, whose specifications are described in Figure 7-11 and Table 7-4. One of the steady-state models represents the reference core model at full power. Another steady-state model has all its coolant voided to facilitate the calculation of the coolant-voiding reactivity (CVR) coefficients. This is done by changing the coolant density to  $10^{-4} \text{ g/cm}^3$ . The third steady-state model is referred to as a toy model as it employs many simplifying assumptions, e.g., constant fuel, coolant, and moderator temperature throughout the core, all fuel is fresh, no thermal-hydraulic feedback, and no reactivity device insertion.

For reference, the core effective multiplication factor, k-eff, for each core model and cross-section library combination is listed in Table 7-4. The differences in k-eff are shown in Table 7-4,

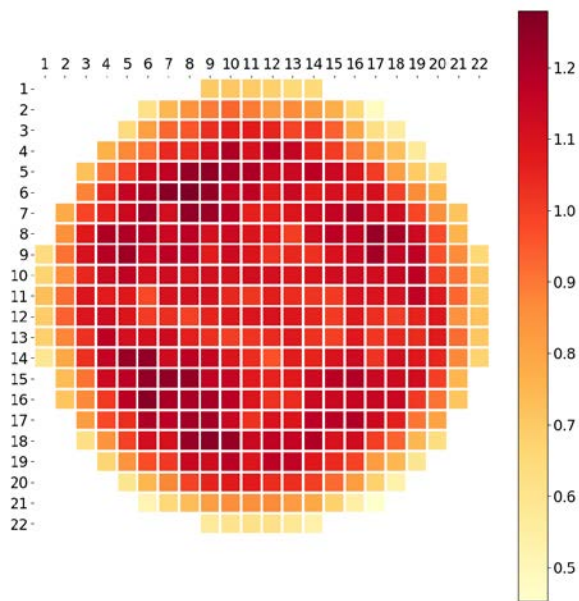
$\Delta k$ -eff, in units of milli-k (mk), are the k-eff values deviating from the k-eff of the corresponding reference core model, except that the k-eff of the reference models are compared to the HELIOS-2G reference model. For the coolant-voided cases, the CVR values are calculated with the Eq. (7-3), and the results are also presented in Table 7-4. The CVR values are around 16 [mk] for all reference cross-section libraries, while the HELIOS-based CVR is slightly higher than CVRs of SERPENT-base libraries.

$$\Delta\rho = \rho_{cvr} - \rho_{ref} = \frac{k_{eff,cvr} - k_{eff,ref}}{k_{eff,cvr} k_{eff,ref}} \times 1000 \quad [mk] \quad (7-3)$$

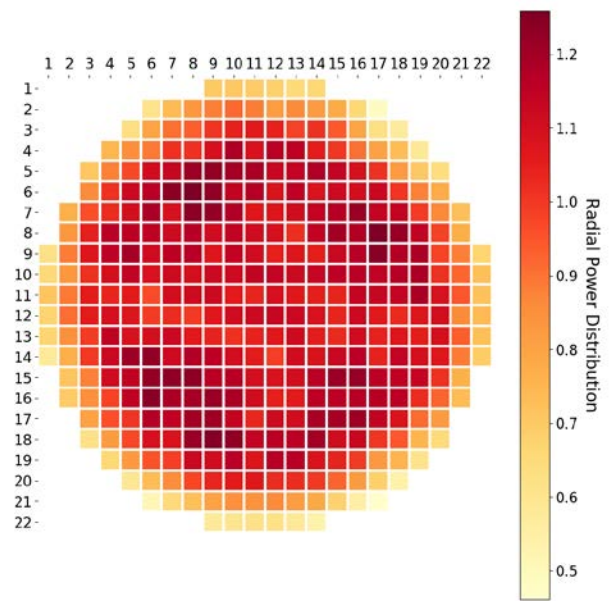
Table 7-4 Reference k-eff and comparison in various core models.

<b>Core Model</b>	<b>Core k-eff</b>	<b>CVR (<math>\Delta\rho</math>) [mk]</b>
H2G_ref	0.9995891	
S2G_ref	0.9706204	
S4G_ref	0.9712535	
H2G_cvr	1.0161754	16.33
S2G_cvr	0.9858744	15.94
S4G_cvr	0.9863787	15.79
H2G_toy	1.000664	
S2G_toy	0.9677108	
NEWT_2G_ref	0.9821152	
NEWT_4G_ref	0.982553	

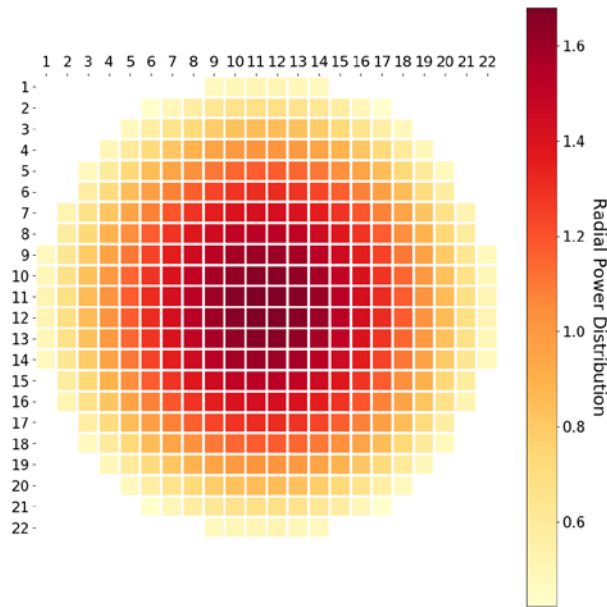
Representative results for the steady-state cases using two-group models are shown in Figure 7-11 (a) (b) and (c) representing, respectively, the radial channel power distribution for the reference, coolant voided and toy core models, all evaluated using the HELIOS-based reference cross-sections. Similar results are obtained using the SERPENT and NEWT-based libraries as shown in Figure 7-12 comparing the core power distribution in four-group energy structure. Finally, representative uncertainty results for the channel power distribution are shown in Figure 7-13 for the reference steady-state core model.



(a) Reference Core Model

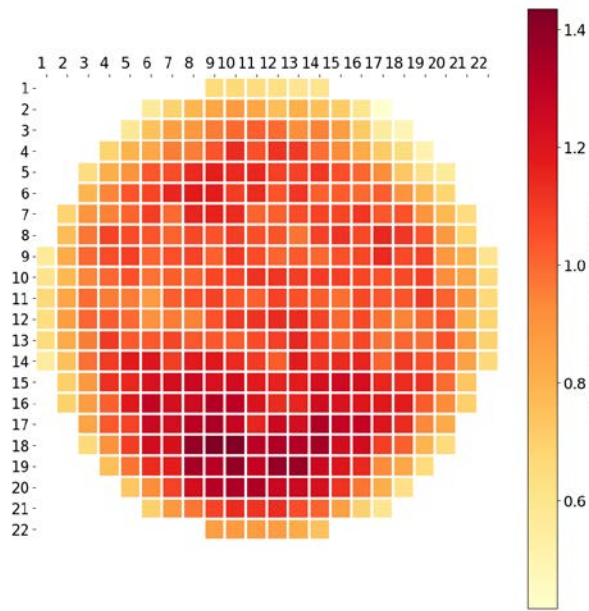


(b) Coolant Voided Core Model

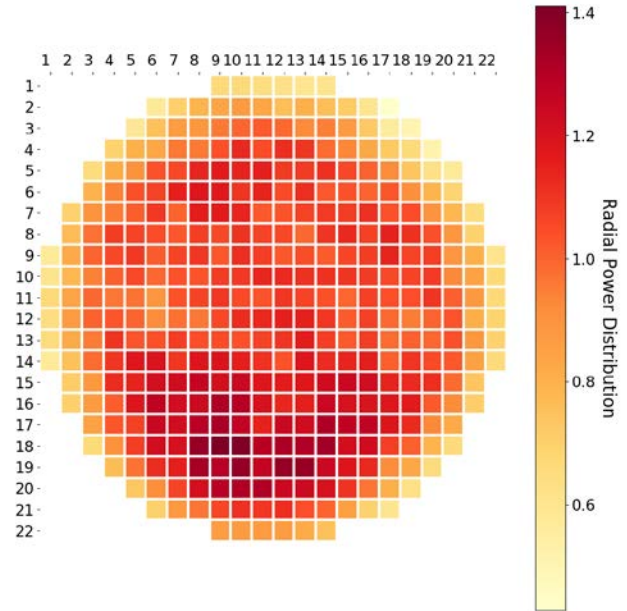


(c) Toy Core Model

Figure 7-11 Channel power distributions in three steady-state core models w/ HELIOS-based cross-section library.

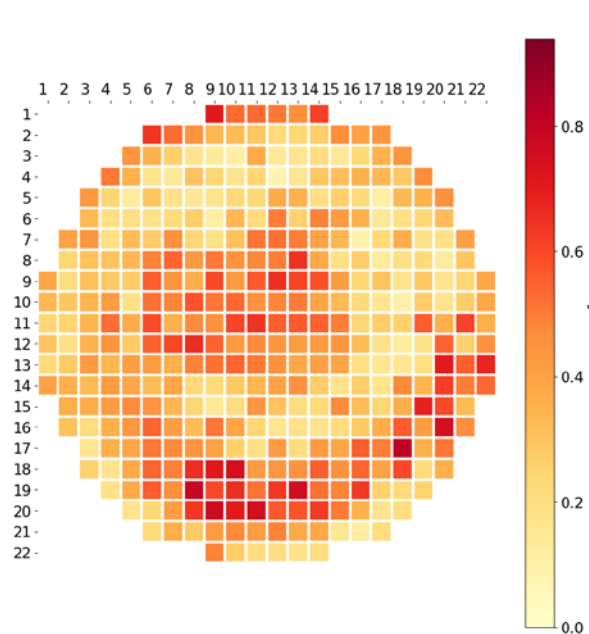


(a) Four-Group SERPENT-based

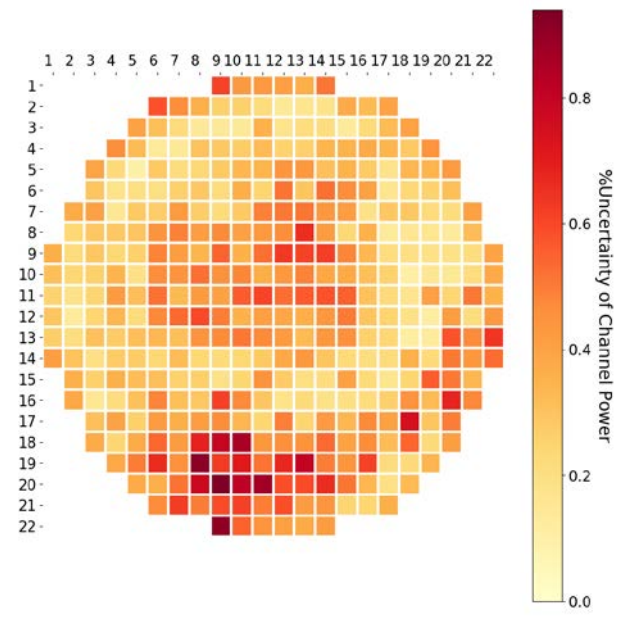


(b) Four-Group NEWT-based

Figure 7-12 Reference channel power distribution w/ SERPENT- or NEWT-based cross-section library in four-group energy structure.



(a) HELIOS-based



(b) SERPENT-based

Figure 7-13 Reference channel power uncertainty distribution w/ HELIOS-based or SERPENT-based cross-section library in two-group energy structure.

### 7.2.2 ROM-based few-group uncertainty propagation results on CANDU core responses

The next set of figures depict the uncertainties for both the core k-effective and the mesh-based power distribution, calculated using the deterministic approach. The goal is to study the impact of  $r$  on the propagated uncertainties. Figure 7-14 depicts the uncertainty in k-effective as a function of the number of active DOFs as done before with the results indicating that only 10 active DOFs are required to accurately calculate the k-effective uncertainty. Similar trend is shown in Figure 7-15 for the mesh-based power, shown for three representative mesh nodes throughout the core, in the center of the core (a), on the periphery of the core (b) and a random selected node (c). The results indicate that at most 20 active DOFs are required.

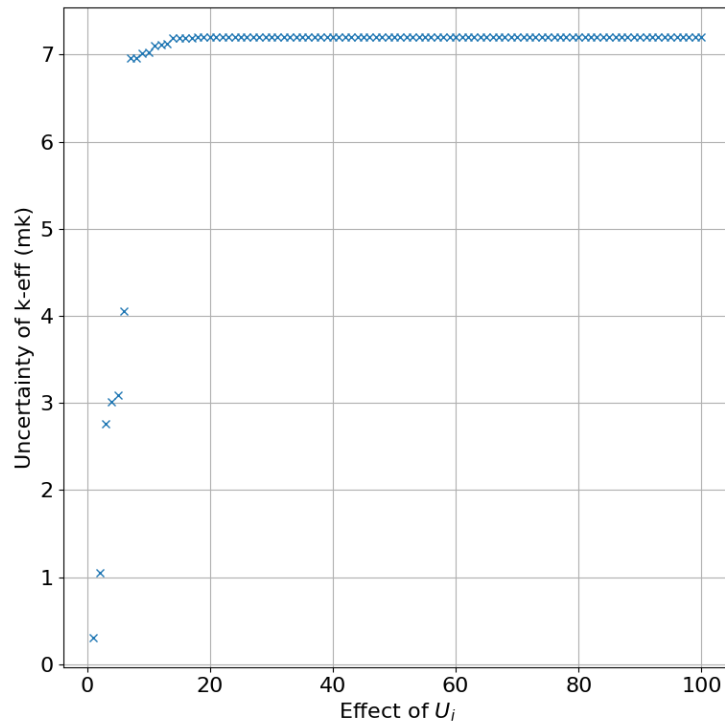
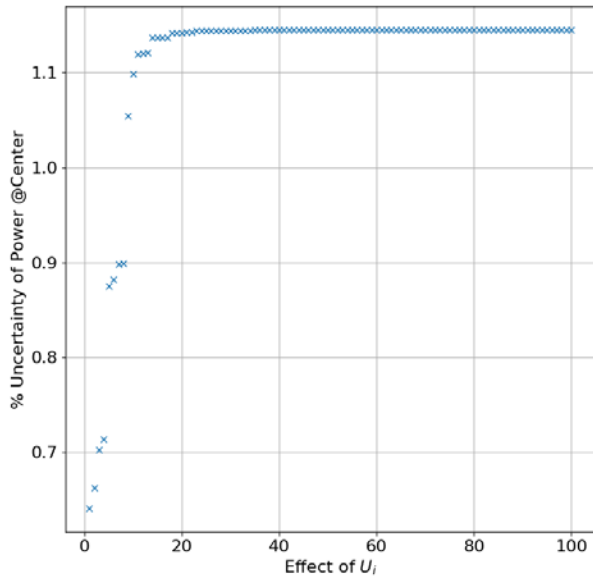
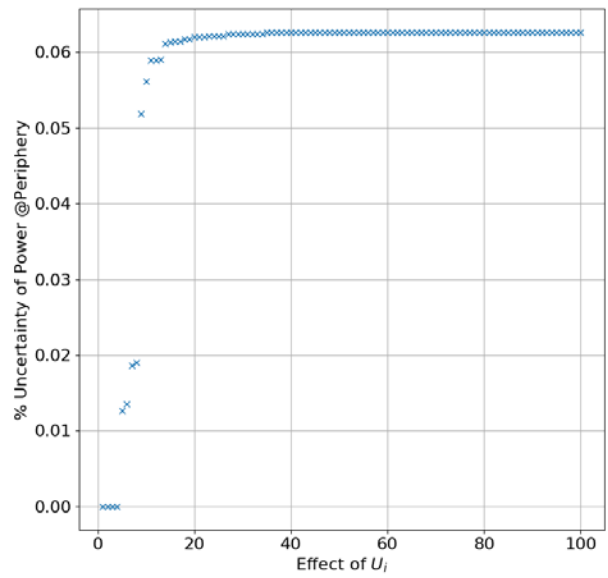


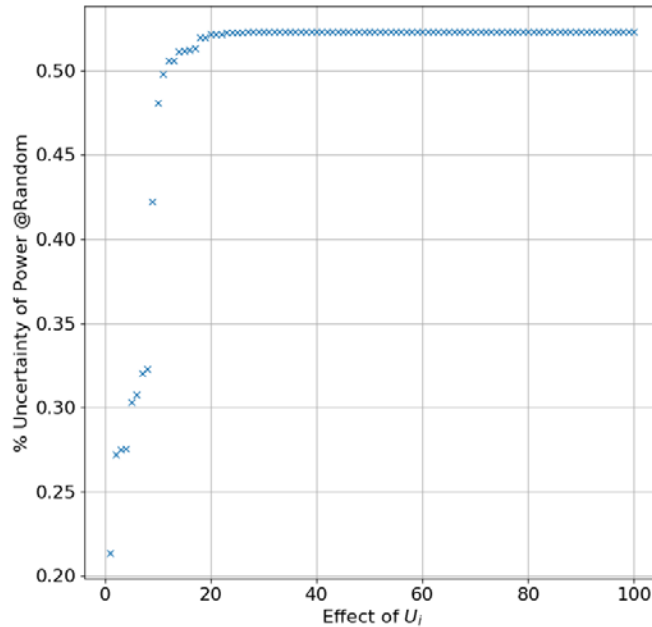
Figure 7-14 ROM-based core k-eff uncertainty.



(a) Power Uncertainty in the Center



(b) Power Uncertainty on the Periphery

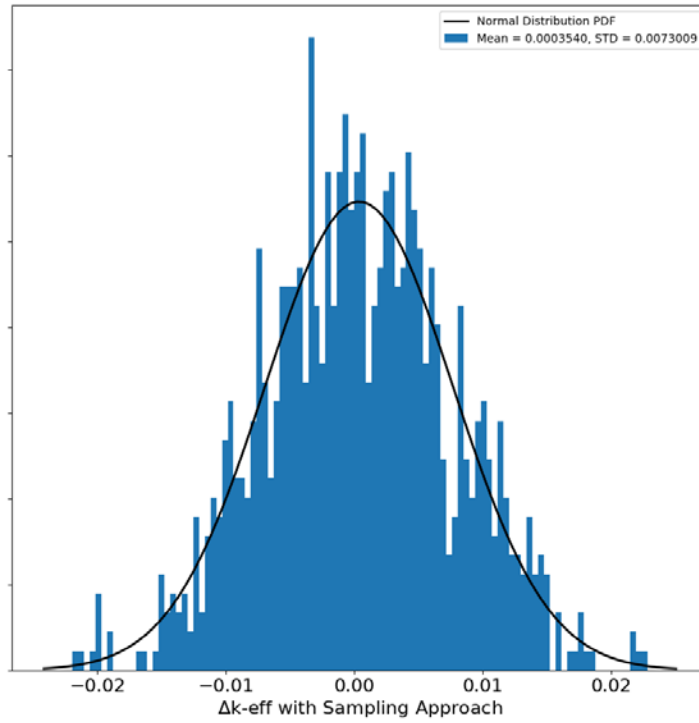


(c) Power Uncertainty at a Random Position

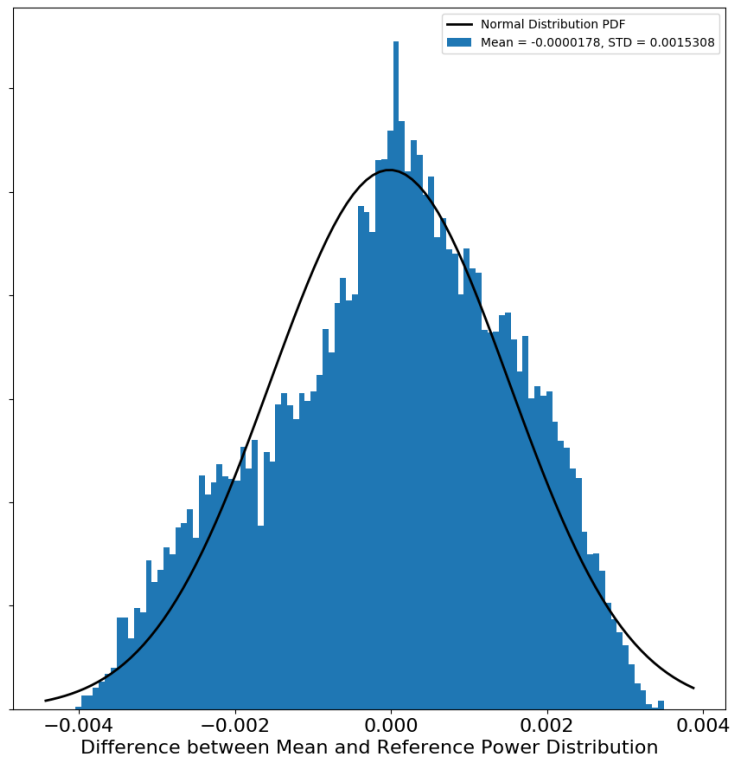
Figure 7-15 ROM-based core channel power uncertainty at certain channel.

Next, the results of the stochastic uncertainty propagation approach are shown. Plots in Figure 7-16 are histograms of  $\Delta k_{eff}$  and difference of power distribution between the mean values of random samples and the reference values, denoting as  $\Delta P_{mean}$ . In this CANDU-6 core model, the number of mesh nodes forming the power distribution is in order of 20,000. The  $\Delta k_{eff}$  values

from  $N=1000$  random samples follow a Gaussian distribution, with mean value almost zero and the standard deviation 7.3 milli-k as shown in Figure 7-15 (a). The k-eff results from the sampling approach is consistent with the deterministic approach (ROM-based), where the uncertainty of k-eff saturates at 7.2 milli-k due to the first ten singular vectors of lattice parameters uncertainties. Note that the mean values of the deterministic executions and the reference values are assumed the same due to the linearity assumption. Table 7-5 summarizes some statistics on the k-effective and mesh-based power distribution mean and reference values. The  $\Delta P_{mean}$  from the random samples slightly deviates from the Gaussian distribution, the mean value is close to zero and the standard deviation is 0.153% according to Figure 7-15 (b) and Table 7-5. Table 7-5 also lists the average of standard deviation of each nodal power distribution, where the power average standard deviation is 0.491% with the deterministic approach and is 0.486% with stochastic approach. The standard deviation of the difference between mean and reference power distribution is about 1/3 of the average standard deviation for all the mesh-based power values.



(a) Histogram of k-eff deviation from reference k-eff



(b) Histogram of Difference between Mean and Reference Power Distribution

Figure 7-16 Histograms of core attributes via stochastic approach.

Table 7-5 Deterministic- vs. stochastic-based uncertainty.

	Deterministic	Stochastic
Reference k-eff	1.0050826	1.0050826
Mean - k-eff	1.0050826	1.0054366
Standard deviation - k-eff	7.2 mk	7.3 mk
Standard deviation of average – difference between mean and reference power distribution	0	0.1531%
Average of standard deviation – power distribution	0.491%	0.486%

### 7.2.3 sUncertainties propagation results in Core CVR

This section calculates the core CVR uncertainties resulting from the few-group parameter uncertainty and compares its value using both the deterministic and stochastic UQ approaches. This can be achieved by running both the “ref” and “cvr” models  $N$  times, where  $N$  represents the number of samples. The core CVR calculation follows the expression in Eq. (7-3), which is given by for the  $i^{\text{th}}$  run as follows:

$$\Delta\rho_i = \rho_{cvr,i} - \rho_{ref,i} = \frac{k_{eff,cvr,i} - k_{eff,ref,i}}{k_{eff,cvr,i} k_{eff,ref,i}} \times 1000 \text{ [mk]}$$

For the deterministic approach  $N$  is selected to be the number of active DOFs and the uncertainty is aggregated whereas in the stochastic approach  $N$  represents the number of random samples employed, and the uncertainty is represented by the standard deviation calculated over the samples. Figure 7-17 shows the results of the deterministic approach using different number of active DOFs on the x-axis. These results indicate that approximately 50 active DOFs is sufficient to calculate the uncertainty and this number is insensitive to the group structure or the reference NESTLE-C library employed. These results are compared to those obtained using the stochastic approach in Table 7-6. As shown earlier with the k-eff results, the CVR results further confirm the consistency between the deterministic- and stochastic-based uncertainties.

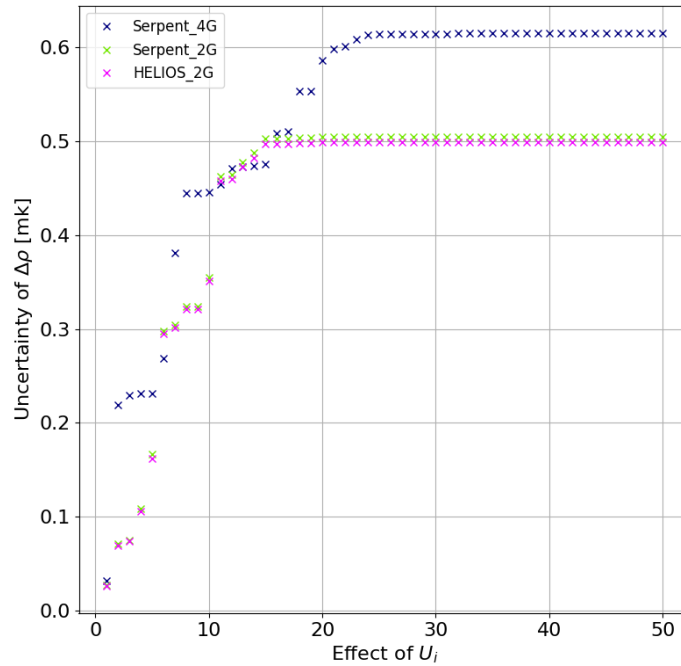


Figure 7-17 ROM-based core CVR uncertainty.

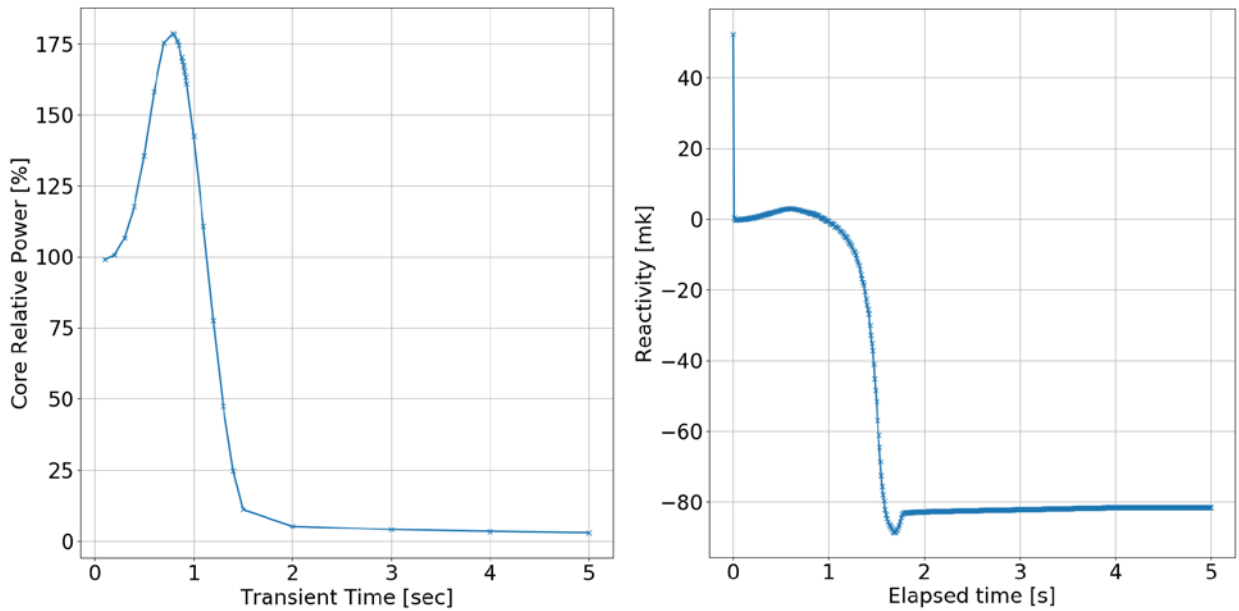
Table 7-6 Core CVR uncertainties via deterministic vs. via stochastic approaches.

Core CVR ( $\Delta\rho$ ) [mk]	Deterministic		Stochastic	
	Mean Value	Uncertainty	Mean Value	Uncertainty
Reference Cross-section Library				
HELIOS_2G	16.33	0.50	16.32	0.54
SERPENT_2G	15.94	0.50	15.96	0.54
SERPENT_4G	15.79	0.61	15.76	0.59

### 7.2.4 Uncertainty Propagation Results in LOCA Core Model

This section presents the uncertainty analysis results for the transient LOCA core model. The total number of NESTLE-C samples employed is 1000. The reference NESTLE-C cross-section library employed is HELIOS\_2G. Figure 7-18 shows two of the core attributes versus time as calculated by the reference transient model. Figure 7-19 plots the percentage discrepancies between each sample of the stochastic approach and the reference execution (golden plots), as well as the resulting core power level uncertainties along time (shown as light blue envelope around

reference solution). The few-group parameter uncertainties result in a maximum core power uncertainty of 15% around 0.9 [sec] when the core power reaches a maximum. Figure 7-20 contains the histograms of core relative power from the 1000 samples at four representative time steps during the transient. It is noted that the few-group parameter uncertainties propagated follow a normal distribution, however, the resulting core relative power distributions are not always normal. Shifting from normal distribution around the peak location indicates nonlinearity in the model in the transient time period.



(a) Core Relative Power

(b) Core Reactivity

Figure 7-18 Reference core attributes in LOCA core model.

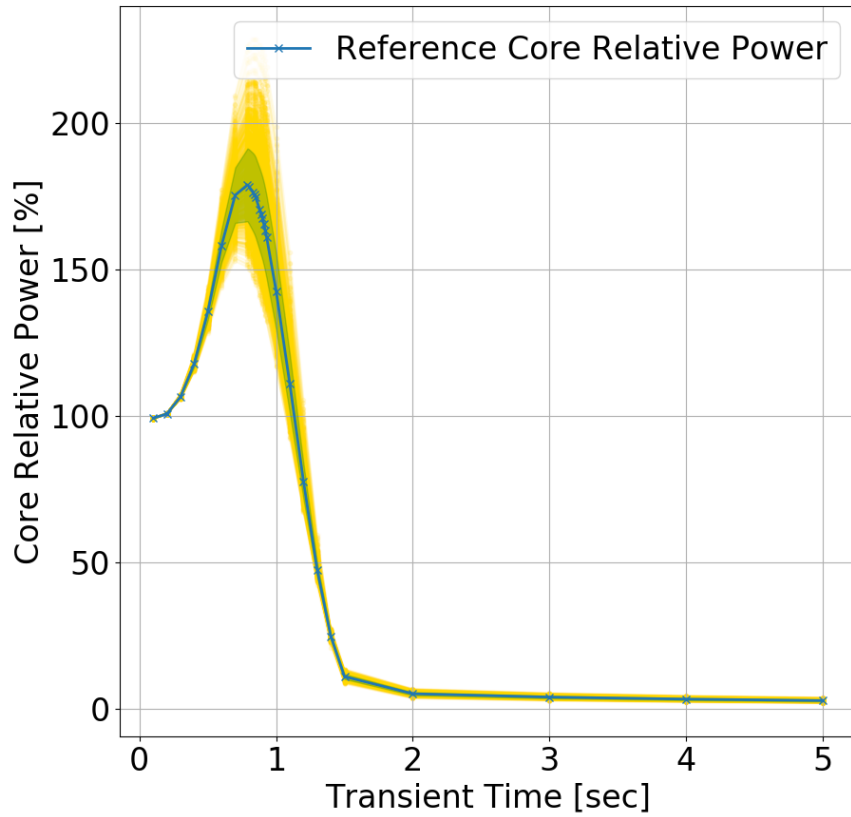


Figure 7-19 Uncertainty of transient core power.

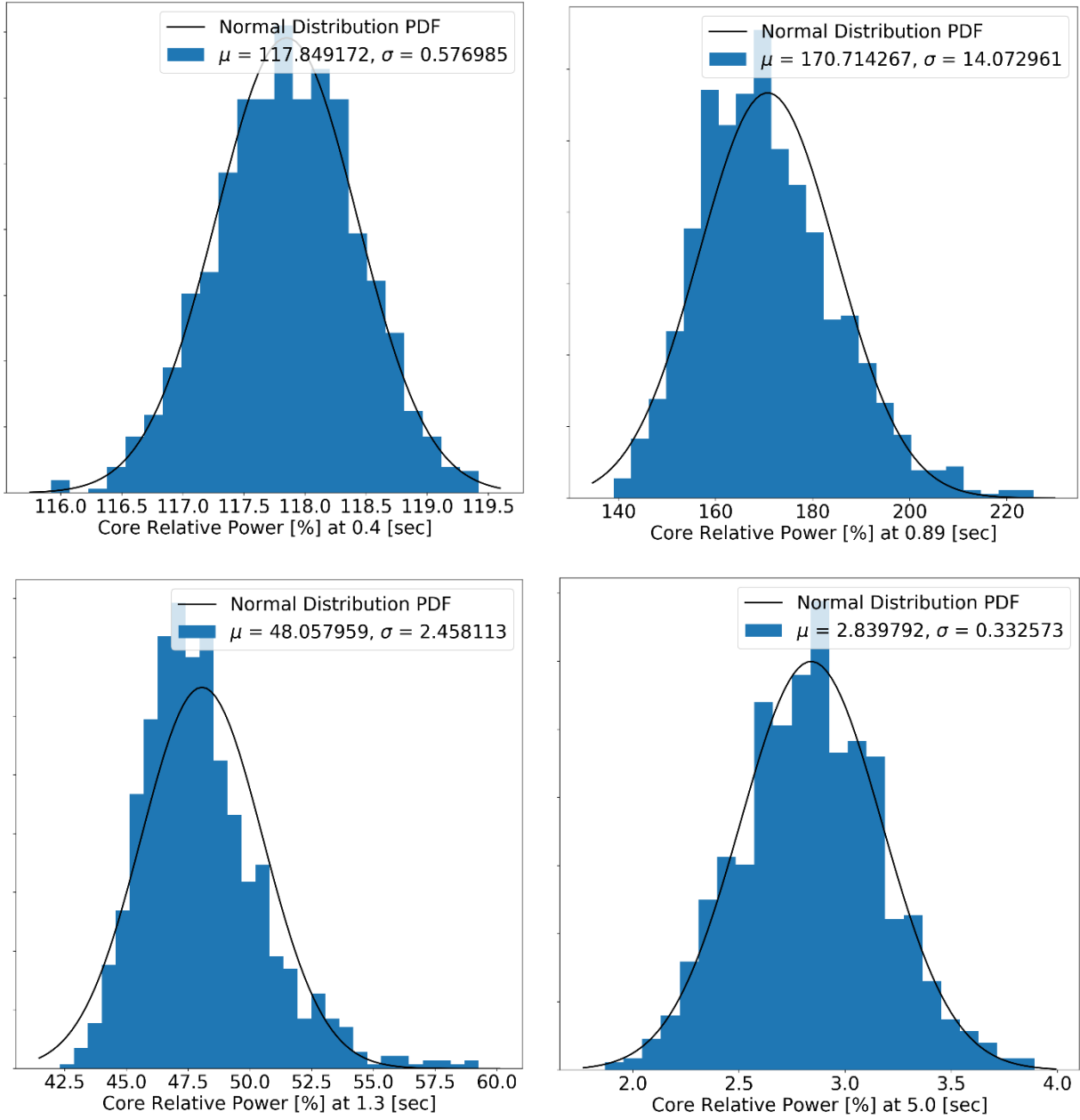


Figure 7-20 Uncertainties of core power at selected time steps.

### 7.3 Conclusions

This chapter reports the few-group parameter uncertainties propagated from multi-group covariance, as well as the uncertainty analysis results through the core simulations based on the ROM-based compression of the few-group uncertainties. Both deterministic method and stochastic method are applied in core uncertainty propagation based on the compressed cross-section uncertainty libraries. Results are based on various few-group structures and core models in both steady-state and transient scenarios. The resulted core uncertainties are, in general, consistent with different reference cross-section libraries, energy structures and uncertainty analysis methods. The nuclear data uncertainty (parameter uncertainties) results in 7 to 8 [mk] (700-800 [pcm]) uncertainty in the core multiplication factor and 1% channel power uncertainty in the steady-state core simulations, and 15% maximum core relative power uncertainty in LOCA core simulations based on the compressed uncertainty libraries.

However, discrepancies and nonlinearity exist in some cases, such as reference power uncertainty shown in Figure 7-13 depicting different distributions, and the mean value of nodal power via stochastic UQ method slightly different from the reference nodal power in deterministic UQ method, indicating the necessity to further investigate the impact on uncertainty analysis with different modeling assumptions and approximations (modeling uncertainties).

### 7.4 References

1. Huang, D. and H. Abdel-Khalik, *Application of Cross Sections Uncertainty Propagation Framework to Light and Heavy Water Reactor Systems*. Journal of Nuclear Engineering and Radiation Science, 2019.
2. Turinsky, P. and H. Sarsour, *NESTLE-C: Few-group neutron diffusion equation solver utilizing the nodal expansion method for eigenvalue, adjoint, fixed-source steady-state and transient problems: CANDU version*. 2003, North Carolina State University: Raleigh, NC (United States).
3. Williams, M.L., et al., *A statistical sampling method for uncertainty analysis with SCALE and XSUSA*. Nuclear technology, 2013. **183**(3): p. 515-526.
4. Leppänen, J., et al. *The Serpent Monte Carlo code: Status, development and applications in 2013*. in *SNA+ MC 2013-Joint International Conference on Supercomputing in Nuclear Applications+ Monte Carlo*. 2014. EDP Sciences.
5. Pounders, J.M., et al., *A 3D stylized half-core CANDU benchmark problem*. Annals of Nuclear Energy, 2011. **38**(4): p. 876-896.
6. Petrie, L.M. and N.F. Landers, *KENO Va: an improved Monte Carlo criticality program with supergrouping*. 1984.

## **8. MODELING ERROR IN CANDU CORE UNCERTAINTY PROPAGATION**

A comprehensive uncertainty analysis should characterize all sources of uncertainties in a computationally-feasible and scientifically-defendable manner. This dissertation employs a well-established reduced order modeling (ROM) based uncertainty quantification methodology to propagate uncertainties throughout neutronic calculations. ROM relies on recent advances in randomized data mining techniques applied to large data streams. In our proposed implementation, the nuclear data uncertainties are first propagated from multi-group level through lattice physics calculation to generate few-group parameters uncertainties, described using a vector of mean values and a covariance matrix. Employing an ROM-based compression of the covariance matrix, the few-group uncertainties are then propagated through downstream core simulation in a computationally efficient manner. This straightforward approach, albeit efficient as compared to brute force forward and/or adjoint-based methods, often employs a number of assumptions that have been unquestioned in the literature of neutronic uncertainty analysis. This dissertation argues that these assumptions could introduce another source of uncertainty referred to as modeling uncertainties, whose magnitude need to be quantified in tandem with nuclear data uncertainties.

This chapter explores the interactions between these two uncertainty sources in order to assess whether modeling uncertainties have an impact on parameter uncertainties. To explore this endeavor, the impact of a number of modeling assumptions on core attributes uncertainties is quantified. The study employs a CANDU reactor model, with SERPENT and NEWT as lattice physics solvers and NESTLE-C as core simulator. The modeling assumptions investigated include those related with the uncertainty propagation method employed, e.g., deterministic vs. stochastic, the few-group energy structure employed to represent the cross-sections, the resonance treatment in lattice physics calculation, the reference values for the cross-section, and the number of samples employed to render ROM compression. Results indicate that some of the modeling assumptions could have a non-negligible impact on the core responses propagated uncertainties, highlighting the need for a more comprehensive approach to combine parameter and modeling uncertainties.

The numerical study is based on the simulation and uncertainty propagation of a CANDU reactor model, which develops two steps integrated in an automated manner for the NESTLE-C [1] simulator with uncertainties propagated through the SCALE's NEWT [2] code for lattice

physics calculations. The first step is to generate an uncertainty library for all neutronic data that are input to NESTLE-C, automating the processing and generation of NESTLE-C uncertainty library. The second step is to evaluate the impact of modeling uncertainties during the process of uncertainty propagation through the core simulation. With regard to the first step, this will be accomplished using the SERPENT [3] and SCALE's NEWT codes for the calculation of the few-group parameters, NESTLE-C for core-wide calculations, and SCALE's SAMPLER [4] for the propagation of multi-group cross-section uncertainties using NEWT. The SERPENT code is used to generate the reference two-group and four-group libraries, and to verify the reference NEWT models. This is because the NEWT is a deterministic neutron transport model which employs a number of standard modeling assumptions, e.g., group structure, resonance treatment, etc., while SERPENT is based on a continuous cross-section Monte Carlo transport model which is considered a gold standard for neutron transport calculations. By employing both models, the impact of modeling uncertainties can be initially assessed on the propagated cross-sections uncertainties.

### **8.1 Modeling Assumptions Setup**

All reference NESTLE-C libraries are based on either the HELIOS or SERPENT-based models. For the two-group case, both HELIOS and SERPENT-based libraries are available. For four and eight group models, only SERPENT-based NESTLE-C libraries are available. The NESTLE-C core models and the reference cross-section libraries applied in this study are listed in Table 8-1. All the core simulations in this section are executed with NESTLE-C version 3.0.0, made available through Canadian Nuclear Laboratories (CNL).

Table 8-1 Core models and reference cross-section libraries with abbreviations in the thesis context.

Core Model	Alias	Reference NESTLE-C Library	Abbreviation
Reference model	ref	Two-group HELIOS	H2G_ref
		Two-group SERPENT	S2G_ref
		Four-group SERPENT	S4G_ref
Coolant voided model	cvr	Two-group HELIOS	H2G_cvr
		Two-group SERPENT	S2G_cvr
		Four-group SERPENT	S4G_cvr
Toy model	toy	Two-group HELIOS	H2G_toy
		Two-group SERPENT	S2G_toy
LOCA model	loca	Two-group HELIOS	H2G_loca

For reference, the core effective multiplication factor, k-eff, for each core model and cross-section library combination is listed in Table 7-4. The differences in k-eff are shown in Table 7-4,  $\Delta k_{eff}$ , in units of milli-k (mk), are the k-eff values deviating from the k-eff of the corresponding reference core model, except that the k-eff of the reference models are compared to the HELIOS-2G reference model. For the coolant-voided cases, the core coolant void reactivity (CVR) values are calculated with the Equation (3), and the results are also presented in Table 7-4. The CVR values are around 16 [mk] for all reference cross-section libraries, while the HELIOS-based CVR is slightly higher than CVRs of SERPENT-base libraries.

## 8.2 Modeling Uncertainties in CANDU Lattice Modeling

The CANDU-6 lattice contains 37 fuel elements composed of natural uranium [26] with heavy water serving as both coolant and moderator. The heavy water inside the pressure tubes serves as the coolant at a temperature of 563 K, and the heavy water outside the pressure tubes acts as moderator at a temperature of 341 K. The CANDU-6 lattice is modeled using SERPENT, KENO-CE, and NEWT codes to provide initial estimates of the modeling uncertainties, representing the discrepancies in the estimated few-group parameters resulting from different modeling assumptions/approximations. SERPENT is a Monte Carlo Radiation Transport code

with depletion capabilities; it uses the ENDF cross-sections in ACE format, and has a capability to collapse the cross-sections into user-specified energy-group format.

As shown in Figure 8-1, comparison of k-eff between SERPENT and KENO-CE, both based on the same solution strategy and same cross-sections, is within 1 [mk], which is considered reasonable for most practical reactor calculations. Regarding NEWT, it appears to slightly under-predict k-eff as compared to SERPENT, with the discrepancies being acceptable in magnitude. These initial results indicate that the models all provide reasonable approximation of neutronic behavior at the lattice level.

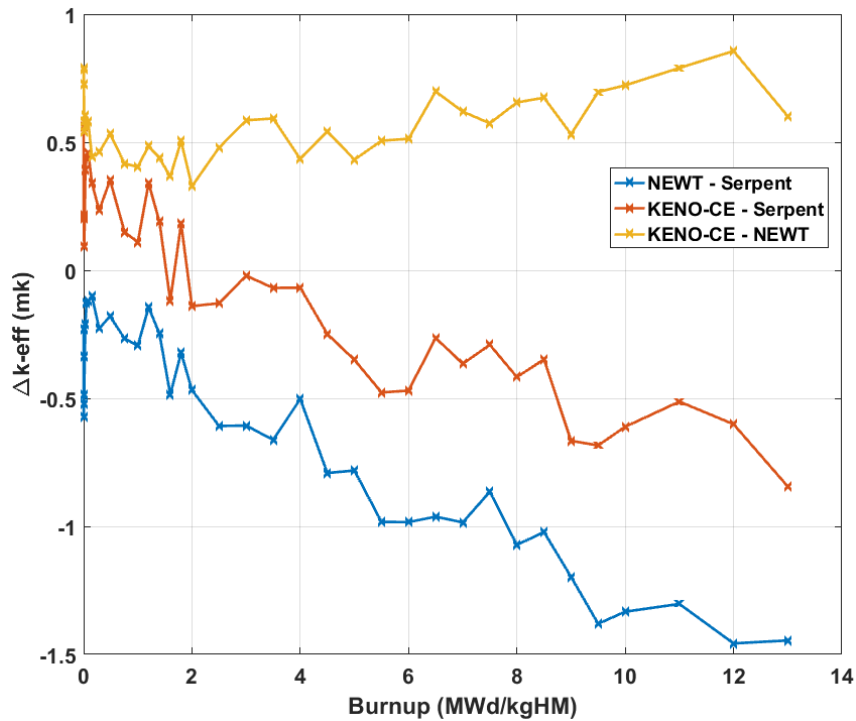


Figure 8-1 Discrepancies in CANDU bundle k-eff generated by different lattice calculation codes.

Figure 8-2 plots a number of representative few-group parameters' burnup-discrepancies as calculated by SERPENT and NEWT. The nomenclature is as described in Table 7-2 with the subscripts indicating the group number. These results show a wide range of discrepancies, with the fast absorption being the most different, followed by the fast transport and fast fission times prompt neutron fraction. The thermal absorption and fission tend to have the same bias, and kappa times sigma fission is four times smaller than sigma fission, implying that kappa values must have similar but opposite discrepancies to render much smaller errors for the product of kappa and

fission cross-section. This was verified by detailed analysis of the kappa and fission cross-section values. Finally, the delayed neutron fraction tends to have the smallest discrepancies as would be expected being the most important quantity for k-eff.

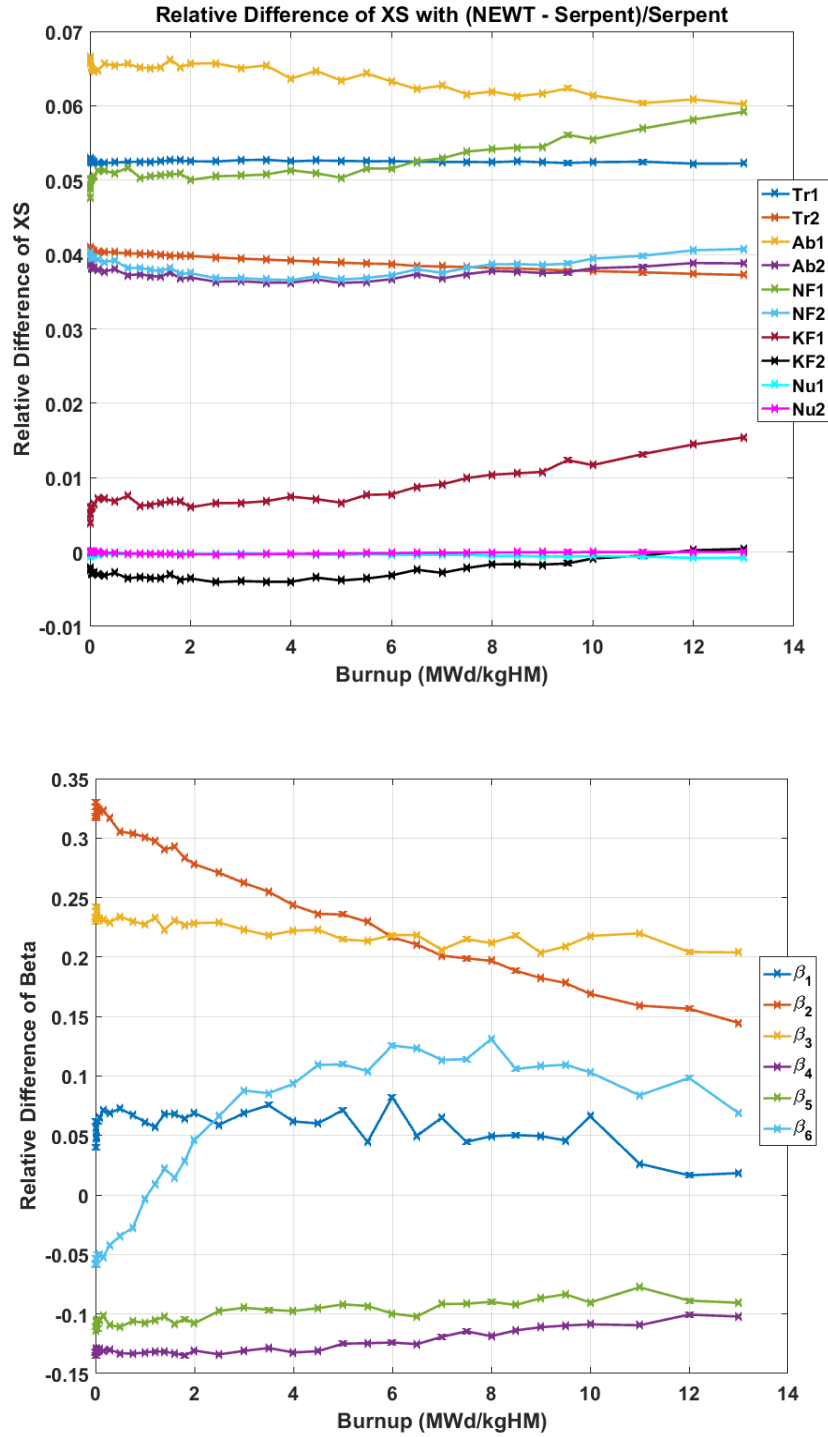
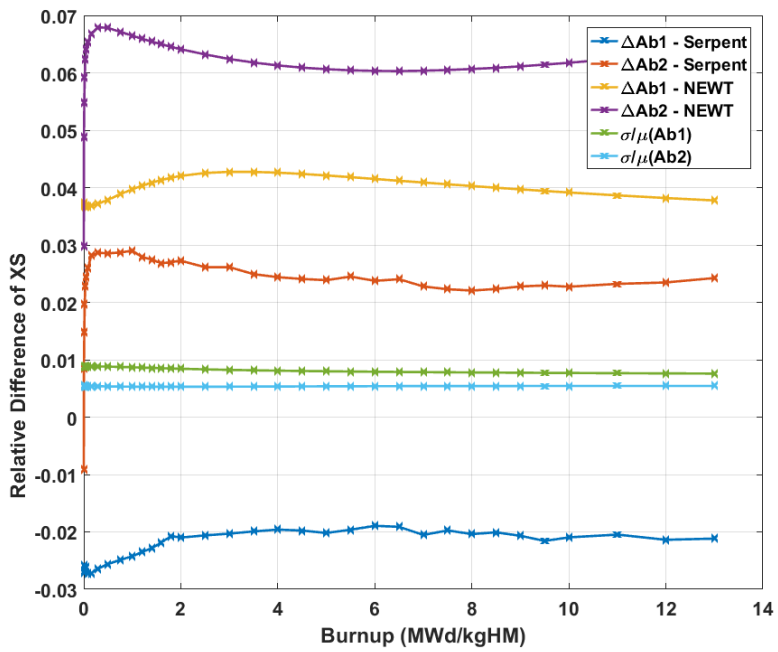
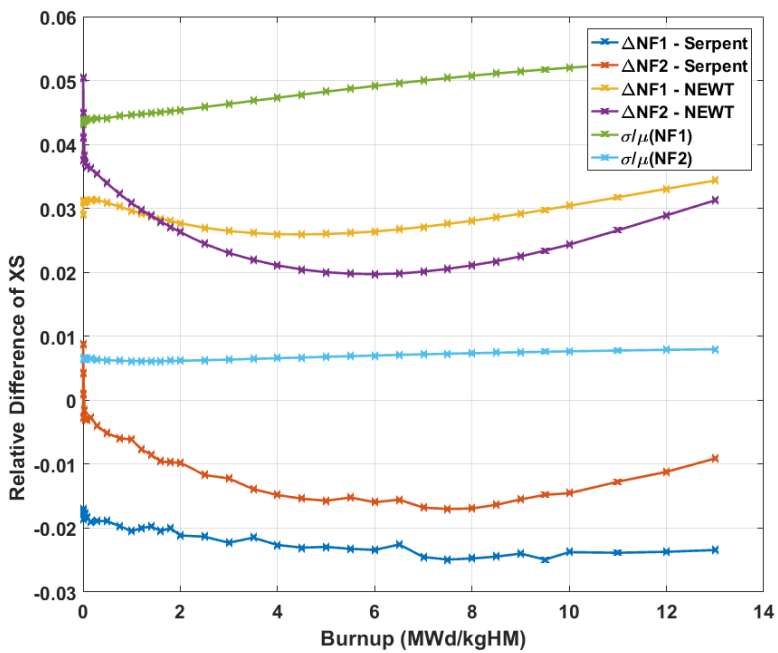


Figure 8-2 SERPENT vs. NEWT few-group cross-section modeling discrepancies.

Next, in support of assessing the impact of modeling errors on the propagated uncertainties, Figure 8-3 compares the standard deviations for a representative set of few-group parameters versus the discrepancies (also referred to as modeling errors) in their reference values as calculated by two different codes. Specifically, the modeling errors in Figure 8-3 are based on the differences of two-group parameters from SERPENT or NEWT calculations comparing to HELIOS data as reference. Note that both modeling errors and the cross-section standard deviations are unit-less as they are both normalized using the mean values of the few-group cross-sections, thereby providing a convenient way for their comparison. Results indicate that the modeling errors can be much bigger in magnitude than the cross-section uncertainties.



(a) Absorption Cross-Section



(b) Nu-Fission Cross-Section

Figure 8-3 Burnup-dependent modeling and cross-Section uncertainties.

### 8.3 Modeling Assumptions Impact during Parameter Uncertainty Propagation

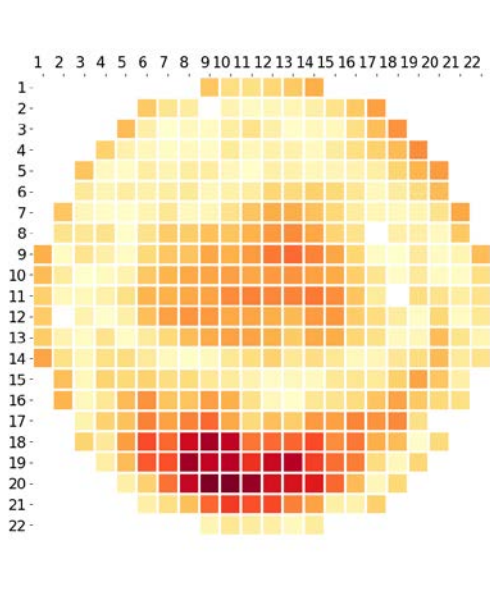
This section describes the details of the propagation of the multi-group cross-sections through the NEWT code to evaluate the few-group parameter uncertainties for NESTLE-C downstream core calculations with particular emphasis on the various assumptions made and how they impact the propagated uncertainties. First, the performance of both the deterministic and stochastic approaches for UQ are compared. Next, the UQ results are assessed against the impact of different modeling approximations. This study is done to provide an initial assessment of the impact of modeling errors for potentially expanding the scope of the study for future work. In particular, the assessment will explore the impact of the few-group structure, the resonance treatment, the number of uncertainty source basis and the impact of the reference values for the few-group parameters.

Regarding the first source of modeling error, the CANDU-6 bundle model is built with NEWT code employing two different treatments for resonance self-shielding calculation, denoted by MULTIREGION and LATTICECELL unit cell definitions, referred to hereinafter as ‘\_Mul’ and ‘\_Lat’, respectively. As another source of modeling error, the few-group parameters are generated in both two- and four-group structures. Also, the impact of the number of samples used to generate the covariance matrix is analyzed using a small and moderate number of samples, e.g., 50 and 300, respectively. Different combinations of these assumptions are employed to analyze the singular and combined effects of the various sources of modeling errors considered as shown in Table 8-2.

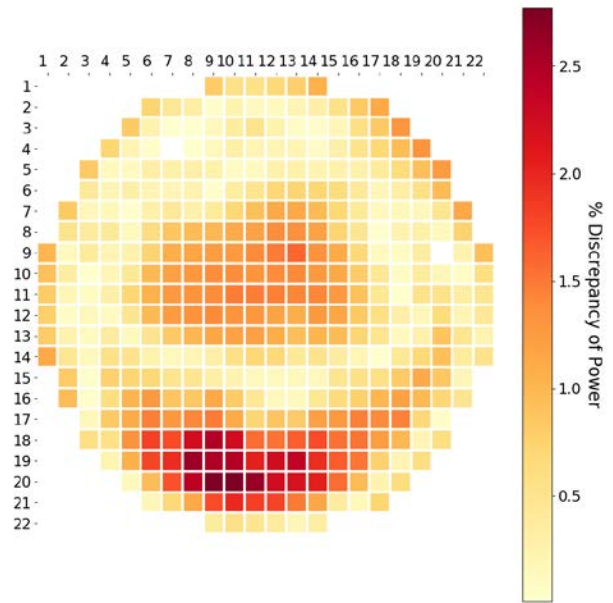
Table 8-2 Few-group uncertainties generation in group structure and number of samples through NEWT calculation.

Resonance treatment	MULTIREGION		LATTICECELL	
Group structure	2G	4G	2G	4G
# of samples completed	300	50	50	50

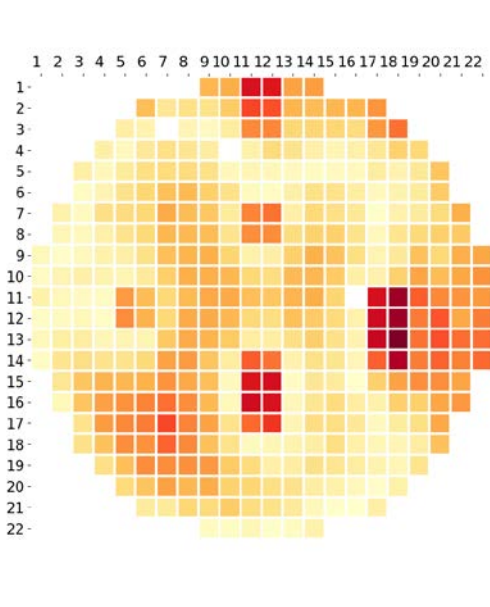
Figure 8-4 (a) and (b) show the power distribution discrepancy between different reference values of few-group parameters within the same group structure, while (c) and (d) show the power distribution discrepancy between using two-group structure data and using four-group structure data.



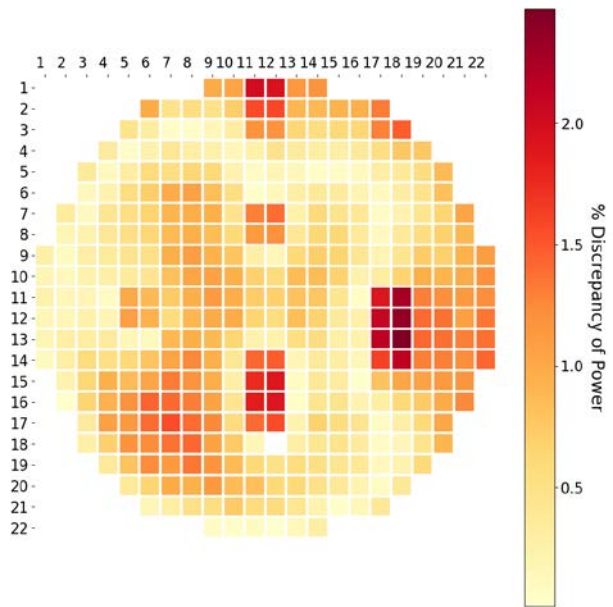
(a) NEWT\_2G vs. SERPENT\_2G



(b) NEWT\_4G vs. SERPENT\_4G



(c) NEWT\_2G vs. NEWT\_4G



(d) SERPENT\_2G vs. SERPENT\_4G

Figure 8-4 Percentage discrepancy of channel power between different reference cross-section libraries.

### 8.3.1 Assessing impact of uncertainty propagation method

This section discusses the impact of the uncertainty propagation method -- including deterministic vs. stochastic, and the associated number of samples used to generate the covariance matrix -- on the core responses uncertainty. To achieve that, the few-group parameter uncertainties are propagated through NESTLE-C core models using both deterministic and stochastic approaches. With regard to the deterministic approach, the conventional sandwich-based equation is used, where the core response to the uncertainties is assumed to be linear. This can be done by executing the code  $r$  times, with each time corresponding to a perturbation of the cross-sections along the  $r$ th singular vector of the few-group covariance matrix. The resulting response variations are compounded together using the sandwich equation formula as shown below:

$$\sigma_y = \sqrt{\frac{1}{N-1} \sum_{i=1}^r s_i^2 \left\{ \frac{f(\sigma_0[1 + \beta u_i]) - f(\sigma_0)}{\beta} \right\}^2} \quad (8-1)$$

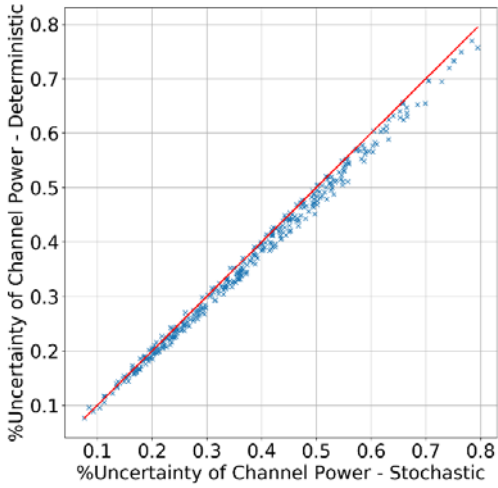
This representation assumes that the singular vectors are in relative units, i.e., consistent with the covariance matrix, also generated in relative units. While in the stochastic approach,  $N=1000$  randomly-generated NESTLE-C libraries are first constructed, in the same way SAMPLER generates its random libraries, where each library is a perturbation off of the reference library with the perturbation selected to be consistent with the few-group covariance matrix. The core attribute uncertainties are represented by the standard deviations of the random samples execution results. These two approaches tend to give similar results if the model responds linearly to the perturbations. Comparison of the core attribute uncertainties calculated by the stochastic and deterministic approaches, as done in Table 8-3 and Figure 8-5, serves as another measure of the validity of the linearity assumption.

Table 8-3 records the mean values and uncertainties of resulting core k-eff with both deterministic and stochastic approaches. Note that the mean value with the deterministic method is the reference value, while with the stochastic method it is the sample mean. Results in Table 8-3 indicate that the core k-eff uncertainties are very close -- within 0.3 [mk] -- as compared to the actual uncertainty and the reference value for k-eff for all cases analyzed. In Figure 8-5 scatter-plots are shown of the channel power uncertainties as calculated by both the deterministic and stochastic approaches using both the HELIOS- and SERPENT-based cross-section data libraries in two-group structure for the three steady-state models analyzed. Each point on these scatter plots

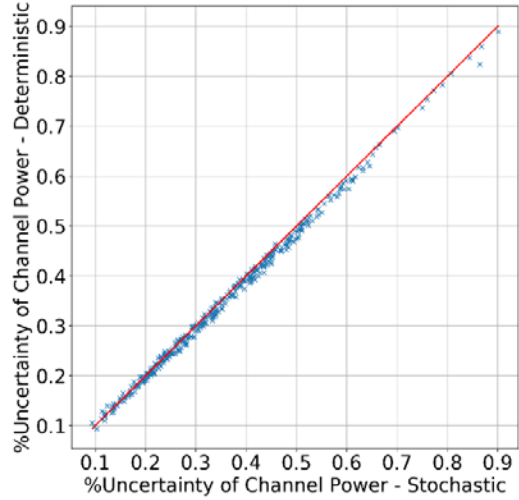
represents the uncertainty of a given channel power as calculated by both the deterministic and stochastic approaches. Ideally, all points should lie on a 45-degree line if the two approaches produce exactly the same results. Results indicate that the data generally show this trend with small deviations, possible at high and low levels of uncertainties. The toy model shows the least amount of deviations from the 45-degree line indicating that local conditions have an impact, albeit small in the cases analyzed, on the propagated uncertainties.

Table 8-3 Core k-eff uncertainty quantification through deterministic vs. stochastic approach.

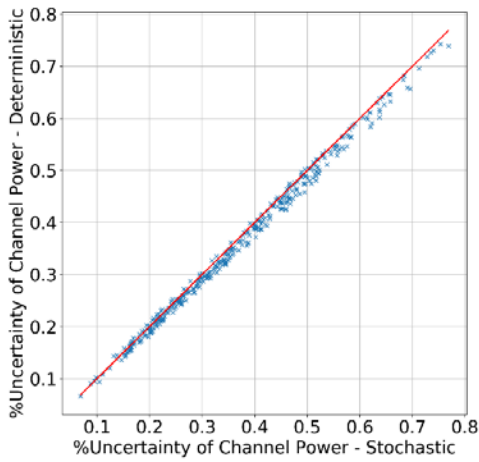
	<b>k-eff</b>	<b>Deterministic</b>	<b>Stochastic</b>
H2G_50U_Mul	Mean value	0.99959	0.99976
	Uncertainty [mk]	8.7	8.8
H2G_300U_Mul	Mean value	0.99959	0.99941
	Uncertainty [mk]	7.4	7.5
S2G_50U_Mul	Mean value	0.97062	0.97131
	Uncertainty [mk]	8.4	8.1
S2G_300U_Mul	Mean value	0.97062	0.97063
	Uncertainty [mk]	7.2	7.3
S4G_50U_Mul	Mean value	0.97125	0.97104
	Uncertainty [mk]	8.4	8.4
H2G_ref_Lat	Mean value	0.99959	0.99975
	Uncertainty [mk]	8.9	8.9
S2G_ref_Lat	Mean value	0.97062	0.97053
	Uncertainty [mk]	8.6	8.5
S4G_ref_Lat	Mean value	0.97125	0.97183
	Uncertainty [mk]	8.4	8.3
H2G_cvr_Lat	Mean value	1.01618	1.01632
	Uncertainty [mk]	8.7	8.7
S2G_cvr_Lat	Mean value	0.98587	0.98579
	Uncertainty [mk]	8.5	8.3
S4G_cvr_Lat	Mean value	0.98638	0.98695
	Uncertainty [mk]	8.2	8.1
H2G_toy_Lat	Mean value	1.00066	1.00020
	Uncertainty [mk]	9.2	8.9
S2G_toy_Lat	Mean value	0.96771	0.96759
	Uncertainty [mk]	8.9	8.7



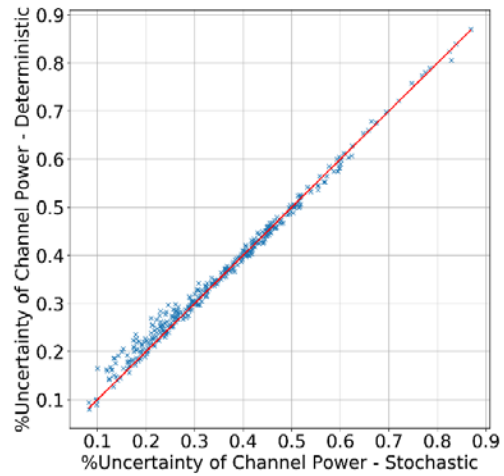
(a) HELIOS\_2G\_ref



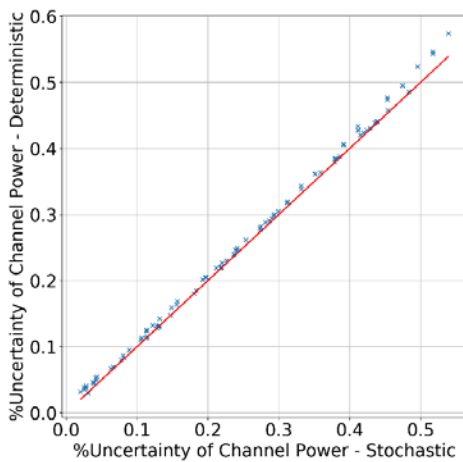
(b) SERPENT\_2G\_ref



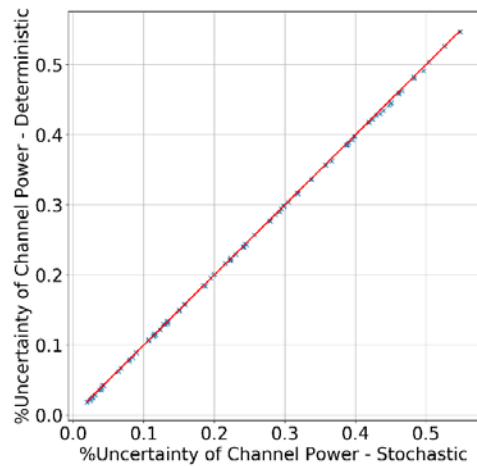
(c) HELIOS\_2G\_cvr



(d) SERPENT\_2G\_cvr



(e) HELIOS\_2G\_toy



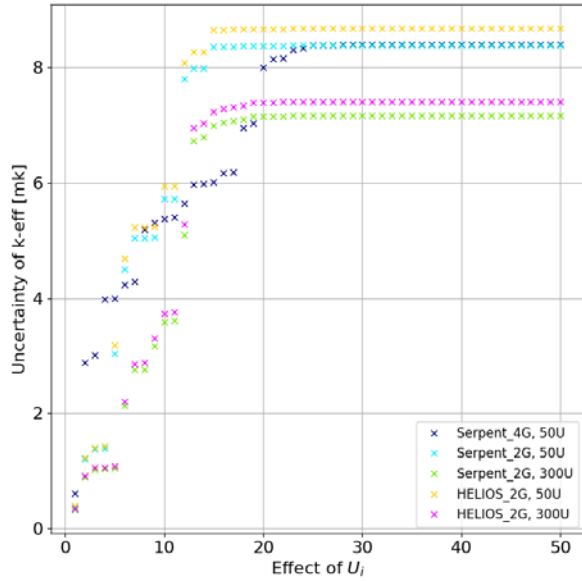
(f) SERPENT\_2G\_toy

Figure 8-5 Scatter plot of channel power uncertainty quantified via deterministic vs. stochastic approach.

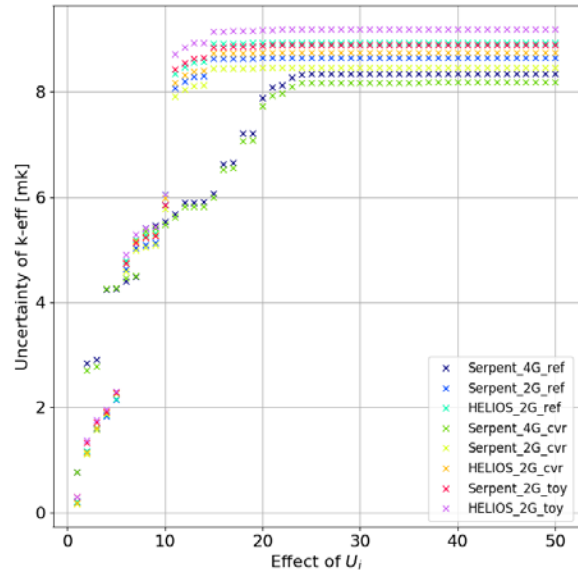
### 8.3.2 Assessing impact of modeling approximations

Next, we compare the impact of using a different number of SAMPLER runs to approximate the few-group covariance matrix. Specifically, two sets of samples are employed, as shown in Table 8-2. In one resonance treatment, 300 samples are generated in two-group structure and 50 samples are generated in four-group structure, denoted as “300U” and “50U” respectively. Note that when 300 samples are used, the covariance matrix will have up to 300 singular values, however for the 50 samples case, only the first 50 singular values will be non-zero. This study allows one to assess whether the number of samples has a strong impact on estimating the most dominant singular values, captured by ROM techniques. The NESTLE-C libraries are then generated based on these two sets of samples and around different reference values for the few-group parameters. Figure 8-6 (a) and (b) show some of these typical results for core k-eff uncertainty for the two noted resonance treatment methodology, i.e., Mul and Lat, respectively. Each figure shows the results of investigation of a number of core models with a different number of group structure and different number of samples, and different reference libraries. Considering the huge number of combinations that one can envision, only representative set of results are displayed.

Both figures show that, regardless of the number of samples, or the choice of the reference library or the resonance treatment method, one needs no more than 25 dominant directions to capture the uncertainty space. Results imply that number of vectors used to represent the few-group uncertainty space provides the largest impact on the core k-eff uncertainty, in order of 2 [mk] based on comparison between HELIOS\_2G\_50U (yellow markers) and HELIOS\_2G\_300U (pink markers) or between SERPENT\_2G\_50U (light blue) and SERPENT\_2G\_300U (green). The group structure shows no impact on core k-eff uncertainty based on comparison of SERPENT\_2G\_50U (light blue) and SERPENT\_4G\_50U (dark blue), but the number of active DOFs differs in the two group structures. Moreover, using different reference cross-section libraries generates about 0.2 [mk] difference in core k-eff uncertainty comparing the HELIOS\_2G\_50U and SERPENT\_2G\_50U results.



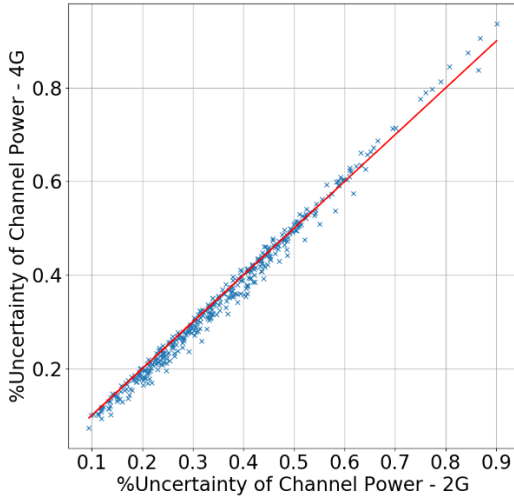
(a) Reference Libraries and # of Uncertainty Basis Comparison



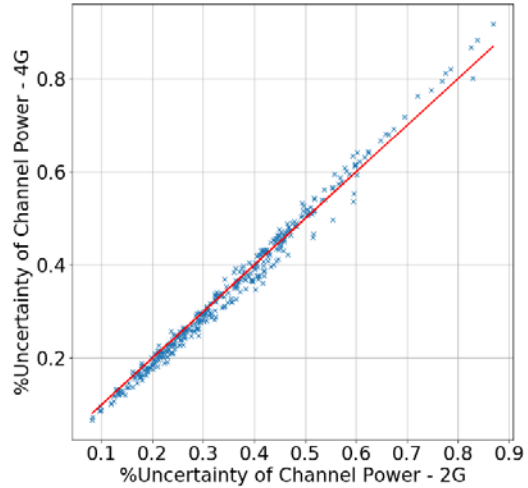
(b) Reference Libraries and Core Models Comparison

Figure 8-6 Comparison of core k-eff uncertainty under different modeling assumptions and approximations, including impact of few-group structures, number of basis from ROM-based compression, core models, and reference cross-section libraries.

Figure 8-7 compares the channel power uncertainties using two different group structures for two different core conditions. Each point represents the uncertainty for a given channel power calculated using two-group and four-group covariance matrices. The reference few-group parameter values are calculated by SERPENT. Results indicate that the group structure has some influence on the calculated uncertainties, which is more pronounced for the lower channel power. The impact is less -- as measured in terms of the total uncertainty -- to channels with higher power.



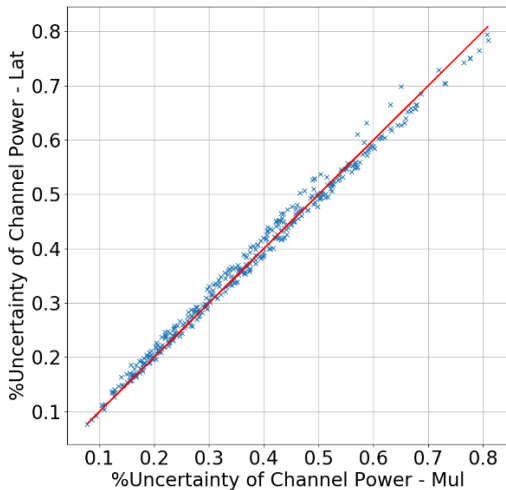
(a) Reference Core Model



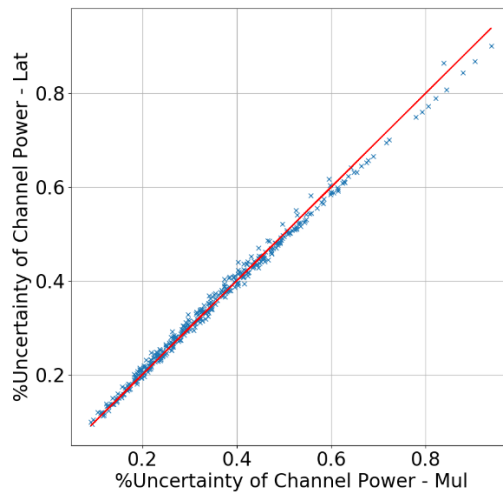
(b) Coolant Voided Core Model

Figure 8-7 Scatter plot of channel power uncertainty based on two-group vs. four-group few-group energy structures.

In Figure 8-8 the power uncertainties are compared in a similar manner to the previous figure, but now to assess the impact of modeling the resonances, with the x-axis representing the Mul treatment and the y-axis the Lat treatment, defined in Table 8-3, and with two different reference values for the cross-sections as shown in subplots (a) and (b). Results indicate that the impact of modeling errors is similar in magnitude to the impact of group structure, and the reference values for the cross-section appear to have less impact on the propagated uncertainties.



(a) HELIOS\_2G-based



(b) SERPENT\_2G-based

Figure 8-8 Scatter plot of channel power uncertainty based on LATTICECELL vs. MULTIREGION resonance treatment.

Next, Figure 8-9 compares the uncertainties as generated based on two different number of SAMPLER runs, specifically, 50 and 300 runs. The core model used here is the reference core model, and subplot (a) and (b) compare the uncertainties using both HELIOS and SERPENT libraries in two-group format.

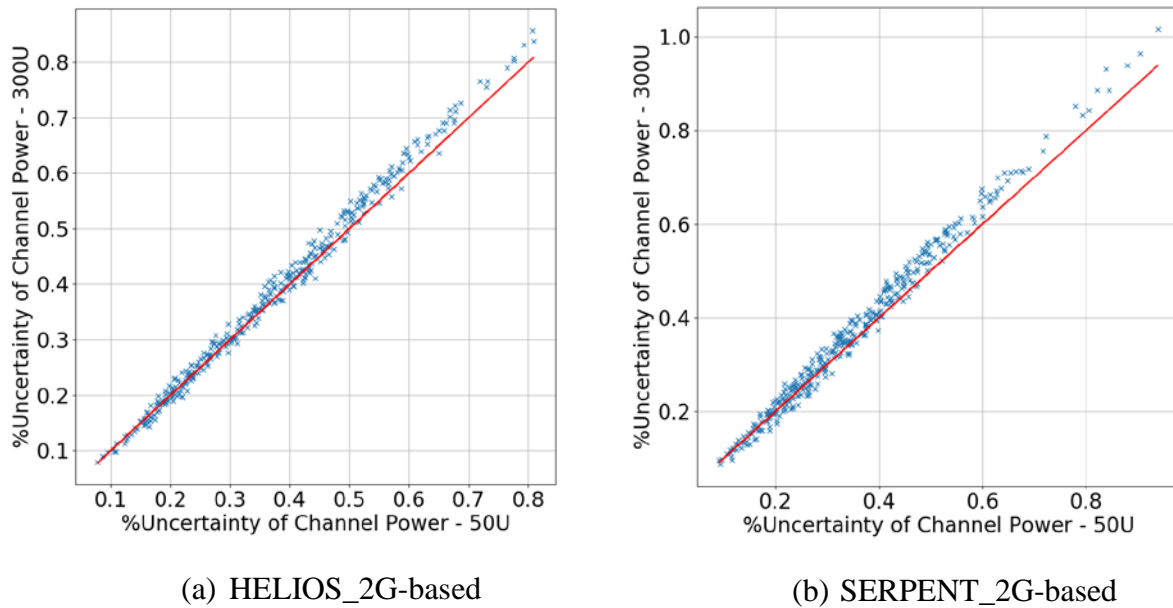


Figure 8-9 Scatter plot of channel power uncertainty based 300 vs. 50 few-group uncertainty source basis.

The results indicate that the use of 50 samples slightly under-predicts the uncertainties. However, the trend observed is still very close to the 45-degree line, indicating that one can get a fairly reasonable estimate of uncertainties with relatively small number of samples which is useful for scoping studies.

#### 8.4 Modeling Uncertainties Interaction with Parameter Uncertainties

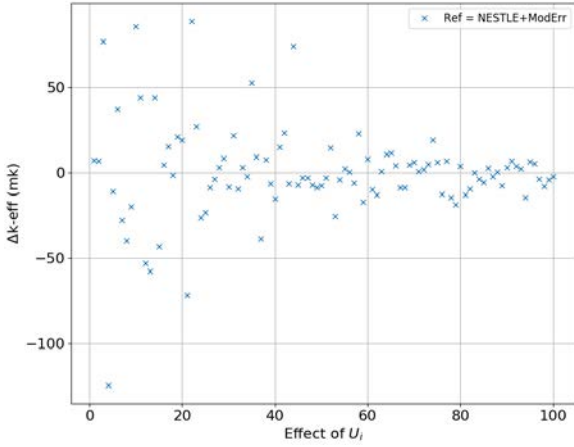
To study the impact of the ROM-based compression on the propagated uncertainties, Figure 8-10 (a) shows the individual k-eff variations resulting from one-at-a-time perturbations along the singular vectors, representing the differences in the curly bracket in Eq. (8-1) with the arbitrary constant  $\beta=1$ . For three different cases, wherein each case, the reference NESTLE cross-sections, denoted as ‘RefXS’, are selected as follows:

$$\sigma_0 = \sigma_{NESTLE} \left( 1 + \frac{\sigma_{NEWT} - \sigma_{SERPENT}}{\sigma_{SERPENT}} \right), \sigma_0 = \sigma_{NEWT}, \sigma_0 = \sigma_{SERPENT}.$$

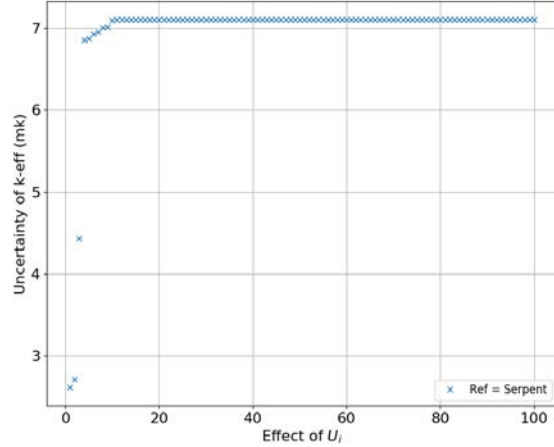
In the first case, the reference NESTLE cross-section (generated using HELIOS [5]) are perturbed by the discrepancies found between NEWT and SERPENT, which is denoted as ‘ModErr’ in the figure subtitles. In the second and third cases, respectively, NEWT and SERPENT cross-sections are used directly as the reference cross-sections for NESTLE model. Regarding cross-section uncertainties, these figures clearly show that one only needs no more than ten singular vectors to propagate the few-group uncertainties (recall that the singular vectors ordering follows the singular value spectrum according to Eq. (5-21)).

Regarding Figure 8-10 (b)-(d), they are designed to investigate the impact of cross-section modeling errors. Each case is generated with different reference cross-section. Results indicate two things. First, the modeling errors do not impact the number of required singular vectors, and the propagated uncertainty show few percent discrepancies due to the modeling errors. Note that in this experiment, we expect the reference k-eff to change due to a change in the reference cross-sections, however if the linearity assumption is valid, the propagated uncertainties should be similar.

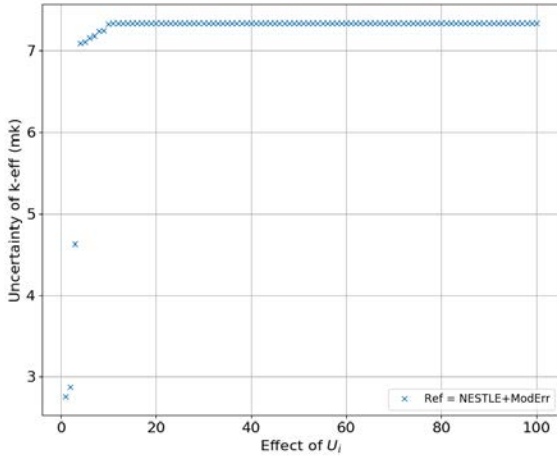
Another important result of Figure 8-10 (a) is that most of the singular vectors have strong impact on k-eff, i.e., k-eff is sensitive to variations along the singular vectors; however only the first ten singular vectors are shown to contribute to the propagated k-eff uncertainty. This is because the singular values of the few-group cross-section drop very quickly with the singular value index. The implication is that singular vectors beyond the tenth vector have very small uncertainties and hence they cannot impact core responses’ uncertainties, even if they have strong sensitivities. This situation is interesting when considering modeling errors, because it is not clear how much correlation exists between modeling errors and the singular vectors of the cross-sections covariance matrix. To explore this correlation, one can project the vector of the modeling errors, representing the differences between two different codes, onto the singular vectors of the covariance matrix.



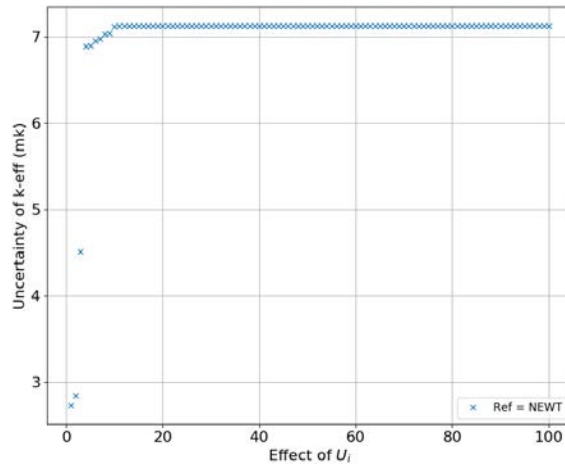
(a) RefXS = NESLTE + ModErr



(b) RefXS = Serpent



(c) RefXS = NESTLE + ModErr



(d) RefXS = NEWT

Figure 8-10 ROM-based core k-eff uncertainty with selected reference cross-section libraries.

The procedure may be described as follows:

- Let the modeling discrepancies, say between NEWT and SERPENT, be described by a vector  $\Delta\sigma_m = (\sigma_{NEWT} - \sigma_{SERPENT}) / \sigma_{SERPENT}$ . The division is to ensure all errors are in relative units as done with the cross-sections covariance matrix.
- Project this vector along the first  $r$  singular vectors of the covariance matrix, such that the  $i^{\text{th}}$  component of  $\Delta\sigma_m$  along the  $u_i$  vector is given by:  $u_i^T (\Delta\sigma_m)$ .
- Aggregate the first  $j$  components of  $\Delta\sigma_m$  in a vector  $\Delta\sigma_m^j = \sum_{i=1}^j u_i^T (\Delta\sigma_m)$ .

- Plot the norms of the vectors  $\|\Delta\sigma_m^j\|$  and  $\|\Delta\sigma_m - \Delta\sigma_m^j\|$  as functions of  $j$  in Figure 8-11.

Figure 8-11 shows that the modeling error vector can be described using the singular vectors of the covariance matrix. Interesting though, one needs more than ten vectors to fully describe it. This implies that some of the modeling error components are collinear with cross-section uncertainties, i.e., the first ten components, and the remaining components are orthogonal to the cross-section uncertainties, i.e., independent. The contributions of each singular vector to the total propagated uncertainty, it is instructive to create a similar graph for the modeling errors components. This is done in Figure 8-12, which shows the change in core k-eff due to the first  $j$  components of the vector of the modeling errors. This can be achieved by running the NESTLE-C model with the perturbation:

$$f\left(\sigma_0\left[1 + \sum_{i=1}^j u_i^T(\Delta\sigma_m)\right]\right) - f(\sigma_0)$$

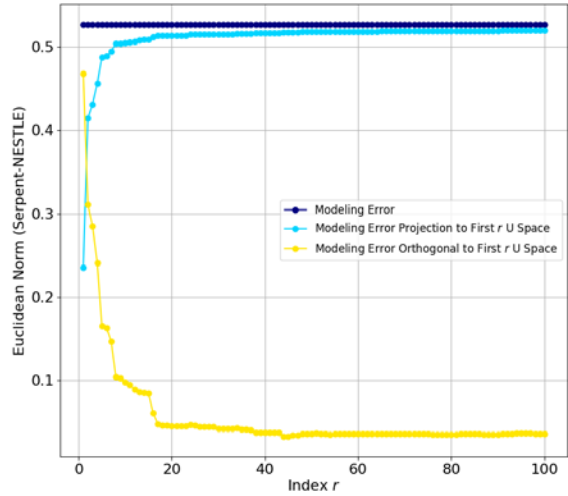
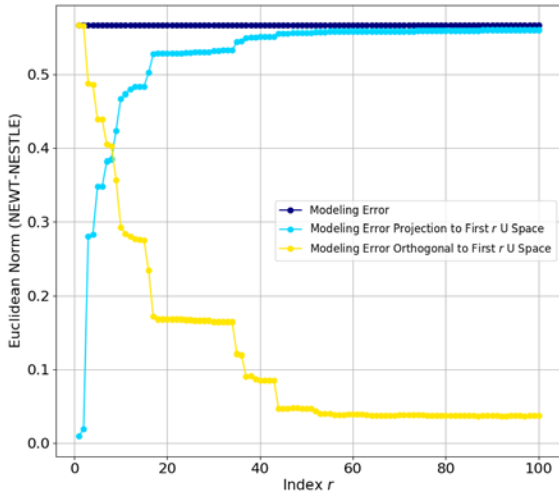
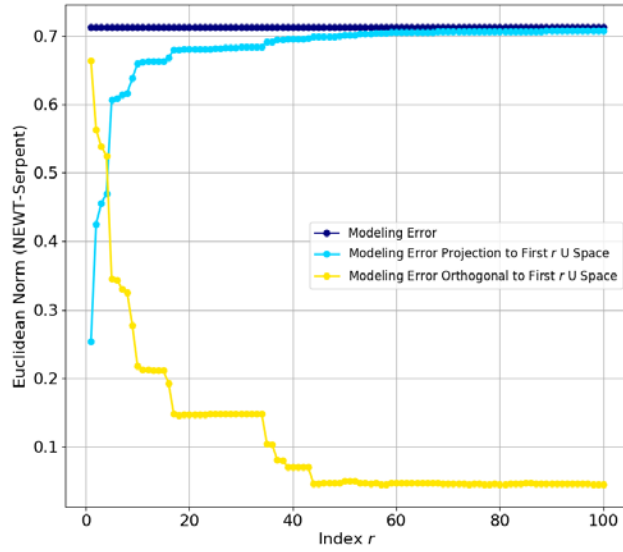


Figure 8-11 Relationship between modeling and parameter uncertainties.

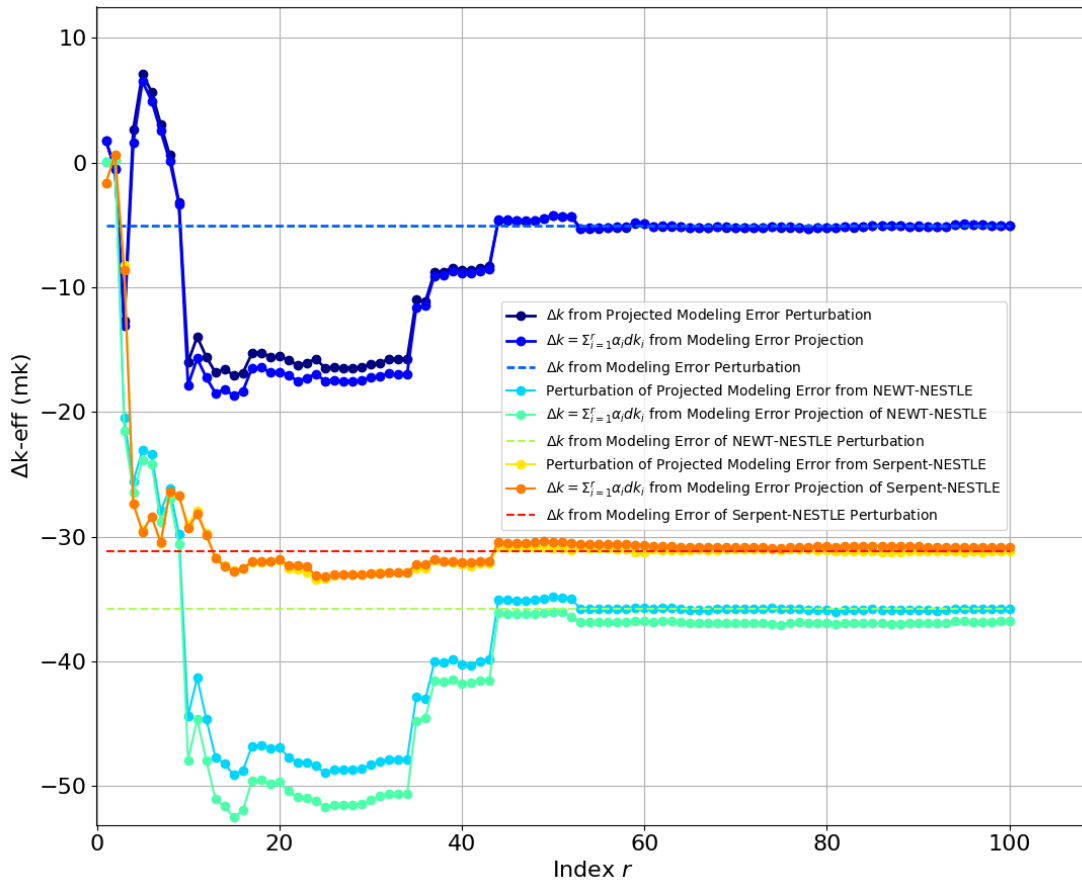


Figure 8-12 Decomposition of modeling errors along parameter uncertainties.

Figure 8-12 shows three sets of figures, each corresponding to one of the three cases mentioned earlier for the modeling errors. Each case shows two graphs that are closely related, one generated by executing the NESTLE-C code to calculate the impact of the modeling errors, and one generated by using linearity approximation, obtained from the previous set of runs used to generate the cross-sections uncertainties. Recall that to propagate cross-section uncertainties, the NESTLE-C code was executed  $r$  times, wherein each time the cross-sections were perturbed along one of the  $u_i$  directions. One can thus use these runs to estimate, assuming linearity, the impact on k-eff for a general modeling errors vector. Results indicate that the linearity assumption is adequate for most of the components, with the exception of a few jumps. More interesting, the graphs show that the first ten components have huge impact on the k-eff, which is much larger than the actual discrepancy calculated using the entire modeling errors vector. For example, for the SERPENT-NEWT discrepancies, the first ten components create a big swing in k-eff which is

then canceled out by the remaining components, resulting in a total of 5 [mk] modeling error. The NEWT cross-sections introduce a bigger initial swing in the negative direction, up to 40 [mk] then recover back to 25 [mk]. The SERPENT cross-sections introduce an initial drop of 30 [mk] followed by almost no additional change due to the rest of the components. To further understand this behavior, the modeling errors components are further separated into components based on key cross-section types, e.g., fast and thermal absorption and fission cross-sections. Figure 8-13 shows the results of this exercise for the modeling errors representing discrepancies between NEWT and SERPENT which gives rise to 5mk error in the core k-eff. Results indicate that there exists a great deal of error compensation between the different cross-section types.

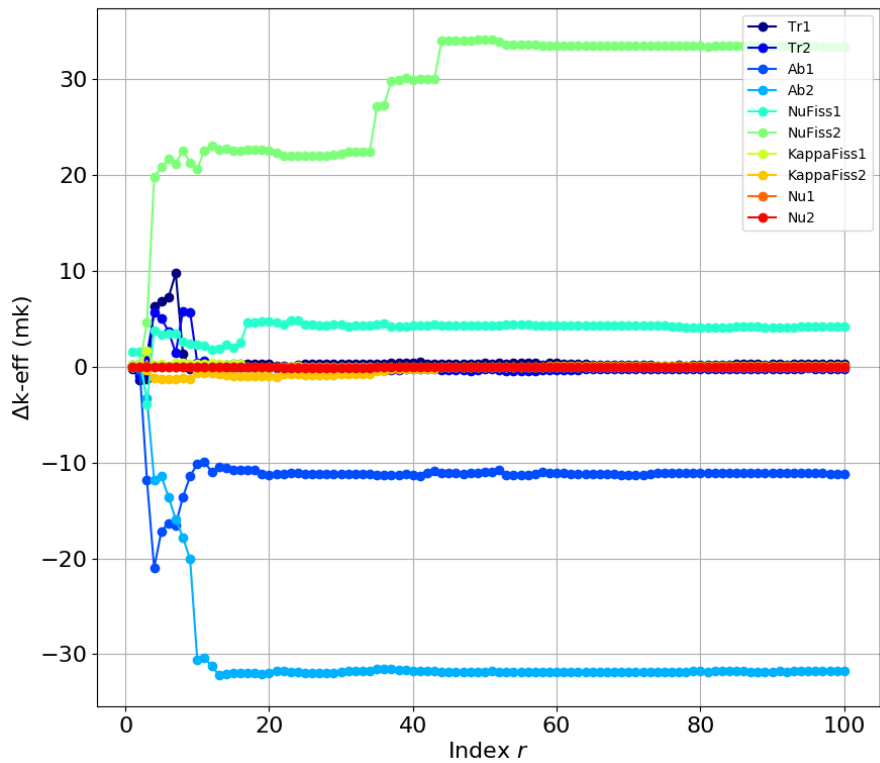


Figure 8-13 Decomposition of modeling errors based on reaction type of few-group parameters.

Next, Figure 8-14 plots the mesh-based nodal power distribution uncertainties using different reference cross-sections for core calculations. For example, the top left graph compares the uncertainties calculated by NESTLE using both NESTLE and NEWT as reference cross-sections. To understand the impact of different cross-section types, the right three graphs compare the uncertainties when the reference cross-sections are perturbed by the modeling errors from a

single type of cross-section. For example, the bottom right graph compares the uncertainties when the reference NESTLE cross-sections are modified by the thermal nu-fission cross-sections and the thermal absorption cross-sections. These results indicate strong sensitivity of the propagated uncertainties to the modeling errors.

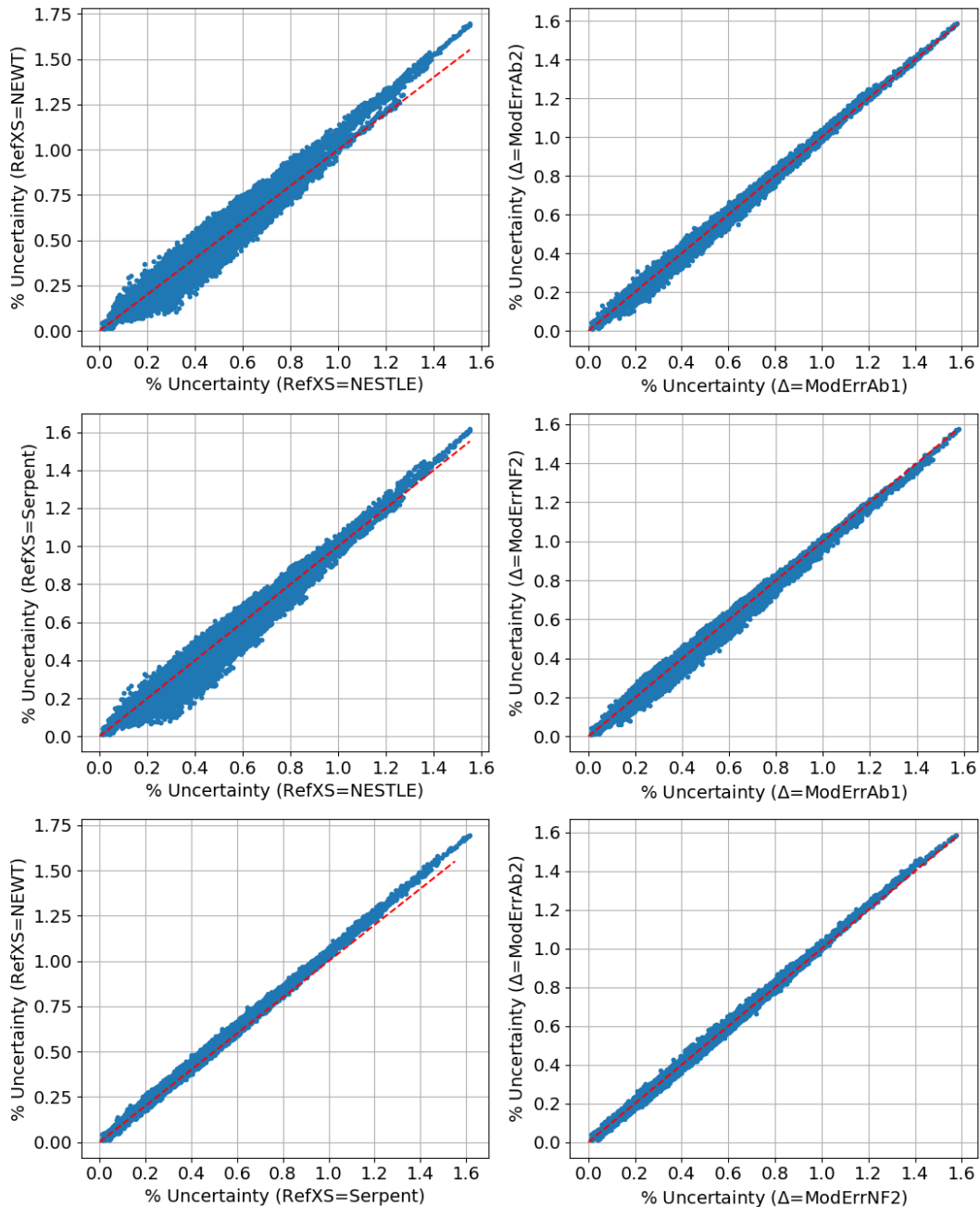


Figure 8-14 Scatter plot of percentage power distribution uncertainties between selected (indicated in the axis label) reference cross-section libraries, implying the impact of modeling uncertainties by switching the reference values.

## 8.5 Conclusion

This chapter provides a detailed discussion on major sources of uncertainties in uncertainty propagation on reactor core calculations, the nuclear data uncertainty and key modeling approximations and assumptions that are generally made during process of neutronics simulation. The proposed ROM-base uncertainty propagation method is applied to deal with the enormous few-group uncertainty space due to wide range of reactor core conditions. Based on the insight on the modeling uncertainties during nuclear data uncertainty propagation, we have found non-neglectable impact of modeling uncertainties on standalone neutronics uncertainty quantification to evaluate the uncertainties of main core attributes, i.e., core multiplication factor and core power distribution. The various modeling assumptions include propagation methods, few-group structures, number of ROM-based uncertainty basis, etc. An algorithm via replacing the reference cross-section library (setting different reference points) is proposed to evaluate the impact of different modeling assumptions. The proposed algorithm is flexible in all the applications and could be extended with other modeling assumptions and approximations.

## 8.6 References

1. Turinsky, P. and H. Sarsour, *NESTLE-C: Few-group neutron diffusion equation solver utilizing the nodal expansion method for eigenvalue, adjoint, fixed-source steady-state and transient problems: CANDU version*. 2003, North Carolina State University: Raleigh, NC (United States).
2. DeHart, M. and M. Jessee, *NEWT: a new transport algorithm for two-dimensional discrete ordinates analysis in non-orthogonal geometries*. ORNL/TM-2005/39, Oak Ridge National Laboratory, 2005.
3. Leppänen, J., et al. *The Serpent Monte Carlo code: Status, development and applications in 2013*. in *SNA+ MC 2013-Joint International Conference on Supercomputing in Nuclear Applications+ Monte Carlo*. 2014. EDP Sciences.
4. Williams, M.L., et al., *A statistical sampling method for uncertainty analysis with SCALE and XSUSA*. Nuclear technology, 2013. **183**(3): p. 515-526.
5. Rahnema, F., *Lattice Database Development for Static and Transient Analyses*. 2002, NazConsulting: Canadian Nuclear Safety Commission.

## 9. CONCLUSION AND FUTURE WORK

This dissertation has developed an ROM-based uncertainty quantification process to reduce the dimensionality of large parameter uncertainty source in neutronics core simulations, which makes the uncertainty analysis computationally feasible. A comprehensive discussion of the uncertainty sources in each stage of neutronics calculations is provided in order to promote the importance of propagating and prioritizing all sources of uncertainties in the uncertainty characterization process. A literature review on uncertainty propagation methods, including stochastic and deterministic methods, as well as the efforts made to increase the efficiency of uncertainty analysis, is provided in detail. Also, the status of development in uncertainty characterization framework and the modeling uncertainty evaluation is also presented in the literature review.

The proposed uncertainty characterization process, including the propagation of parameter uncertainties in a compressed format and modeling uncertainties in form of modeling assumptions and approximations, is illustrated with PCM methodology and ROM techniques implemented. The impact of a number of modeling assumptions and approximations on the resulting uncertainty in core attributes is evaluated. The interactions between the two major sources of uncertainties, the nuclear data uncertainty and the modeling uncertainty, are investigated and assessed. The implication is that one must take into account of modeling uncertainty when propagating uncertainties in uncertainty analysis on nuclear reactor calculations.

This Ph.D. work manages to create the first comprehensive library of nuclear data uncertainties for reactor physics calculations in CANDU reactor application. This UCF can be extended to other types of reactors or multi-physics uncertainty analysis. Further, the UCF can also be extended to include other sources of uncertainties, such as thermal physics uncertainties.